

AD-774 264

ROLLING ELEMENT BEARING RETAINER
ANALYSIS

Joseph A. Mauriello, et al

Avco Lycoming Division

Prepared for:

Army Air Mobility Research and Development
Laboratory

November 1973

DISTRIBUTED BY:

NTIS

National Technical Information Service
U. S. DEPARTMENT OF COMMERCE
5285 Port Royal Road, Springfield Va. 22151

ACCESSION FOR	
STC	Write Section <input checked="" type="checkbox"/>
DOC	Sub. Section <input type="checkbox"/>
MEANS/PROCS	<input type="checkbox"/>
JUSTIFICATION	
BY	
DISTRIBUTION/AVAILABILITY GROUPS	
Size	AVAIL. NO. OF SPECIAL
A	

DISCLAIMERS

The findings in this report are not to be construed as an official Department of the Army position unless so designated by other authorized documents.

When Government drawings, specifications, or other data are used for any purpose other than in connection with a definitely related Government procurement operation, the United States Government thereby incurs no responsibility nor any obligation whatsoever; and the fact that the Government may have formulated, furnished, or in any way supplied the said drawings, specifications, or other data is not to be regarded by implication or otherwise as in any manner licensing the holder or any other person or corporation, or conveying any rights or permission, to manufacture, use, or sell any patented invention that may in any way be related thereto.

Trade names cited in this report do not constitute an official endorsement or approval of the use of such commercial hardware or software.

DISPOSITION INSTRUCTIONS

Destroy this report when no longer needed. Do not return it to the originator.

1b

Unclassified

Security Classification

AD-774264

DOCUMENT CONTROL DATA - R & D

(Security classification of title, body of abstract and indexing annotation must be entered when the overall report is classified)

1. ORIGINATING ACTIVITY (Corporate author)		2A. REPORT SECURITY CLASSIFICATION	
Avco Lycoming Division 550 S. Main Street Stratford, Connecticut 06497		Unclassified	
2. REPORT TITLE		2B. GROUP	
ROLLING ELEMENT BEARING RETAINER ANALYSIS			
3. DESCRIPTIVE NOTES (Type of report and inclusive dates)			
Final Report			
4. AUTHOR(S) (First name, middle initial, last name)			
Joseph A. Mauriello A. B. Jones Normand Lagasse William Murray			
5. REPORT DATE		7A. TOTAL NO. OF PAGES	
November 1973		273 267	
6A. CONTRACT OR GRANT NO.		7B. NO. OF REFS	
Contract DAAJ02-67-C-0080		11	
B. PROJECT NO.		8A. ORIGINATOR'S REPORT NUMBER(S)	
Task IG:62203D14414		USAAMRDL Technical Report 72-45	
C.		8B. OTHER REPORT NO(S) (Any other number that may be assigned this report)	
D.		Lycoming Report No. 195.7.10	
9. DISTRIBUTION STATEMENT			
Approved for public release; distribution unlimited.			
11. SUPPLEMENTARY NOTES		12. SPONSORING MILITARY ACTIVITY	
		Eustis Directorate U. S. Army Air Mobility R&D Laboratory Fort Eustis, Virginia	
13. ABSTRACT			
<p>An integrated analytical and experimental program was conducted to analyze the operation of rolling element bearing retainers and attendant lubrication effects. Analytical models to represent ball and roller bearing operation were derived with regard to the elastic deflections at the rolling element/race contacts, tractive forces generated at the bearing component interaction surfaces, and viscous drag effects.</p> <p>Program objectives were conducted in two phases. The first phase was to analyze the forces and the lubrication conditions that exist between the rolling element and retainer pockets when the bearing is operating at high-load and high-speed conditions. Once completed, the derived analysis was incorporated into an iterative computer program to produce bearing solutions for arbitrary load and speed conditions.</p> <p>The second phase of the program was to conduct an experimental test program to validate the computer analysis. Bearing performance was investigated over a wide range of loads, speeds, and lubrication conditions. Also, data were acquired on ball bearings subjected to retainer skid at high-speed, low-load operating conditions. To accomplish the test program, it was necessary to modify an existing test rig and to design special instrumentation for acquisition of the desired operating data.</p>			

DD FORM 1473

REPLACES FORM 1473, 1 JAN 64, WHICH IS OBSOLETE FOR ARMY USE.

Unclassified

Reproduced by
NATIONAL TECHNICAL
INFORMATION SERVICE
U.S. Department of Commerce
Springfield, VA 22151

Unclassified
Security Classification

1A KEY WORDS	LINK A		LINK B		LINK C	
	ROLE	WT	ROLE	WT	ROLE	WT
Bearing Retainer Lubrication of Bearings Rolling Element Bearing Retainer						

Unclassified
Security Classification

1a

12036-73



DEPARTMENT OF THE ARMY
U. S. ARMY AIR MOBILITY RESEARCH & DEVELOPMENT LABORATORY
EUSTIS DIRECTORATE
FORT EUSTIS, VIRGINIA 23604

The research described herein was conducted by AVCO Lycoming Division under the terms of Contract DAAJ02-69-C-0080. The work was performed under the technical management of Mr. E. R. Givens, Propulsion Division, Eustis Directorate, U.S. Army Air Mobility Research and Development Laboratory.

The objectives of the program were to analyze the forces exerted on the retainer pockets of rolling element bearings during high-load, high-speed operating conditions that exist within the rolling-contact areas of the bearing.

Appropriate technical personnel of this Directorate have reviewed this report and concur with the conclusions contained herein.

12

Task IG162203D14414
Contract DAAJ02-69-C-0080
USAAMRDL Technical Report 72-45
November 1973

ROLLING ELEMENT BEARING RETAINER ANALYSIS

Final Report

Avco Lycoming Report No. 105.7.10

By

Joseph A. Mauriello
Normand Lagasse
A. B. Jones
William Murray

Prepared by

Avco Lycoming Division
Stratford, Connecticut

for

EUSTIS DIRECTORATE
U. S. ARMY AIR MOBILITY
RESEARCH AND DEVELOPMENT LABORATORY
FORT EUSTIS, VIRGINIA

Approved for public release; distribution unlimited.

SUMMARY

An integrated analytical and experimental program was conducted to analyze the operation of rolling element bearing retainers and attendant lubrication effects. Analytical models to represent ball and roller bearing operation were derived with regard to the elastic deflections at the rolling element/race contacts, tractive forces generated at the bearing component interaction surfaces, and viscous drag effects.

Program objectives were conducted in two phases. The first phase was to analyze the forces and the lubrication conditions that exist between the rolling element and retainer pockets when the bearing is operating at high-load and high-speed conditions. Once completed, the derived analysis was incorporated into an iterative computer program to produce bearing solutions for arbitrary load and speed conditions.

The second phase of the program was to conduct an experimental test program to validate the computer analysis. Bearing performance was investigated over a wide range of loads, speeds, and lubrication conditions. Also, data were acquired on ball bearings subjected to retainer skid at high-speed, low-load operating conditions. To accomplish the test program, it was necessary to modify an existing test rig and to design special instrumentation for acquisition of the desired operating data.

FOREWORD

This final report describes a program conducted by Avco Lycoming Division for the U. S. Army Air Mobility Research and Development Laboratory under Contract DAAJ02-69-C-0080, Task 1G162203D14414.

U. S. Army technical direction was provided by Mr. R. Givens.

We wish to acknowledge Mr. R. Chasman of the Air Force Aero Propulsion Laboratory for his support of the program, and Drs. J. Walowit and A. L. Cu of Mechanical Technology, Inc., for their contributions to the elastohydrodynamic traction computer subroutines and to the equations of shear forces on the high-speed bearing retainers.

TABLE OF CONTENTS

	<u>Page</u>
SUMMARY	iii
FOREWORD	v
LIST OF ILLUSTRATIONS	ix
LIST OF TABLES	xiv
LIST OF SYMBOLS	xv
INTRODUCTION	1
MATHEMATICAL ANALYSIS	5
Ball Bearing Mathematical Model	5
Roller Bearing Mathematical Model	21
Elastohydrodynamic Film Thickness Calculation	41
Elastohydrodynamic Traction Coefficients	46
Analysis of Shear Forces on a Lubricated, High-Speed Bearing Retainer	62
VERIFICATION TEST PROGRAM	83
Test Rig Description and Operation	83
Test Bearing Description	93
Instrumentation	121
Data Acquisition	129
Test Procedure	134
Test Results	140
COMPUTER PROGRAM RESULTS	176
Ball Bearing Computer Deck	176
Roller Bearing Computer Deck	134
CONCLUSIONS	183
RECOMMENDATIONS	189
LITERATURE CITED	190

	<u>Page</u>
APPENDIXES	
I. Ball Bearing Computer Program FORTRAN Source Deck	191
II. Format for Ball Bearing Computer Input Information .	222
III. Typical Ball Bearing Problem for Computer Program	224
IV. Roller Bearing Computer Program FORTRAN Source Deck	227
V. Format for Roller Bearing Computer Program Input Information	244
VI. Typical Roller Bearing Problem from Computer Program	246
VII. MIL-L-23699-Type Oil Properties Available for Use in Program Inputs	248
VIII. Solution for Roller Bearing Case Operating at 20,000 RPM and Radial Load of 200 Pounds	249
DISTRIBUTION	251

LIST OF ILLUSTRATIONS

<u>Figure</u>		<u>Page</u>
1	Race Control Concept	2
2	Ball Referred to XYZ Coordinate System	7
3	Initial and Final Positions of Inner and Outer Race Curvature Centers	11
4	Bearing Referred to XYZ Coordinate System.	15
5	Forces and Moments Acting on Outer-Piloted Cage .	18
6	Forces and Moments Acting on Inner-Piloted Cage .	19
7	Bearing Details	22
8	Roller Contact Forces and Roller Orientation Schematic	25
9	Roller Pocket Forces and Cage Whirl Forces	33
10	Ball Motion Occurring in High-Speed Angular- Contact Ball Bearing; General Case	43
11	Contact Areas on Race and Ball	44
12	Coefficient of Friction Versus Shear Rate Parameter for Heating Parameter = 10^{-6}	48
13	Coefficient of Friction Versus Shear Rate Parameter for Heating Parameter = 5×10^{-4}	49
14	Velocity Components Active in Contact Areas	51
15	Tractive Force Versus Slip Velocity	55
16	Race Contact, Velocity Distribution, and Tractive Force Distribution in a Ball-Race Contact	56

<u>Figure</u>		<u>Page</u>
17	Sliding Velocity and Tractive Force Distribution in a Ball-Race Contact	57
18	Analysis of Retainer-Ball Traction; Schematic . . .	63
19	Dimensionless Pressure Profile for Ball-Retainer Contact ($\eta = 0$).	67
20	Dimensionless Load per Unit Length	71
21	Film Thickness and Maximum Pressure for Retainer-Ball Contact	73
22	Traction Versus Load for Ball and Roller Contacts	76
23	Film Thickness and Maximum Pressure for Retainer-Roller Contact,	77
24	Geometry Used in Calculating Retainer-Race Traction; Schematic.	79
25	Section Used in Calculating Drag on Ball; Schematic	82
26	Bearing Test Rig; Cross-Sectional View,	85
27	Bearing Test Facility	86
28	Bearing Test Rig; Right Front View	87
29	Bearing Test Rig; Front View	88
30	Air Pressure Differential Versus Bearing Thrust Load	89
31	Test Rig Facilities; Schematic Diagram	91
32	Typical Data Sheets	92
33	Ball Bearing PSK 18123	95

<u>Figure</u>		<u>Page</u>
34	Ball Retainer Rework PSK 17438	97
35	Ball Bearing S/N 003 Inner Race Roundness and Concentricity	100
36	Ball Bearing S/N 003 Outer Race Roundness and Concentricity	101
37	Ball Bearing S/N 006 Inner Race Roundness and Concentricity	102
38	Ball Bearing S/N 006 Outer Race Roundness and Concentricity	103
39	Ball Bearing S/N 003 Outer Race Surface Texture and Groove Radius	105
40	Ball Bearing S/N 003 Thrust Inner Race Surface Texture and Groove Radius	107
41	Ball Bearing S/N 006 Outer Race Surface Texture and Groove Radius	109
42	Ball Bearing S/N 006 Thrust Inner Race Surface Texture and Groove Radius	111
43	Roller Retainer Rework PSK 17478	115
44	Roller Bearing Outer Ring Roundness and Concentricity	117
45	Roller Bearing Inner Ring Roundness and Concentricity	118
46	Roller Bearing Outer Race Surface Finish	119
47	Roller Bearing Inner Race Surface Finish	120
48	Instrumentation Location	122

<u>Figure</u>		<u>Page</u>
49	Ball Bearing Retainer Strain-Gage Location and Rework	124
50	Hall Generators Installed in Ball Bearing Retainer Pockets	127
51	Ball Bearing Magnetic Field Mapping	128
52	Slip Ring and Driving Plate	130
53	Typical Multiplexer Outputs	132
54	Build No. 2 Bearing Failure; Shaft Unbalance. . .	133
55	Build No. 2 Bearing Failure; Insufficient Pocket Clearance	135
56	Improved and Original Retainer to Driving Ring Strain-Gage Lead Paths	136
57-64	Retainer Web Force and Retainer Speed Versus Time, Showing Nature of Impact Loads.	142-149
65-72	Retainer Web Force Expanded With Computed Web Force Superimposed	150-157
73-74	Harmonic Analysis of Experimentally Determined Retainer Web Force (Average of 16 Spectra) for Ball Bearing Smooth Race	159-160
75	Harmonic Analysis of Computed Retainer Web Force for Ball Bearing Smooth Race.	161
76-79	Retainer Web Filtered and Unfiltered Retainer Force Wave Form With Computed Forces Superimposed	162-165
80	Retainer Speed Ratio Versus Axial Thrust Load .	167

<u>Figure</u>		<u>Page</u>
31-82	Expanded Trace of Rough-Race Bearing Retainer Web Forces	169-170
83-86	Bearing Retainer Web Force and Speed Versus Time	172-175
87	Pocket Loading Versus Radial Load (Axial Load = 1000 Pounds)	178
88	Pocket Film Thickness Versus Pocket Load (Axial Load = 1000 Pounds, Radial Load = 500 Pounds)	179
89	Retainer Speed Versus Axial Load	181
90	Roller Bearing Program Data; Residual Cage Torque Versus Cage Slip (Inner Race Speed = 20,000 RPM)	186
91	Roller Bearing Program Data; Cage Slip Versus Radial Load (Inner Race Speed = 20,000 RPM)	187

LIST OF TABLES

<u>Table</u>		<u>Page</u>
I	Stability Map - FRCTN Subroutine.	60
II	Stability Map - Analytical Function From FRCTN Subroutine.	60
III	Stability Map - $f = C_1 G_1^{1/4}$	61
IV	Stability Map - $f = C_1 G_1^{1/2}$	61
V	Physical Properties of MIL-L-23699 Oil, Code 0-64-2	90
VI	Test Ball Bearing Inspection Data, Detail Internal Geometry	99
VII	Roller Bearing Engineering Data	113
VIII	Ball Bearing Test Conditions	137
IX	Roller Bearing Test Conditions.	138
X	Summary of Test Results, Build No. 2	141
XI	Inner and Outer Race Temperatures, Build No. 3	168
XII	Inner and Outer Race Temperatures, Build No. 4	171
XIII	Bearing Problem Parameters.	177
XIV	Ball Kinematics; Inner Ring Speed = 20,000 RPM, Radial Load = 0	183
XV	Roller Bearing Problem Parameters	185

LIST OF SYMBOLS

A	area of cage guiding surface, in. ²
A_1	axial distance between inner and outer race curvature centers, in.
A_2	radial distance between inner and outer race curvature centers, in.
A_3	drag area on rolling elements, in. ²
A_i	drag area on races, in. ²
$A_{Y, Z}$	pilot surface load parameters for Y and Z directions, lb
a_i	semimajor axis of contact ellipse, in.
b	semiwidth of roller contact, in.
b_i	semiminor axis of pressure ellipse, in.
\bar{C}	radial clearance of rolling element in retainer pocket, in.
C_D	drag coefficient
C_f	friction factor for flow between race and retainer
C_i	$C_1 = 1.0, C_2 = -1.0$
D_1	outside diameter of retainer or pilot surface, in.
D_2	inside diameter of retainer or pilot surface, in.
D'	retainer pilot diameter, in.
D_{C_1}	outside diameter of cage, in.
D_{C_2}	inside diameter of cage, in.
d	rolling element diameter, in.

E	pitch diameter, in.
$E(\epsilon_j)$	complete elliptical integral of the second kind
E_R, E	Young's modulus for bearing rings (R) and rolling elements (E), lb/in. ²
E'	instantaneous pitch diameter of ball, in.
E''	materials parameter in Dowson and Higginson equation, lb/in. ²
F	reaction of bearing, in.
\bar{F}	external radial load, lb
F_1, F_2	hydrodynamic forces in retainer pocket, lb
F_C	rolling element centrifugal force, lb
\bar{F}_C	centrifugal force on cage, lb
F_D	viscous drag force on rolling element, lb
F_F	retainer pilot surface Coulomb drag force, lb
F_P	normal force in roller/pocket contact, lb
F_{P_i}	total load of roller against retainer pocket, lb
F_{P_x}	friction force generated at retainer contact in pocket in X direction, lb
F_{P_z}	friction force generated at ball retainer contact in ball pocket in Z direction, lb
F_R	net viscous drag force on retainer, lb
F_T	tractive force in roller/race contact, lb
F_V	tangential force in roller/pocket contact, lb
F_X	bearing reaction force in X direction, lb

F_{X_i}	friction force directed along major axis (X) of pressure ellipse, lb
F_Y	bearing reaction force in Y direction, lb
F_{Y_i}	friction force directed along minor axis (Y) of pressure ellipse, lb
F_Z	bearing reaction force in Z direction, lb
F'_{p_x}	load per unit length of roller against retainer pocket, lb/in.
F'_Z	total tractive force between roller and retainer pocket, lb
$F'_Z{}_y$	tractive force per unit length between roller and retainer pocket, lb/in.
\bar{F}_V	roller bearing externally applied radial load in the Z direction, lb
\tilde{F}_i	dimensionless tractive forces
f	friction factor/coefficient - rolling element to race contacts
f_i	race curvature - groove radius divided by ball diameter
f_r	coefficient of sliding friction for pilot surface
G_1	shear rate parameter
G_2	thermal heating parameter
G_3	pressure-viscosity parameter
H	horizontal component of pilot surface load (P_c), lb
H_j	spacing between retainer and race, in.
h	elastohydrodynamic film thickness, in.
h_0	minimum elastohydrodynamic film thickness, in.

h_p	film thickness of midpoint of roller to cage contact, in.
h_{p_x}	film thickness at any point X along roller to cage contact, in.
\tilde{h}	dimensionless film thickness
I	mass moment of inertia of rolling element, in.-sec ² -lb
i	$i = 1$ for outer race contact; $i = 2$ for inner race contact
K	coefficient of friction for retainer-rolling element contacts
$K(\epsilon_1)$	complete elliptical integral of the first kind
K_c	Coulomb friction coefficient for roller-retainer contact
K_f	thermal conductivity of the lubricant, Btu/ ^o F-hr-ft
K'_f	constant = 0.5482
K'_w	constant = 2.447
l_F	flat length of roller, in.
l_T	total length of roller less two corner radii, in.
l'	distance from roller dim point to contact pattern end, in.
M_c	total torque on retainer, lb-in.
m	mass of rolling element, lb-sec ² /in.
m_c	mass of cage, lb-sec ² /in.
$\mu_{R, E}$	Poisson's ratio for bearing rings (R) and rolling element (E)
M_V	viscous drag between rings and retainer, lb-in.
M_Y	inertial moment of ball about Y axis, lb-in.
M_Z	inertial moment of ball about Z axis, lb-in.
M'_Y	bearing reactive moment about Y axis, lb

n	number of rolling elements
P	race contact force, lb
P_c	retainer pilot surface to guiding race land load, lb
P_{c_r}	normal pilot contact force if \bar{F}_c is absent, lb
P_D	diametral clearance of bearing, in.
P_{HZ}	Hertz pressure, lb/in. ²
P_i	race contact normal loads, lb
P_{ix}	load per unit length of contact at X along roller contact, lb/in.
P_p	normal contact load between ball and retainer in pocket, lb
\tilde{P}	dimensionless load per unit length
p	pressure, lb/in. ²
p_x	roller loading, lb-in.
\tilde{p}	dimensionless pressure
Q_p	spin torque at ball to retainer pocket contact, lb-in.
Q_{s_i}	spin torque at race contact, lb-in.
Q_v	viscous drag torque on cage, lb-in.
\bar{Q}	torque unbalance on cage, lb-in.
q	roller azimuth index
R	equivalent radius of contact against a plane surface, in.
R_c	roller crown radius, in.

R_E	radius of rolling element, in.
R_R	radius of race surface, in. /sec
Re	Reynolds number
r	corner radius of roller, in.
r_r	roller radius, in.
S_m	maximum Hertz stress, psi
S_R, S_B	RMS surface roughness parameters
T_i	inlet lubricant temperature, $^{\circ}F$
T_o	temperature of lubricant, $^{\circ}F$
t_r	thickness of retainer, in.
U	velocity term in Dowson and Higginson equation, in. /sec
U_i	sliding velocity of ring on cage, in. /sec
U_R	linear velocity of roller, in. /sec
U_y	linear velocity of race, in. /sec
u_s	sliding speed at rolling element to race contact, in. /sec
u_x, u_y	rolling element to retainer sliding velocities, in. /sec
V	vertical component of pilot surface load (P_c), lb
V_{Bi}	linear velocity in the Y direction at a strip on a ball, in. /sec
V_E	surface velocity of roller, in. /sec
V_o	orbital velocity of rolling element, rad/sec
V_{Ri}	linear velocity in the Y direction at a strip on the race, in. /sec

V_{XR_i}	linear velocity on a strip on the race in the X direction, in. /sec
V_{YB_i}	linear velocity of the ball in the Y direction at the center of the contact area, in. /sec
V_{XB_i}	linear velocity on a strip on the ball in the X direction, in. /sec
V_{y_i}	surface velocity of ring relative to retainer, in. /sec
V_{XB_i}	linear velocity on a strip on the ball in the X direction, in. /sec
V_{YR_i}	linear velocity of a raceway in the Y direction at the center of the contact area, in. /sec
W	normal pocket load = P_p , lb
w	load per unit width of contact, lb/in.
\tilde{W}	dimensionless load
W'_i	total axial effective contact length between retainer and ring, in.
X_1	ball center (axial) coordinate relative to outer race center of curvature, in.
X_2	ball center (radial) coordinate relative to outer race center of curvature, in.
y^*	semistrip width, in.
Z	radial clearances at cage outside and inside diameter
α_o	pressure coefficient of viscosity, in. ² /lb
β_1^*	temperature viscosity coefficient used by Crook, °F
β_i	race contact angle, deg
γ_j	geometric parameter = $d/\cos \beta_i/E'$
Δ	total approach of inner and outer rings, in.

Δ_0	total compression at roller to race contact, in.
Δ_i	approach of ball to race at the i^{th} contact, in.
Δ_{ix}	approach of roller to race at X along roller contact, in.
δ	total approach of inner to outer race, in.
Δ_q	total compression of roller, in.
δ_0	maximum compressive stress in contact area, Hertz stress
δ_x	inner ring displacement in X direction, in.
δ_y	inner ring displacement in Y direction, in.
δ_z	inner ring displacement in Z direction, in.
ϵ_i	modular angle of a pressure ellipse, rad
ξ, η	dimensionless coordinates
σ	angular position of pilot surface load line, rad
μ	lubricant viscosity, lb-sec/in. ²
μ_0	lubricant viscosity in inlet region of elastohydrodynamic contacts, lb-sec/in. ²
ρ	mass density of lubricant, lb-sec ² /in. ⁴
τ	shear stress, lb/in. ²
$\tilde{\tau}$	dimensionless shear stresses
τ_i	Hertz auxiliary parameter
τ_y	shear stress in lubricant film in Y direction, lb/in. ²
ω	rolling element azimuth angle measured clockwise, deg

ω_i	angular velocity of the i^{th} ring relative to the retainer, rad/sec
ω_{s_i}	spin velocity component at race contact, rad/sec
ω_x	rolling element angular velocity about X axis, rad/sec
ω_y	rolling element angular velocity about Y axis, rad/sec
ω_z	rolling element angular velocity about Z axis, rad/sec
$\dot{\omega}_x$	angular acceleration of rolling element about X axis, rad/sec ²
Ω_1	angular velocity of ball about X axis = ω_x rad/sec
Ω_2	angular velocity of ball about Z axis = ω_z rad/sec
Ω_E	retainer (cage) speed, rpm
Ω_i	absolute angular velocity of the bearing rings, rad/sec
e	elastic constants, in. ² /lb

INTRODUCTION

The analysis of rolling element bearing systems, which had earlier been prohibitive for manual calculation, has been facilitated by the advent of digital computers. Bearing systems present highly redundant, nonlinear mathematical models for which closed-form solutions are not available. Solutions must be obtained by numerical iterative techniques.

During the past ten years, many computer programs for bearing analysis have been created to meet the varying needs of industry. The best known is a five-degree-of-freedom program derived and written by A. B. Jones.² This program forms the basis of most of the computer work accomplished in the bearing analysis field, and is extensively used throughout the aerospace industry for the design and analysis of high-speed rolling element bearings.

The program uses Newton-Raphson iterative techniques to solve for equilibrium of the individual bearings and the entire bearing system simultaneously under the action of applied external loads while considering high-speed effects. Solutions are arrived at by systematically varying the shaft deflections until the integrated reaction forces of the rolling elements against the races balance the applied forces.

This analysis for ball bearings, however, does not consider the forces acting among the retainer, the rolling elements, and the piloting surfaces of the bearings, nor does it account for the tractive forces generated at the race contact areas. Bearing kinematics are established by constraining the balls' angular velocity vector to lie in a radial plane, i. e., no ball rotation about the axis dictated by the ball gyroscopic moment. Also, the analysis is subject to the race control hypothesis, which dictates that the ball will roll without spin at the race contact (inner or outer) that offers the greatest resistance to spinning. High-speed bearings with relatively large centrifugal ball loads against the outer race would, therefore, be predominantly outer race controlled. The significance of outer and inner race control is shown geometrically in Figure 1.

A race control assumption was imposed in the previous analysis because a ball in angular contact cannot exhibit pure rolling at both inner and outer race contacts simultaneously. Therefore, the ball must have a

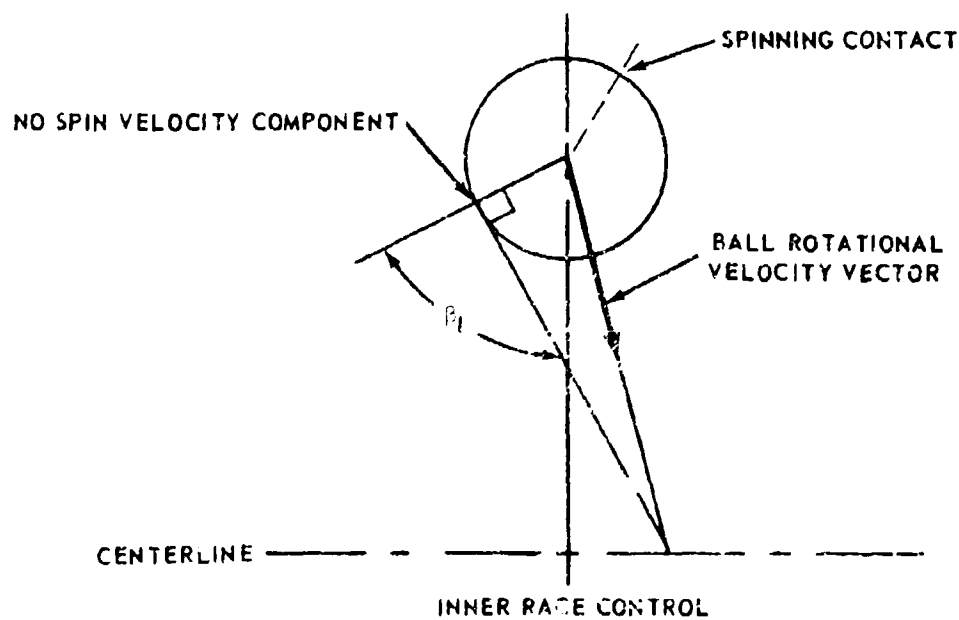
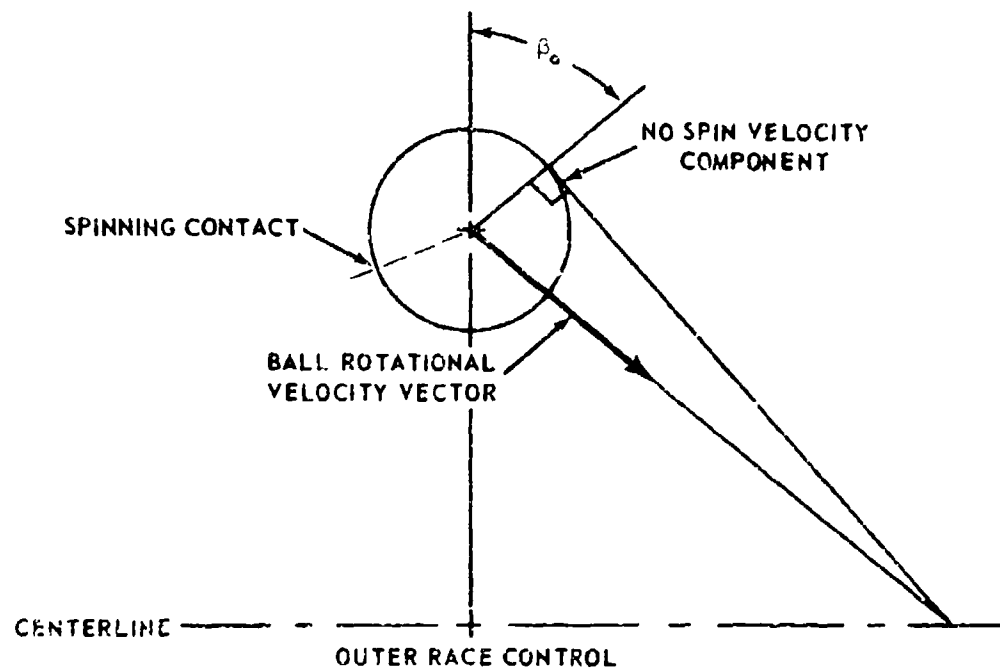


Figure 1. Race Control Concept.

spin velocity component at one or both race contacts which is equivalent to a twisting of the race body with respect to the ball about the normal to the center of the pressure area. Outer race control is considered to be advantageous for high-speed bearings because it results in minimum ball gyroscopic moments and maximum stability. It does have the disadvantage of placing the spin velocity component at the inner race with attendant heat generation, where oil cooling is most difficult.

Also implicit in the analysis is the concept that all friction resistance to the gyroscopic moment is generated at the controlling race and that tractive slip does not occur at any of the race contacts, which, of course, results in analytical solutions predicated upon zero retainer slip. The roller bearing analysis used is, in general, subject to the same limitations as those described for the ball bearing with the obvious exception of the race control and gyroscopic considerations, which are not applicable to rollers.

Recent work conducted by Harris,⁵ Poplawski and Mauriello,⁹ Boness,³ and others has indicated that some of the assumptions discussed above and incorporated within the basic Jones analysis are only approximately valid. Specifically:

1. The ball angular velocity vector in an angular contact ball bearing does not lie exclusively in a radial plane. There is an angular velocity component in the circumferential direction.
2. The raceway control hypothesis is not applicable to all modes of bearing operation.
3. Tractive slip does occur at the rolling element-to-race contacts with attendant retainer slippage.
4. Resistance to the ball gyroscopic moment is not confined exclusively to the controlling race.

Some of these weaknesses have been resolved by various analysts in special computer models treating individual bearings. However, some fundamental problem areas have yet to be addressed, most notably the thermal effects due to contact area slip upon the tractions generated in an EHD (elastohydrodynamic) contact. This effect is of the utmost importance

in that the contact area traction is the key element in the establishment of the ball kinematics and thereby the entire solution.

The task undertaken as reported herein was to derive a new mathematical model for ball and roller bearings that is general and is not subject to the assumptions and restrictions described above. This undertaking required a reformulation of the existing Jones analytical model to include the following salient points:

1. EHD tractive forces and moments in the contact areas accounting for the thermal effects accompanying sliding
2. EHD film thickness accounting for spin as well as rolling velocities in the contact areas
3. Ball angular velocity in three degrees of freedom
4. Traction and normal loads acting at the rolling element-to-retainer contacts
5. Viscous forces acting among the retainer inside diameter, outside diameter, and their respective bearing race surfaces
6. Rolling element viscous drag forces
7. Equilibrium of the retainer assembly to be established to predict retainer speed deviation from the theoretical epicyclic value.

Rig testing was conducted to verify and modify the theoretical analysis. The test program included the modification of a test rig and the design of special instrumentation to obtain the required verification data. Tests were run on a 100-millimeter ball bearing at speeds up to 20,000 rpm with axial and radial loads up to 1,000 pounds.

MATHEMATICAL ANALYSIS

BALL BEARING MATHEMATICAL MODEL

A complete presentation of the mathematical model developed for the ball bearing solution is presented in this section. The approach taken is an extension of the analysis related in Reference 2 to include retainer loads and lubrication considerations. The numerical procedure that has been employed is composed of essentially two major iterative loops, one within the other. Each loop has specific criteria which must be satisfied to obtain the desired solution. The innermost loop of the analysis deals with individual ball equilibrium which is achieved when Equations (26) through (30) are simultaneously satisfied. These equations represent force equilibrium in the X and Z directions, and moment equilibrium about the X, Y, and Z axes, respectively. The second loop of the analysis establishes equilibrium of the bearing rings with respect to externally applied loads. These criteria are achieved when Equations (34) through (37) are satisfied. These equations represent force equilibrium on the bearing races in the X, Y, and Z directions and moment equilibrium about the Y axis, respectively. A second function of this loop establishes retainer torque balance by iterating upon retainer speed accounting for ball-to-race tractive forces, ball-to-retainer loads, viscous drag between retainer and ring surfaces, and ball drag. In this manner, the retainer speed is established and its deviation from the theoretical epicyclic value can be determined. These considerations are expressed in Equations (46) through (49), which deal with force equilibrium in the X, Y, and Z directions and moment equilibrium about the X axis.

The balls in a high speed ball bearing operating under other than a centric thrust load do not orbit at uniform speed if unrestrained by the cage. Consequently, they move fore and aft within the clearance of the pockets, and at times they may be in contact with the fore or aft wall of the retainer pocket.

When a ball is in contact with either the fore or aft wall of the pocket, its orbital speed is that of the cage and is generally different from its unconstrained orbital speed. Slippage between ball and race, always present to some degree, is greatly altered in form and intensity at this time. Also, frictional forces of the ball in the pocket are significantly increased.

At the instant a ball contacts a pocket wall, an impact force is produced. This force may be the maximum force exerted on the pocket when speeds are high and bearing loadings are light. As loading intensity is increased, the impact severity changes little, whereas the slippage-dependent forces increase greatly.

The mathematical model for this study neglects the impact forces and constrains the ball to orbit at the constant speed of the cage. Also, the fore and aft clearance in the pocket is zero to ensure the worst possible case of cage loading, neglecting impact forces; i. e., all balls are in contact with their pockets at all times. For purposes of assessing the properties of the film between ball and pocket, the true clearance is employed.

The ball referred to an XYZ coordinate system is shown in Figure 2. The X axis is parallel to the axis of the bearing and rotates about the latter with the angular cage (retainer) velocity Ω_E .

In the following, the subscript 1 refers to the outer ring or outer-ring contact. The subscript 2 refers to the inner ring or inner-ring contact.

$$\left. \begin{array}{l} C_1 = 1 \\ C_2 = -1 \end{array} \right\} \quad (1)$$

ω_i is the angular velocity of the i^{th} ring relative to the cage and is related to the absolute angular velocity Ω_i of the ring and the cage velocity Ω_E .

$$\omega_i = \Omega_i - \Omega_E \quad (2)$$

$i = 1$ for outer ring

$i = 2$ for inner ring

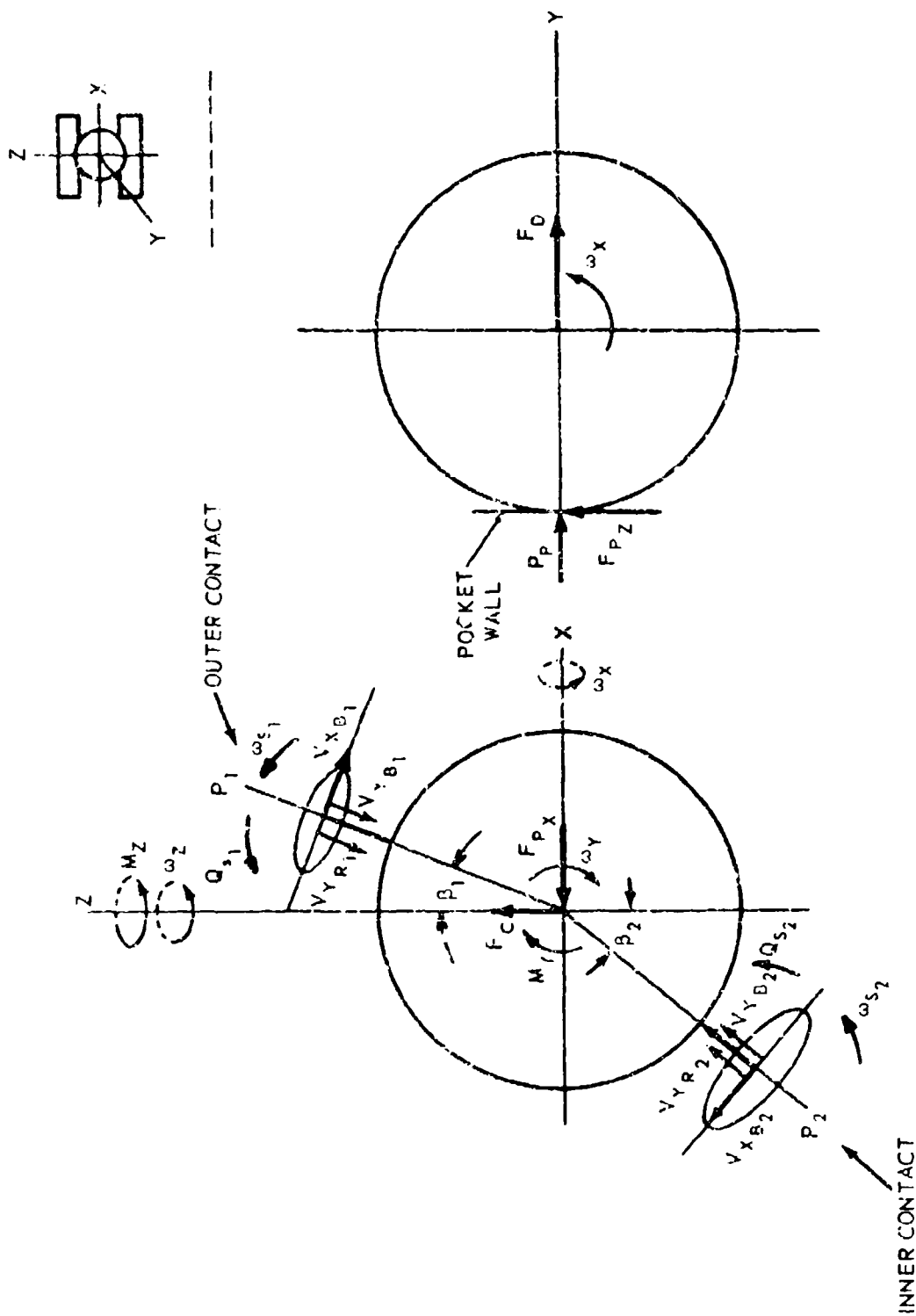


Figure 2. Ball Referred to XYZ Coordinate System.

ω_X , ω_Y , and ω_Z are the angular velocities of the ball about X, Y, and Z.

F_C is the centrifugal force, and M_Y and M_Z are the inertial moments about Y and Z.

$$M_Y = I \omega_Z \Omega_E \quad (3)$$

$$M_Z = -I \omega_Y \Omega_E \quad (4)$$

$$F_C = m \frac{E'}{2} \Omega_E^2 \quad (5)$$

I is the mass moment of inertia of the ball about its center, and m is the mass of the ball. E' is the instantaneous pitch diameter.

P_i is the contact force, and a_i and b_i are the semimajor and semiminor axes of the pressure ellipse.

V_{YR_i} is the linear velocity of a raceway in the Y direction at the center of a pressure area.

$$V_{YR_i} = \frac{(\Omega_i - \Omega_E) (E' + c_i d \cos \beta_i)}{2} \quad (6)$$

V_{YB_i} is the linear velocity of the ball at the i^{th} contact in the Y direction.

$$V_{YB_i} = \frac{c_i d}{2} (\omega_X \cos \beta_i - \omega_Z \sin \beta_i) \quad (7)$$

β_i is the operating contact angle at the i^{th} contact.

V_{XB_i} is the velocity of slip of race on ball in the X direction.

$$V_{XB_i} = -\frac{d}{2} \omega_Y \quad (8)$$

ω_{S_i} is the angular velocity of spin of the i^{th} race with respect to the ball and is

$$\omega_{S_i} = C_i \left[(\Omega_i - \Omega_E - \omega_X) \sin \beta_i - \omega_Z \cos \beta_i \right] \quad (9)$$

F_{X_i} and F_{Y_i} are friction forces directed along the major and minor axes of the pressure ellipse. Q_{S_i} is a friction moment about the normal at the center of the ellipse. These items are the result of sliding between the race and ball, which are separated by an EHD film. Their values and the values of their derivatives are calculated in a subroutine, BALFTJ. *

Input to subroutine BALFTJ¹¹ consists of:

- **1. Pressure-viscosity coefficient of the lubricant - in.²/lb
- **2. Temperature-viscosity coefficient of the lubricant - /°F
- 3. Viscosity of the lubricant at inlet temperature - lb-sec/in.²
- **4. Thermal conductivity of the lubricant - Btu/°F-hr-ft
- 5. Inlet temperature - °F
- 6. Young's modulus for ball and for race - lb/in.²
- 7. Poisson's ratio for ball and race
- 8. Dimensions a_i and b_i of the pressure area - in.
- 9. Load on the contact P_i - lb
- 10. Linear velocity of the race VY_{R_i} - in./sec
- 11. Linear velocity of the ball VY_{B_i} - in./sec
- 12. Velocity of slip of race on ball in the direction of the major axes VX_{B_i} - in./sec
- 13. Angular velocity of spin ω_{S_i} - rad/sec

* Discussed under "Elastohydrodynamic Traction Coefficients"

**Values can be obtained from Appendix VII.

14. Ball diameter d - in.
15. Race groove radius $f_1 d$ - in.
16. Pitch diameter E' - in.
17. Cosine of the contact angle $\cos \beta_i$
18. Value of C_i
19. Incrementing factor for V_{YB_i}
20. Incrementing factor for V_{XB_i}
21. Incrementing factor for ω_{S_i}
22. Incrementing factor for P_i

BALFTJ returns FX_i , FY_i , and QS_i and their derivatives with respect to VX_i 's, VY_i 's, ω_{S_i} 's, and P_i 's. It also returns minimum film thickness h_o .

P_P is the normal force of retainer on ball.

$$P_P = F_{Y_1} + F_{Y_2} - F_D \quad (10)$$

F_D is a viscous drag force. *

P_i is the contact force and is the result of the elastic approach Δ_i of ball and race body.

Figure 3 shows the initial and final positions of the inner and outer race curvature centers. β is the initial contact angle and f_1 the race curvature factor.

From Figure 3,

$$\Delta_1 = \left[X_1^2 + X_2^2 \right]^{1/2} - (f_1 - .5) d \quad (11)$$

$$\Delta_2 = \left[(A_1 - X_1)^2 + (A_2 - X_2)^2 \right]^{1/2} - (f_2 - .5) d \quad (12)$$

A_1 and A_2 are defined analytically in Equations (31) and (32).

*Calculated as described under "Analysis of Shear Forces on a Lubricated, High-Speed Bearing Retainer,"

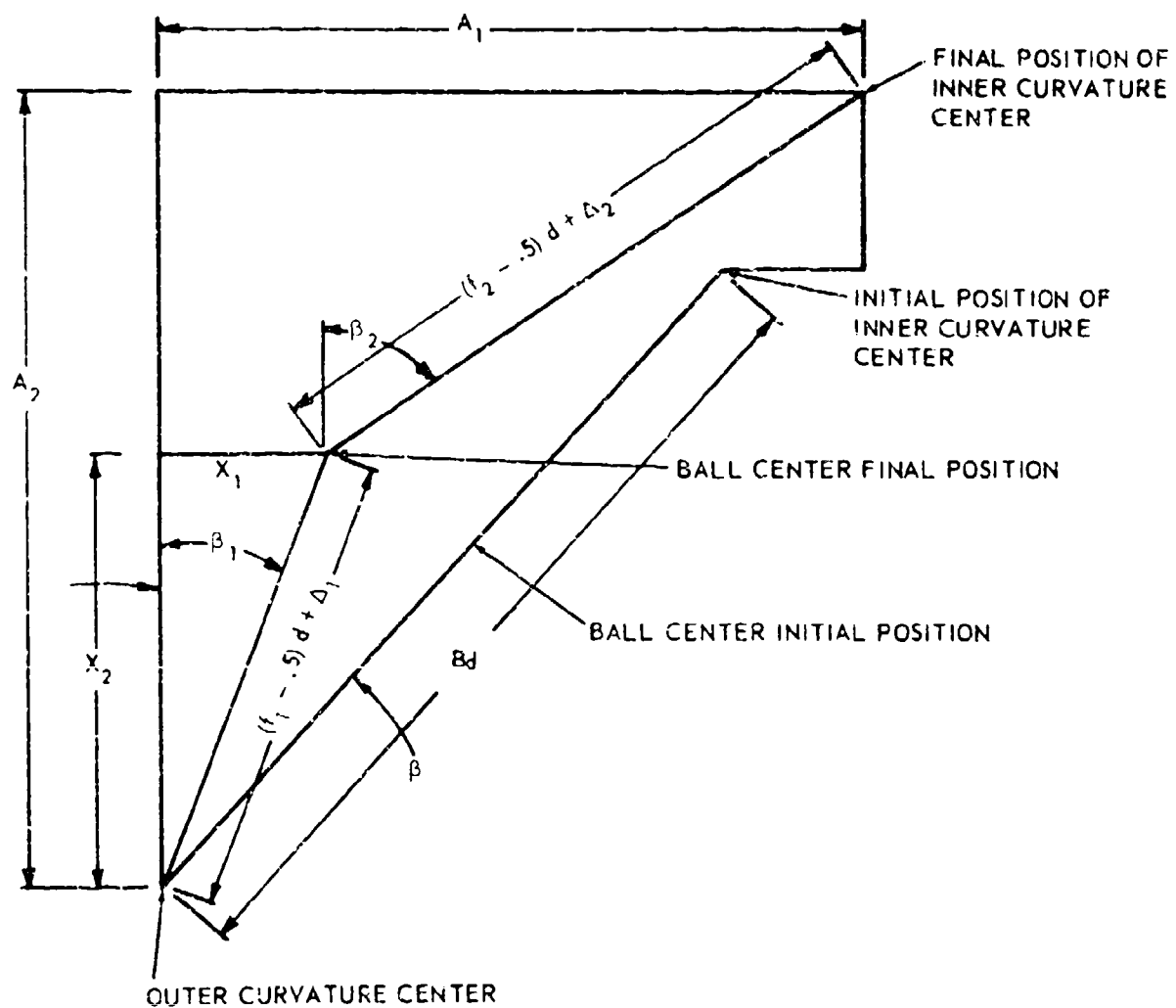


Figure 3. Initial and Final Positions of Inner and Outer Race Curvature Centers.

$$\tan \beta_1 = \frac{X_1}{X_2} \quad (13)$$

$$\tan \beta_2 = \frac{A_1 - X_1}{A_2 - X_2} \quad (14)$$

$$E' = E + 2 \left[X_2 - (f_1 - .5) d \cos \beta \right] \quad (15)$$

The dimensions of the pressure area are found as follows:

ϵ_i is the modular angle of the ellipse.

$$\epsilon_i = \sin^{-1} \left[1 - \left(\frac{b_i}{a_i} \right)^2 \right]^{1/2} \quad (16)$$

It is related to the geometries of the bodies in the neighborhood of the contact by an auxiliary parameter τ_i .

$$\cos \tau_i = \frac{\frac{1}{f_i} - \frac{2C_i \gamma_i}{1 + C_i \gamma_i}}{4 - \frac{1}{f_i} - \frac{2C_i \gamma_i}{1 + C_i \gamma_i}} \quad (17)$$

where

$$\gamma_i = \frac{d \cos \beta_i}{E'} \quad (18)$$

ϵ_i and τ_i are related by

$$\cot^2 \epsilon = \frac{(1 - \cos \tau_i) E(\epsilon_i)}{2[K(\epsilon_i) - E(\epsilon_i)]} \quad (19)$$

$K(\epsilon_i)$ and $E(\epsilon_i)$ are the complete elliptic integrals of the first and second kind having the modular angle ϵ_i .

The semiminor axis of the pressure area is

$$b_i = \left[\frac{3(\vartheta_R + \vartheta_E) E(\epsilon_i) P_i d \cos \epsilon_i}{4\pi \left(4 - \frac{1}{f_i} - \frac{2C_i \tau_i}{1 + C_i \tau_i} \right)} \right]^{1/3} \quad (20)$$

and the semimajor axis is

$$a_i = \frac{b_i}{\cos \epsilon_i} \quad (21)$$

ϑ_R and ϑ_E are elastic constants for race and ball, respectively.

$$\vartheta_R = \frac{4(1 - m_R^2)}{E_R} \quad (22)$$

$$\vartheta_E = \frac{4(1 - m_E^2)}{E_E} \quad (23)$$

The symbols m_R and m_E are Poisson's ratio for race and ball. E_R and E_E are Young's modulus for race and ball.

The relation between contact force and elastic deflection is nonlinear.

$$\Delta_i = \frac{3 P_i (\vartheta_R + \vartheta_E) K(\epsilon_i)}{8 \pi \sigma} \quad (24)$$

The maximum normal pressure occurs at the center of the pressure area and is

$$\delta_{o_i} = \frac{3 P_i}{2 \pi \sigma_i b_i} \quad (25)$$

The equilibrium of the ball requires that

$$-P_1 \sin \beta_1 + P_2 \sin \beta_2 + F_{X_1} \cos \beta_1 - F_{X_2} \cos \beta_2 - F_{P_X} = 0 \quad (26)$$

$$-P_1 \cos \beta_1 + P_2 \cos \beta_2 - F_{X_1} \sin \beta_1 + F_{X_2} \sin \beta_2 + F_C + F_{P_Z} = 0 \quad (27)$$

$$(F_{Y_1} \cos \beta_1 - F_{Y_2} \cos \beta_2 - F_{P_Z}) \frac{d}{2} + Q_{S_1} \sin \beta_1 - Q_{S_2} \sin \beta_2 = 0 \quad (28)$$

$$(F_{X_1} + F_{X_2}) \frac{d}{2} + M_Y - Q_P = 0 \quad (29)$$

$$\begin{aligned} (-F_{Y_1} \sin \beta_1 + F_{Y_2} \sin \beta_2 - F_{P_X}) \frac{d}{2} + Q_{S_1} \cos \beta_1 \\ - Q_{S_2} \cos \beta_2 + M_Z = 0 \end{aligned} \quad (30)$$

F_{P_X} and F_{P_Z} are pocket frictional forces.*

The variables in the above set of equations are X_1 and X_2 and the angular velocities ω_X , ω_Y , and ω_Z . The equations are solved numerically.

Figure 4 shows the bearing referred to an XYZ coordinate system. The outer ring is fixed while the inner ring can move. The inner ring can have three linear displacements, δX , δY , and δZ , relative to the outer ring and is constrained from rotations about Y and Z.

The YZ plane in Figure 4 contains the locus of the inner race curvature centers.

For arbitrary values of the three displacements, there will be the reactions F_X , F_Z , and M_Y , which act in the directions shown in Figure 4.

* Calculated as described under "Analysis of Shear Forces on a Lubricated, High-Speed Bearing Retainer."

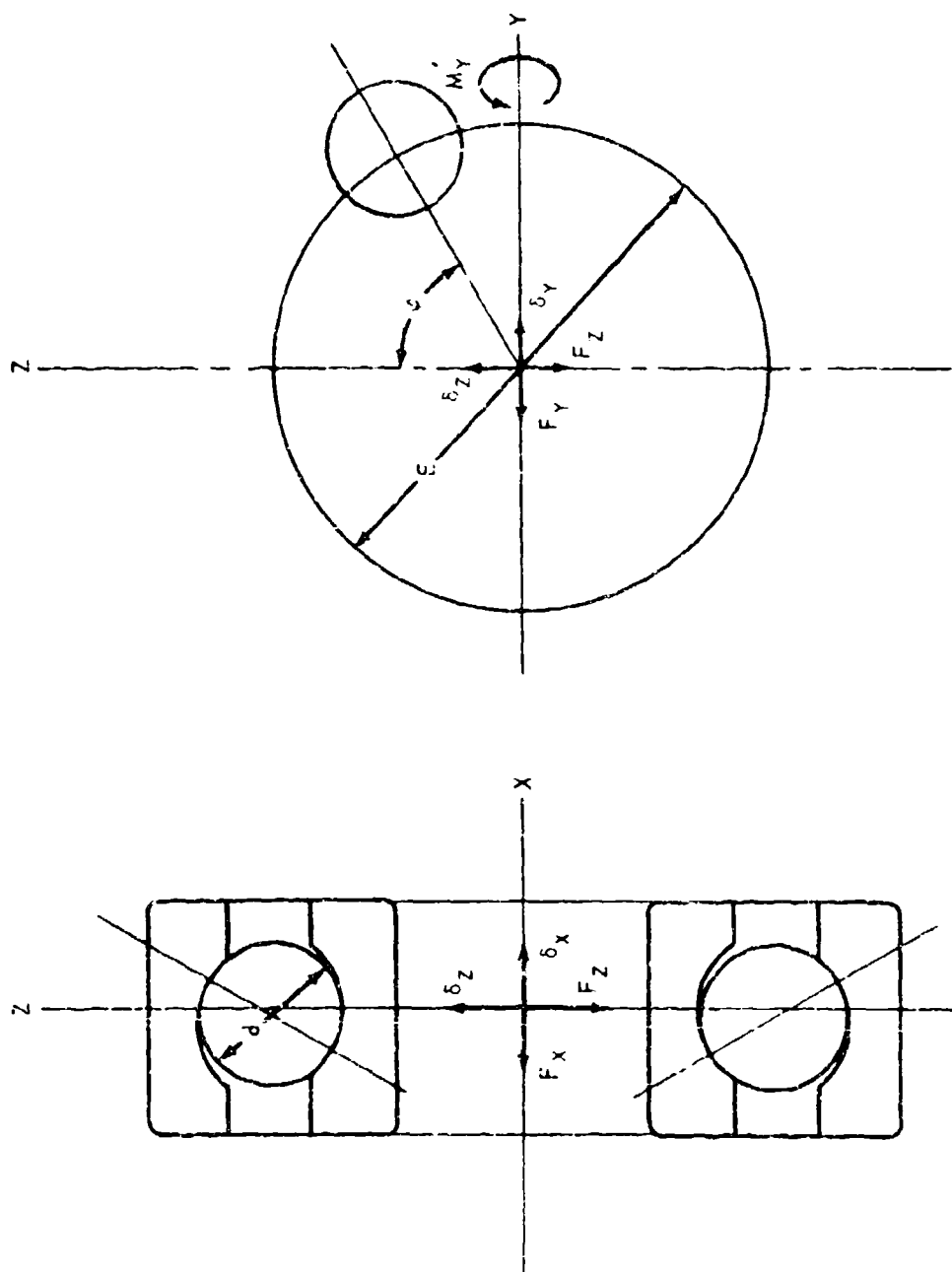


Figure 4. Bearing Referred to XYZ Coordinate System.

The values of A_1 and A_2 in Equation (14) depend on the displacements at the inner ring center.

$$A_1 = Bd \sin \beta + \delta_x \quad (31)$$

$$A_2 = Bd \cos \beta + \delta_y \sin \varphi + \delta_z \cos \varphi \quad (32)$$

$$B = f_1 + f_2 - 1 \quad (33)$$

φ is the ball azimuth measured clockwise from the YZ plane as viewed from +X.

The bearing reactions are:

$$F_x = \sum_{j=1}^n \left[P_{2j} \sin \beta_{2j} - F_{x_{2j}} \cos \beta_{2j} \right] \quad (34)$$

$$F_y = \sum_{j=1}^n \left[\left(P_{2j} \cos \beta_{2j} + F_{x_{2j}} \sin \beta_{2j} \right) \sin \varphi_j - F_{y_{2j}} \cos \varphi_j \right] + A_y \quad (35)$$

$$F_z = \sum_{j=1}^n \left[\left(P_{2j} \cos \beta_{2j} + F_{x_{2j}} \sin \beta_{2j} \right) \cos \varphi_j + F_{y_{2j}} \sin \varphi_j \right] + A_z \quad (36)$$

$$M_y = \sum_{j=1}^n \left\{ \left[P_{2j} R \sin \beta_{2j} - F_{x_{2j}} \left(R \cos \beta_{2j} - f_{2j} d \right) \right] \cos \varphi_j + F_{y_{2j}} f_2 d \sin \beta_{2j} \sin \varphi_j \right\} \quad (37)$$

where n is the number of balls.

A_y and A_z are zero for an outer-piloted cage and are nonzero for inner-piloted cage; they are calculated as follows:

$$R = \frac{E}{2} + (f_2 - .5) d \cos \beta \quad (38)$$

M_Y^1 does not enter into the calculations but is an item of interest.

Figure 5 shows the forces and moments acting on an outer-piloted cage. Q_{V1} and Q_{V2} are viscous shear moments.* P_C is the reaction of the piloting ring against the cage. F_F is a Coulomb friction force between cage and guiding surface and acts at the angle θ .

$$P_C = [H^2 + V^2]^{1/2} \quad (39)$$

$$H = \sum_{j=1}^n [-P_{P_j} \cos \varphi_j - F_{P_{Z_j}} \sin \varphi_j] \quad (40)$$

$$V = \sum_{j=1}^n [-P_{P_j} \sin \varphi_j - F_{P_{Z_j}} \cos \varphi_j] \quad (41)$$

$$F_F = \mu P_C \quad (42)$$

$$\tan \theta = \frac{H}{V} \quad (43)$$

Figure 6 similarly illustrates an inner-piloted cage. Equations (37) through (41) apply here also.

With an inner-piloted cage, P_C and F_F are reactive on the inner ring, and A_Y and A_Z for use with Equations (35) and (36) are

$$A_Y = - P_C (\sin \theta - \mu \cos \theta) \quad (44)$$

$$A_Z = - P_C (\cos \theta + \mu \sin \theta) \quad (45)$$

* Calculated as described under "Analysis of Shear Forces on a Lubricated, High-Speed Bearing Retainer."

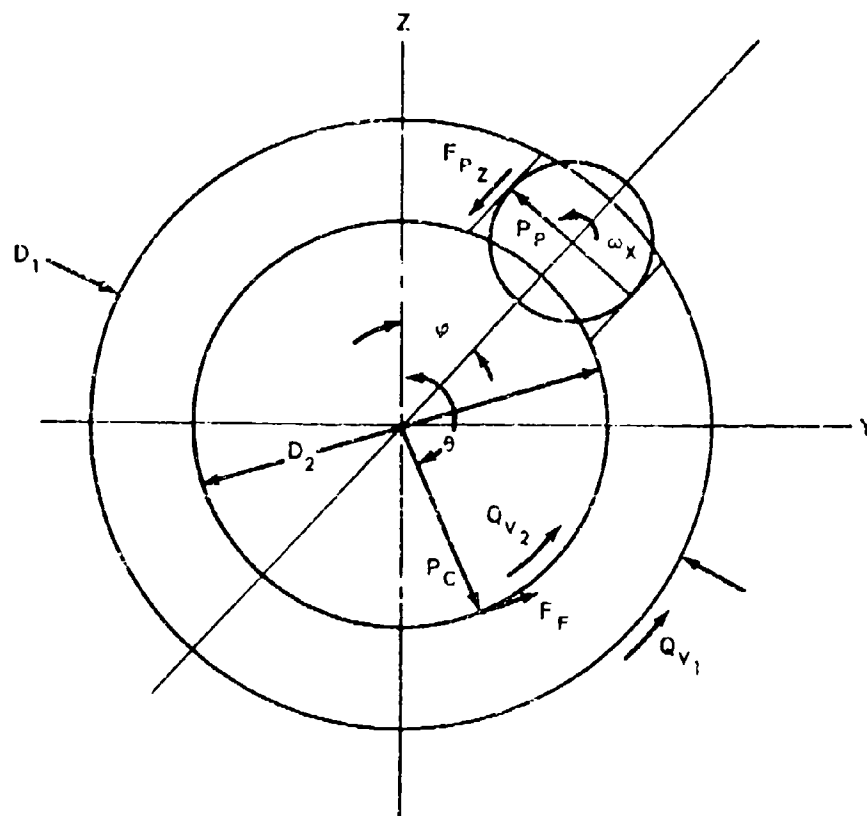


Figure 6. Forces and Moments Acting on Inner-Piloted Cage.

The requirements for equilibrium of the bearing and cage system may now be written:

$$F_X + \bar{F}_X = 0 \quad (46)$$

$$F_Y = 0 \quad (47)$$

$$F_Z + \bar{F}_Z = 0 \quad (48)$$

$$Q_{V_1} + Q_{V_2} + \frac{F_F D'}{2} + \frac{1}{2} \sum_{j=1}^n \left[P_{P_j} E' + F_{P_{Z_j}} d \right] = 0 \quad (49)$$

D' is D_1 for an outer-piloted cage and D_2 for an inner-piloted cage. \bar{F}_X and \bar{F}_Z are external thrust and radial loads.

Equations (46) through (49) are nonlinear in the variables δX , δY , δZ , and Ω_E . They are solved numerically by iterative procedures.

ROLLER BEARING MATHEMATICAL MODEL

The determination of the forces on the cage of a high-speed roller bearing requires the evaluation of the internal load distribution, the friction forces in the EHD films at the race contacts, and the friction and normal forces in the roller to cage pocket contacts.

The calculation of individual roller loads is made without consideration of friction forces in the race contact film or in the pocket contact film. This procedure is valid since the tangential friction force of the roller against the pocket is small compared to the load at an outer-race contact.

For an assumed value of roller orbital speed (cage speed) the internal load distribution is obtained as follows. A first assumption of orbital speed is made close to the theoretical value for no slip.

$$\Omega_E = \frac{1}{2} \left[\Omega_1 \left(1 + \frac{d}{E} \right) + \Omega_2 \left(1 - \frac{d}{E} \right) \right] \quad (1-S) \quad (50)$$

where Ω_E = cage speed

Ω_1 = outer ring speed

Ω_2 = inner ring speed

d = roller diameter

E = pitch diameter

S = a slip factor

A suggested value of S for the first pass is 0.001.

Figure 7 illustrates a typical radial roller bearing and shows the detail of the roller's profile.

Let Δ_0 be the approach of the roller to the race body measured at the midpoint of the roller's length. The approach is the same at all points of the cylindrical surface. The approach at a point on the crowned portion is less. At any location x along the roller's length, measured from the midpoint, the approach is

$$\Delta_x = \Delta_0 \quad -l_F \leq x \leq l_F \quad (51)$$

$$\Delta_x = \Delta_0 - \sqrt{R_c^2 - \frac{l_F^2}{2}} + \sqrt{R_c^2 - x^2} \quad \frac{l_F}{2} < |x| < \frac{l_T}{2} \quad (52)$$

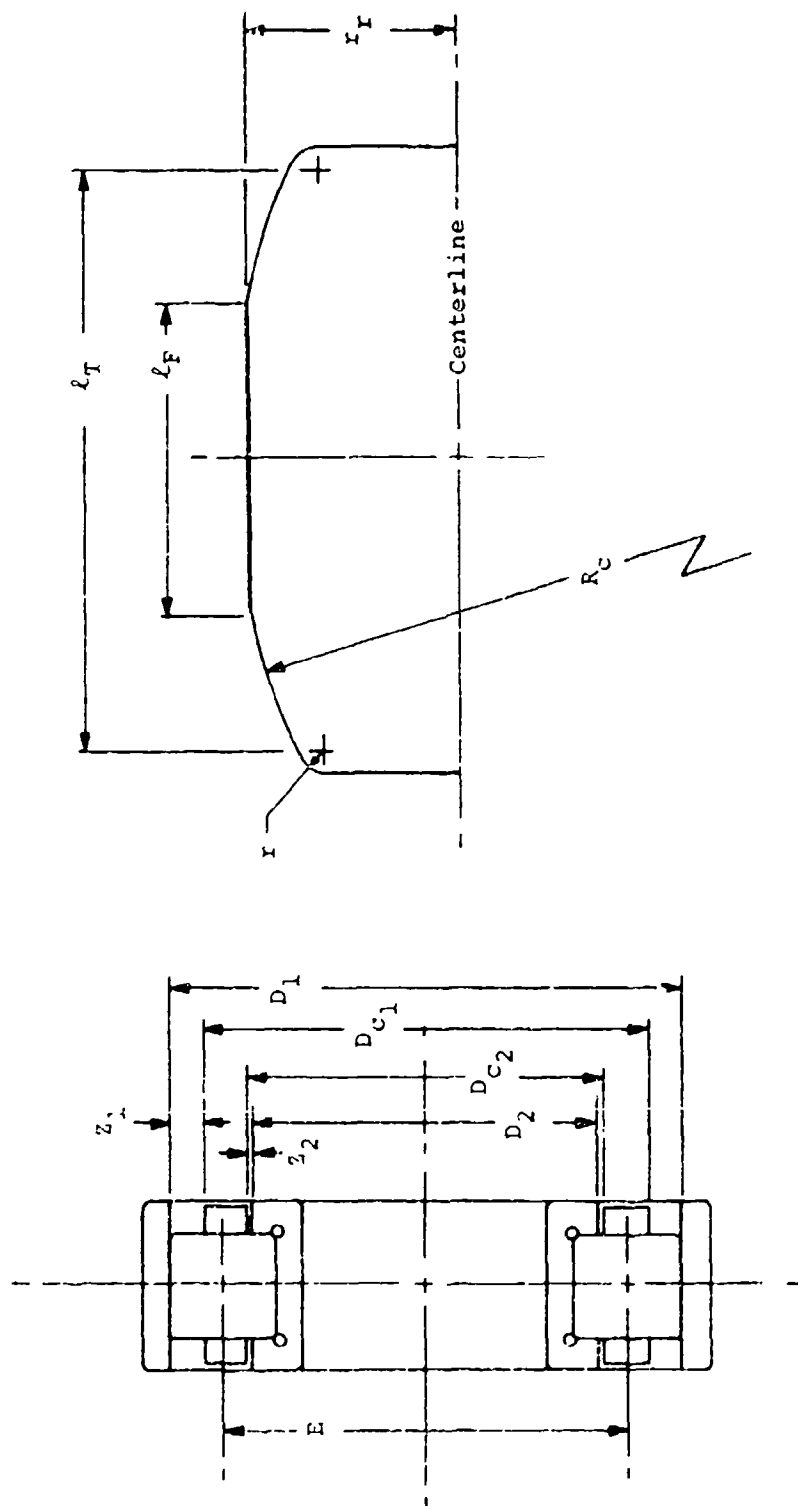


Figure 7. Bearing Details.

Lundberg, Reference 7, gives the relation between load and approach for a cylindrical roller of length l as

$$\Delta = \frac{(\nu_R + \nu_E) P}{2 \pi l} \left[1.8864 + \ln \left(\frac{l}{2b} \right) \right] \quad (53)$$

where $\left. \begin{matrix} \nu_R \\ \nu_E \end{matrix} \right\} =$ elastic constants for race and roller, respectively, and are of the form

$$\nu = \frac{4(1-m^2)}{E} \quad (54)$$

m = Poisson's ratio
 E = modulus of elasticity
 P = total force on the contact
 b = semiwidth of the contact area
 l = length of roller

Setting p_x as the lb/in. loading at point x , one may write

$$\Delta_x = \frac{(\nu_R + \nu_E)}{2 \pi} p_x \left[1.8864 + \ln \left(\frac{l}{2b_x} \right) \right] \quad (55)$$

b_x is given by

$$b_x = \left[\frac{(\nu_R + \nu_E) p_x d (1 \pm \frac{d}{E})}{2 \pi} \right]^{1/2} \quad (56)$$

The upper sign is used for an outer-race contact and the lower for an inner-race contact.

l' is the distance from the roller midpoint to the end of the contact area.

$$l' = \sqrt{R_c^2 - \left[\sqrt{R_c^2 - \left(\frac{l_F}{2} \right)^2} - \Delta_o \right]^2} \quad (57)$$

If l' from Equation (57) is greater than $\frac{l_T}{2}$, l' is set equal to $\frac{l_T}{2}$.

The contact force resulting from an approach Δ_o is

$$P = 2 \int_0^{e'} p_x dx \quad (58)$$

Equation (58) is evaluated numerically by Simpson's rule. In the process of evaluating the integral it is necessary to assume discrete values of x and to calculate the value of p_x . From Equations (55) and (56) with Δ_x known,

$$\frac{d\Delta_x}{dp_x} = \frac{(\vartheta_R + \vartheta_E)}{2\pi} \left[1.3864 + \ln \left(\frac{r'}{2b_x} \right) \right] \quad (59)$$

An assumption of p_x is made and the corresponding Δ_x calculated from Equation (55). An improved value of p_x is

$$p'_x = p_x - \frac{(\Delta'_x - \Delta_x)}{\left(\frac{d\Delta_x}{dp_x} \right)} \quad (60)$$

The process can be repeated until p'_x is to the desired accuracy.

Figure 8 shows a roller in contact with both races and acted upon by centrifugal force F_c and contact loads P_1 and P_2 .

Assuming that the shear forces due to the pocket contact are small with respect to P_1 ,

$$-P_{1q} + P_{2q} + F_c = 0 \quad (61)$$

$$F_c = m_R \frac{E}{2} \Omega_E^2 \quad (62)$$

where m_R = mass of roller

Ω_E = orbital velocity of roller

$$\Delta_{o1} + \Delta_{o2} = \Delta_q \quad (63)$$

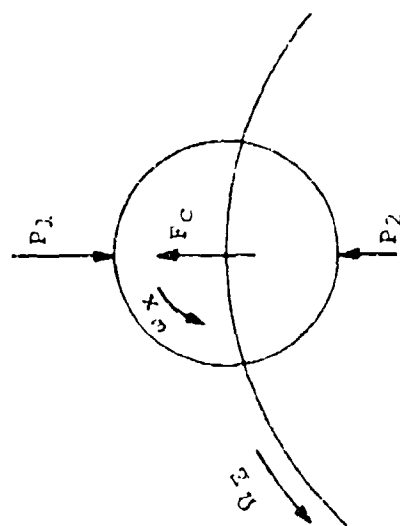
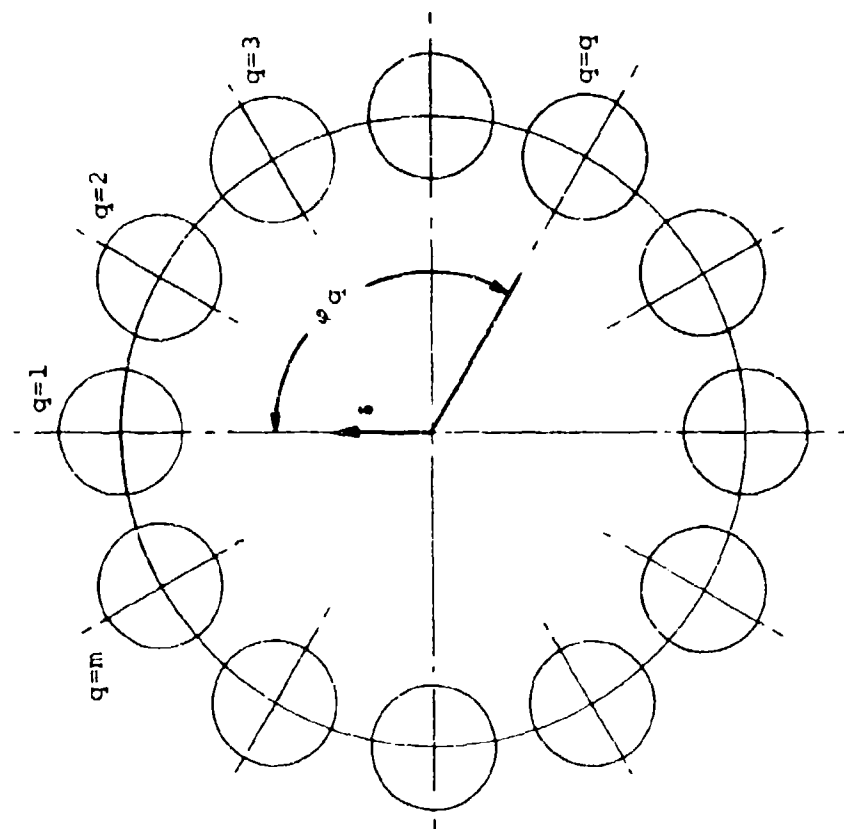


Figure 8. Roller Contact Forces and Roller Orientation Schematic.

Figure 8 also shows the numbering scheme for the rollers in relation to the displacement δ of the inner race with respect to the outer. The azimuth of the q^{th} roller is

$$\varphi_q = \frac{2 \pi (q - 1)}{n} \quad (64)$$

The total approach of inner race to outer at the q^{th} roller is

$$\Delta_q = \delta \cos \varphi_q - \frac{P_D}{2} \quad (65)$$

where P_D = operating diametral clearance of bearing

Δ_{o1} = elastic approach of roller and race at outer contact

Δ_{o2} = elastic approach of roller and race at inner contact

For an assumed value of bearing displacement δ , Δ_q can be calculated. An estimate of Δ_{o1} is made and Δ_{o2} is given by Equation (63). P_{1q}

and P_{2q} can be evaluated and substituted in Equation (61). In general,

Equation (61) will not be satisfied and the residue ψ exists.

$$\psi = -P_{1q} + P_{2q} + F_c \quad (66)$$

An improved value of Δ_{o1} is

$$\Delta'_{o1} = \Delta_{o1} - \frac{\psi}{\left(\frac{d\psi}{d\Delta_{o1}}\right)} \quad (67)$$

$$\frac{d\psi}{d\Delta_{o1}} = -\frac{dP_{1q}}{d\Delta_{o1}} - \frac{dP_{2q}}{d\Delta_{o2}} \quad (68)$$

The derivative of P with respect to the corresponding Δ_o is of the form

$$\frac{dP}{d\Delta_o} = 2 \frac{\frac{d_x}{\left(\frac{d\Delta_x}{dp_x}\right)}}{\Delta_o} \quad (69)$$

Repetition of the process leading to Equation (67) enables Δ_{o1} to be determined to any desired accuracy.

The reaction of the bearing to the displacement δ is

$$F = \sum_{q=1}^n P_{2q} \cos \varphi_q \quad (70)$$

Equilibrium requires that

$$F - \bar{F} = 0 \quad (71)$$

where \bar{F} = external radial load

For an assumption of δ , Equation (71) may not be satisfied. An improved value of δ is

$$\delta = \varepsilon - \frac{(F - \bar{F})}{\left(\frac{dF}{d\delta}\right)} \quad (72)$$

$$\frac{dF}{d\delta} = \sum_{q=1}^n \frac{dP_{2q}}{d\Delta_{o2q}} \frac{d\Delta_{o2q}}{d\Delta_q} \cos^2 \varphi_q \quad (73)$$

Differentiating Equations (61) and (63) with respect to δ_q ,

$$-\frac{dP_1}{d\Delta_{o1q}} \cdot \frac{d\Delta_{o1q}}{d\Delta_q} + \frac{dP_2}{d\Delta_{o2q}} \cdot \frac{d\Delta_{o2q}}{d\Delta_q} = 0 \quad (74)$$

$$\frac{d\Delta_{o1q}}{d\Delta_q} + \frac{d\Delta_{o2q}}{d\Delta_q} = 1 \quad (75)$$

From these is obtained

$$\frac{d\Delta_{o2q}}{d\Delta_q} = \frac{\frac{-dP_1}{d\Delta_{o1q}}}{\frac{-dP_1}{d\Delta_{o1q}} - \frac{dP_2}{d\Delta_{o2q}}} \quad (76)$$

Figure 9 shows the forces acting on the roller which arise from the lubricant effects. These are assumed small in comparison with P_1 .

ω_1 and ω_2 are the velocities of the outer and inner races with respect to the cage:

$$\omega_i = \Omega_i - \Omega_E \quad i = 1, 2 \quad (77)$$

where Ω_i = angular velocity of a ring relative to ground

Ω_E = angular velocity of the cage relative to ground

The linear velocity of a race relative to the cage is

$$U_{yi} = \frac{(E + C_i d)}{2} \omega_i \quad i = 1, 2 \quad (78)$$

where $C_1 = +1$ for an outer contact

$C_2 = -1$ for an inner contact

The evaluation of the integral in Equation (58) by Simpson's rule requires the establishment of an odd number of stations over the contact length. The stress conditions and the sliding velocities of race on roll at these stations will be utilized in calculating the friction forces in the EHD film.

The maximum Hertz pressure at any location x within the pressure area is

$$S_{m_x} = \frac{2 p_x}{\pi b} \quad (79)$$

For stations within the cylindrical portion of the roll, the radius of the roll is

$$r_r = \frac{d}{2} \quad (80)$$

For stations within the crowned portion of the roll,

$$r_{rx} = \frac{d}{2} - \sqrt{r^2 - \left(\frac{f F}{2}\right)^2} + \sqrt{R^2 - x^2} \quad (81)$$

The linear velocity of the roll at any station is

$$U_{R_{x_i}} = C_i r_x \omega_x \quad i = 1, 2 \quad (82)$$

where ω_x is the angular velocity of roller about its center

The slip velocity of race on roll is

$$U_{S_{x_i}} = U_{y_i} - U_{R_{x_i}} \quad i = 1, 2 \quad (83)$$

The minimum film thickness at any station is*

$$h_{x_i} = \frac{1.6 R_{x_i}^{.43} a^{.6} (\mu_0 |\bar{U}_{x_i}|)^{.7}}{P_{x_i}^{.13} (E'')^{.03}} \quad i = 1, 2 \quad (84)$$

where R_{x_i} = the radius of a roll having the same conformity with regard to a flat plate that the actual contact has

$$R_{x_i} = \frac{1}{-\frac{2C_i}{(E + C_i d)} + \frac{1}{r_{x_i}}} \quad i = 1, 2 \quad (85)$$

a = the pressure-viscosity coefficient of the lubricant

μ_0 = the lubricant viscosity at inlet temperature

\bar{U}_{x_i} = the average rolling velocity at the station

$$\bar{U}_{x_i} = \frac{1}{2} (U_{y_i} + U_{R_{x_i}}) \quad (86)$$

$$E'' = \frac{8}{\nu_R + \nu_E} \quad (87)$$

The friction or tractive force generated in the EHD film depends on the coefficient of friction at the various stations along the contact length.

*Calculated as discussed under "Elastohydrodynamic Traction Coefficients"

A computer program provided by the Air Force Aero Propulsion Laboratory and Mechanical Technology, Inc. calculates the friction coefficient as a function of three parameters: G_1 , G_2 and G_3 .

$$G_{1_{x_i}} = \frac{G_A |U_{S_{x_i}}|}{S_{m_{x_i}} h_{x_i}} \quad (88)$$

$$G_{2_{x_i}} = G_B U_{S_{x_i}}^2 \quad (89)$$

$$G_{3_{x_i}} = a_3 S_{m_{x_i}} \quad (90)$$

where

$$G_A = \mu_3 \left(\frac{a}{a_3} \right)^{.6} \left(\frac{\mu_0}{\mu_3} \right)^{.7} \quad (91)$$

$$G_B = \frac{\mu_3 \beta}{1.728 K_F} \quad (92)$$

$$a_3 = \frac{0 + 930 a (T_1 - 86)}{546 (T_1 + 460)} \quad (93)$$

$$\mu_3 = \mu_0 e^{\beta (T_1 - 86)} \quad (94)$$

The tractive force is obtained by numerical integration of the following:

$$F_{T_1} = 2 \int_0^L f_{x_1} p_{x_1} dx \quad (95)$$

The derivative of F_{T_i} with respect to ω_x will be required. These are obtained by calculating F_{T_i} values for $\omega_x + \Delta\omega_x$ and $\omega_x - \Delta\omega_x$ and substituting them in:

$$\frac{dF_{T_i}}{d\omega_x} = \frac{(F_{T_i})_{\omega_x + \Delta\omega_x} - (F_{T_i})_{\omega_x - \Delta\omega_x}}{2 (\Delta\omega_x)} \quad (96)$$

Turning now to the pocket contacts, the following expressions for F_p and F_v are obtained* (Figure 9 also shows a roller in a pocket and those forces acting on the roller from the cage):

$$F_{p_x} = \frac{2.447 \mu_o |\omega_x| \left(\frac{d_x}{2}\right)^2}{h_{p_x}} \quad (97)$$

$$F_{v_x} = \frac{.5482 \mu_o \omega_x \left(\frac{d_x}{2}\right)^{3/2}}{h_{p_x}^{1/2}} \quad (98)$$

Along the cylindrical portion, the film thickness is h_{p_o} . When $x > \frac{\ell_F}{2}$ the film thickness is

$$h_{p_x} = h_{p_o} + \sqrt{R_c^2 - \left(\frac{\ell_F}{2}\right)^2} - \sqrt{R_c^2 - x^2} \quad (99)$$

The pocket forces are obtained by numerical integration of

$$F_p = 2 \int_0^{\ell_T} F_{p_x} dx \quad (100)$$

*Calculated as described under "Analysis of Shear Forces on a Lubricated, High-Speed Bearing Retainer."

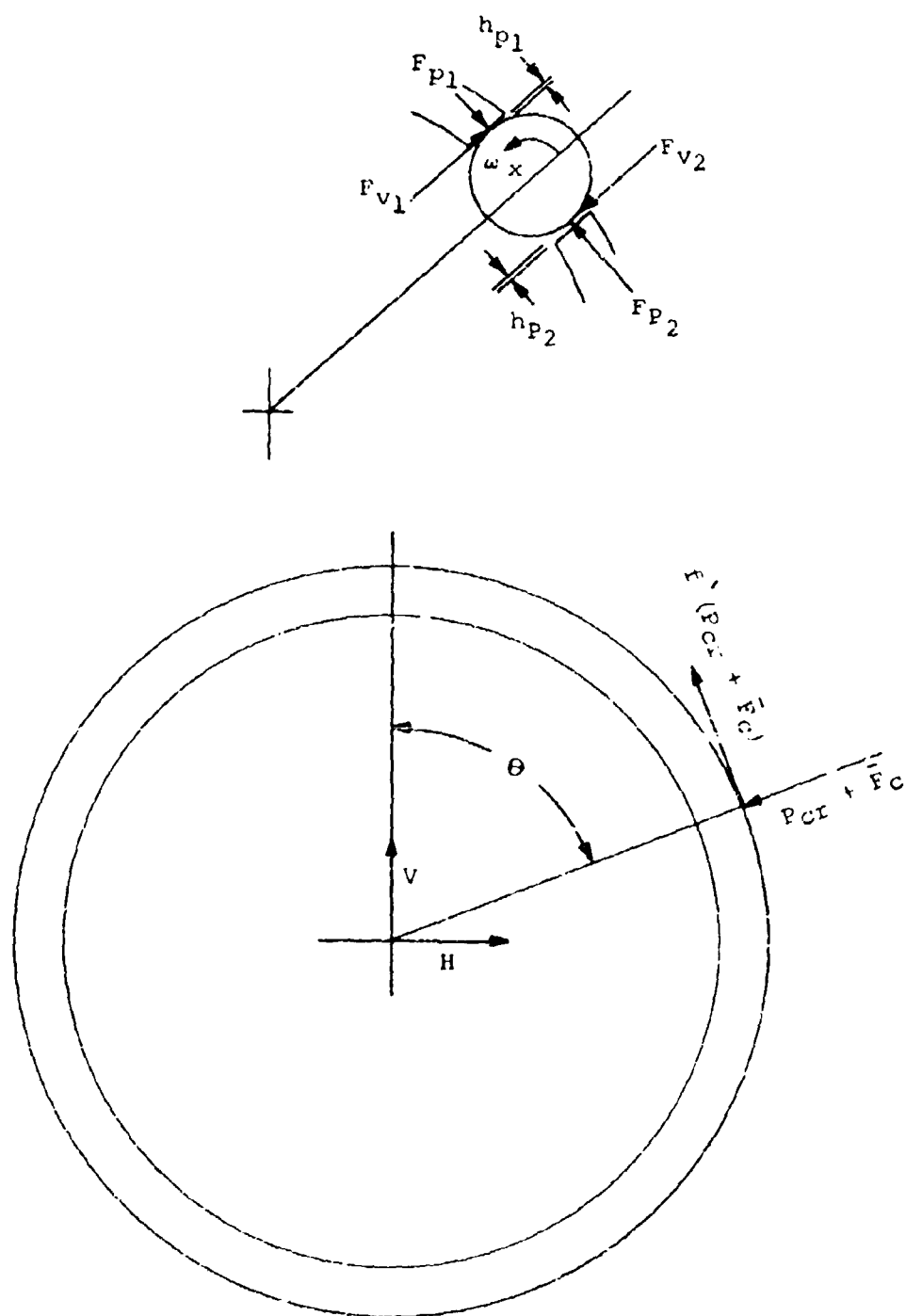


Figure 9. Roller Pocket Forces and Cage Whirl Forces.

and

$$F_v = 2 \int_0^{l_T} F_{v_x} dx \quad (101)$$

The derivatives of F_p and F_v with respect to ω_x and h_o are required.

$$\frac{dF_p}{d\omega_x} = \frac{F_p}{|\omega_x|} \quad (102)$$

$$\frac{dF_v}{d\omega_x} = \frac{F_v}{\omega_x} \quad (103)$$

Differentiating Equations (97) and (98) gives

$$\frac{dF'_{p_x}}{dh_{p_x}} = \frac{-2.447 \mu |\omega_x| \left(\frac{d_x}{2}\right)^2}{h_{p_x}^2} \quad (104)$$

$$\frac{dF'_{v_x}}{dh_{p_x}} = \frac{-.2741 \mu \omega_x \left(\frac{d_x}{2}\right)^{3/2}}{h_{p_x}^{3/2}} \quad (105)$$

Then the required derivatives are

$$\frac{dF_p}{dh_{p_o}} = 2 \int_0^{l_T} \frac{dF'_{p_x}}{dh_{p_o}} dx \quad (106)$$

$$\frac{dF_v}{dh_{p_0}} = 2 \int_0^{\frac{1}{2}T} \frac{dF'_{v_x}}{dh_{p_0}} dx \quad (107)$$

The viscous drag on a roller orbiting at high speed is*

$$F_D = -\frac{\rho \ell L}{64} \sum_{i=1}^2 Z_i \left[|D_i - D_{c_i}| \Omega_E \right]^2 \quad (108)$$

- where ρ = lubricant density
 Z_1 = radial riding clearance at outer pilot surface
 Z_2 = radial riding clearance at inner pilot surface
 D_1 = bore of outer ring
 D_{c_1} = outside diameter of cage
 D_2 = outside diameter of inner ring
 D_{c_2} = bore of retainer

If $Z_1 > Z_2$ the cage is inner-ring piloted. If $Z_1 < Z_2$ the cage is outer-ring piloted.

From Figure 9, assuming the forces F_{v_1} or F_{v_2} are small in comparison with P_1 , let

$$\Phi = F_{T_1} + F_{T_2} - F_D \quad (109)$$

*Calculated as described under "Analysis of Shear Forces on a Lubricated, High-Speed Bearing Retainer."

If $\Phi > 0$, the roller contacts the leading wall of the pocket and drives the cage, and the value of an index, I , is 1.

If $\Phi < 0$, the roller contacts the trailing wall of the pocket and is driven by the cage. The value of the index is 2.

F_p and F_v need be calculated only for the end of the pocket corresponding to I . The forces at the other end of the pocket are negligible due to the pocket clearance, which is large compared to the lubricant film at the I end.

Two modes of operation are recognized. In the first mode the roller is in contact with both outer and inner races. In the second the roller contacts the outer race only. In neither mode is the angular acceleration of the roller in orbit or about its own axis considered. In other words the transition from motion with contact at both races to steady-state motion with outer-race contact only is assumed to be instantaneous.

When the roller is in contact with both races,

$$F_{pI} - |F_{T1} + F_{T2} - F_D| = 0 \quad (110)$$

Equation (110) is calculated using an assumed value of ω_x . For the first pass, ω_x is obtained from

$$\omega_x = \frac{(\Omega_1 - \Omega_E)(E + d)}{d} \quad (111)$$

Equation (110) is also evaluated using an assumed value of $h_{p_{oI}}$, and

Equation (110) will probably have the residue ψ .

An improved value of $h_{p_{oI}}$ is

$$h_{p_{oI}} = h_{p_{oI}} - \frac{\psi}{\left(\frac{dh}{dh_{p_{oI}}}\right)} \quad (112)$$

where

$$\frac{d\Psi}{dh_{p_{oI}}} = \frac{dF_{pI}}{dh_{p_{oI}}} \quad (113)$$

Repetition of the process yields $h_{p_{oI}}$ to desired accuracy.

Taking moments about the roll center,

$$(F_{T1} - F_{T2} - F_{vI}) \frac{d}{2} = 0 \quad (114)$$

For the initial assumption of ω_x , Equation (114) will not be satisfied and there will be the residue ψ . An improved value of ω_x is

$$\dot{\omega}_x = \omega_x - \frac{d\Psi}{\left(\frac{d\Psi}{d\omega_x}\right)} \quad (115)$$

$$\frac{d\Psi}{d\omega_x} = \frac{dF_{T1}}{d\omega_x} - \frac{dF_{T2}}{d\omega_x} - \frac{dF_{vI}}{d\omega_x} - \frac{dF_{vI}}{dh_{p_{oI}}} \cdot \frac{dh_{p_{oI}}}{d\omega_x} \quad (116)$$

where

$$\frac{dh_{p_{oI}}}{d\omega_x} = - \frac{\left(\frac{dF_{pI}}{d\omega_x}\right)}{\left(\frac{dF_{pI}}{dh_{p_{oI}}}\right)} \quad (117)$$

Repeated application of Equation (115) yields ω_x to desired precision. After each pass the process returns to Equation (82).

The solution for the case of outer contact only is solved in a similar manner except that F_{y_2} and its derivatives are nonexistent.

The viscous drag force between retainer and ring is, from Reference 3,

$$F_{R_i} = .008 \rho^{3/4} \mu_o^{1/4} \sum_{i=1}^2 \frac{|U_i|^{7/4}}{Z_i^{1/4}} \frac{A_i U_i}{|U_i|} \quad (118)$$

where ρ = lubricant density
 μ = lubricant viscosity
 U = sliding velocity of ring on cage
 A = total guiding area
 Z = 1/2 cage ring diametral clearance

$$U_i = \frac{(\omega_i - \omega_E) D_i}{2} \quad i = 1, 2 \quad (119)$$

The torque on the cage due to viscous drag is

$$Q_v = \frac{1}{2} \sum_{i=1}^2 F_{R_i} D_i \quad (120)$$

The total horizontal and vertical loads on the cage due to pocket forces are

$$H = \sum_{q=1}^n \left[-C_{I_q} (F_{p_{I_q}} \cos \varphi_q + F_{v_{I_q}} \sin \varphi_q) \right] \quad (121)$$

$$V = \sum_{q=1}^n \left[C_{Iq} (F_{Prq} \sin \varphi_q - F_{Vrq} \cos \varphi_q) \right] \quad (122)$$

Figure 9 shows the reactions of the piloting surface on the cage. The radial force consists of a component, P, and a centrifugal force due to cage whirl with a rotating load. From Figure 9,

$$V + f' (P + \bar{F}_c) \sin \Theta - (P + \bar{F}_c) \cos \Theta = 0 \quad (123)$$

$$H - f' (P + \bar{F}_c) \cos \Theta - (P + \bar{F}_c) \sin \Theta = 0 \quad (124)$$

$$f' = \frac{U_J}{|U_J|} f_r \quad (125)$$

where f_r = coefficient of sliding friction at the pilot interface

J = 1 for an outer-piloted retainer and 2 for an inner-piloted retainer

$$\bar{F}_c = \frac{m_c Z_J \omega_w^2}{2} \quad (126)$$

m_c = mass of cage

ω_w = speed of whirl

From Equations (120) and (121),

$$\tan \Theta = - \frac{(f' V - H)}{(f' H + V)} \quad (127)$$

$$P = \frac{H}{f' \cos \Theta + \sin \Theta} - \bar{F}_c \quad (128)$$

The total torque on the cage may now be evaluated.

$$\bar{Q} = \frac{1}{2} \sum_{q=1}^n \left[C_{I_q} (F_{p_{I_q}} E + F_{v_{I_q}} D_p) \right] + \frac{f (P + \bar{F}_c)}{2} D_{c_j} + Q_v \quad (129)$$

The cage speed is now decremented and the value of \bar{Q} recalculated. This is equivalent to returning to Equation (77) with the new value of Ω_E .

The decrementing process is continued until \bar{Q} changes sign. The method of false position is then applied to drive $|Q|$ to a satisfactory minimum.

ELASTOHYDRODYNAMIC FILM THICKNESS CALCULATION

The minimum EHD film thickness is calculated within the computer program by a subroutine provided by the Air Force Aero Propulsion Laboratory and Mechanical Technology, Inc., in accordance with Reference 11. The fundamental relationship employed is the Dowson and Higginson¹ equation as indicated below for cylindrical contacts. Ball and roller race contacts are reduced to equivalent contacts in the analysis by dividing the contact zones into strips.

$$h_o = 1.6 R \frac{\left[a_o E'' \right]^{.6} \left[\frac{u \mu_o}{E'' R} \right]^{.7}}{\left[\frac{w}{E'' R} \right]^{.13}} \quad (130)$$

where a_o = pressure coefficient of viscosity $\left[\frac{\text{in.}}{\text{lb}} \right]^2$

$$E'' = \left[\frac{1-m_R^2}{2E_R} + \frac{1-m_E^2}{2E_E} \right] \left[\frac{\text{lb}}{\text{in.}} \right]^2$$

m = Poisson's ratio (rolling element, race)

E = Young's modulus (rolling element, race)

μ_o = viscosity at ambient pressure and film inlet temperature $\left[\frac{\text{lb-sec}}{\text{in.}^2} \right]$

$u = \frac{1}{2} \left[V_R + V_E \right]$ velocity term $\left[\frac{\text{in.}}{\text{sec}} \right]$

$R = \left[\frac{1}{R_R} + \frac{1}{R_E} \right]^{-1}$ equivalent radius $[\text{in.}]$

w = load per unit width of contact $\left[\frac{\text{lb}}{\text{in.}} \right]$

h_o = minimum film thickness

The application of this equation to ball bearings requires the establishment of various kinematic and geometric parameters that will be developed here. The general case of ball motion occurring in a high-speed angular contact ball bearing is represented in Figure 10. The case depicted is with the ball fixed in the plane of the paper with relative outer and inner ring speeds of ω_1 and ω_2 , respectively. As indicated, the ball is free to rotate about all three axes.

The operating contact angles at the inner and outer races are unequal owing to ball centrifugal forces and gyroscopic moments. As is evident, the relative motion between ball and race at each contact will be a combined rolling and spinning action. Proper calculation of the EHD film thickness in these contact areas must consider this combined motion. This was accomplished by dividing the contact area into a number of strips parallel to the y axis as shown in Figure 11. These strips are treated as individual cylindrical contacts rolling in the y direction.

Figure 11 represents the contact zone on the race, which has a velocity due to race rotation of

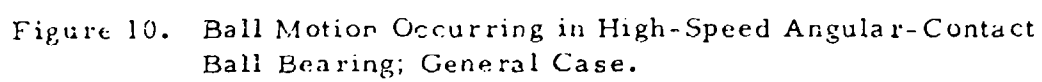
$$V_{YR_i} = \frac{\omega_i}{2} \left(E + C_i d \cos \beta_i \right) \quad (131)$$

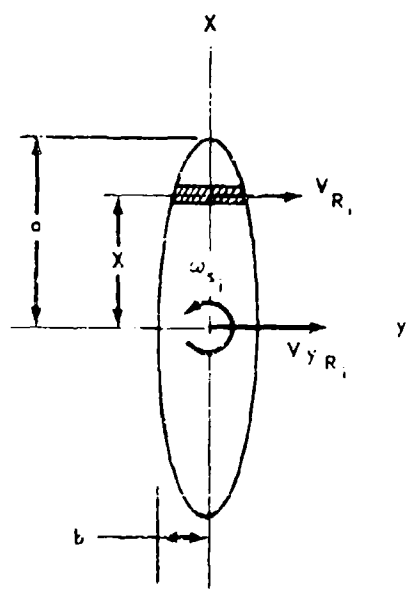
where $i = 1$ designates outer contact
 $i = 2$ designates inner contact

$$\left. \begin{aligned} C_1 &= +1 \\ C_2 &= -1 \end{aligned} \right\} \text{sign terms}$$

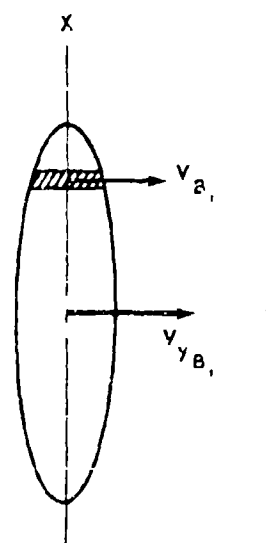
and $\omega_i = \Omega_i - \Omega_c$

where Ω_1 = outer ring speed
 Ω_2 = inner ring speed
 Ω_c = retainer speed





CONTACT AREA ON RACE



CONTACT AREA ON BALL

Figure 11. Contact Areas on Race and Ball.

and an angular spin velocity relative to the ball of

$$\omega_{s_i} = C_i \left[(\omega_i - \omega_x) \sin \beta_i - \omega_z \cos \beta_i \right] \quad (132)$$

Combining these two velocity components, we can now calculate the velocity in the y direction of any point on the race contact by

$$V_{R_i} = V_{Y_{R_i}} - X \omega_{s_i} \quad (133)$$

The velocities within the contact zone on the ball as shown in Figure 11 in the Y direction can be calculated from

$$V_{B_i} = V_{Y_{B_i}} = \frac{C_i d}{2} (\omega_x \cos \beta_i - \omega_z \sin \beta_i) \quad (134)$$

The race radii of curvature in the plane of rolling required to calculate the equivalent radius of contact against a flat surface can be stated as

$$R_{R_i} = -\frac{C_i}{2} \left(\frac{E}{\cos \beta_i} + C_i d \right) \quad (135)$$

and the ball radius of curvature

$$R_{B_i} = \frac{d}{2} \quad (136)$$

Finally, w , the load per unit width of contact, can be found from

$$w = \frac{3P}{4a} \left(1 - \frac{X^2}{a^2} \right) \quad (137)$$

The film thickness is calculated for each strip in the contact, $-a < x < a$, and the minimum value, all strips considered, is presented in the computer output as the minimum thickness for the contact.

The application of the Dowson and Higginson equation to cylindrical roller bearing contacts is treated in the same manner as in the above ball bearing method. The roller bearing case, however, is simpler because of the absence of spin velocities.

ELASTOHYDRODYNAMIC TRACTION COEFFICIENTS

Traction Model

The mechanics by which EHD oil films are generated in heavily loaded rolling element contacts such as those encountered in ball and roller bearings is well understood. The magnitude of the EHD film thicknesses can be accurately calculated using the Dowson and Higginson equation as indicated in the previous section. This is the case even though the analysis is predicated upon isothermal flow conditions, because the film thickness is determined primarily by the oil properties in the inlet region of the contact where the oil pressure is nearly ambient, and the oil temperature is approximately the same as that of the rolling surfaces.

Traction effects, however, present a more complicated picture to be analyzed in that the traction forces transmitted by the contacting surfaces are strongly influenced by the rheology of the fluid within the film. In the race contacts, high Hertz pressures are in effect accompanied by appreciable sliding with the attendant heating of the oil film. The rheological behavior of the lubricant film in the contact is strongly affected by these elevated pressures and temperatures. Currently, information regarding the shear properties of lubricant films under these high contact pressures and sliding velocities is incomplete, and sufficient understanding of the rheology of the lubricants in this regime is not available to produce analytical solutions.

The traction coefficients appearing within the computer programs were established with the use of computer program subroutines BALFTJ and TRAC provided by the Air Force Aero Propulsion Laboratory and Mechanical Technology, Inc. In these subroutines, sliding frictional coefficients were generated based upon the experimental data reported by Johnson and Cameron⁶. To apply this experimental data to a wide range of load, speed, and lubricant parameters, an analysis of friction similar to that developed by Crook⁴ was conducted by Mechanical Technology, Inc., to identify the pertinent dimensionless parameters governing frictional behavior.

The results indicated that the friction coefficients are governed by three dimensionless parameters for a given inlet temperature and lubricant.

$$G_1 = \frac{\mu_o u_s}{P_{Hz} h_o}$$

$$G_2 = \frac{\beta_1^* \mu_o u_s^2}{8 K_f}$$

$$G_3 = \alpha_o P_{Hz}$$

where μ_o = inlet viscosity
 u_s = sliding speed
 P_{Hz} = maximum Hertz pressure
 h_o = film thickness
 β_1^* = temperature viscosity coefficient based on the function used by Crook
 K_f = thermal conductivity of the lubricant
 α_o = pressure viscosity coefficient based on the viscosity function used by Crook

Physically, G_1 is a direct measure of the shear rate effects, whereas G_2 and G_3 measure the thermal heating effects and the pressure-viscosity effects respectively. With the use of these three parameters, Johnson's experimental frictional coefficients were plotted against G_1 for a constant G_2 with G_3 as parameters. Typical graphs for a low and high value of G_2 are given in Figures 12 and 13. Portions of the curves are extrapolations of Johnson's data to cover broader ranges of speed, load, and lubricant properties.

It is seen that at small values of G_1 , all curves have a constant slope. This corresponds to the fact that at small sliding speeds the frictional coefficient varies linearly with sliding speed. In each graph, all curves merge at large values of G_1 to a common value, which is the "ceiling" found by Johnson and Cameron and also by Plint.⁸ The ceiling decreases with increasing G_2 . The existence of a ceiling in friction suggests that there is a limiting shear stress in a lubricant film.

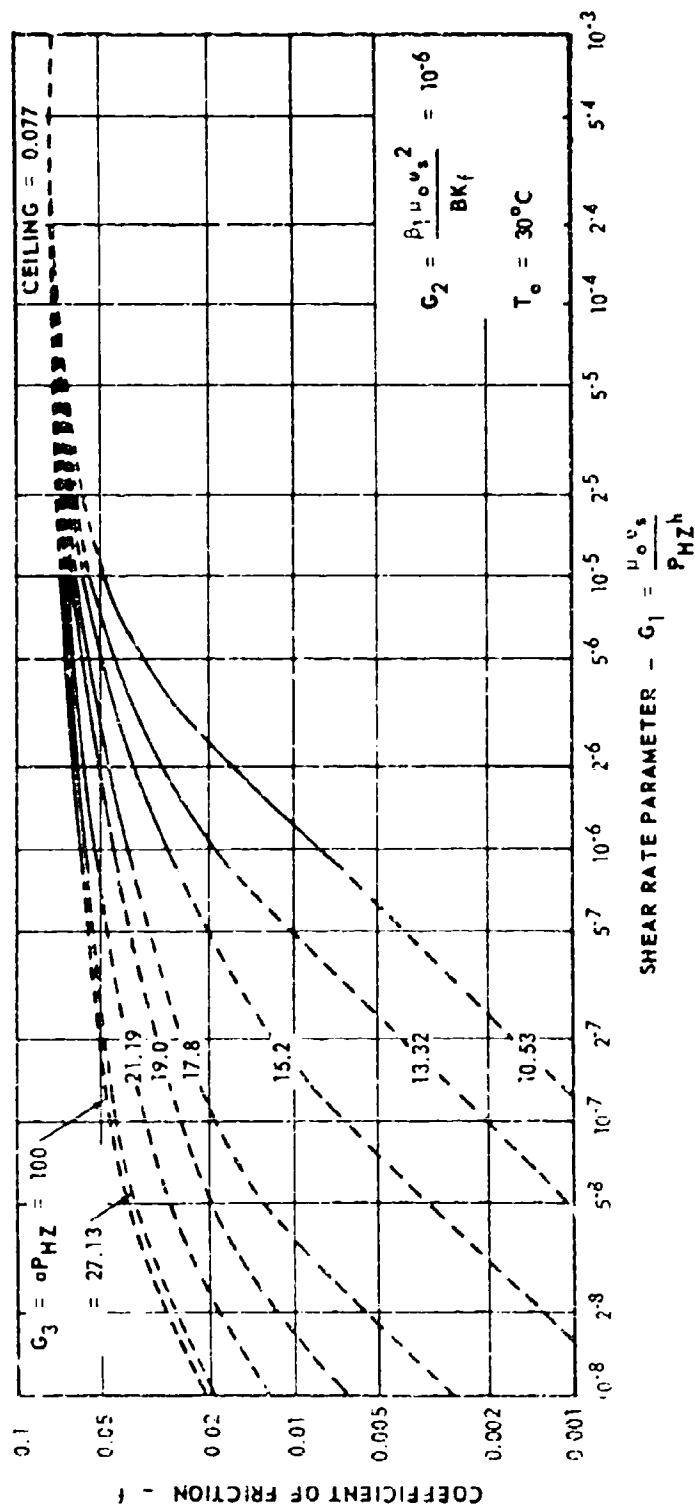


Figure 12. Coefficient of Friction Versus Shear Rate Parameter for Heating Parameter = 10^{-6} . Reference (11), Figure 93.

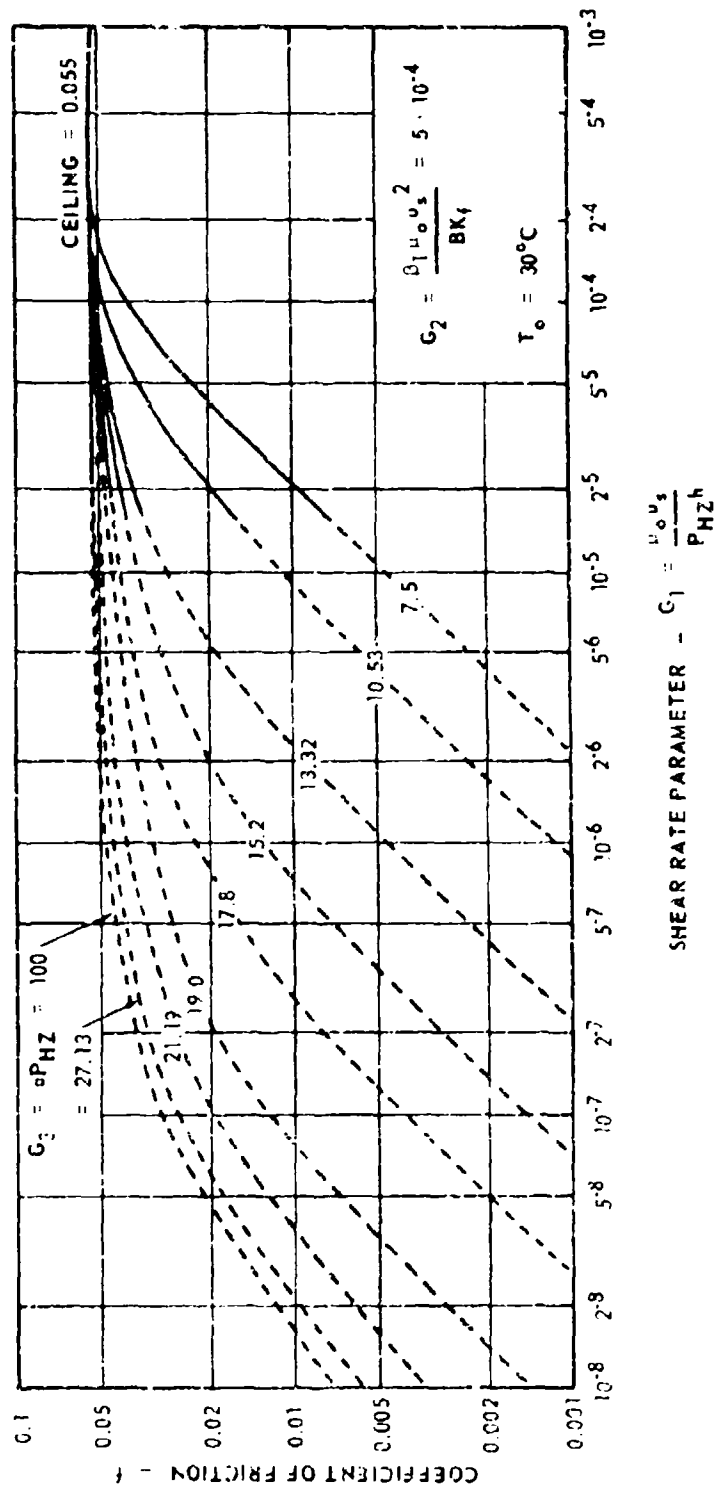


Figure 13. Coefficient of Friction Versus Shear Rate Parameter for Heating Parameter = 5×10^{-4} . Reference (11), Figure 97.

It should be noted that all the frictional coefficient graphs are for a given inlet lubricant temperature, 30° C. Change of inlet temperature affects the frictional coefficient due to the dependence of the limiting shear stress upon the inlet temperature. Johnson and Cameron and Plint investigated this inlet temperature effect. Plint's experiment shows that the variation of frictional coefficient with inlet temperature is approximately linear, and the slope does not seem to vary much with either rolling or sliding speed. The slope was found to be -0.001 per degree Fahrenheit. This relationship is used to predict frictional coefficients for inlet temperatures other than 30° C.

Tractive Forces and Spin Torque

To facilitate the general kinematic solutions desired while accounting for gyroscopic slip and ball spin, it is necessary to calculate the tractive forces between the balls and races with the assumption of motion about all three ball axes. Figure 14 illustrates the velocity components active in the contact areas on the ball and race of a common contact. Each ellipse is divided into a number of strips parallel to the direction of rolling (Y axis). The dimensions a and b are the semimajor and the semiminor axes of the contact, respectively. The sliding velocity in the Y direction at each strip can be found from Equations (133) and (134) and is

$$u_{s_y} = \left| V_{R_i} - V_{B_i} \right| \quad (138)$$

With this sliding velocity established and the Hertz stress, lubricant properties, and EHD film thickness known, the tractive coefficient f for the strip can be calculated with the procedure previously described. The tractive force acting on each strip in the y direction is

$$dF_y = 2 \tau_y y^* dx \quad (139)$$

where y^* is the semistrip width dimension as shown in Figure 14 and

$$\tau_y = \frac{f_w}{2y^*} \quad (140)$$

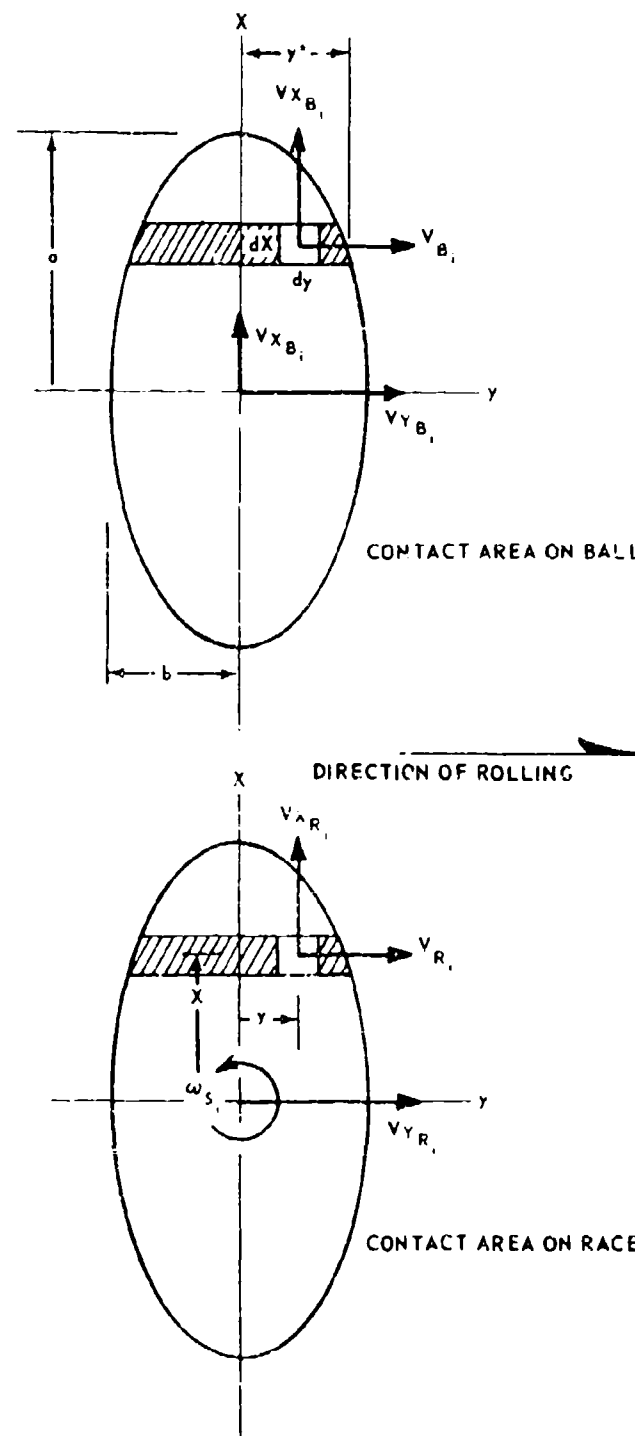


Figure 14. Velocity Components Active in Contact Areas.

The total tractive force for the contact at the y direction is the sum of the tractive forces within the individual strips, or

$$F_{y_i} = \int_{-a}^a 2 \tau_{y \cdot y} \cdot dx = \int_{-a}^a f_w dx \quad (141)$$

The shear stress in the x direction is calculated with the assumption that the ratio of the two mutually perpendicular shear stresses is proportional to their shear rates. The previously defined strip is then further divided into differential elements to evaluate the velocity variations along the Y axis as shown in Figure 14.

Therefore,

$$\frac{\tau_x}{\tau_y} = \frac{u_{s_x}}{u_{s_y}} \quad (142)$$

$$\tau_x = \left| \frac{V_{x_{R_i}} - V_{x_{B_i}}}{V_{R_i} - V_{B_i}} \right| \tau_y \quad (143)$$

where

$$V_{x_{R_i}} = y \cdot \omega_{s_i} \quad (144)$$

is the velocity at each element on the race relative to the ball owing to ball spin and

$$V_{x_{B_i}} = -\frac{d}{2} \omega_y \quad (145)$$

is the velocity of the ball relative to the race resulting from gyroscopic precession of the ball. The velocity component ω_y is the ball angular velocity about the axis dictated by the ball's gyroscopic movement and is one of the independent variables employed in the overall iterative bearing solution.

The total tractive forces in the x direction can be written

$$F_{x_i} = \int_{-a}^a \int_{-y^*}^{y^*} \tau_x dy dx \quad (146)$$

The spin torque normal to the contact ellipse can be expressed as

$$Q_{s_i} = \int_{-a}^a f_w x dx + \int_{-a}^a \int_{-y^*}^{y^*} \tau_x y dy dx \quad (147)$$

Each of these integrals, Equations (141), (146), and (147), was evaluated numerically in the subroutine BALFTJ to provide the tractive forces and moments along with their derivatives with respect to the velocity components and normal contact loads needed for the computer analysis.

Tractive forces and derivatives for the roller bearing contacts were calculated in the same manner in the subroutine ROLFTN subject to the simplification of zero spin velocity and torque.

Tractive Instability

The most significant difficulty encountered during the computer program development stems from the rheological behavior of the fluid and the resulting traction forces developed at high slip speeds. At high values of G , the slope of the traction curve in Figures 12 and 13 becomes progressively flatter, and finally reaches a zero slope at the ceiling, i.e., the limiting shear stress is reached. In this regime, changes in the sliding velocity do not strongly affect the tractive forces generated;

consequently, all derivatives of forces and moments with respect to the velocity components are nearly zero. This behavior creates a breakdown within the iterative procedure because velocity changes are not then affecting bearing tractive forces, and the load adjustments with velocity changes required to achieve solutions are not forthcoming.

Another phenomenon that caused problems at high slip rates is illustrated in Figure 15, where tractive force is plotted against slip velocity directly. Note that at low slip rates the tractive forces increase with increasing slip rates, while at high slip rates the tractive forces decrease with increasing slip rates. This decrease in traction with increasing slip rate is primarily the result of heating of the oil film with an attendant temperature increase combined with a strong temperature dependence of the oil viscosity. In this regime, the heating effect overrides the increasing slip rate to produce a net decrease in traction.

This effect produces a surprising result when combined linear and spin slip velocities are superimposed on a race contact. In some cases, the computed reactive spin torque on the ball opposes the spinning velocity, as one would intuitively expect. However, in other cases, the reactive spin torque is in the same sense of the spinning velocity; i.e., the calculated reaction torque is in a direction so as to accelerate the spinning action of the ball. This anomaly can be explained by considering the two points A and B on the tractive curve, Figure 15. Point A is in the regime where shear rate predominates over tractive behavior, while point B is in the regime where thermal effects are predominant. Consider race contact as shown in Figure 16, with the ball sliding in the y direction with a sliding velocity V_y . The tractive force picture in the contact for this case would be as indicated in Figure 16. If angular velocity ω is now superimposed, different tractive profiles are obtained as indicated in Figure 17, depending upon whether we were initially operating at point A or B. In this manner, the torque reaction to ball spin can either oppose or reinforce the ball spin velocities, depending on whether the dominant slip velocities are on the increasing or decreasing section of the traction curve. This phenomenon is not fully understood at this point, and it must be remembered that the base friction data have been obtained in cylindrical contacts in the absence of spin.

This traction behavior certainly implies that the ball motion would be unstable in these regimes and solutions are unattainable. This phenomenon hampers convergence not only when the desired solution is in the unstable regime, but also if these instabilities are encountered during intermediate passes through the iterative loop for a case which ultimately is stable.

To study this traction-slip behavior in depth, an auxiliary computer program was created. The program treats a single ball-race contact for which the linear and spinning slip velocities are introduced. The program first calculates the tractive forces and moments resulting from

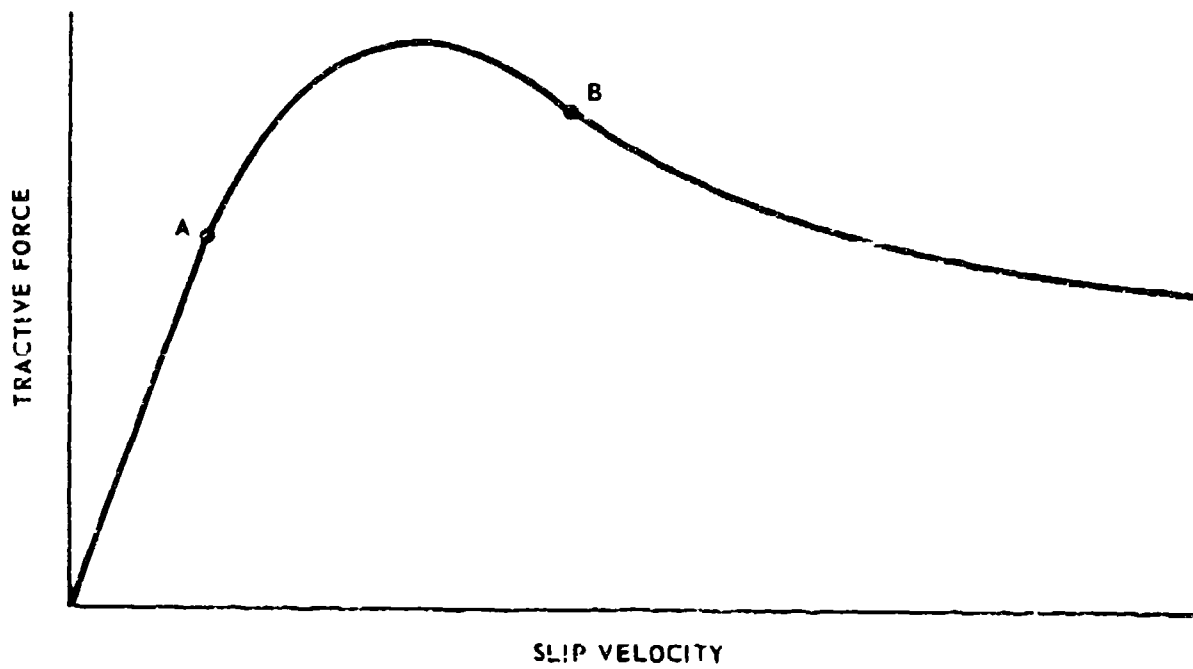


Figure 15. Tractive Force Versus Slip Velocity.

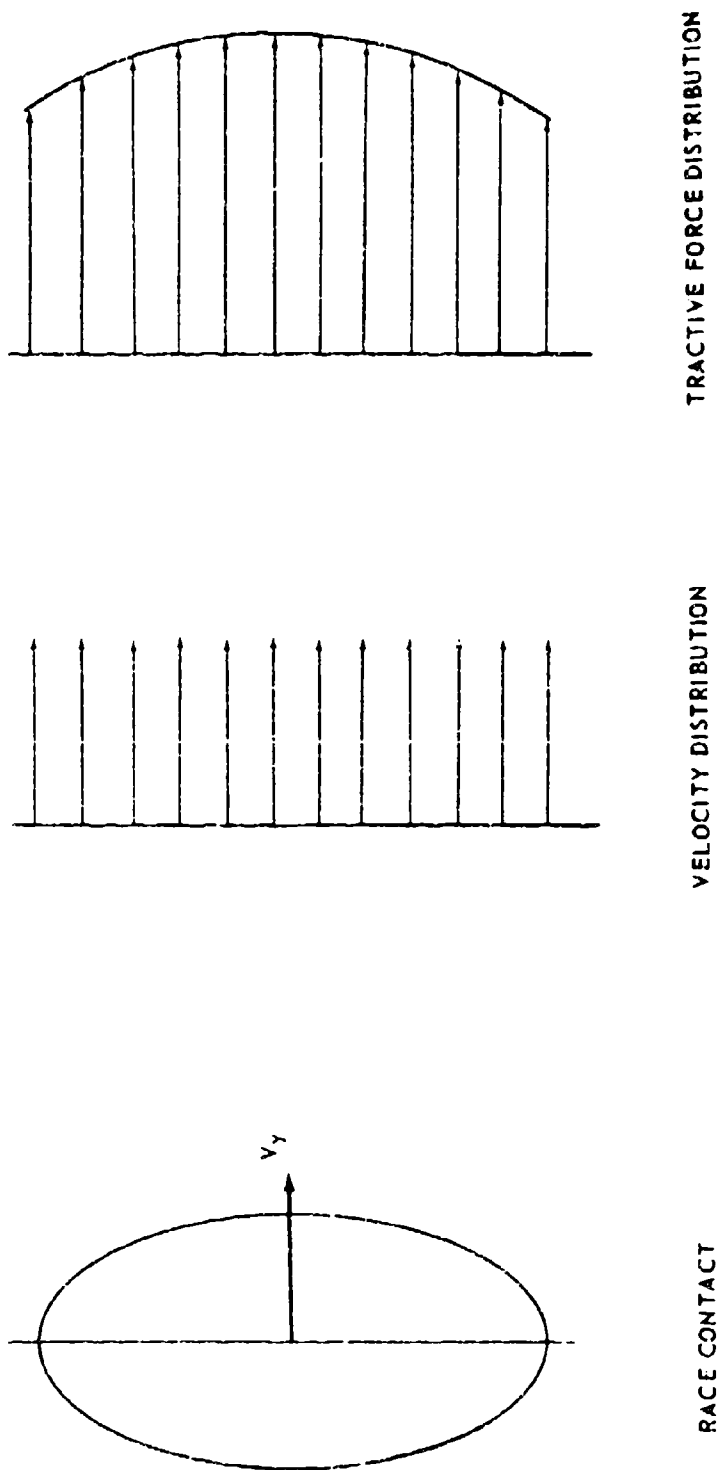


Figure 14. Race Contact, Velocity Distribution, and Tractive Force Distribution in a Ball-Race Contact.

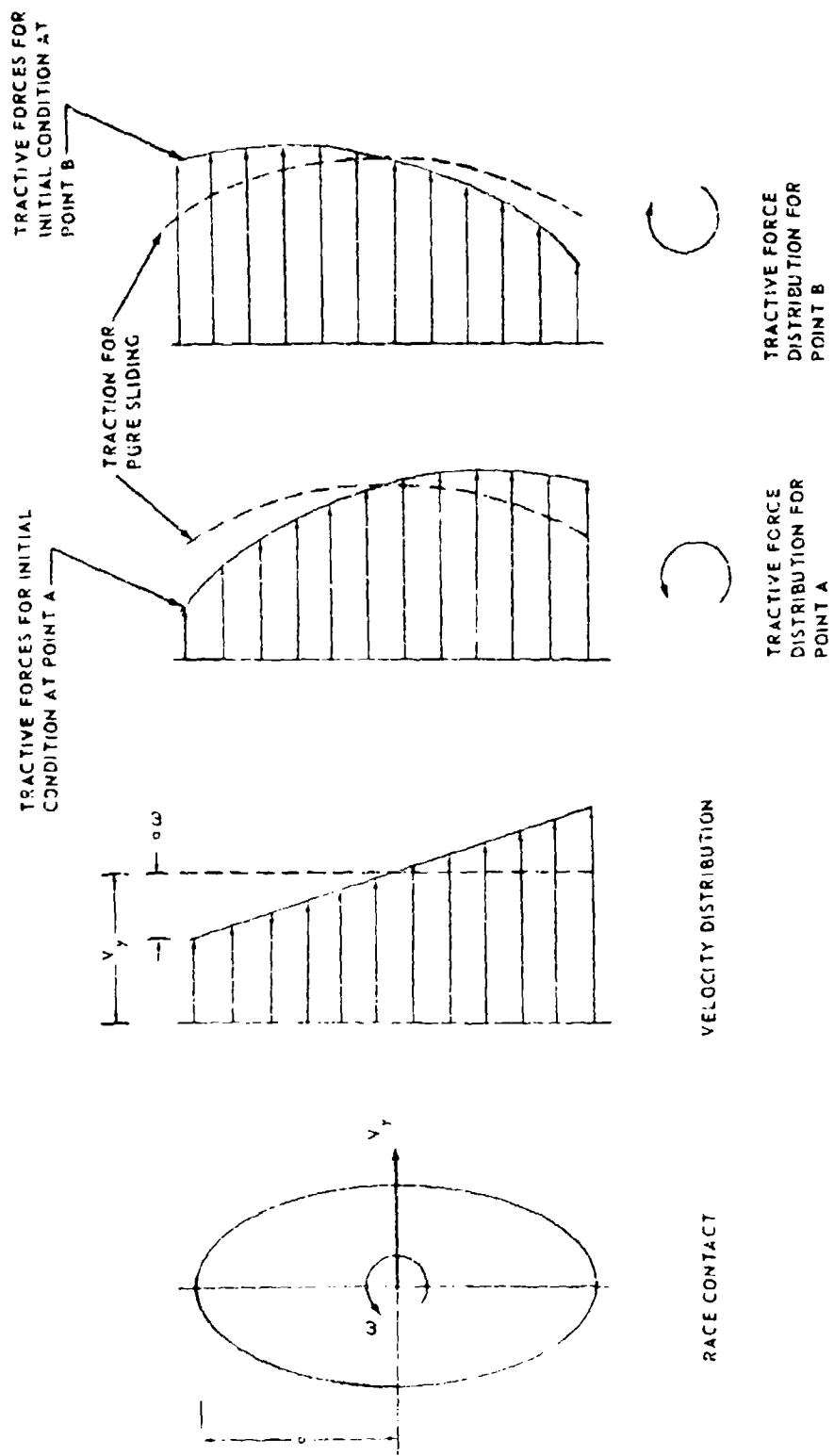


Figure 17. Sliding Velocity and Tractive Force Distribution in a Ball-Race Contact.

the input slip values, increments the input velocities a small amount, and then attempts to iterate back to the initial sliding velocities while knowing their corresponding tractive forces and moments. In this manner the areas of instability can be established as a function of linear and spin slip velocities.

The program incorporates three options to consider different traction versus slip relationships. The first relationship uses the aforementioned Johnson empirical data integrated into a table look-up/interpolation subroutine FRCTN written by Mechanical Technology, Inc. The second relationship is an analytical function that was derived to fit the FRCTN data by scaling and shifting of G_1 , G_2 , and G_3 terms. This smooth analytical function was formulated to eliminate any local numerical discontinuities that could creep into the table look-up interpolation procedure. The following analytical expression resulted:

$$f = \frac{.073 G_1 \left(\frac{G_1}{G_2'} \right)^{-.221}}{G_1 \left(\frac{G_1}{G_2'} \right)^{-.171} + 2.65 \left(10^{-7.4 \log_{10} G_3 + 2.4} \right)} \quad (148)$$

where

$$G_2' = 1 \times 10^{-5}$$

which represents, relatively well, the trends of the charts prepared by Mechanical Technology, Inc. However, the deviation in the absolute value of the traction coefficients can be relatively large. The third relationship is a general power law function of the type

$$f = C_1 G_1^C \quad (149)$$

Cases of combined linear and spin slip up to 10,000 inches per second and 1,000,000 rpm, respectively, were investigated. Tables I through IV present the results in a matrix of linear versus spin

slip velocity indicating the number of iterations required to achieve the back solution. The letter "D" that appears in some positions designates a divergence in the iterative process and is indicative of the tractive instability.

The test case used for the study is typical of ball bearing contacts with a semimajor axis of 0.050, a semiminor axis of 0.005, and a Hertz pressure of 150,000 psi.

Table I presents the stability picture for the FRCTN subroutine. As is evident, instabilities for the case studied occur at moderate and high spin slip velocities and do not seem to be as strongly influenced by linear slip. The constant divergence at 1,000 inches per second sliding velocity at all spin slip velocities does not seem to follow the general trend depicted.

Table II is the result when the smooth analytical function is used instead of the interpolation procedure for the same empirical data. The result is generally the same with an apparent slight improvement at higher linear slip velocities. The strong instability previously seen at 1,000 inches per second is not present. The nature of the stability maps indicates that, in general, as the slope of the curve (Figures 12 and 13) diminishes, the instability tendency increases; therefore, some further studies were conducted with various slopes. The subject curves being log-log plots of traction versus C_1 implies that the slope of the curve is dictated by the exponent term e in Equation (149). Again referring to Figures 12 and 13, the slope of the straight-line portion of the curves at low values of C_1 has an e equal to 1.0. As the slope becomes progressively flatter, while C_1 is increasing, the value of e is decreasing and approaches 0. Tables III and IV give the results when the power law, Equation (149), is used with e values of 1/4 and 1/2 respectively. As is evident, the greater the value of e (greater slope), the greater the stability. In addition to investigating the effects of e , a number of numerical values for C_1 were also run. Results indicated that stability of the system is not a function of C_1 , which establishes the magnitude of the traction coefficient, but, as intuitively expected, is a strong function of the traction coefficient's relationship to the slip velocity.

Roller Bearing Tractive Instability

Difficulties encountered with nonconvergence of the ball bearing program were also present in the roller bearing program. As a result, the power law function for friction, developed previously for the ball bearing program, was adopted. The roller bearing program was thus developed and solutions for all cases inputted were realized.

TABLE 1 . STABILITY MAP - FRCTN SUBROUTINE *							
Linear Slip (in. /sec)	Spin Slip (rpm)						
	0	10	10 ²	10 ³	10 ⁴	10 ⁵	10 ⁶
0	-	1	3	D	D	D	D
1	1	1	2	D	D	D	D
10	4	4	6	D	D	D	D
10 ²	3	4	4	4	13	D	D
10 ³	D	D	D	D	D	D	D
10 ⁴	6	8	7	7	7	D	D
* - Values indicate number of iterations required for solution D - Divergence in iterative process							

TABLE II . STABILITY MAP - ANALYTICAL FUNCTION FROM FRCTN SUBROUTINE *							
Linear Slip (in. /sec)	Spin Slip (rpm)						
	0	10	10 ²	10 ³	10 ⁴	10 ⁵	10 ⁶
0	-	2	2	3	3	D	D
1	6	9	D	D	D	D	D
10	3	4	5	6	D	D	D
10 ²	5	5	5	5	6	D	D
10 ³	6	7	7	6	6	8	L
10 ⁴	11	12	13	15	9	15	10
* - Values indicate number of iterations required for solution D - Divergence in iterative process							

TABLE III. STABILITY MAP - $f = C_1 G_1^{1/4}$ *							
Linear Slip (in. /sec)	Spin Slip (rpm)						
	0	10	10^2	10^3	10^4	10^5	10^6
0	-	2	2	3	3	4	6
1	3	4	5	D	D	D	D
10	4	4	4	5	D	D	D
10^2	4	4	4	5	6	D	D
10^3	6	5	5	5	5	6	D
10^4	9	9	5	7	7	8	7
* - Values indicate number of iterations required for solution D - Divergence in iterative process							

TABLE IV. STABILITY MAP - $f = C_1 G_1^{1/2}$ *							
Linear Slip (in. /sec)	Spin Slip (rpm)						
	0	10	10^2	10^3	10^4	10^5	10^6
0	-	2	2	3	3	3	6
1	3	3	4	8	9	9	9
10	4	4	4	4	9	11	13
10^2	4	4	4	4	5	9	15
10^3	9	4	4	4	5	5	15
10^4	14	5	6	15	5	5	8
* - Values indicate number of iterations required for solution							

ANALYSIS OF SHEAR FORCES ON A LUBRICATED, HIGH-SPEED BEARING RETAINER

Until recently, very little attention has been paid to the effects of the retainer on the operating characteristics of a ball or roller bearing assembly. A knowledge of the forces on the retainer is important with respect to both their effect on the dynamics of the other components of the bearing and their influence on the life of the retainer itself.

In this section, simplified analyses are developed to estimate the shear forces imposed on the retainer by retainer-rolling element and retainer-race interactions in a high-speed oil-lubricated bearing assembly. These analyses require geometry, speeds, lubricant properties, and normal loading as inputs, and are intended to provide relationships to be incorporated as subroutines in a bearing dynamics analysis. Consideration is given to ball and roller bearings.

Traction and Load Analyses for Retainer-Ball Contact

Simplified relationships may be presented for predicting the shear forces on the retainer when in hydrodynamic contact with a ball. A schematic for a single ball in its pocket is shown in Figure 18. The ball imparts a normal load W to the retainer in the direction of orbital motion. For an angular contact bearing having angular velocity components Ω_1 and Ω_2 (Ω_2 is neglected) and a given lubricant and given geometry, it is desired to determine the relationship between the vertical and circumferential tractive forces F_1 and F_2 and the load W .

Development of Analysis

The analysis of the ball-retainer contact will start with a few basic assumptions:

1. Hydrodynamic forces at the contact can be described by Reynolds equation for steady, isoviscous, incompressible, laminar flow.
2. The radial clearance C is assumed large compared with the minimum film thickness h_0 and small compared with the ball radius R_p .
3. The ball-retainer contact will be considered rigid as opposed to EHD.

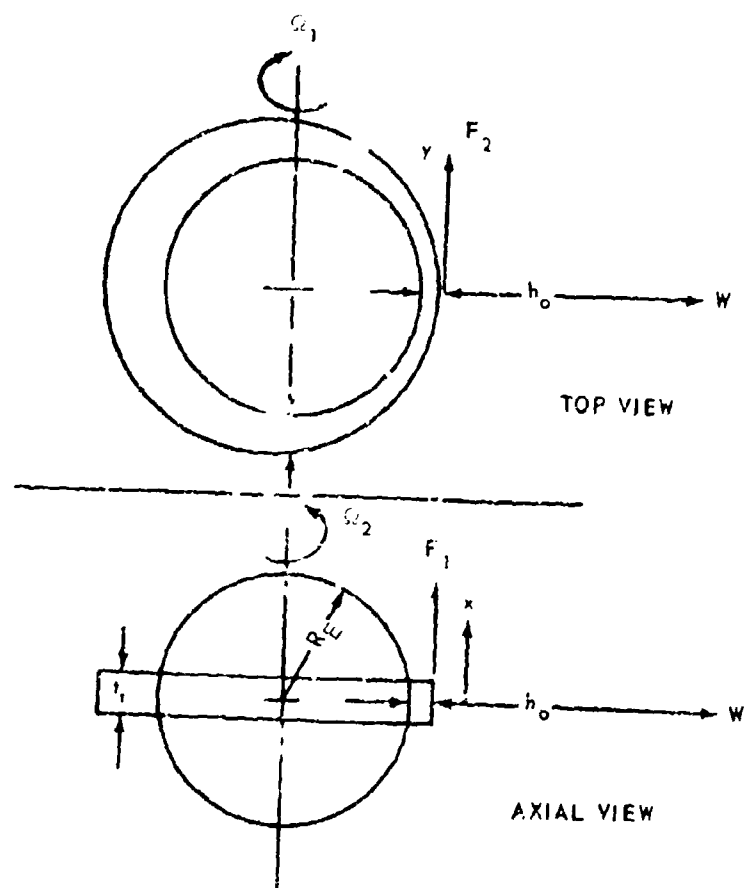


Figure 18. Analysis of Retainer-Ball Traction; Schematic.

The Reynolds equation for steady, isoviscous, incompressible flow is given by

$$\frac{\partial}{\partial x} \left(h^3 \frac{\partial p}{\partial y} \right) + \frac{\partial}{\partial y} \left(h^3 \frac{\partial p}{\partial x} \right) = 6\mu u_x \frac{\partial h}{\partial x} + 6\mu u_y \frac{\partial h}{\partial y} \quad (150)$$

If $h_0/C \ll 1$, the load will be supported in a very small region in the neighborhood of the point of contact ($x = y = 0$). Each of the surfaces can be represented by its quadratic approximation, thus giving a film thickness shape of the form

$$h = h_0 + \frac{x^2}{2R_E} + \frac{y^2}{2} \left(\frac{1}{R_E} - \frac{1}{R_E + C} \right)$$

or approximately,

$$h = h_0 + \frac{x^2}{2R_E} + \frac{y^2}{2R_E} \left(\frac{C}{R_E} \right) \quad (151)$$

The surface velocity u_y is given by $u_y = R\Omega_2$, and if h_0/C is small, the velocity u_y may be approximated by the constant value $u_y = R\Omega_1$.

Equations (150) and (151) may be put into convenient dimensionless form by substituting the dimensionless variables

$$\begin{aligned} \xi &= \frac{x}{\sqrt{2R_E h_0}} \\ \eta &= \frac{y}{\sqrt{2R_E h_0}} \sqrt{\frac{C}{R_E}} \\ p &= \frac{6\mu R\Omega_1}{h_0} \sqrt{\frac{2R_E}{h_0}} \tilde{p} \\ \tilde{h} &= \frac{h}{h_0} \end{aligned}$$

for the respective dimensional quantities in Equations (150) and (151) to obtain the equation

$$\frac{\partial}{\partial \xi} \left(\tilde{h}^3 \frac{\partial \tilde{p}}{\partial \xi} \right) + \frac{C}{R_E} \frac{\partial}{\partial \eta} \left(\tilde{h}^3 \frac{\partial \tilde{p}}{\partial \eta} \right) = - \frac{\partial \tilde{h}}{\partial \xi} + \frac{\Omega_2}{\Omega_1} \sqrt{\frac{C}{R_E}} \frac{\partial \tilde{h}}{\partial \eta}$$

where

$$\tilde{h} = 1 + \xi^2 + \eta^2 \quad (152)$$

In accordance with assumption (2), terms of order $\sqrt{C/R}$ are neglected to obtain the approximate form of Reynolds equation

$$\frac{d}{d\xi} \left(\tilde{h}^3 \frac{d\tilde{p}}{d\xi} \right) = - \frac{d\tilde{h}}{d\xi} \quad (153)$$

The usual downstream separation condition is imposed on Equation (153), which requires the pressure and pressure gradient to vanish simultaneously at some point downstream of the center of contact $\xi = -\xi_1(\eta)$. Hence,

$$p = \frac{dp}{d\xi} = 0 \quad (154)$$

at $\xi = -\xi_1(\eta)$.

We may now integrate Equation (153) with respect to ξ subject to the boundary condition given by Equation (154) to obtain the equation

$$\frac{d\tilde{p}}{d\xi} = \frac{\xi_1^2 - \xi^2}{(1 + \xi^2 + \eta^2)^3} \quad (155)$$

It can be seen that the pressure gradient dies out at $1/\xi^4$ as ξ becomes large. The upstream edge of the retainer $x = -t_r/2$ corresponds to a value of $\xi = -t_r/(2\sqrt{2Rh_0})$, which will be much larger under the general range of conditions of interest than the value of ξ required for the pressure to approach its limiting value; hence, we may invoke the boundary condition

$$\lim_{\xi \rightarrow \infty} \tilde{p} = 0 \quad (156)$$

The results of this analysis will thus be independent of the width of the retainer. The two constraints imposed by Equations (154) and (156) are sufficient for determining the constant of integration associated with Equation (155), the separation point $\xi_1(\eta)$, and hence the pressure profile $\tilde{p}(\eta)$.

The pressure profile satisfying Equations (154) and (155) is given by

$$\tilde{p}(\xi, \eta) = \int_{-\xi_1(\eta)}^{\xi} \frac{\xi_1^2(\eta) - \xi'^2}{(1 + \xi'^2 + \eta^2)^3} d\xi' \quad (157)$$

and $\xi_1(\eta)$ is determined from Equation (156). The result is given below:

$$\xi_1(\eta) = 0.4751 \sqrt{1 + \eta^2} \quad (158)$$

Film Thickness-Load Relationship for Retainer-Ball Contacts

The dimensionless pressure profile at $\eta = 0$ $\left[\tilde{p}(\xi, 0) \right]$ is shown graphically in Figure 19. It can be seen that the pressure dies out rapidly in the inlet region and at $\xi = 3$ is 10 percent of its peak value. Hence the error in pressure introduced by our upstream boundary approximation will be small if $t_r / (2/\sqrt{2} R h_0) > 3$.

The pressure at any value of η is given by

$$\tilde{p}(\xi, \eta) = \frac{1}{(1 + \eta^2)^{3/2}} \tilde{p}(\xi, \sqrt{1 + \eta^2}, 0) \quad (159)$$

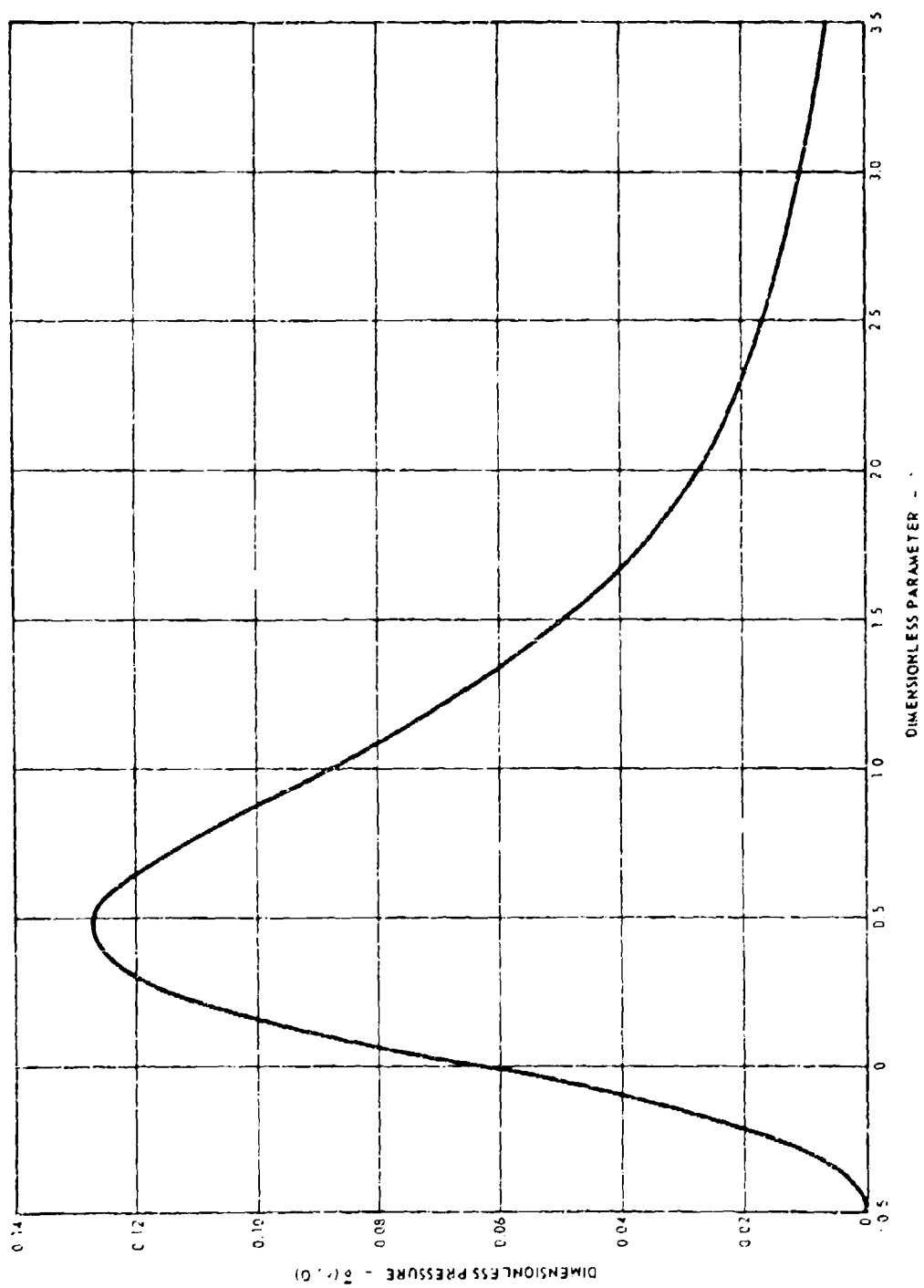


Figure 19. Dimensionless Pressure Profile for Ball-Retainer Contact ($\eta = 0$).

Equation (159) may be integrated with respect to ξ over the interval $-\xi_1 < \xi < \infty$ to obtain the dimensionless load per unit length $\tilde{P}(\eta)$, which is given by

$$\tilde{P}(\eta) = \int_{-\xi_1(\eta)}^{\infty} \tilde{p}(\xi, \eta) d\xi = 0.2040 (1 + \eta^2)$$

and the total dimensionless load \tilde{W} may be obtained by integrating $\tilde{P}(\eta)$ over all η ($-\infty < \eta < \infty$). It can be shown that the error introduced here will be of the order of $\sqrt{h_0}/C$.

The dimensionless load \tilde{W} is

$$\tilde{W} = \int_{-\infty}^{\infty} \tilde{P}(\eta) d\eta = 0.6407$$

and the load-film thickness relationship in terms of physical parameters is

$$\boxed{W = \frac{\mu \Omega_1 R^3}{\sqrt{h_0 C}} K_w} \quad (160)$$

where $K_w = 10.87$

Traction Relationships

The shear stress relationships on the retainer consistent with lubrication theory for isoviscous, incompressible flow are as follows:

$$\tau_{xz} = -\frac{h}{2} \frac{dp}{dx} + \frac{\mu u_x}{h}$$

$$\tau_{yz} = -\frac{h}{2} \frac{dp}{dy} + \frac{\mu u_y}{h}$$

The above equations may be put in their dimensionless form:

$$\tilde{\tau}_1 = \frac{h_0}{\mu R_E \Omega_1} \tau_{xz} = 3 \tilde{h} \frac{d\tilde{p}}{d\tilde{x}} + \frac{1}{\tilde{h}} \quad (161)$$

$$\tilde{\tau}_2 = \frac{h_0}{\mu R_E \Omega_2} \tau_{yz} = 3 \tilde{h} \frac{\sqrt{C}}{\sqrt{R_E}} \frac{d\tilde{p}}{d\tilde{y}} \frac{\Omega_1}{\Omega_2} + \frac{1}{\tilde{h}} \quad (162)$$

The first term on the right side of Equation (162) is of the order $\sqrt{C/R_E}$ and will be neglected. Equation (155) may be used to replace the pressure gradient appearing in Equation (161).

The resulting shear stress equations are

$$\tilde{\tau}_1 = 3 \frac{(\xi^2 - \xi_1^2)}{(1 + \xi^2 + \eta^2)^2} + \frac{1}{(1 + \xi^2 + \eta^2)} \quad (163)$$

and

$$\tilde{\tau}_2 = \frac{1}{1 - \xi^2 - \eta^2} \quad (164)$$

The shear stresses die out as the reciprocal of the square of the coordinate variables as they get large. If integrated over an infinite area, the tractions will diverge logarithmically. Rather than introduce new parameters into the system to limit the area that stresses act upon, it is convenient to define an effective length in the y direction and to consider variations in shear stress in the x direction only. In other words, an effective length will be used to treat the traction problem as one of lubricated line (rather than point) contact.

For the case of a roller bearing, line contact would actually occur and the effective length would be the flat portion of the roller.

An effective length for a ball bearing will be selected by examining the variation of the dimensionless load per unit length \tilde{P} with the dimensionless circumferential coordinate η , which is shown in Figure 20. An effective dimensionless length η_{eff} for calculating load can be defined such that $\tilde{P}_{\text{max}} \eta_{\text{eff}} = \tilde{W}$, which corresponds to a value of $\eta_{\text{eff}} = \pi$ or an effective length of $L_{\text{eff}} = \sqrt{2} \pi R \sqrt{h_0/C}$.

This effective circumferential length is used to calculate the dimensionless tractive forces:

$$\tilde{F}_1 = \eta_{\text{eff}} \int_{-\xi_0}^{\xi_0} \tilde{\tau}_1 d\xi = 1.218$$

and

$$\tilde{F}_2 = \eta_{\text{eff}} \int_{-\xi_0}^{\xi_0} \tilde{\tau}_2 d\xi = 0.328$$

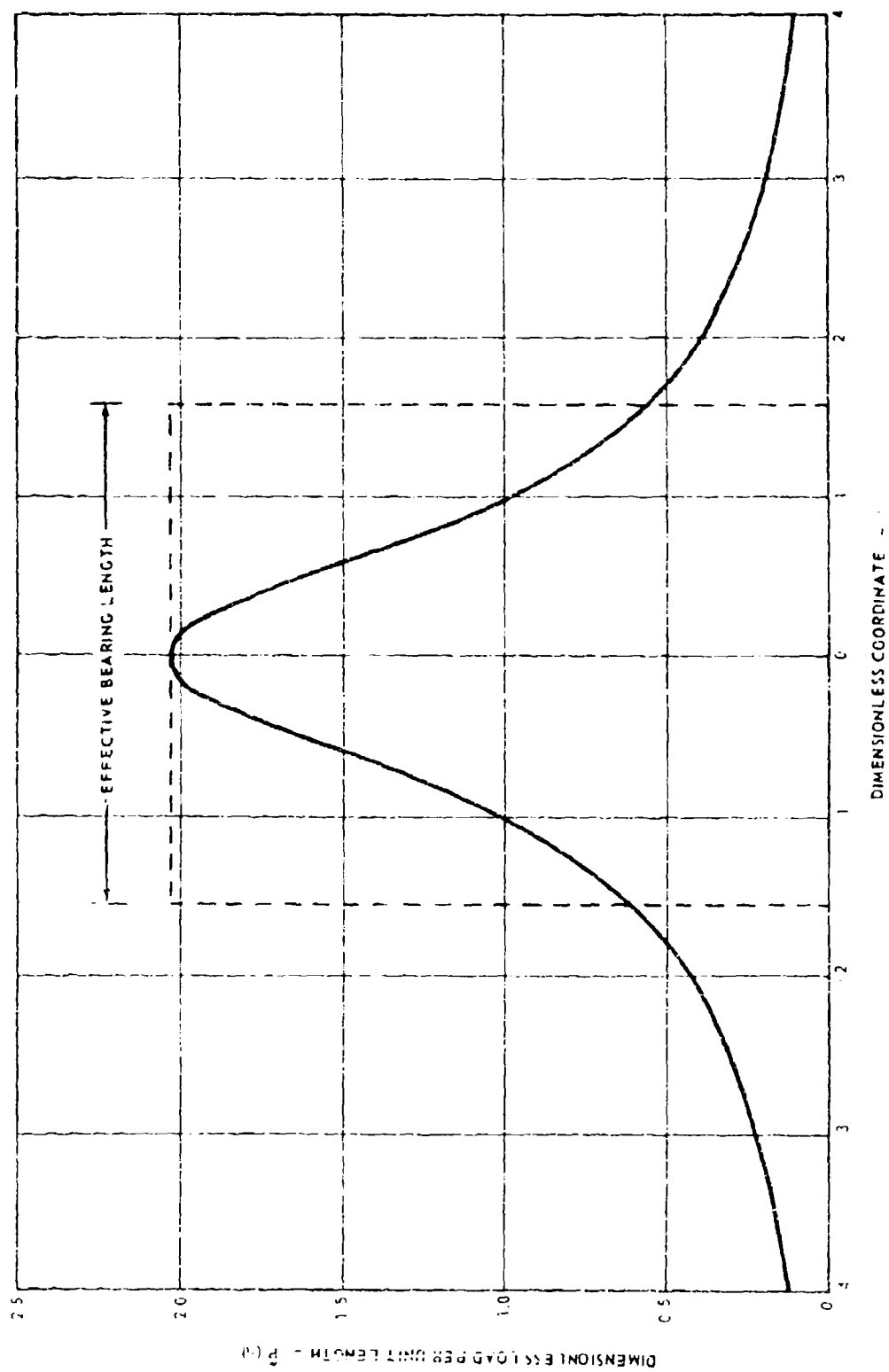


Figure 20. Dimensionless Load per Unit Length.

The hydrodynamic tractions may be expressed in terms of physical parameters as

$$F_i = \frac{\mu \Omega_i R_E^{5/2}}{C^{1/2}} K_i, \quad i = 1, 2 \quad (165)$$

where $K_1 = 2.436$ and $K_2 = 12.66$.

The traction formulas presented above are extremely simple to use for predicting hydrodynamic tractions. Some consideration should be given to the predicted film thickness and surface roughness to determine whether or not the contact is indeed hydrodynamic. Since the retainer ball contact is a concentrated contact, some consideration should also be given to the possibility of EHD effects. Further insight can be obtained here with the use of a numerical example.

Our numerical example will deal with a 0.5-inch-diameter ball spinning with an angular velocity of $\Omega_i = 50,000$ rpm in a retainer pocket having a 5-mil radial clearance, lubricated with a 2-centipoise-viscosity oil. When EHD effects are considered, a pressure coefficient of viscosity of 10^{-4} in.²/lb will be used and elastic properties will be taken to correspond to those of steel. Film thickness and peak pressure versus load relationships are shown in Figure 21 for rigid-hydrodynamic and EHD contacts.

The EHD results were obtained using Hertz contact and Grubin's film thickness relationships. Both pressure and film thickness are shown to vary much more rapidly with load for rigid contact. At low loads, hydrodynamic effects spread the load out over a larger area than the Hertz contact zone, and EHD effects will be small. At loads where the rigid hydrodynamic pressures are predicted to be much higher than EHD pressures, EHD effects will be dominant and the analysis presented here will not be valid. It can be seen, however, that the film thickness at that point as predicted by either theory will be of the same order of magnitude as the surface roughness, and it is quite likely that the tractions will more nearly approach those resulting from dry friction.

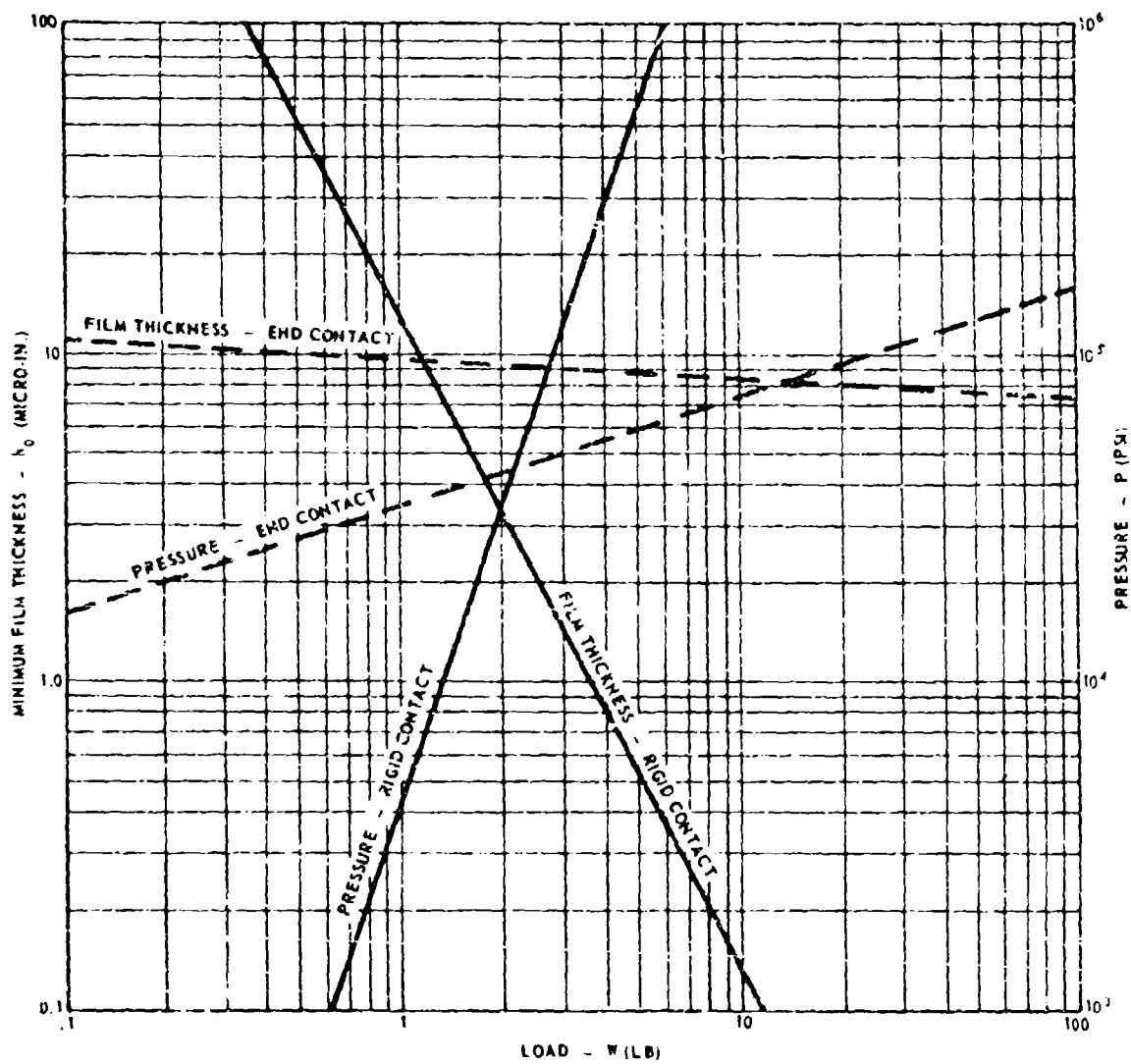


Figure 21. Film Thickness and Maximum Pressure for Retainer-Ball Contact.

The above arguments indicate that a reasonable result can be obtained by dividing the ball-retainer tractions into two regimes, rigid-hydrodynamic contact and dry friction, depending on the film thickness. A critical film thickness separating the two regimes may be determined from the surface roughness. We may define an effective surface roughness S_{eff} as

$$S_{eff} = \sqrt{S_R^2 + S_B^2}$$

where S_R and S_B refer to the RMS (root mean square) surface roughness of the retainer and ball respectively. When $h_0/S_{eff} < 4$, increased surface distress has been found to occur for bearings undergoing severe sliding. At a value of $h_0/S_{eff} = 1.5$, considerable surface distress is present as a result of asperity clashes. We will thus define our critical film thickness h_c for dry friction based on surface distress data as:

$$h_c = 1.5 S_{eff}$$

The resulting ball-retainer traction formulas are

$$F_t = \begin{cases} \frac{\mu \Omega_1 R_E^{5/2}}{C^{1/2}} K_1 \left(\frac{h_0}{h_c} \right)^{1/2} & \text{if } h_0 \geq h_c \\ K_1 W \frac{\Omega_1}{\sqrt{v^2 + \Omega_1^2}} \left(\frac{h_0}{h_c} \right)^{1/2} & \text{if } h_0 < h_c \end{cases} \quad (166)$$

$K_1 = 2,436, \quad K_2 = 12.66, \quad i = 1, 2$

where K denotes coefficient of friction and h_0 is calculated from Equation (160). A reasonable value for h_c is 10 microinches.

The variation of F_1 with W for our numerical example is shown in Figure 22. Inspection of this figure indicates that for practical purposes there is essentially no friction until a threshold load for Coulomb friction is reached. The retainer dynamics will thus probably be much more sensitive to the film thickness formula, Equation (160), than the hydrodynamic traction formulas. It should be noted that the film thickness formula does not contain the effective line contact assumption that was used in developing the traction formulas and hence should be less prone to error.

Tractions for Retainer-Roller Contact

The film thickness-load relationship and the traction relationship for the retainer-roller contact can be obtained from the formulas already presented for the retainer-ball contact. The pressures, shear stresses, and normal and tangential forces per unit length for the retainer-roller contact will be the same as those acting at $y = 0$ for the retainer-ball contact. The forces for the retainer-roller contact are simply the forces per unit length for the retainer-ball contact at $y = 0$ multiplied by the length ℓ of the roller. The equations obtained in this manner are:

$$W = \frac{4\pi R_E^2 L}{h_0} K'_w \quad (167)$$

$$F_1 = 4\pi R_E L \sqrt{\frac{R}{h_0}} K'_1 \quad (168)$$

where $K'_w = 2.447$, $K'_1 = 0.5482$.

Film thickness and peak pressure versus load relationships for a roller-retainer contact are shown in Figure 23. The lines are drawn in a manner analogous to those in Figure 21, and the input parameters are the same except for the additional input of the length of the roller $\ell = 3/8$ inch. Comparison of Figures 21 and 23 indicates that the pressures

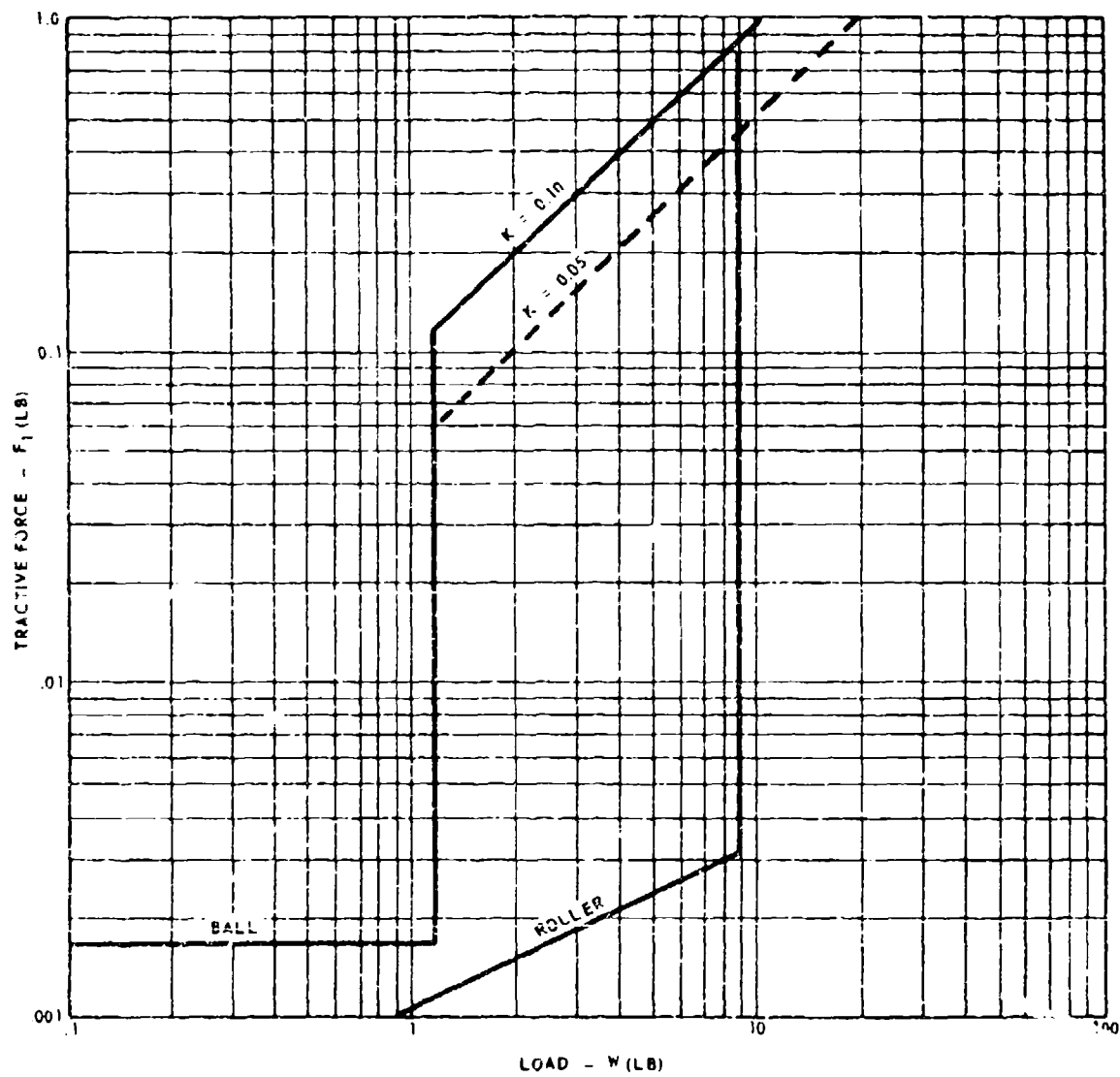


Figure 22. Traction Versus Load for Ball and Roller Contacts.

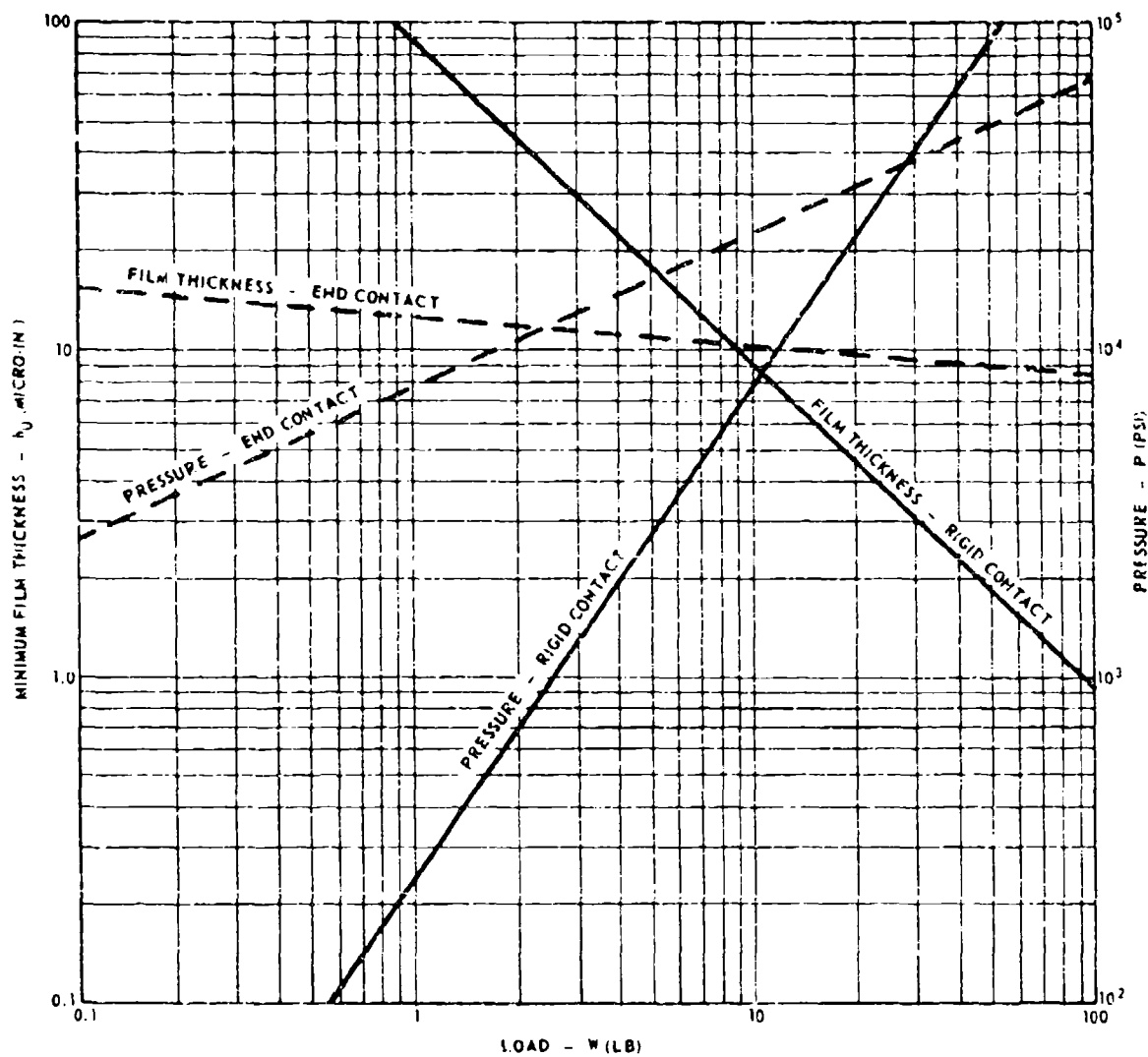


Figure 23. Film Thickness and Maximum Pressure for Retainer-Roller Contact.

will be lower and the retainer-roller contact will tend to be hydrodynamic at somewhat higher loads than in the retainer-ball contact. In other respects the two figures are qualitatively similar, and it should suffice to use the same criteria used in arriving at Equation (166) to obtain the relationship

$$F_1 = \begin{cases} \mu \Omega_1 R_E L \sqrt{\frac{R_E}{h_o}} K_1 & h_o \leq h_c \\ KW & h_o > h_c \end{cases} \quad (169)$$

Tractions calculated from Equation (166) are shown in Figure 22.

Lubricant Drag Between Retainer and Race

A cross-sectional schematic of the retainer and races is shown in Figure 24. At the high speeds of interest here, the flow between the retainer and the races should be turbulent and the shear stress on either surface can be approximated by

$$|\tau_j| = \frac{1}{8} C_f \rho V_j^2 \quad j = 1, 2 \quad (170)$$

where ρ is the fluid density, V_j is the absolute value of the relative velocity between the retainer and race, j , and C_f is the friction factor for flow between the retainer and race, j . The friction factor will in general be a function of the Reynolds number Re_j .

$$Re_j = \frac{V_j H_j \rho}{\mu}$$

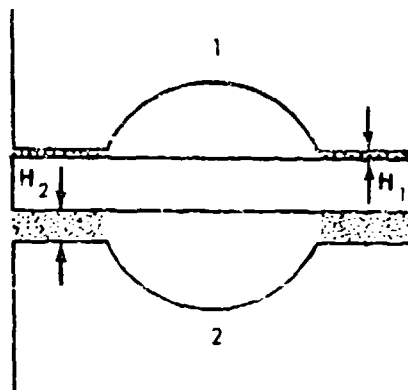


Figure 24. Geometry Used in Calculating Retainer-Race Traction;
Schematic.

It will be assumed that the spacing between the retainer and the guiding surfaces of each race is flooded with oil. We will use the friction factor relationship for Couette flow given by

$$C_f = \frac{0.064}{(Re)^{1/4}} \quad (171)$$

The net drag force on the retainer in the grooved region should be small in comparison with the drag forces between the guiding surfaces, since the flow cross section is larger and the region will probably not be flooded. The drag force on the retainer will thus be calculated based on the area of the guiding surfaces (A_j).

The net force on the retainer, F_R , is given by

$$|F_R| = 0.008 \left| \frac{V_1^2 A_1}{\eta_1 l^4} - \frac{V_2^2 A_2}{\eta_2 l^4} \right| \quad (172)$$

and will in general act in the direction of the relative velocity of the guiding race with respect to the retainer.

It should be noted that when the retainer is under load it will be operating with a high eccentricity with respect to the guiding race. It is doubtful that the retainer-race contact can support a significant amount of load hydrodynamically (as appears to be the case for the retainer-ball contact) because of the large clearances and resulting small area of effective contact. It is thus recommended that a tractive force due to Coulomb friction be added to F_R to obtain the total tractive force on the retainer.

Drag on Ball/Roller

The accurate computation of viscous drag on the ball requires a somewhat more detailed knowledge of the flow field than is currently available.

Drag formulas are available for unconfined motions of bodies of various shapes. The flow in a ball bearing assembly is highly confined; however, it is quite likely that both raceways are not flooded and the flow pattern will be quite complex.

Figure 25 shows the cross section to be considered in estimating drag for the case of a ball bearing. In general, conformity is such that the major open channel for flow will be that existing between the retainer and race 2 shown in the illustration. If we assume that all the flow past the ball occurs around the shaded region and treat this region as a cylinder, the drag force on the ball F_D will be given by

$$F_D = C_D A_3 \frac{\rho V_3^2}{2} \quad (173)$$

where A_3 is the projected shaded region and V_3 is the linear orbital velocity of area A_3 . As a result of the highly approximate nature of these calculations, it will suffice to take A_3 to be $A_3 \approx 2R_E H_2$, V_3 to be the orbital velocity of the ball V_o , and a characteristic drag coefficient of $C_D = 1$ for flow past a cylinder to obtain the formula

$$F_D = \rho R_E H_2 V_o^2 \quad (174)$$

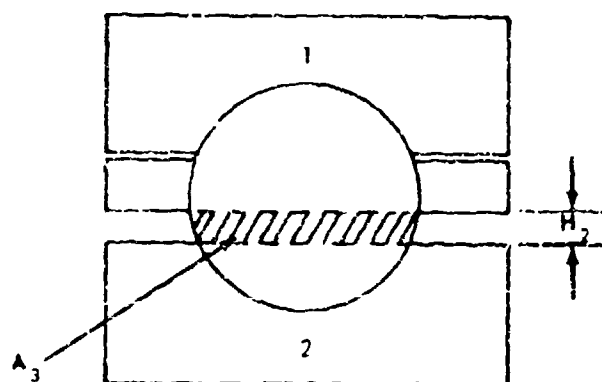


Figure 25. Section Used in Calculating Drag on Ball; Schematic.

VERIFICATION TEST PROGRAM

TEST RIG DESCRIPTION AND OPERATION

The test rig used in this program is shown in Figure 26. The rig simulates a 100-millimeter power turbine bearing and seal package, and it is capable of operating at speeds to 30,000 rpm with 1500° F air temperature and 250 psig air pressure outside the package. The test rig is driven by an 8-inch steam turbine rated at 100 horsepower at 30,000 rpm. A 2:1 speed increaser was installed between the turbine and the test rig. A picture of the test facility is shown in Figure 27. Photographs of the test rig are shown in Figures 28 and 29.

The test rig, Figure 26, incorporates the 100-millimeter bearing, a 100-millimeter radial load bearing, and a 55-millimeter support bearing package. When a roller bearing was installed in the test position, a ball bearing was used in the support position for axial positioning of the shaft.

The axial load for the ball bearing was applied during the test by creating an air pressure differential across the thrust load wheel. The magnitude of the axial load was accurately controlled by modulating the differential pressure across the wheel area. Axial thrust load as a function of air pressure differential is plotted in Figure 30. The radial load on the test bearing was obtained by applying a force to the load bearing. The housing of the load bearing is attached through a rod to a hydraulic piston. The housing is not restrained radially but is prevented from rotating by the loading rod, which is strain gaged to measure the applied radial load. The support bearing package of the test rig was adapted from existing engine hardware (T53-L-13, No. 2 bearing package).

In the main bearing test package, a carbon labyrinth was used to restrict the thrust wheel pressurization air from flowing into the bearing package. The load bearing was lubricated by one jet of 0.050 inch diameter, located on the forward side of the load bearing. The test bearing was lubricated by two jets of 0.035 inch diameter, one located on each side of the test bearing. The oil supply to the load and to the test bearings was controlled independently.

The oil used for the testing was MIL-L-23699, supplied by the Air Force Aero Propulsion Laboratory, oil code 0-64-2. Physical properties for this batch are listed in Table V.

The following parameters were measured and controlled during test rig operation:

1. Oil flow to the bearings, pph
2. Oil temperature in and out, $^{\circ}\text{F}$ }
3. Oil pressure in and out, psig } (test bearing)
4. Bearing cavity pressure, psig
5. Bearing cavity temperature, $^{\circ}\text{F}$
6. Air temperature, $^{\circ}\text{F}$ }
7. Air pressure, psig } (outside test bearing package)
8. Inner and outer race temperatures, $^{\circ}\text{F}$
9. Axial load, lb
10. Radial load, lb
11. Shaft speed, rpm
12. Vibration level (at test bearing housing)
13. Chip detection
14. Cage speed, rpm

The special instrumentation package for measuring retainer data was cantilevered off the rig housing (Figure 26). The retainer drives the instrumentation package, which consists of a multiplexer and mercury slip rings. The multiplexer bearings are oil mist lubricated and air cooled. The mercury slip ring bearings are self-contained and grease packed.

A schematic of the test rig facilities is shown in Figure 31. Typical data sheets are shown in Figure 32.

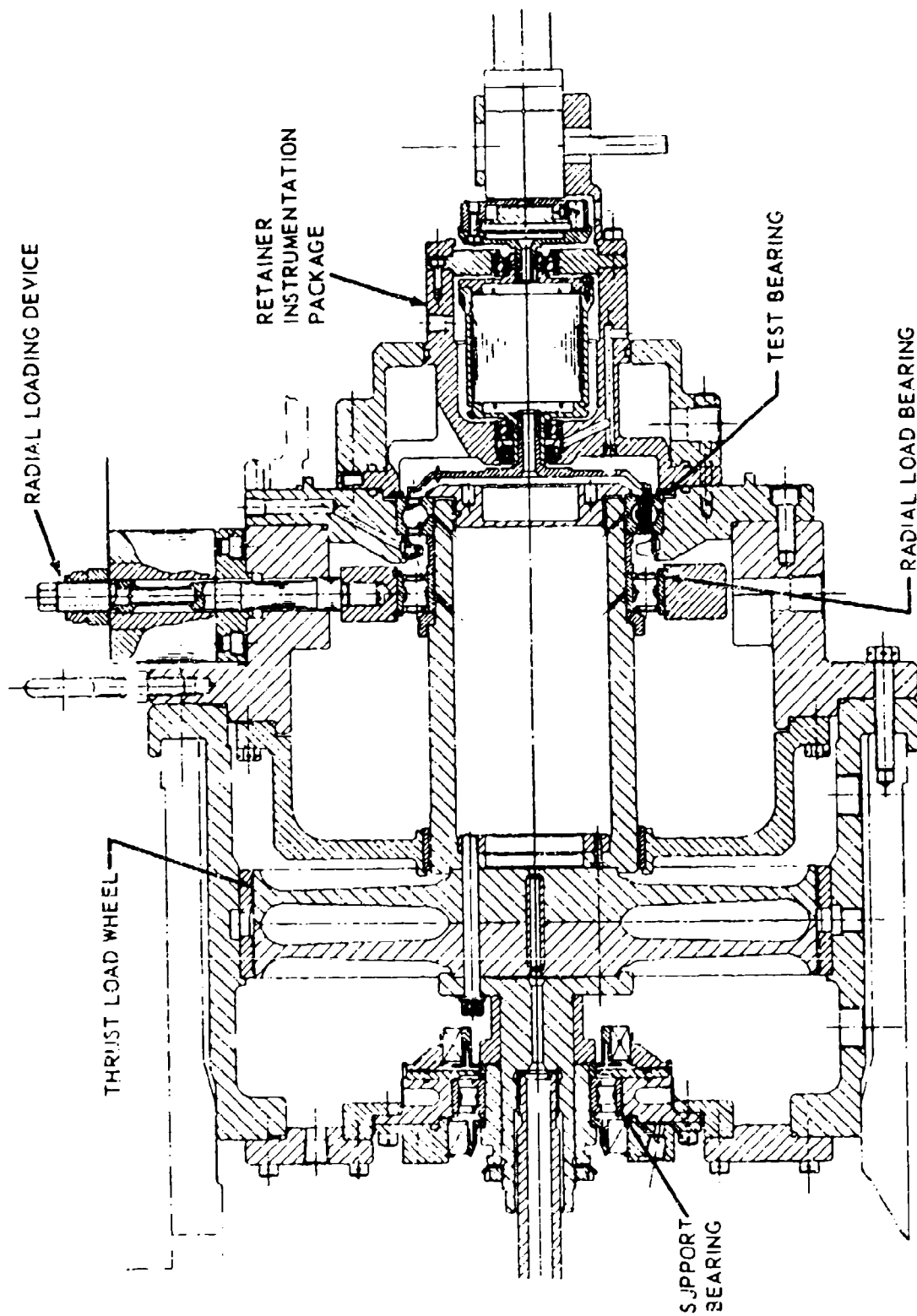


Figure 24. Bearing Test Rig; Cross-Sectional View.

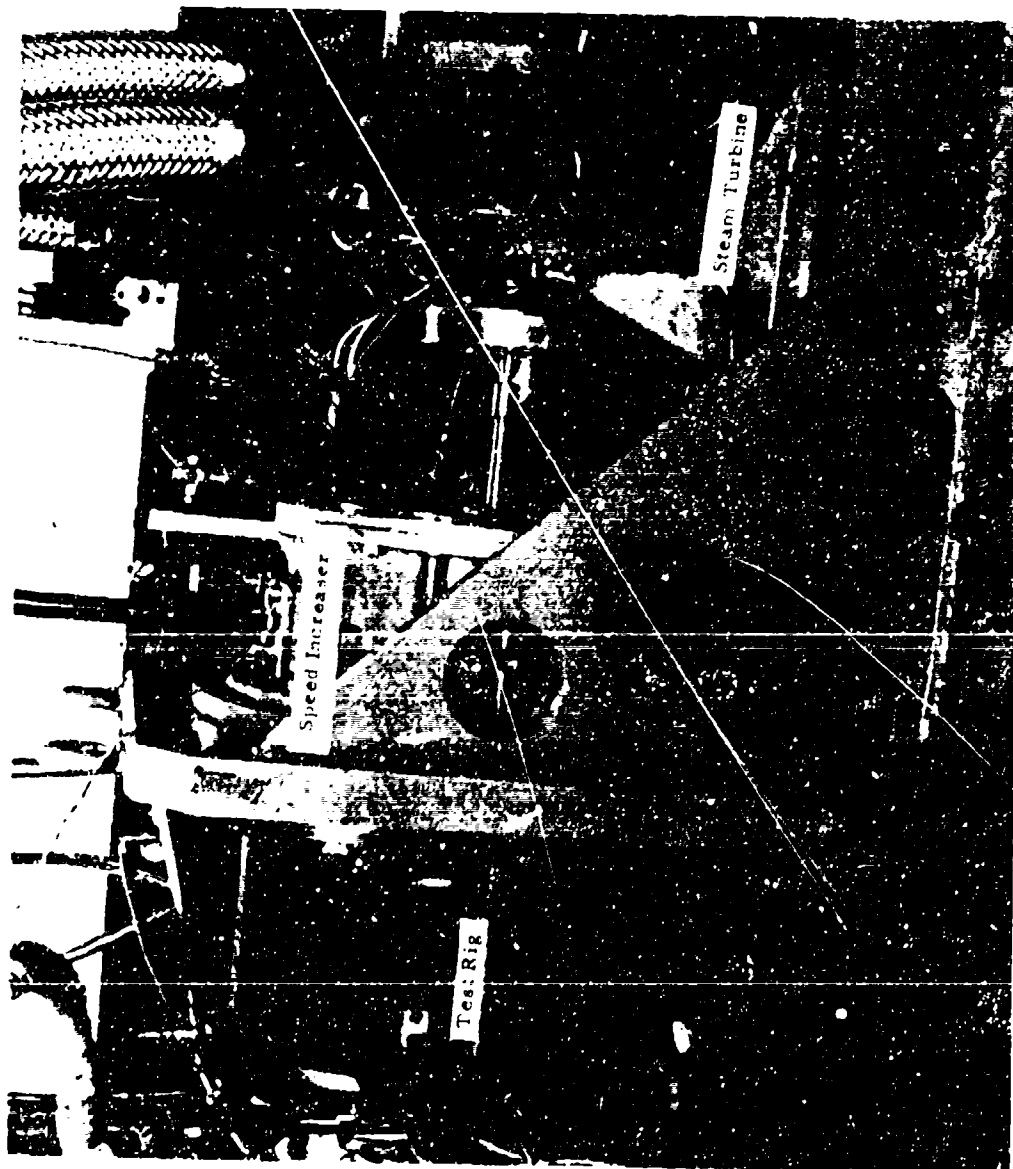


Figure 27. Bearing Test Facility.



Figure 28. Bearing Test Rig: Right Front View.

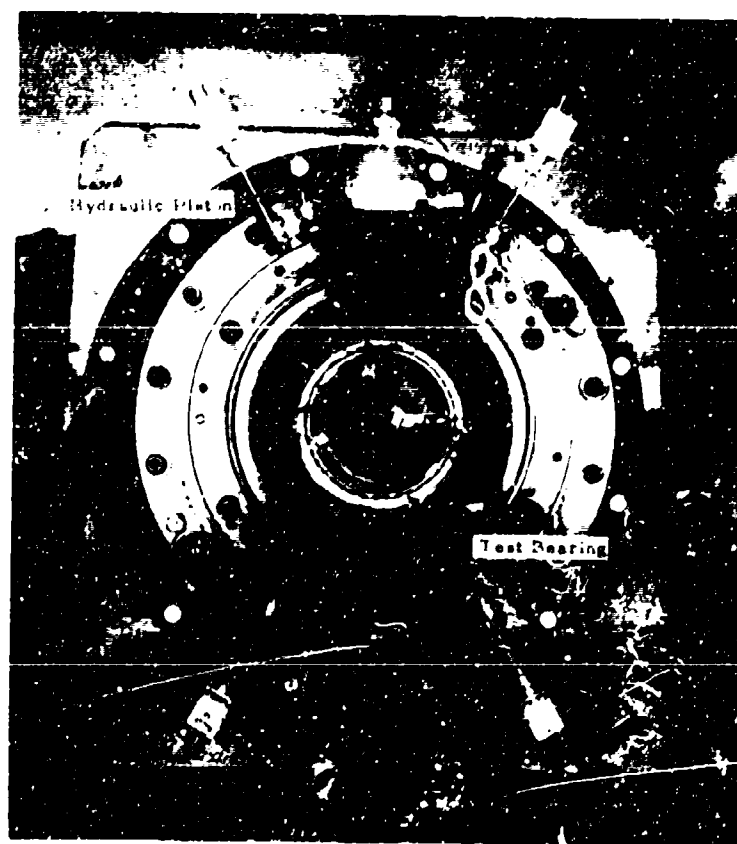


Figure 29. Bearing Test Rig; Front View.

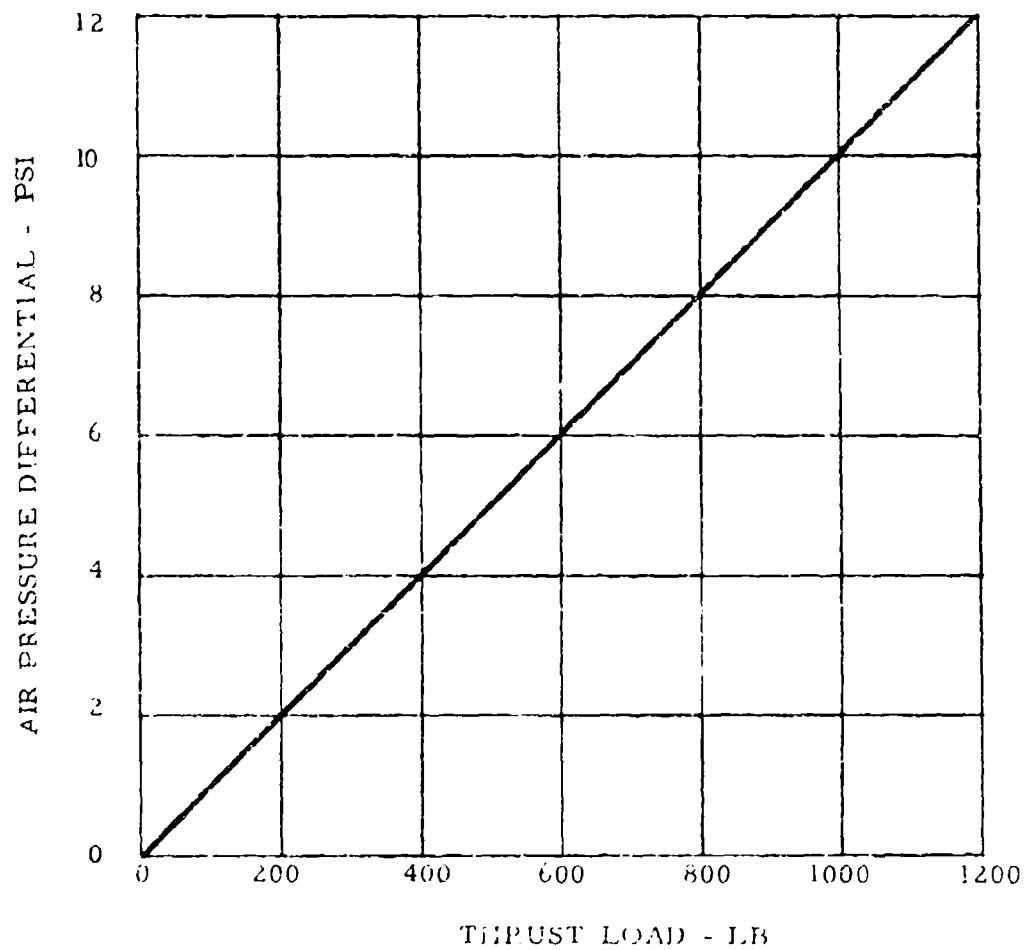


Figure 30. Air Pressure Differential Versus Bearing Thrust Load.

TABLE V. PHYSICAL PROPERTIES OF MIL-L-23699 OIL,
CODE 0-64-2

MATERIAL EXAMINATION REPORT

MATERIALS LABORATORY

0-64-2

AVCO LYCOMING DIVISION

Lab No. _____

Lot No. _____

P. O. _____ R. R. _____ Quantity 1 qt Date 4/28/70

Batch No. _____ Mfr's Dsgn. _____ Date of Synthesis _____

Specification MIL-L-23699 Vendor _____

From _____ Condition _____

TEST	REQUIREMENTS	VENDOR	LYCOMING	DISP.
Viscosity at 100°	25 cs min		27.71	Accept
Viscosity at 210° F	5.0 to 5.5 cs		5.91	Reject
Flash Point, min	450° F		490	See
Pour Point, max	-65° F		L-65	Note
Evap. Loss, 400° F/ 6 hr	10% max by wt		8.3	
Color, ASTM	Report		3	
Foam, max, 75° F	Volume/collapse 25 ml/1 minute		15/45 sec	
200° F	25 ml/1 minute		5/4 sec	
75° F after 200° F	25 ml/1 minute		10/20 sec	
Visual	Transparent, Uniform No sediment, etc.		Clear	
Neutralization No.	0.50 max		.12	
"F" Rubber Swell, % 400° F/72 hr	+10 to +25		23.5	
Cracking Under Tension	None		None	
Trace Sediment	.005 ml		<.005	

By _____ Date 5/25/70

NOTE: Infrared indicates material to be similar to Mobil Jet II

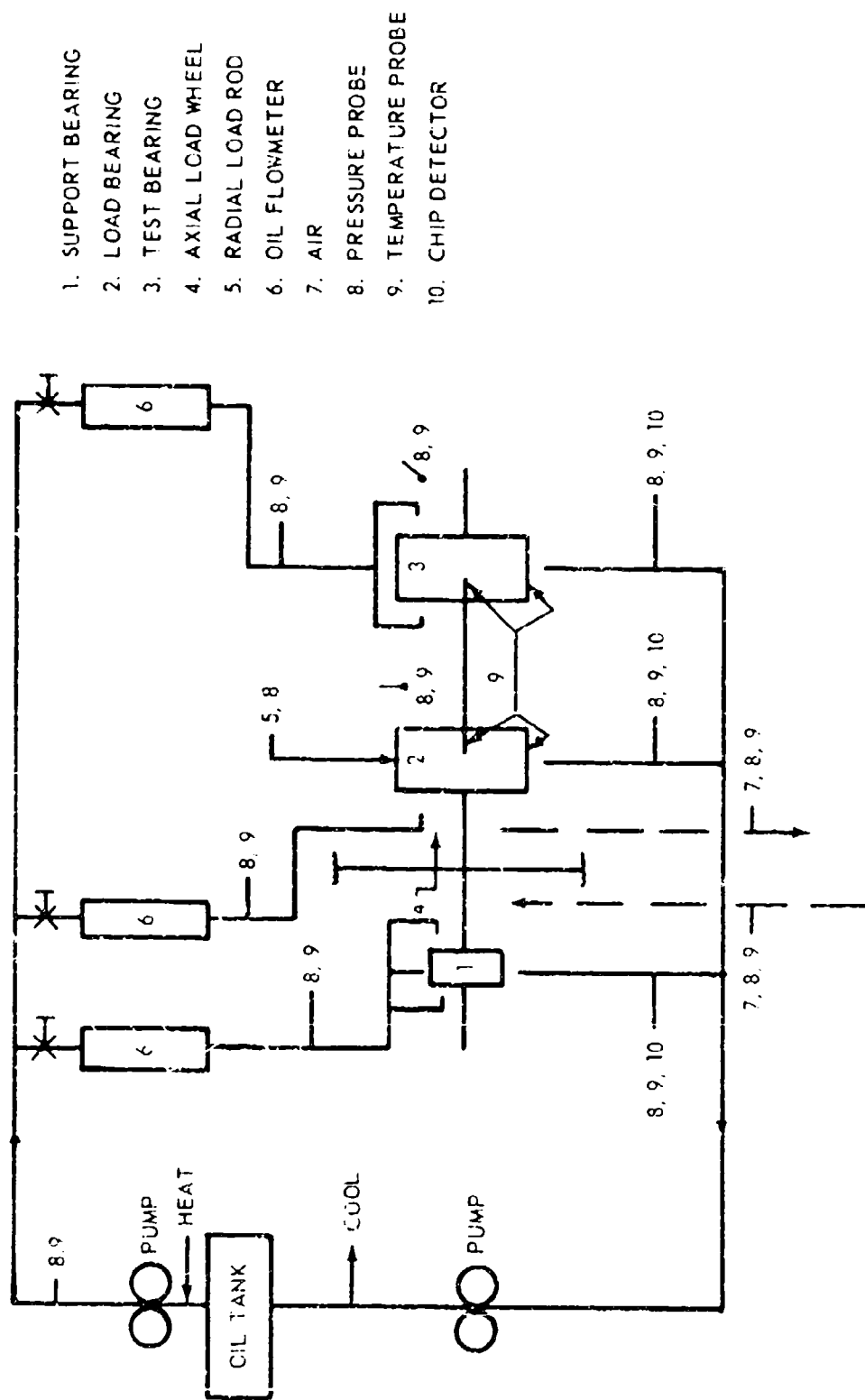


Figure 31. Test Rig Facilities; Schematic Diagram.

Sheet No. 1

ENGINE N/A LYCOMING GAS TURBINE TEST DATA
 TEST TITLE Configuration Ball Brg CONTRACT DATE TEST CELL 4
TEST TITLE Bearing Retainer Analysis Test Rig OPERATOR OBSERVER

RUN NO.	TIME	Temperature										Oil In Test Brg	Oil Out Test Brg	Oil In Sup Brg	Oil Out Sup Brg	Roller Brg	Test Ball Brg
		Brg Output C.B.	C.B. Out	Oil In	Oil Out	Oil In Test Brg	Oil Out Test Brg	Oil In Sup Brg	Oil Out Sup Brg	Oil In Sup Brg	Oil Out Sup Brg						
1		10	11	12	13	14	15	16	17	18	19	20	21	22	23	24	
2																	
3																	

Sheet No. 2

ENGINE N/A LYCOMING GAS TURBINE TEST DATA
 TEST TITLE Configuration Ball Brg CONTRACT DATE TEST CELL 4
TEST TITLE Bearing Retainer Analysis Test Rig OPERATOR OBSERVER

RUN NO.	TIME	Test Brg Cav Press	Oil Mist Multi-Phase	Oil In Sup Brg	Oil Out Sup Brg	Supply Air Mist	Pressure Gear Box Oil	Oil In Test Brg	Oil Out Test Brg	Fwd Wheel Thrust Load	Aft Wheel Thrust Load	Oil Flow Test Brg	Oil Flow Sup Brg	Vib. Turb Dis/ Vel	Vib. G. B. Rig Dis/ Vel
2															
3															

Figure 32. Typical Data Sheets.

TEST BEARING DESCRIPTION

Ball Bearings

The ball bearings used for the test program are typical of main shaft thrust bearing designs of aircraft gas turbine engines. The bearing design is of an angular contact, split inner ring configuration with a one-piece, machined, outer-land-piloted retainer. Complete design details are given in Figure 33 (PSK 18123). Some modifications to the test bearing were made to obtain desired inner and outer race surface texture.

One test bearing, S/N 003, was reworked to produce a race surface roughness of 5AA maximum; another, S/N 006, was reworked to produce a race surface roughness of 24AA maximum. This rework was done in order to evaluate the effect of surface texture/EHD film interaction upon bearing performance. Calculations indicate that the film thickness-to-composite surface roughness factor for the 5AA finish bearing at 100° F oil-in temperature and 20,000 rpm is greater than 4.0, and consequently the bearing would operate with full film separation of the contacting surfaces. In contrast, the bearing with the 24AA surface finish would have a film thickness-to-composite surface finish factor of less than 1.0 at 200° F oil-in and 20,000 rpm, and it should operate without full film lubrication, i. e., with boundary lubrication.

Modifications to the retainer were also required to facilitate the placement of strain gages for pocket load measurements. Undercuts were machined into three adjacent pockets as indicated in Figure 34 (PSK 17438). The undercuts provide a recess in the pocket to prevent contact of the strain gages with the ball, and also increase the flexibility of the cross beam section to produce measurable strain levels for load measurements under the anticipated force levels.

A complete pretest dimensional inspection of the test bearings was performed on critical dimensions and characteristics. Clearances, surface textures, groove radii, race runouts, etc., were measured and recorded, and are presented in Table VI and Figures 35 through 42.

Roller Bearings

The roller bearings employed for the test program are also typical of main shaft gas turbine designs. The bearings incorporate cylindrical rollers in a one-piece, machined retainer that is piloted on inner ring shoulders. Bearing details are presented in Table VII.

Test retainer modifications similar to the ball bearing retainer modifications were required to provide for strain gage placement and suitable beam flexibility to facilitate measurement of the pocket loads, as depicted in Figure 43. Here, also, a complete pretest dimensional inspection was performed on the critical characteristics of the bearing. Results are presented in Figures 44 through 47.

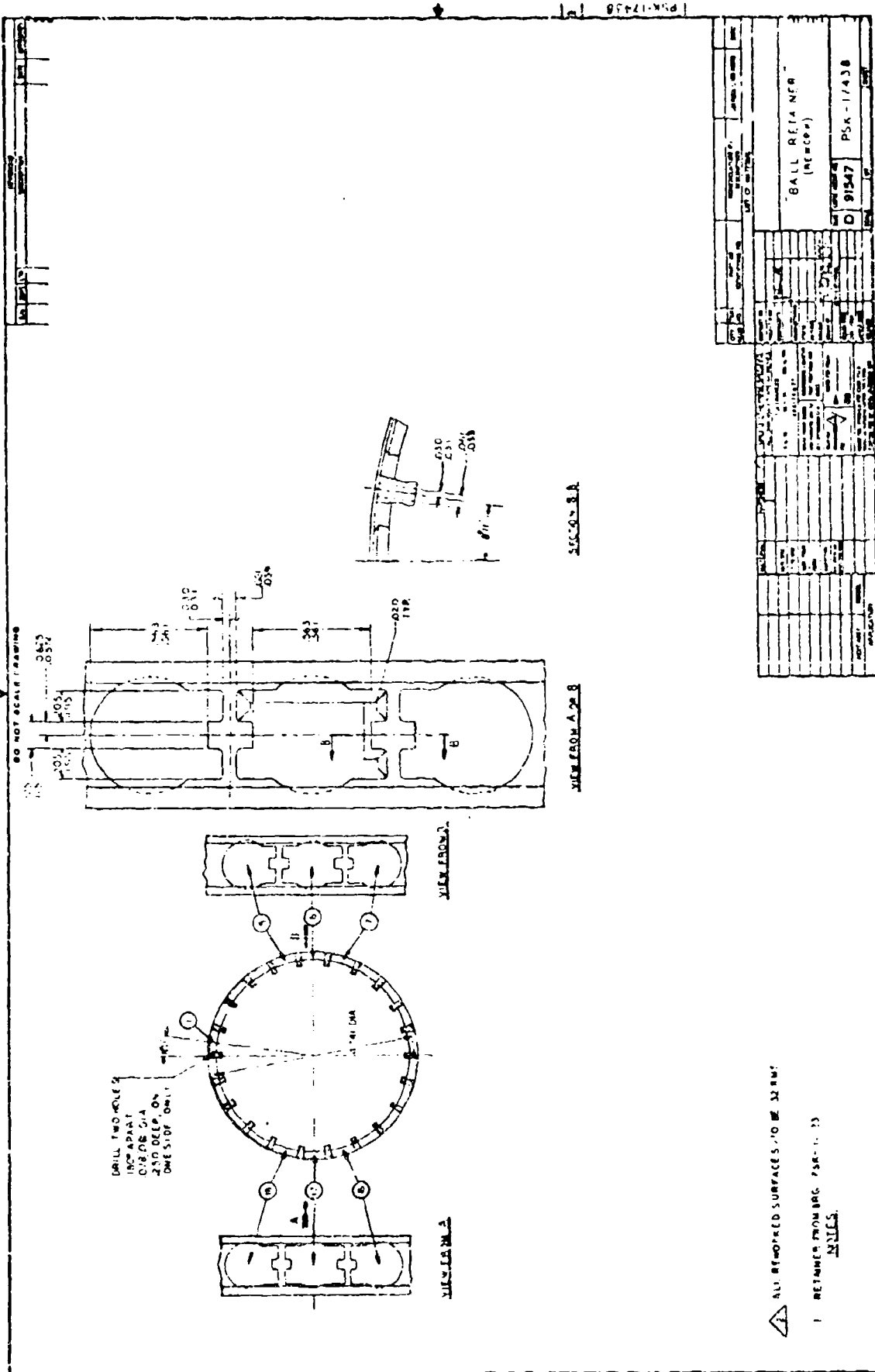


Figure 34. Ball Retainer Rework PSK 17438.

TABLE VI. TEST BALL BEARING INSPECTION DATA, DETAIL INTERNAL GEOMETRY		
	Bearing S/N	
	003	006
Outside Diameter (in.)	5.5110/5.5109	5.51163/5.51162
Inside Diameter (in.)	3.9360/3.93596	3.9366/3.93665
Ball Diameter (in.)	.53105	.53103
Inner Race Finish (AA)	4-5	30-35
Outer Race Finish (AA)	4-5	24
Ball Finish (AA)	3	2.5
Internal Clearance (in.)	.0050	.0045
Inner Race Groove Radius (thrust)	.2728	.27676
Outer Race Groove Radius	.2728	.2753
Inner Race Groove Radius (nonthrust)	.2741	.27676

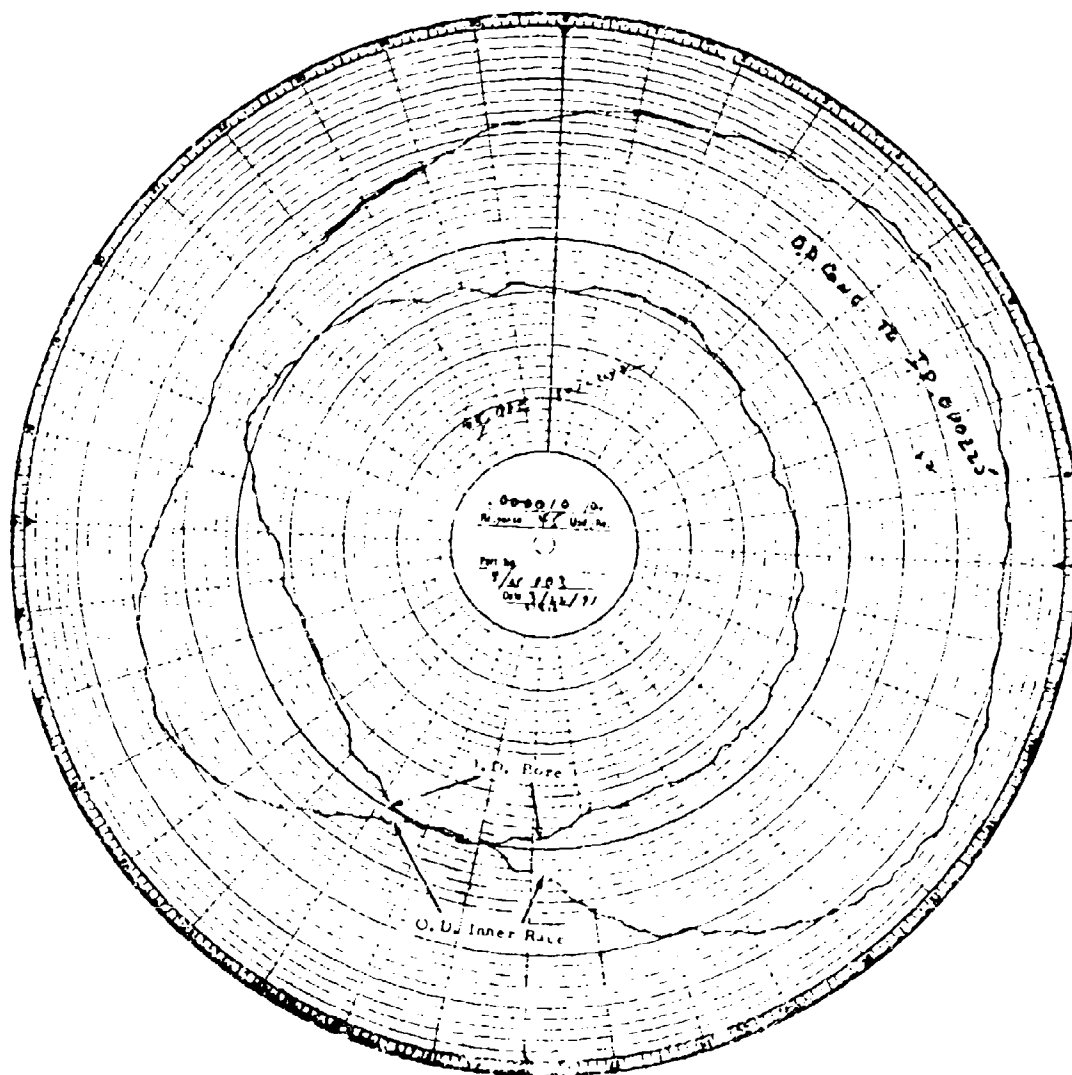


Figure 35. Ball Bearing S/N 003 Inner Race Roundness and Concentricity.

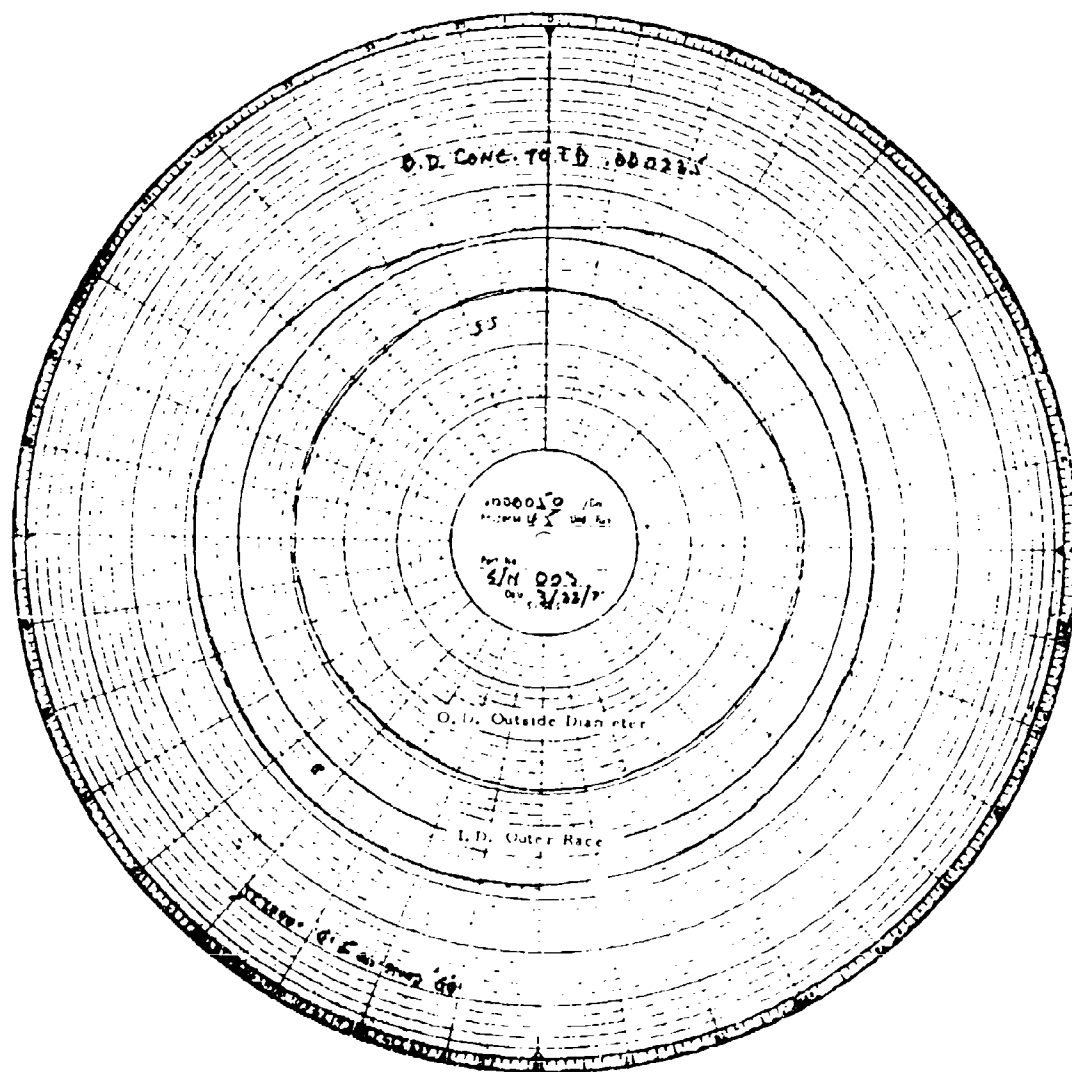


Figure 36. Ball Bearing S/N 003 Outer Race Roundness and Concentricity.

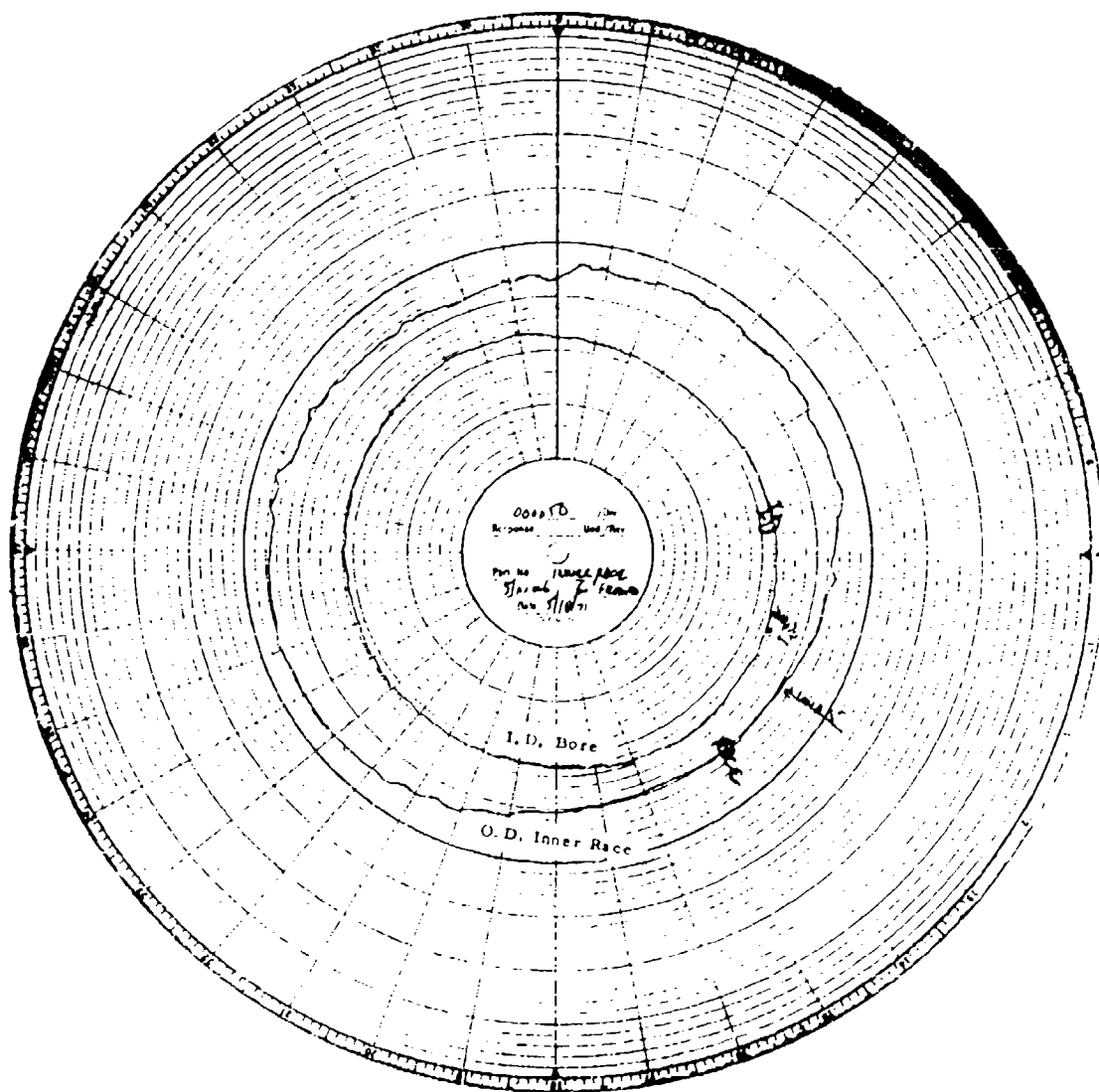


Figure 37. Ball Bearing S/N 006 Inner Race Roundness and Concentricity.

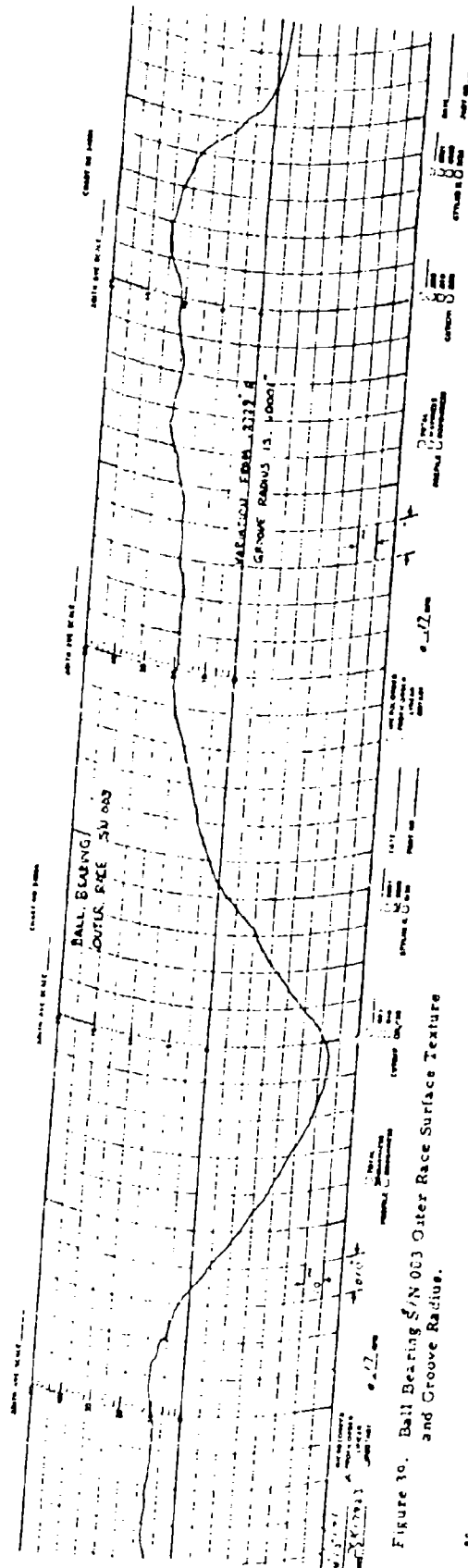
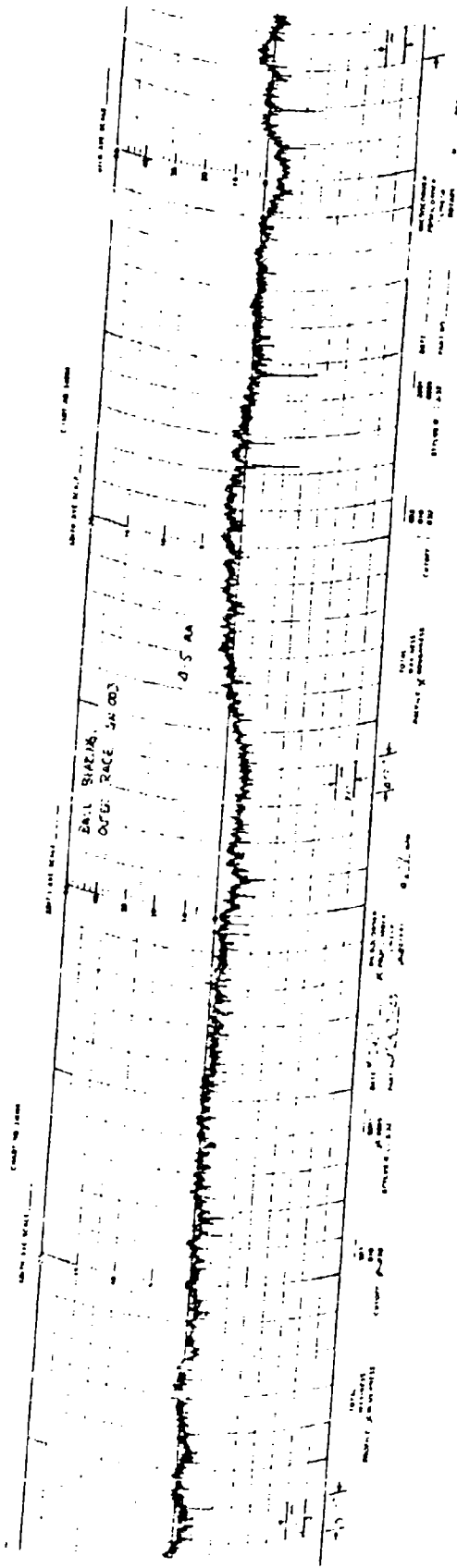


Figure 10. Ball Bearing S/N 003 Outer Race Surface Texture and Groove Radius.

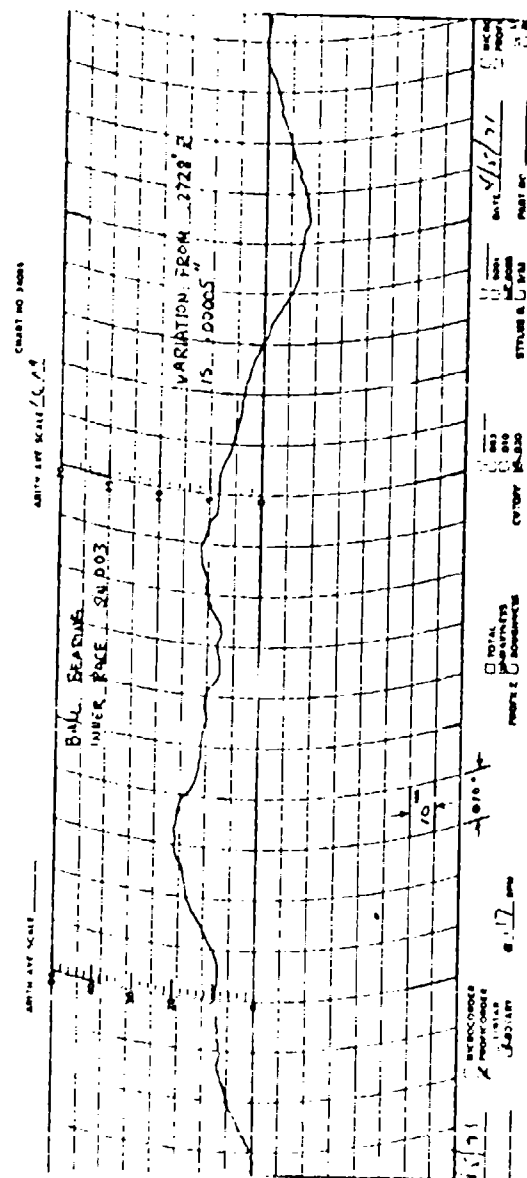
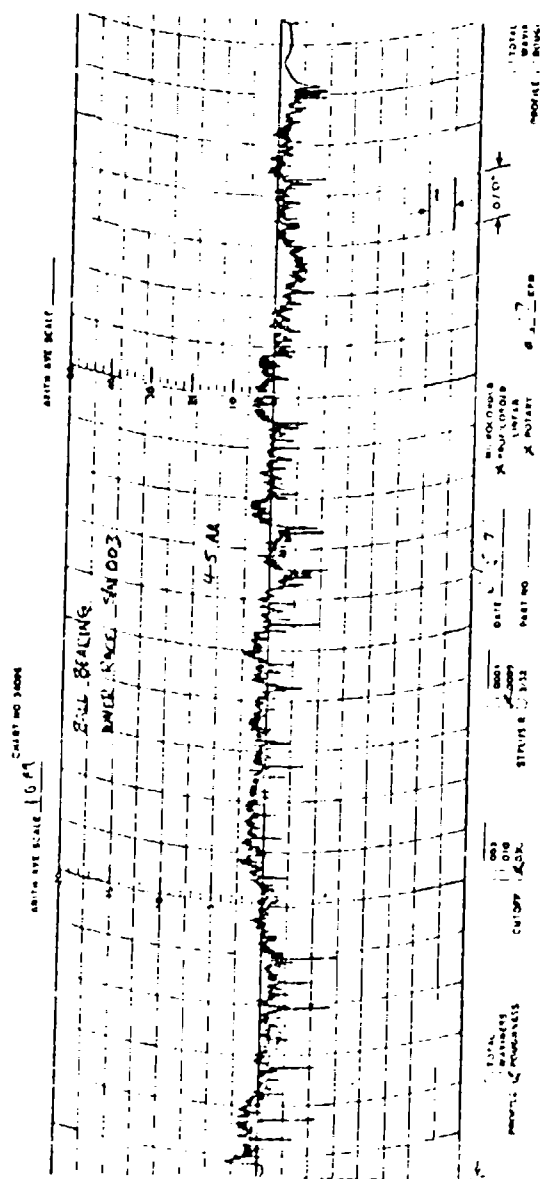


Figure 40. Ball Bearing S/N 003 Thrust Inner Race Surface Texture and Groove Radius.

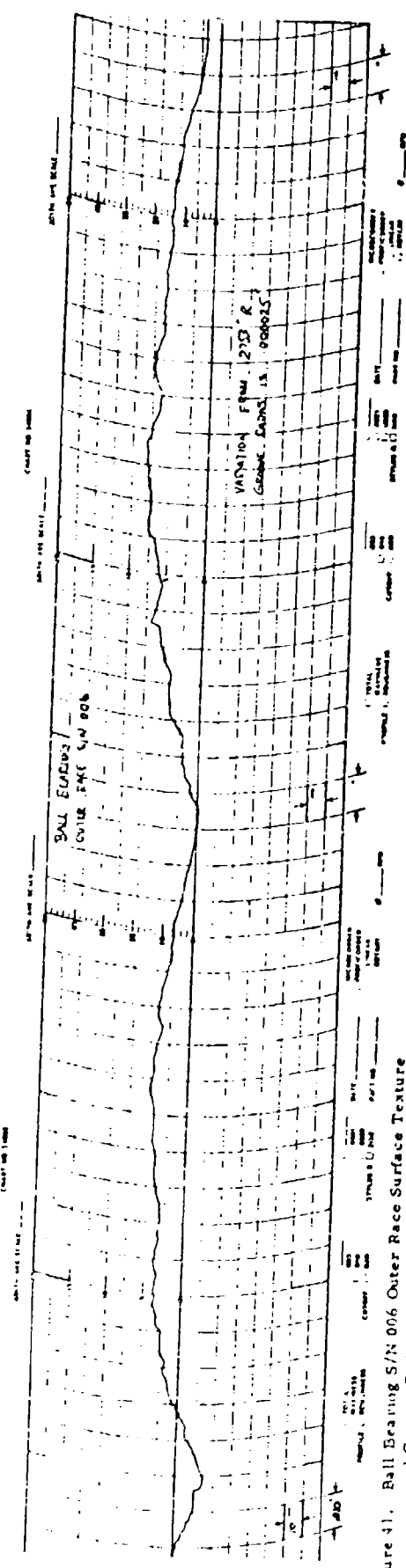
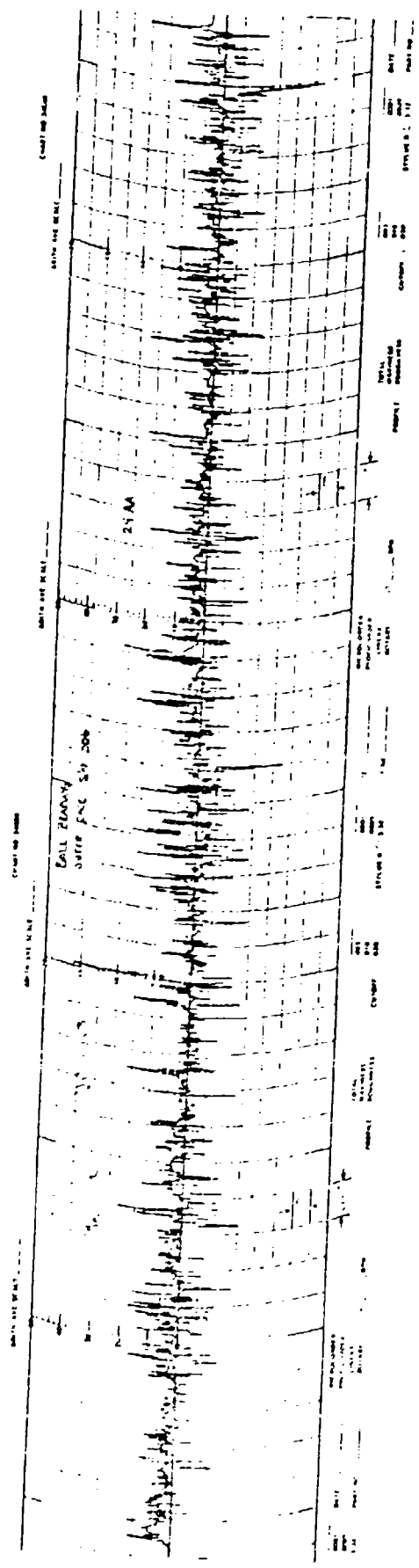


Figure 41. Ball Bearing S/N 006 Outer Race Surface Texture and Groove Radius.

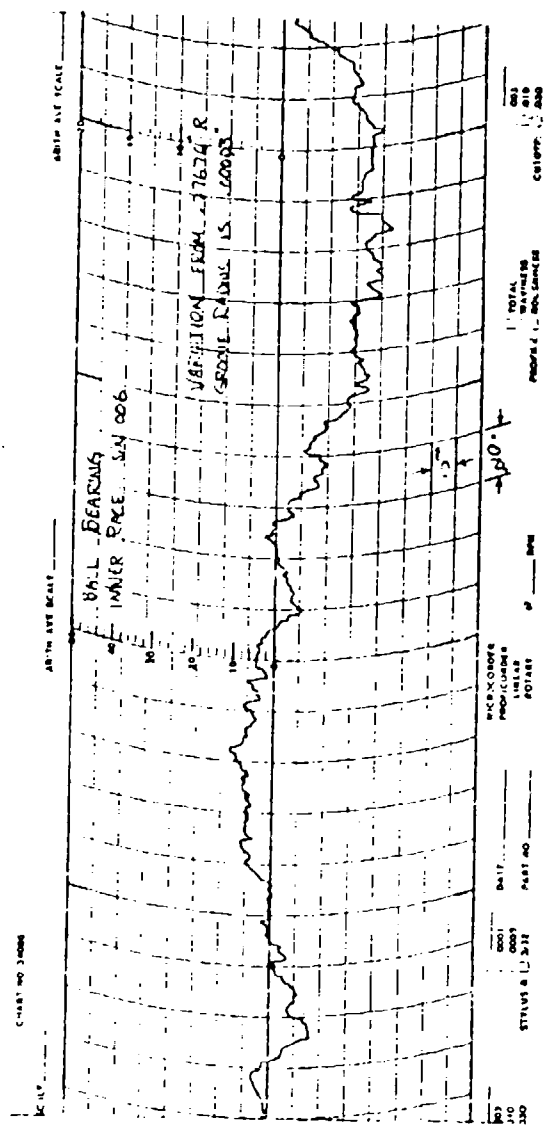
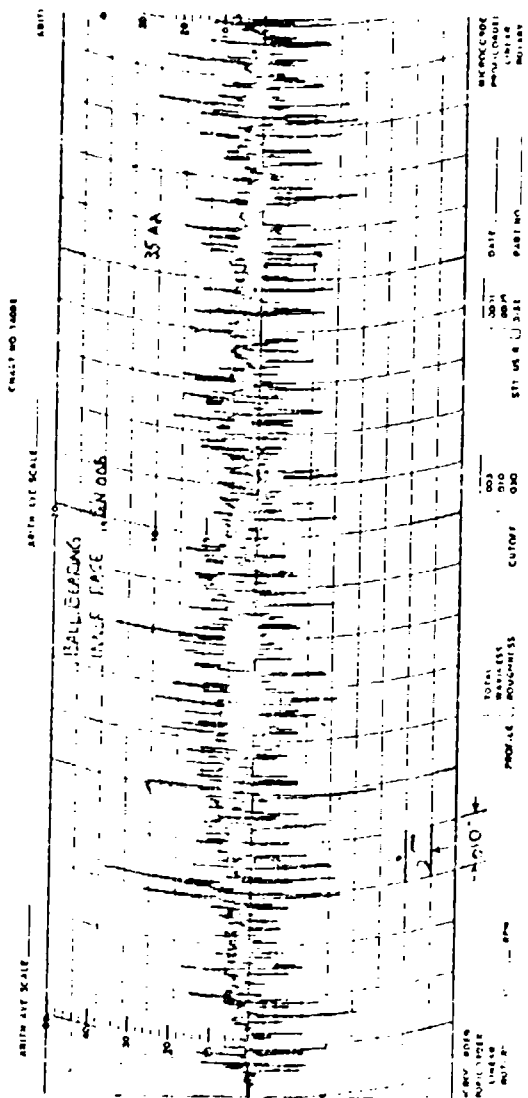


Figure 42. Ball Bearing S/N 006 Thrust Inner Race Surface Texture and Groove Radius.

TABLE VI. ROLLER BEARING ENGINEERING DATA	
Lycoming Identification	MRC R-19 20-C
Bearing Application	Test Rig
Bearing Type	Straight Thru Outer
RBECC Grade	5
Bearing to Conform to Lycoming Specifications	P6903, E-1004
Bore	100 MM
Outside Diameter	140 MM
Width	20 MM
Number of Rollers	28
Roller Diameter	11 MM = .4331
Roller Length	11 MM = .4331
Roller Pitch Diameter	4.7244 Ref.
Roller Diameter Variation	+ .000025
Roller Length Variation	+ .0001
Roller End Radius	.030/.040
Roller Crown Radius	35.0
Roller Flat Length	.144/.271
Roller Ends Square to Outside Diameter	.0001
Parallelism of Roller Active Surface	.000050
Diametral Clearance under 11-lb cage load	.0055
Inner Ring Shoulder Height, $\frac{1}{2}$ of Roller Diameter	22%
Outer Ring Shoulder Height, $\frac{1}{2}$ of Roller Diameter	NA
Inner Ring Shoulder Diameter	4.472/4.469
Outer Ring Shoulder Diameter	NA
Cross Corner Dimension	NA
Roller to Shoulders End Play	.0005
Runway Surface Finish	6RMS
Roller Diameter Surface Finish	3RMS
Roller Ends Surface Finish	3RMS
Ring Pilot Surface Finish	16RMS
Retainer Pilot Surface Finish	20RMS

TABLE VII - Continued

Roller and Ring Material	SAE 52100 Steel
Roller and Ring Hardness	R _C 58-62
Retainer Material	Bronze
Retainer Hardness	
Retainer Plating	AMS 2412
Retainer Plating Thickness	.0005/.0015
Material Stabilized to Operate at	-65° to +350°F
Pilot Surface	Inner
Pilot Clearance (Total Diametral)	.025 - .035
Roller Axial Pocket Clearance	.010/.015
Roller Circumferential Pocket Clearance	.007/.012
Minimum Retainer Pocket Corner Radii	
Retainer Face to Bearing Face Clearance, Min. End Play Removed	
Roller Pocket Location in Retainer - Axially	.001 min
Roller Pocket Location in Retainer - Circumferentially	
Minimum Retainer Web Section	
Minimum Retainer Land Width	
Retainer Pilot Surface Runout	
Retainer O.D. to Bore Concentricity	
Type of Retention	Snap-In Type
Max/Min Diameter Over/Under Roller	
Minimum Roller Drop	.035 max
Runout of Outer Ring Shoulder Diameter	
Runout of Inner Ring Shoulder Diameter	
Note: Cage, Inner Race and Rollers are Nonseparable.	

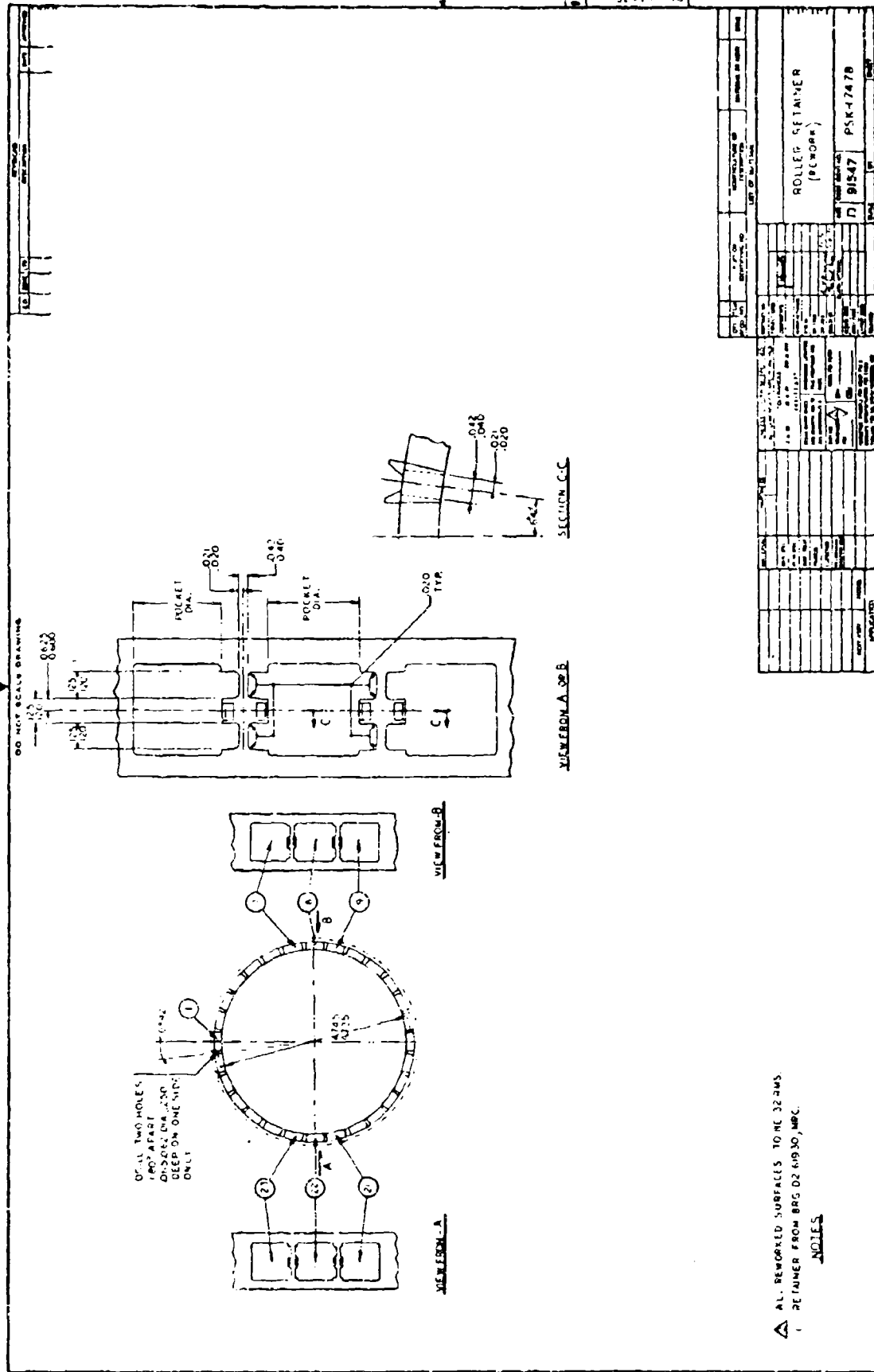


Figure 43. Roller Retainer Rework PSK 17478.

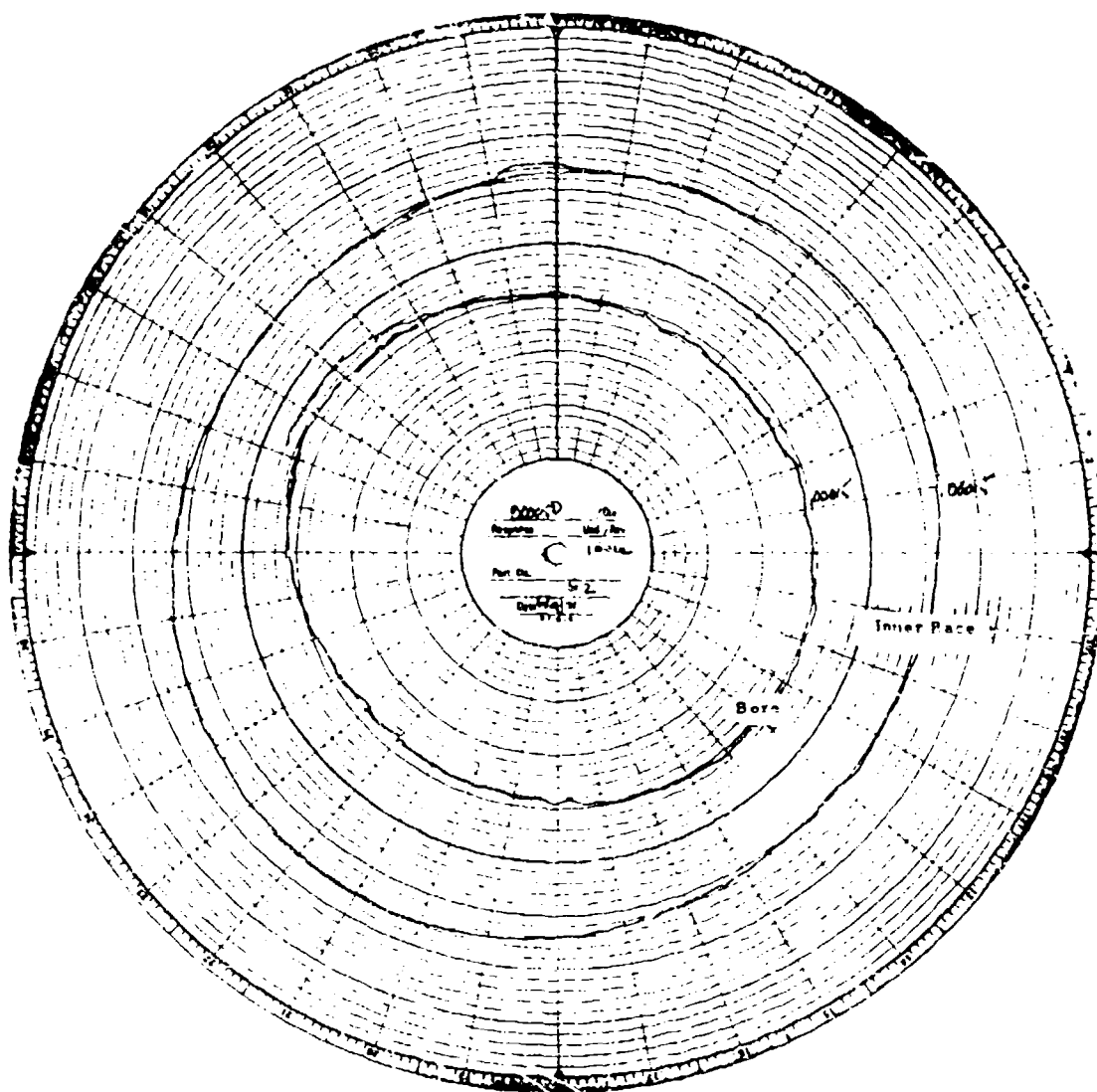


Figure 45. Roller Bearing Inner Ring Roundness and Concentricity.

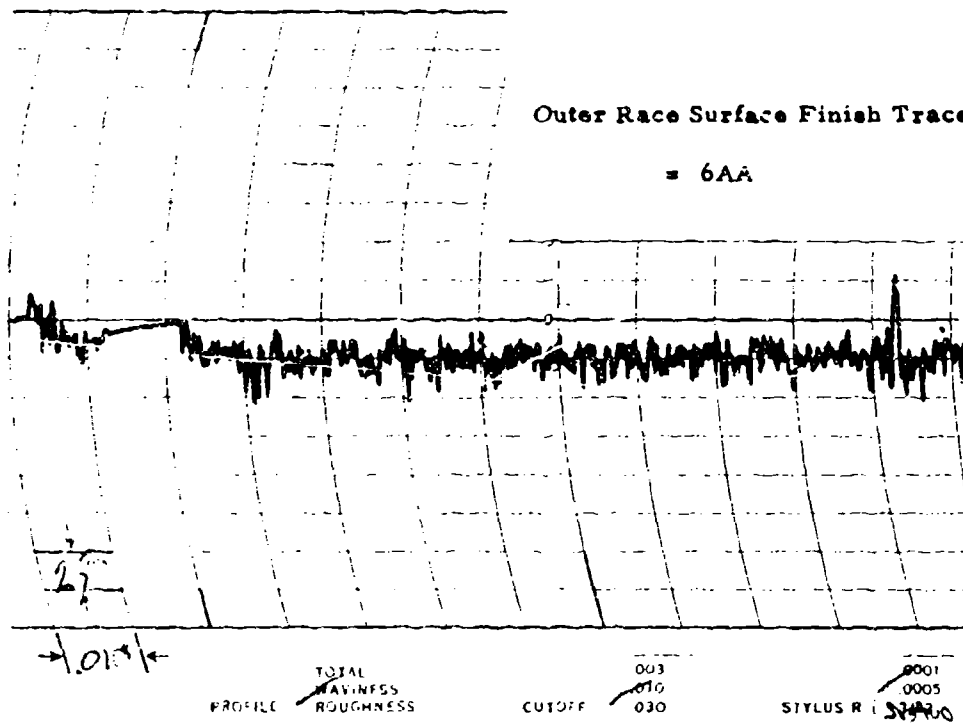


Figure 46. Roller Bearing Outer Race Surface Finish.

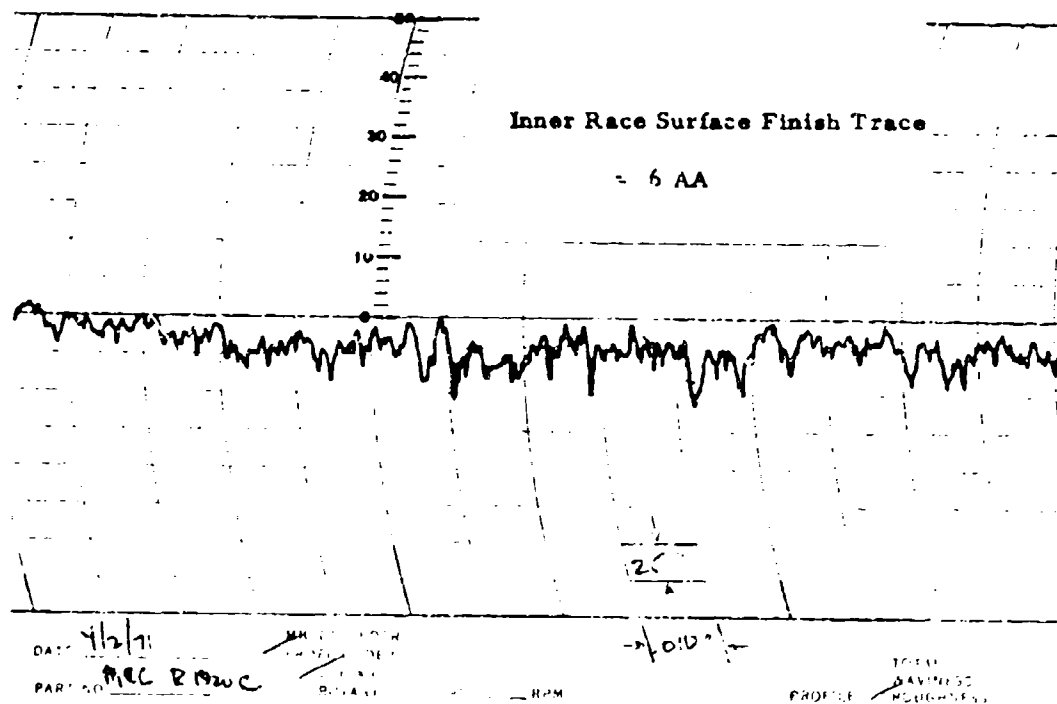


Figure 47. Roller Bearing Inner Race Surface Finish.

INSTRUMENTATION

Instrumentation was incorporated in the bearing retainer test vehicle (F/N TE 21869), Figure 48, to measure the following key parameters:

1. Inner race temperature - °F
2. Outer race temperature - °F
3. Bearing retainer speed - rpm
4. Inner race speed - rpm
5. Radial load on bearing - lb
6. Force exerted by ball/roller on the bearing retainer pocket - lb
7. Ball attitude and three-axis rotational velocity (ball bearing test only)
8. Torque exerted on the retainer by slip ring drag and inertia - in.-lb
9. Bearing retainer and torque element temperature - °F

Items 1 through 7 were required to compare test results with the computer program output. Item 5 was a measurement duplication. Radial force was applied through a hydraulic ram with a known cross-sectional area with a known pressure. Item 7 was to provide an instantaneous ball attitude readout. Item 8 was to measure and divorce the effects of slip ring and associated hardware from the retainer data required by Item 6. Item 9 was to evaluate the effects of the retainer environment on Items 6 through 8.

A description of each item of instrumentation follows:

1. Inner Race Temperature - Inner race temperature measurement on both the bearing under study and the loading bearing was accomplished by embedding thermocouples in the shaft, which provided intimate contact between the thermocouples and the bearing inner race bore.
2. Outer Race Temperature - Outer race temperatures were measured using standard bayonet-type thermocouples in intimate contact with the outer race outer diameter.
3. Ball Retainer Speed - Speed was measured using a magnetic pickup sensing rotation of the slip ring shaft, which was directly coupled to the slip ring driving plate. The slip ring shaft was manufactured with five small lobes and one large lobe. This large lobe produced a magnetic pickup output greater than the other five. The angular relationship between the large lobe and the location of the instrumented

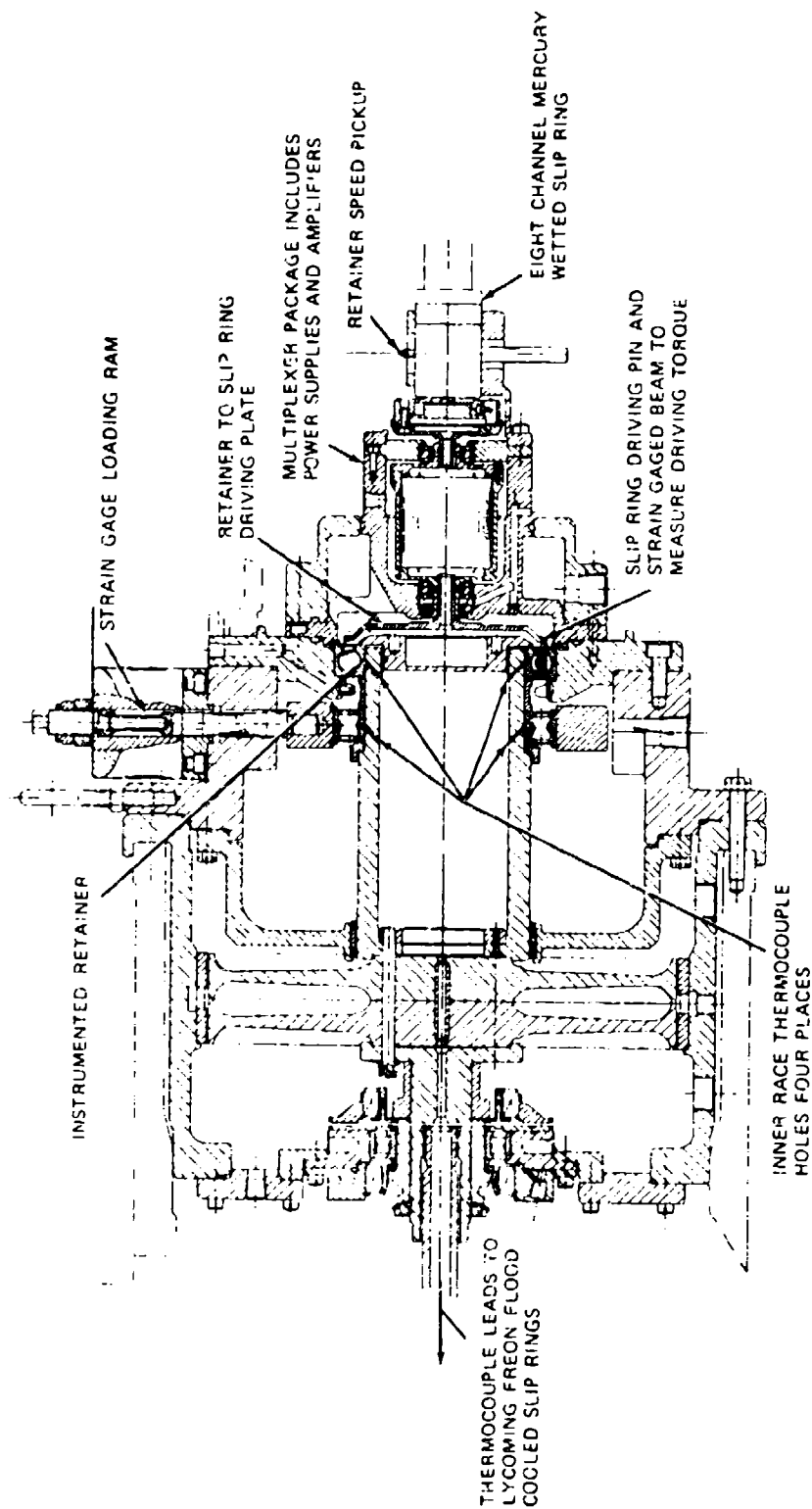


Figure 48. Instrumentation Location.

ball bearing pockets was known, as was the relationship between the stationary magnetic pickup and the point of application of the radial load. A means was thereby provided to relate the speed signal to the angular position of the retainer pockets under study and consequently the ball loading cycle. In the first tests, a strain gage was attached to the outer race to detect ball passing frequency, which is also a function of retainer speed.

4. Inner Race Speed - A magnet pickup was used to detect the speed of a gear directly coupled to the shaft supporting the rotating inner race.
5. Radial Load on Bearing - A hydraulic piston was used to apply radial loads to the bearing. The shaft between the piston loading bearing was instrumented with a four-active-arm strain-gage bridge and was deadweight calibrated. A pressure gage was installed in the line to the piston for cross checking the force on the loading bearing.
- 6a. Ball Force on Bearing Retainer - To measure the force exerted by the ball on the retainer web, two webs were reworked to accommodate the strain gages and increase the strain sensitivity. The two reworked webs were strain gaged with two fully active four-arm bending bridges, Figure 49. The inside of the reworked web was chosen for strain gaging over the outside, as shown. A photoelastic model was used to determine the optimum location. The model showed the outside to be more cross sensitive to other cage loadings (i. e., a ball pushing axially on the cage would cause larger outputs at the outside of the web than at the inside). The strain gage bridges were calibrated. The first retainers were designed for a maximum strain sensitivity for a 50-pound ball load. At the time the retainer instrumentation was designed, accurate estimates of ball forces were not available, and 50 pounds was selected arbitrarily with the knowledge that the retainer could, if found too insensitive, be reworked and made more sensitive. Later retainers were modified for a maximum strain sensitivity at 25 pounds, based on preliminary results of retainer ball load measurements.
- 6b. Roller Force - The same type of strain gage instrumentation employed in the ball force measurements was used in the roller force measurement except that the rework to the retainer was only to accommodate the strain gages, not to increase its strain sensitivity, as the webs were already thin enough for good strain sensitivity.

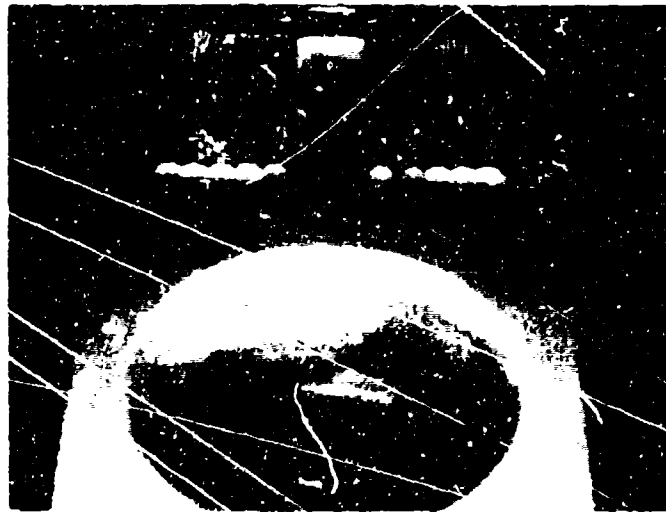


Figure 49. Ball Bearing Retainer Strain-Gage Location and Rework.
 Top: Two additional strain gages are opposite the two shown, and the four gages are wired on a four-arm bending bridge.
 Bottom Left: View looking down through retainer ball pocket shows two instrumented retainer webs, each having a four-active-arm bending bridge. Bottom Right: Overall view of strain-gaged ball retainer pocket webs.

7. Ball Bearing Attitude - Each test ball bearing retainer was instrumented with two sets, three per set, of Hall generators (F. W. Bell Inc. Model 105-225). These generators were not standard. They were built for Lycoming in the smallest size practical (0.050 by 0.060 inch). The temperature resistance was also increased from 200° F for standard items to 248° F for this application. The vendor supplied the characteristics for each generator.

A Hall generator is a device whose voltage output is proportional to a current input and the magnetic field to which the Hall generator is subjected (see sketch below):

$$V_H \propto I_c B (\cos \phi)$$

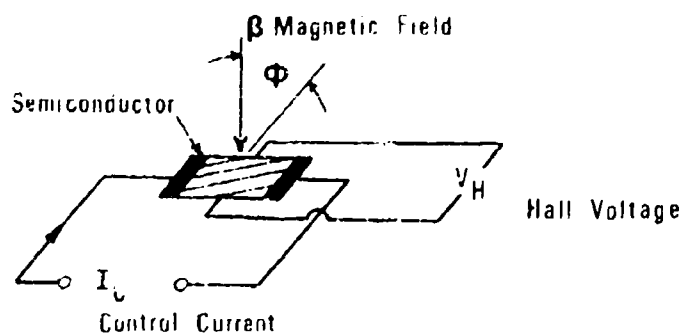
where V_H = Hall voltage

I_c = Hall control current

B = magnetic flux

ϕ = angle between I_c and B

If the control current (I_c) is held constant, the voltage (V_H) is proportional to the magnetic field to which the Hall generator is subjected. Unlike generation of a voltage in a conductor through changing flux fields, the Hall requires no change in flux.



As originally proposed, three mutually perpendicular Hall generators would sense the magnetic field strength of a magnetized ball, making it possible to determine angular location at any instant in time. This was accomplished by producing magnetic poles at 90 degrees to one another. While more than one set of 90-degree poles is possible, it was believed that the resulting confusion and effort required to keep track of similar poles would not be justified. With this arrangement (one set of 90-degree poles), only about 25 percent of the surface of the ball has a field strength sufficient to be detectable by the Hall generators, using the planned generators and ball material. To increase the time during which the ball magnetic field could be sensed, the Hall generators were installed in line at the ball contact point on the retainer, in slightly recessed slots. With the Hall generator and ball bearing material used (M50), sensitivities were so low that the ball clearance had to be reduced to 0.005 inch. Figure 50 shows the Hall generators in place.

Prior to installing the instrumented retainer and magnetized balls in the test rig, each ball was mapped to describe the magnetic field in terms of a Hall generator output versus ball position (Figure 51). This mapping was to be transferred to a large three-dimensional model of the ball. Scale-model Hall generators could then be used to determine the angular position of the ball by rotating the model ball until three voltages obtained from testing matched the three model ball voltages. This position described by three voltages would be unique. It would describe the angular position of the ball with respect to the retainer. This process repeated at defined small time intervals over small azimuth angles would provide three-axis rotational velocities at these angles.

Preliminary static and low-speed laboratory tests indicated the idea to be feasible. In one test a magnetic ball was calibrated as outlined in Figure 51. The ball was spun in a lathe and the output was observed. The output was as expected. In another test the magnetic ball was placed in an instrumented retainer pocket and rotated slowly by hand using a Plexiglas rod bonded to the ball. The three resulting Hall voltages were observed on three oscilloscope channels.

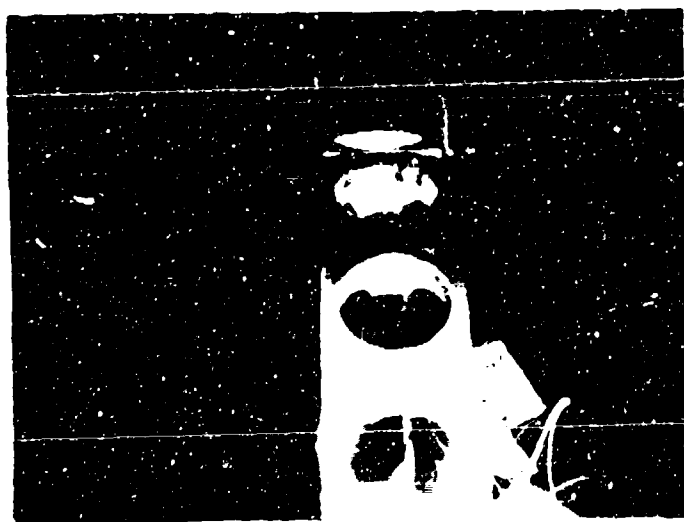
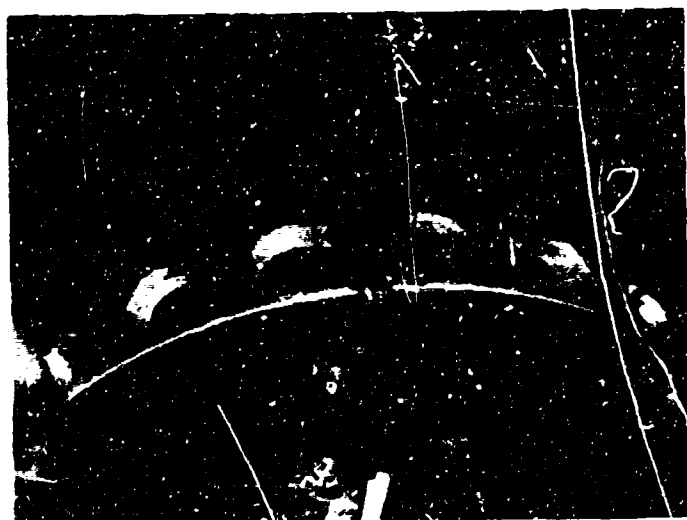


Figure 50. Hall Generators Installed in Ball Bearing Retainer Pockets.
Top: Reworks and Hall lead wire routing. Bottom: Location of Hall generators.



Figure 51. Ball Bearing Magnetic Field Mapping. The magnetic ball is bonded to a Plexiglas rod mounted in a lathe chuck. A Hall generator is mounted on a Plexiglas rod, held in the tool post. In the position shown, the ball is rotated 360 degrees in 20 degree increments. At each increment a reading from the Hall generator is taken. The tool post is then rotated 20 degrees and again the ball is rotated 360 degrees in 20-degree increments. The process is repeated until the mapping is complete.

8. Slip Ring Driving Torque - The bearing retainer would be driving a slip ring and multiplexer system, which it would not normally do. The torque required to drive the slip ring was measured by instrumenting the slip ring driving plate with two strain-gaged cantilever beams. The gaged beams were calibrated for torque and for temperature. The slip ring assembly and driving plate are shown in Figure 52.

The torque system was designed to read torque in one direction, but these tests showed that significant vibratory torques occur.

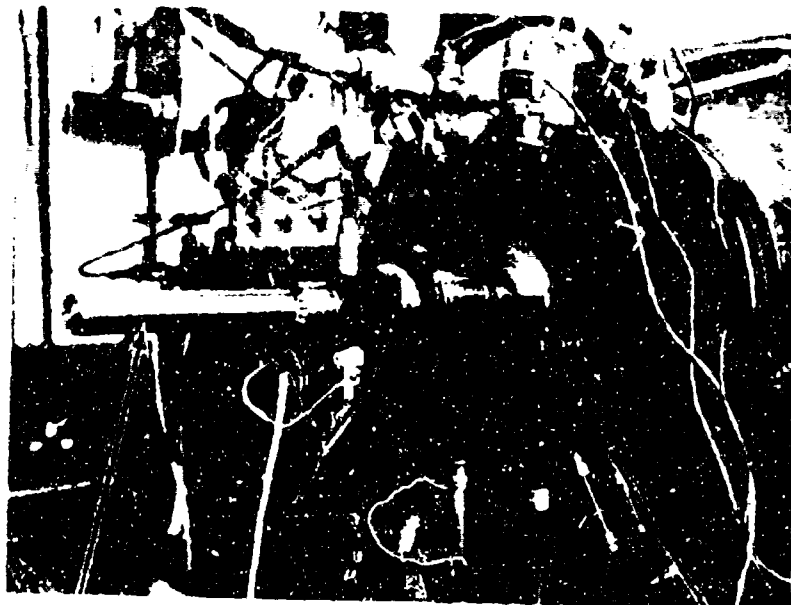
9. Retainer and Torque Element Temperature - To be able to compensate for temperature effects on the retainer strain-gaged bridges, torque element strain-gaged bridges, and Hall generators, thermocouples were installed at these locations.

DATA ACQUISITION

Retainer Data Transmission

The large number of signal leads from the retainer, 12 leads for the Hall generators, 8 leads from the ball force bridges, 4 leads from the torque bridge, and 6 leads from the thermocouples, would have required 30 slip ring channels. If common grounding were used, 26 channels would be required. Slip rings of this size would inherently have large drag characteristics. A mercury-wetted slip ring with 16 channels was proposed, but this is not a developed item and nonrecurring engineering cost would have been excessive. An eight-channel mercury-wetted slip ring was available, but if this were employed, data could not be taken simultaneously from Hall generators, ball force gages, and the torque driving plate. Simultaneous data acquisition was a goal. The problem of a large number of signals and the requirement for simultaneity suggested the use of a multiplexer.

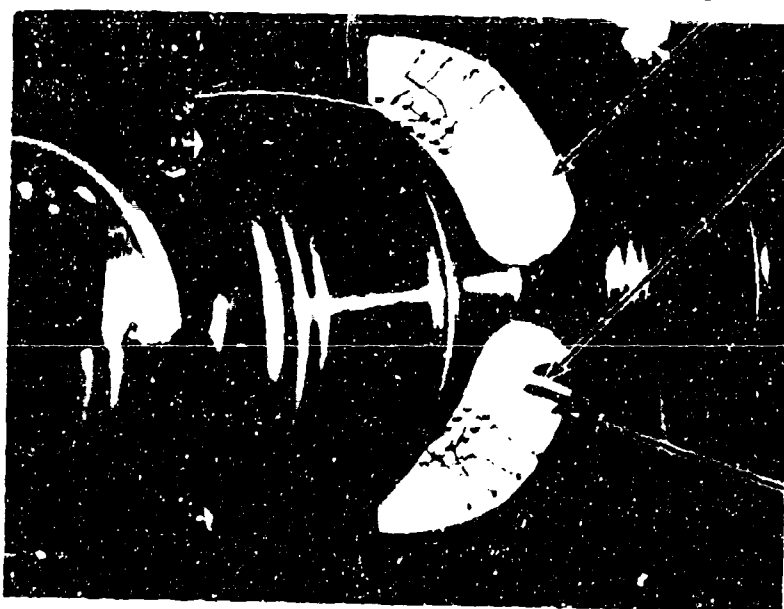
A multiplexer system, which was designed and built at Lycoming, incorporated constant-current power supplies for the Hall generators, constant-voltage power supplies for the strain-gaged bridges, compensating networks and cold-junction reference for the thermocouples, and buffer amplifiers with a gain of 100 for the output from all the previously mentioned channels. Coupled with an eight-channel mercury-wetted slip ring (Vibro-Meter SA Model MT8/A), this system provided close to the



Slip Ring

Driving Plate

Lead Wires From
Bearing Retainer Driving Plate



Instrumented Canti-
lever To Measure Slip
Ring Driving Torque

Driving Pin From
Retainer - A
Second Pin Is 180
Degrees From One
Shown

Figure 52. Slip Ring and Driving Plate. Top: Overall view.
Bottom: Closeup of driving plate. Rotation is
counterclockwise.

desired goal for obtaining simultaneous data from the rotating retainer instrumentation. The 30 leads were reduced to four through multiplexing, and three slip ring channels were required to power and sequence the multiplexer. The multiplexer was time divided, with the output from the Hall generators being multiplexed simultaneously, the output from the strain-gaged bridges being displayed simultaneously, and the output from thermocouples being displayed simultaneously. The switching rate of the multiplexer could be varied from 0.1 time per second to in excess of 10,000 times per second. Figure 53 shows typical outputs from the multiplexer.

Inner Race Temperature Data Transmission

The rotating inner race temperatures were transmitted through Lycoming-developed Freon flood-cooled slip rings coupled to the rear of the shaft supporting the test bearing inner race.

Recording

All signals except the inner race temperatures were recorded on magnetic tape. Lockheed tape recorder Model 417D was used. The frequency response of this system is 10,000 Hertz. Signals from the inner race were displayed on instrumentation in the test cell and were manually recorded.

Monitoring

During all testing, inner race speed, retainer speed, inner race speed ratio, ball force, radial load, and driving torque were monitored before and after magnetic tape recording. This procedure assured that the quality of the signals was maintained throughout the recording process.

Problem Areas

During this test program three bearing failures occurred which resulted in the loss of data and the elimination of certain instrumentation.

The first failure (a smooth-race ball bearing) was due to shaft unbalance. This failure also resulted in the loss of a Hall generator-instrumented retainer and multiplexer (Figure 54).

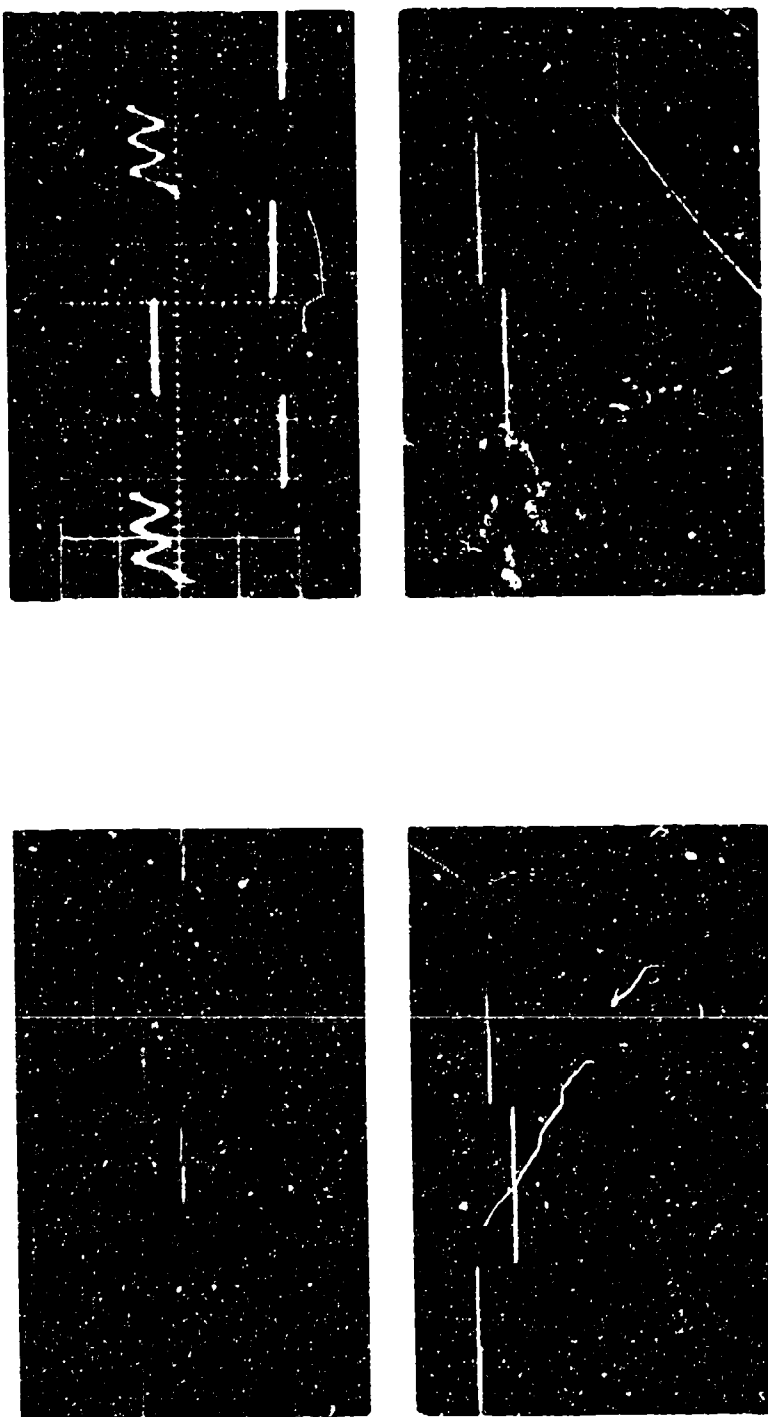


Figure 53. Typical Multiplexer Outputs. Top Left: Output from multiplexer when four different DC voltages are input to the four multiplex channels. Top Right: Output from multiplex when (from left to right) a sine wave is input to the first channel, and a DC voltage is input to the second channel. Zero input to channel (to be used as a reference channel) and same voltage input to channel two is input to channel four. Bottom Left and Right: Outputs from multiplexer just prior to running. Note shift in output of channel four during calibration of one of the web force strain-gage bridges. The shift is approximately 0.2 volt and is equal to 9 pounds of force acting on the retainer pocket web.

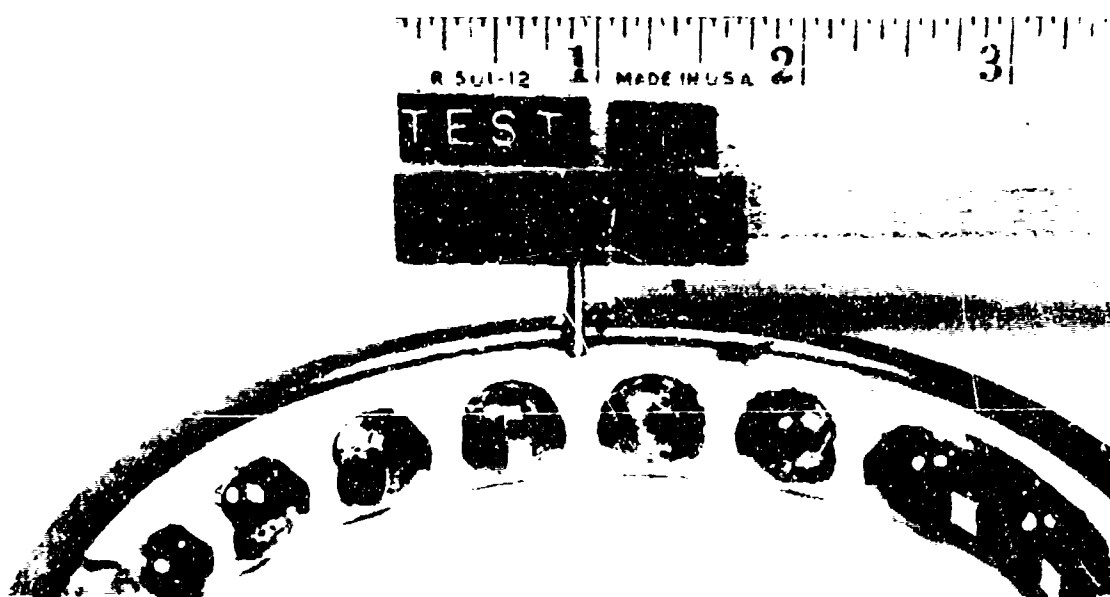


Figure 54. Build No. 2 Bearing Failure; Shaft Unbalance. Top: Inner races. Bottom: Cage, balls, and outer race.

The second failure (a smooth-race ball bearing) was the result of reducing the pocket clearance from 0.022 inch for the normal bearing to 0.005 inch to achieve the necessary Hall generator sensitivity. This failure is shown in Figure 55. When the Hall generators were eliminated to provide the necessary clearance, the multiplexer system was no longer required.

The third failure (a smooth-race roller bearing) was the result of excessive roller skewing during attempts to produce a skid map.

During early test runs, the wire routing from the retainer to the slip ring driving plate was adequate; but during later runs, there were lead wire failures resulting in the loss of data, and improved techniques were devised. The original and the improved lead paths are shown in Figure 56.

TEST PROCEDURE

The test program was accomplished in four builds as follows:

<u>Build</u>	<u>Test Bearing</u>	<u>Lubrication Condition</u>
1	Ball	EHD
2	Ball	EHD
3	Ball	Boundary
4	Roller	EHD

A full EHD oil film was achieved by operating at high speed and moderate loads.

Boundary lubrication was achieved by utilizing races with poor surface finish (24 AA). Experience has shown that this degree of roughness allows metal-to-metal contact.

Load and speed test conditions for the ball and roller bearing tests are defined in Tables VIII and IX respectively.

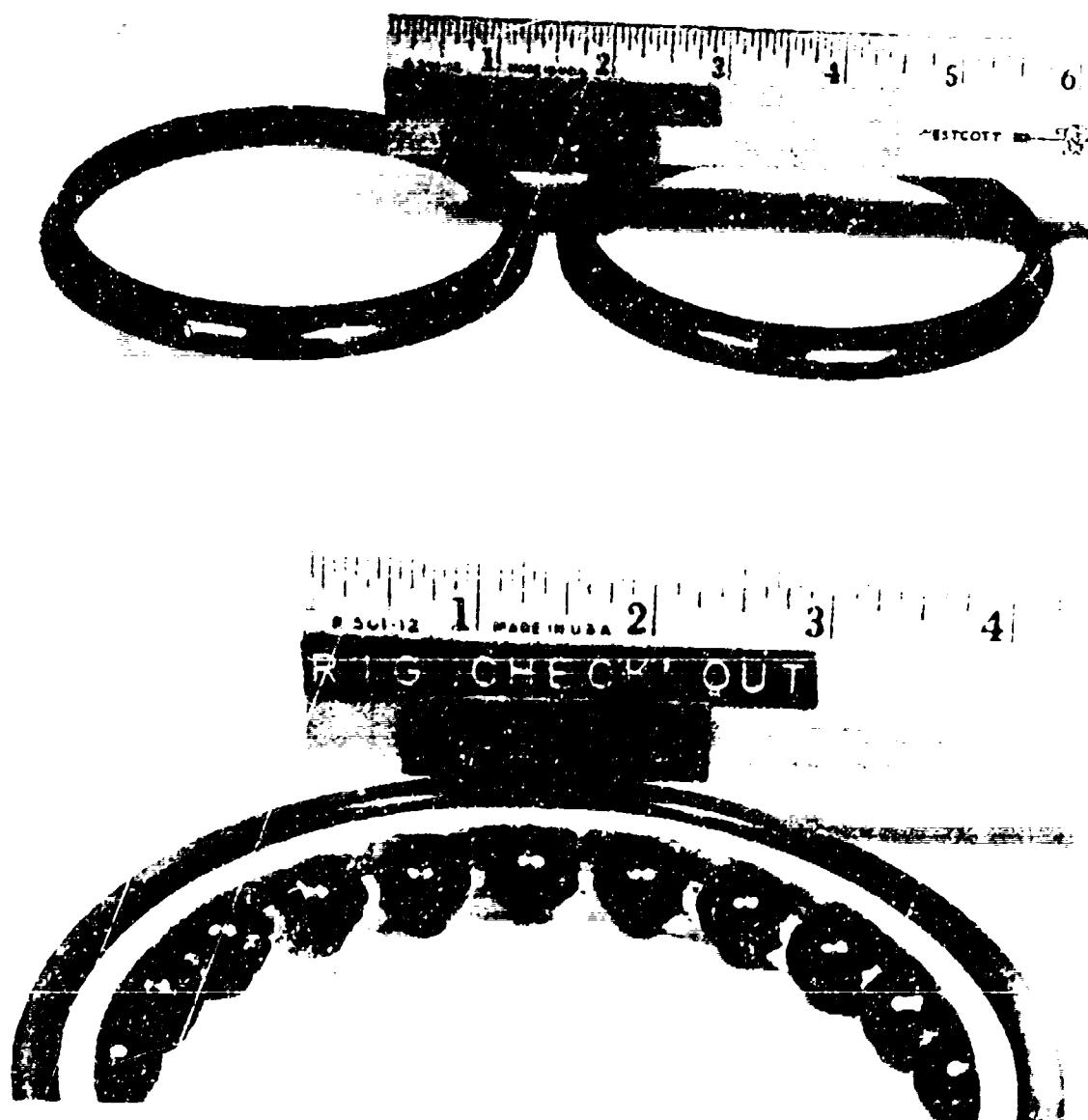


Figure 55. Build No. 2 Bearing Failure; Insufficient Pocket Clearance.
Top: Inner races. Bottom: Cage, balls, and outer race.



Figure 56. Improved and Original Retainer to Driving Ring Strain Gage Lead Paths. Top: Improved lead path showing gage leads fixed to pins attached on retainer; leads are spot welded to plate riveted to driving plate, and the leads are larger than originally. Bottom. Original lead path, unsupported from retainer, epoxy bonded to driving plate.

TABLE VIII. BALL BEARING TEST CONDITIONS			
Data Point	Inner Ring Speed (rpm)	Axial Load (lb)	Radial Load (lb)
1	16,000	1000	0
2	16,000	1000	500
3	16,000	500	500
4	16,000	100	0
5	20,000	1000	0
6	20,000	1000	500
7	20,000	500	500
8	20,000	100	0

TABLE IX. ROLLER BEARING TEST CONDITIONS			
Data Point	Inner Ring Speed (rpm)	Axial Load (lb)	Radial Load (lb)
1	16,000	0	1000
2	16,000	0	600
3	16,000	0	200
4	16,000	0	0
5	20,000	0	1000
6	20,000	0	600
7	20,000	0	200
8	20,000	0	0

Build No. 1, Rig Checkout

The objective of this build was to check out the test rig for the test program. Standard rig instrumentation was used. Retainer instrumentation and inner race temperature probes were not installed for this build. A standard ball bearing was installed in the test position.

The test rig was operated to 23,000 rpm. Oil flows to the test bearing and two support bearings were adjusted at various speed increments to note the effect on scavenge temperature. Radial and axial thrust loads were also varied at different shaft speed settings to determine load effects on vibration. The rig checkout was concluded with a 1-hour run at 23,000 rpm.

Build No. 2, Smooth-Race Ball Bearing

The test rig was rebuilt with bearing instrumentation to take data on the ball bearing in the EHD region.

The oil-in temperature to the test bearing was maintained at $100 \pm 5^\circ \text{F}$ during the test.

The rig was operated through all of the data points defined in Table VIII.

To generate a bearing skid map, the test rig was brought to 20,000 rpm, the radial load was reduced to zero, and the thrust (axial) load was reduced in increments until skidding occurred.

Build No. 3, Rough-Race Ball Bearing

This build was the same as Build No. 2 except that the test bearing had a rough surface finish on the inner and outer races to promote boundary lubrication at the rolling contacts. The same data points defined in Table VIII were evaluated. The oil-in temperature during the test was $200 \pm 5^\circ \text{F}$.

An attempt was made to produce a skid map, but skidding would not occur.

Build No. 4, Smooth-Race Roller Bearing

The test rig was rebuilt with bearing instrumentation to take data on the roller bearing in the EHD region.

The oil-in temperature to the test bearing was maintained at $100 \pm 5^{\circ}\text{F}$ during the test.

The eight data points to be evaluated during this build are defined in Table IX. The test rig was operated through all of these data points.

TEST RESULTS

Build No. 1, Rig Checkout

This build resulted in successful operation of the test rig, without retainer or race instrumentation, to speeds of 23,000 rpm under test load conditions.

Disassembly and inspection of the test rig after checkout operation showed that both the test and facility bearings were in excellent condition.

Build No. 2, Smooth-Race Ball Bearing

The first ball bearing configuration tested was with a smooth-race surface finish (5AA). Test results are summarized in Table X, which includes test race temperatures, measured radial load, slip ring driving torque, radial load frequency, and retainer-to-inner race speed ratio.

These results show that radial load was composed of a steady and an oscillatory component. Retainer driving torque was found to be oscillatory also. When drag was introduced into the driving system by "holding back" the slip ring, torque was still oscillatory, which suggested that the cage motion was not steady but accelerated and decelerated once per revolution. Maximum torque required to drive the slip ring was measured at 7 inch-pounds steady load, ± 7 inch-pounds vibratory.

Samples of the outputs from both ball force strain gage bridges and the cage speed signal as a function of time are shown in Figures 57 through 64. These figures show large pulse-type forces being applied to the cage at a nonuniform amplitude and nonperiodic frequency. In addition, they show a small vibratory (approximately ± 3 to ± 4 pounds) force. This smaller vibratory signal is expanded five times and presented in Figures 65 through 72.

TABLE X. SUMMARY OF TEST RESULTS, BUILD NO. 2							
Data Points (1)	Inner and Outer Race Temperatures			Radial Load (lb) (2)	Radial Load Frequency (Hz) (3)	Retainer to Rig Speed Ratio	Driving Torque (in. - lb) (4)
	Inner Race (°F)	Outer Race (°F)	ΔT (°F)				
1	320	209	-126	0 ± 100 0 ± 20	257 (5)	.46 .46	6 ± 3
2	-	205	-	470 ± 80 470 ± 120	281 254	.46 .46	6 ± 3
3	340	205	-135	470 ± 140 510 ± 150	279 (5)	.46 .45	5 ± 5
4	260	195	-65	0 ± 20 0 ± 20	(5) (5)	.31 (6) .45	5 ± 3
5	320	205	-75	0 ± 20 0 ± 20	(5) (5)	.46 .45	6 ± 6
6	250	220	-29	500 ± 120 480 ± 95	356 334	.45 .45	7 ± 7
7	300	225	-135	500 ± 120 480 ± 100	348 331	.45 .45	6 ± 6
8	200	220	-40	0 ± 20 0 ± 20	(5) (5)	.45 .46	3 ± 3
1. Each test was run twice (once with two web force strain gage bridges, once with one web force and one torque measurement); inner and outer race temperatures were determined during the second run only. Upper values are for test No. 1; lower values are for test No. 2. 2. From strain-gaged radial loading ramp; static and dynamic components. 3. Frequency of oscillation of radial loading ramp; caused by unbalance and/or eccentricity of shaft supporting bearing. 4. Vibratory component not sinusoidal during condition where torque goes to zero. 5. Ability to determine primary frequency limited by low-level dynamic component. 6. Indicate slip during first run but no slippage during second run; also shown in harmonic analysis.							

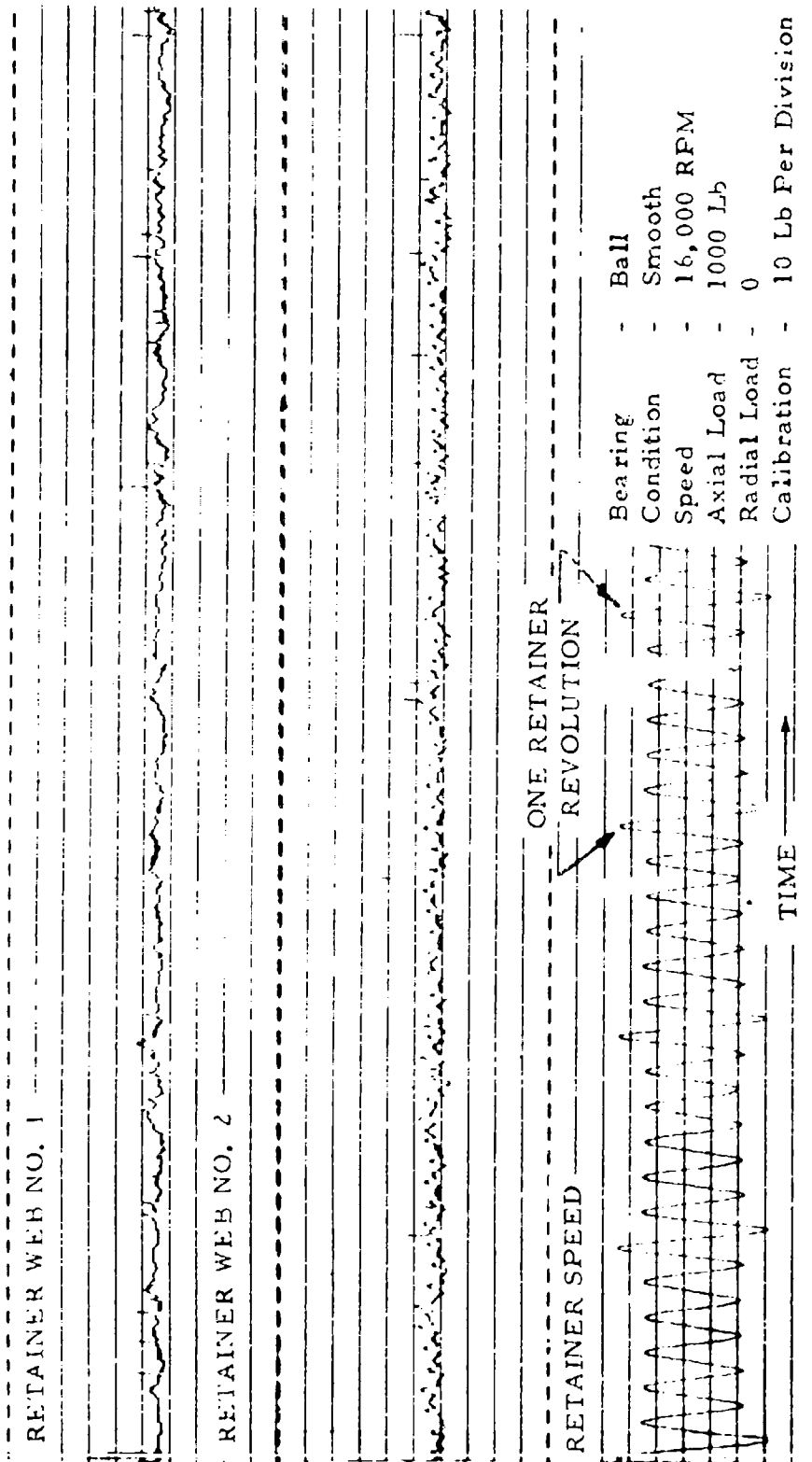


Figure 57. Retainer Web Force and Retainer Speed Versus Time, Showing Nature of Impact Loads.

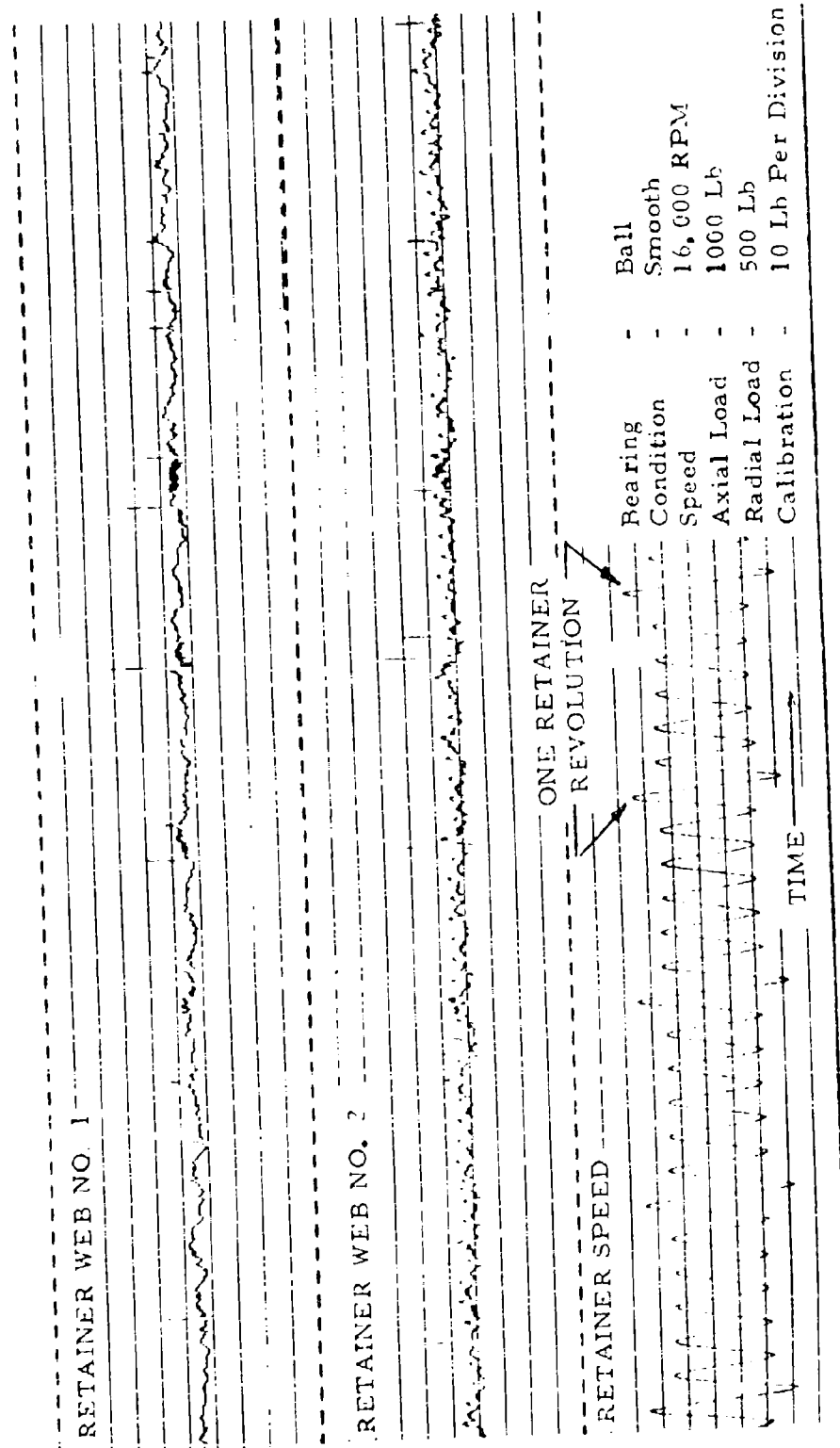


Figure 58. Retainer Web Force and Retainer Speed Versus Time, Showing Nature of Impact Loads.

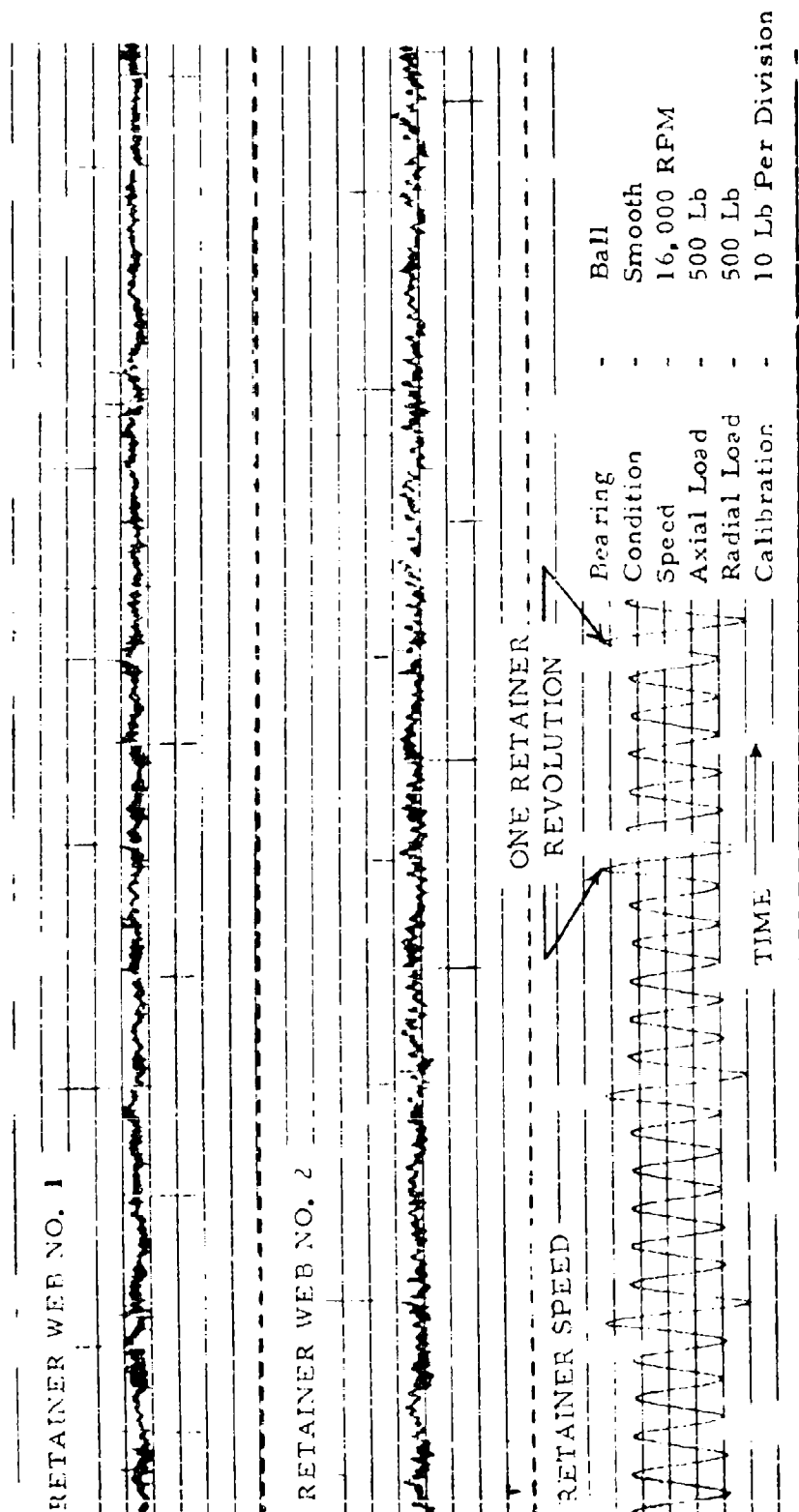


Figure 59. Retainer Web Force and Retainer Speed Versus Time, Showing Nature of Impact Loads.

RETAINER WEB NO. 1

RETAINER WEB NO. 2

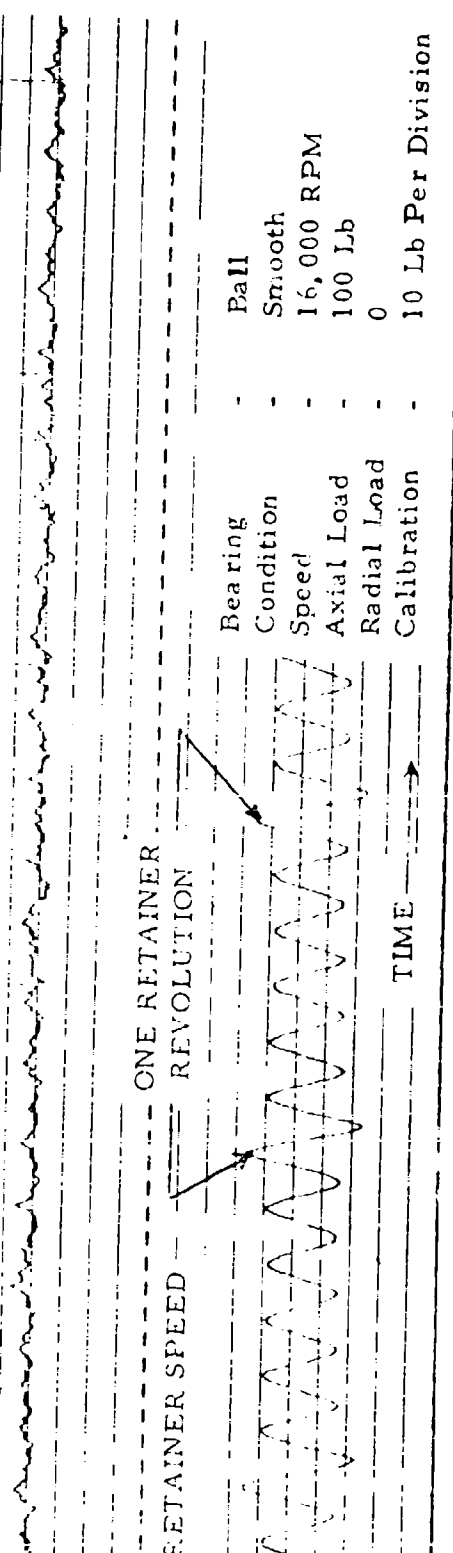


Figure 60. Retainer Web Force and Retainer Speed Versus Time, Showing Nature of Impact Loads.

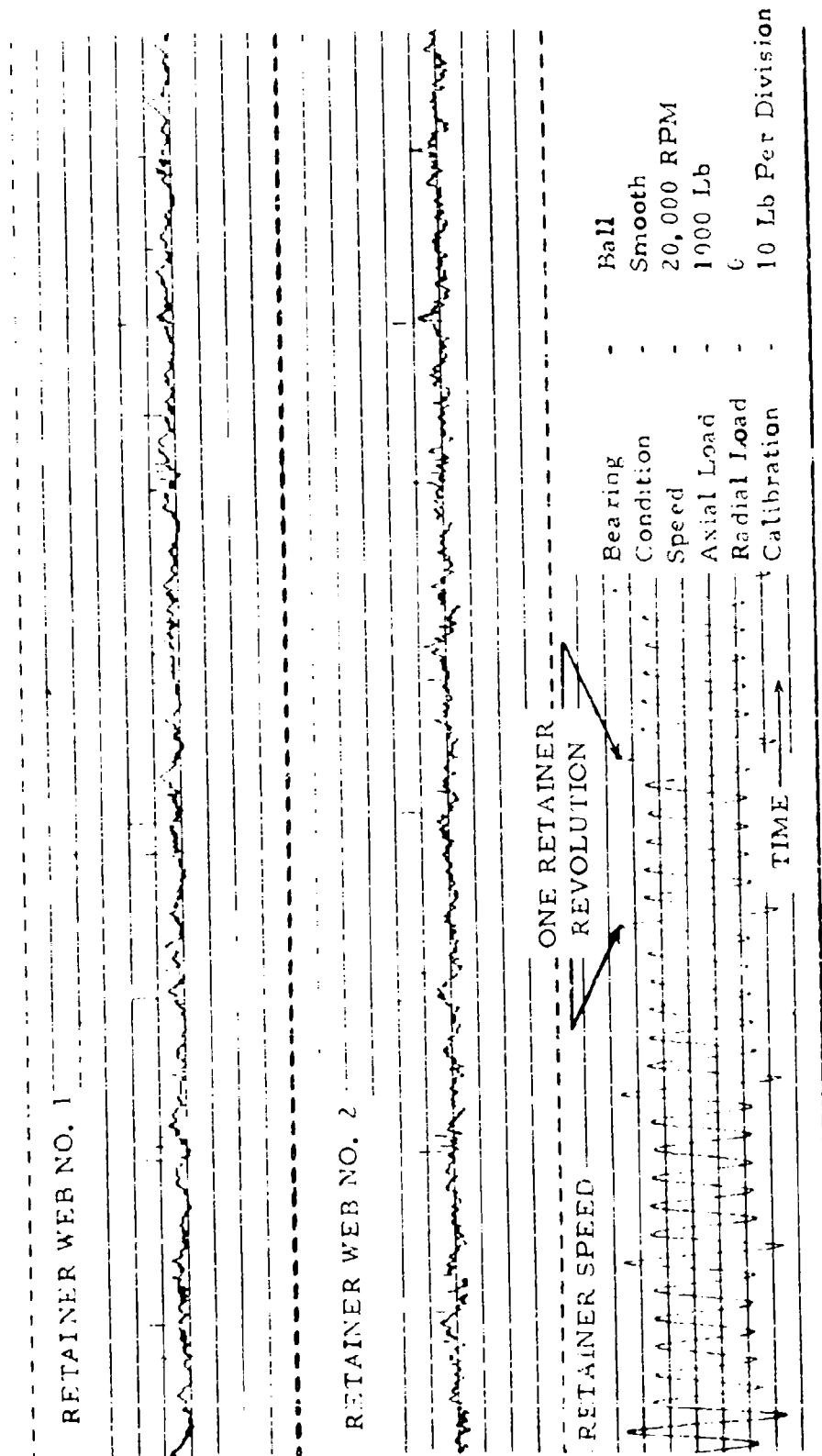


Figure 61. Retainer Web Force and Retainer Speed Versus Time, Showing Nature of Impact Loads.

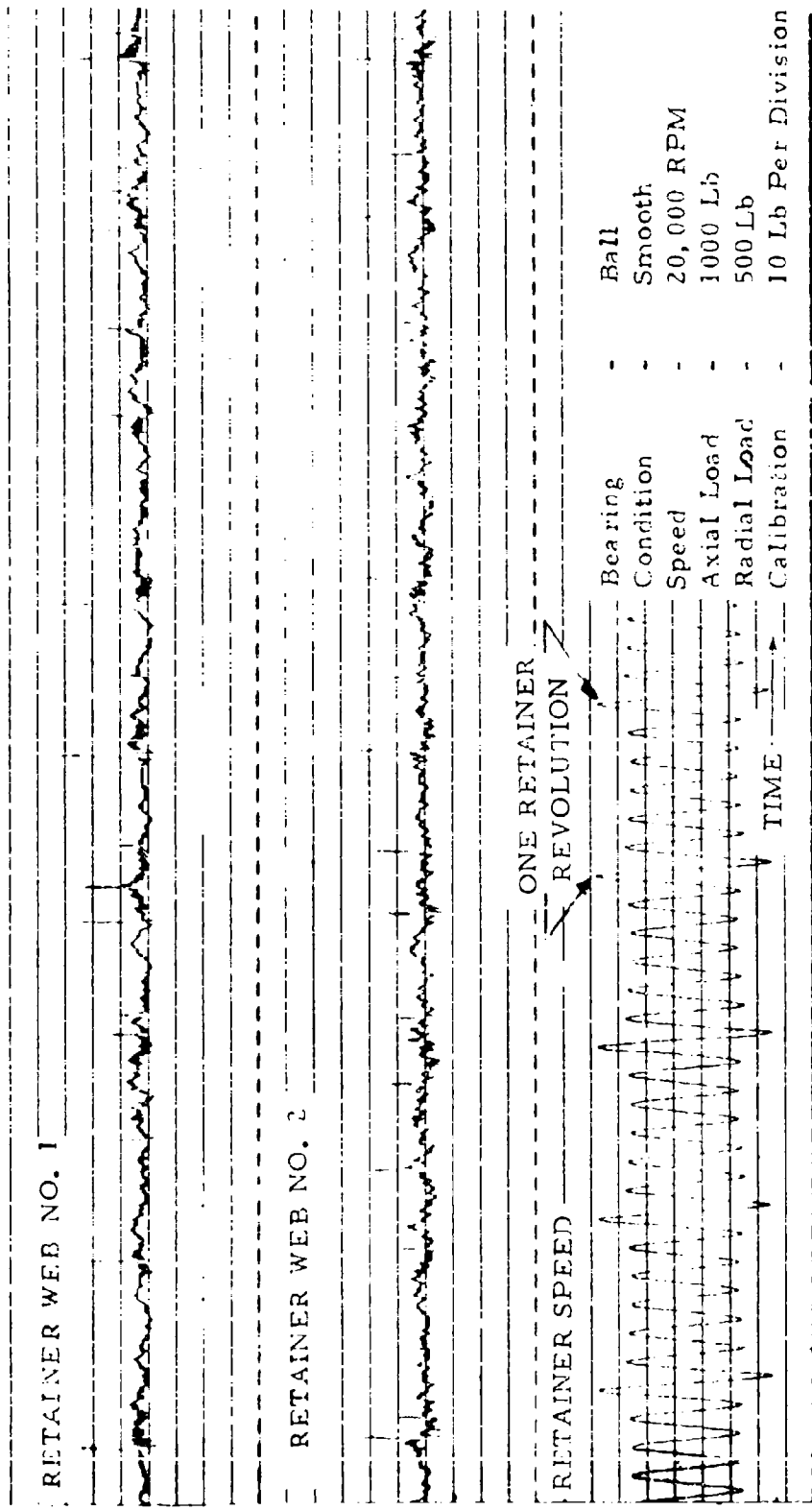


Figure 62. Retainer Web Force and Retainer Speed Versus Time, Showing Nature of Impact Loads.

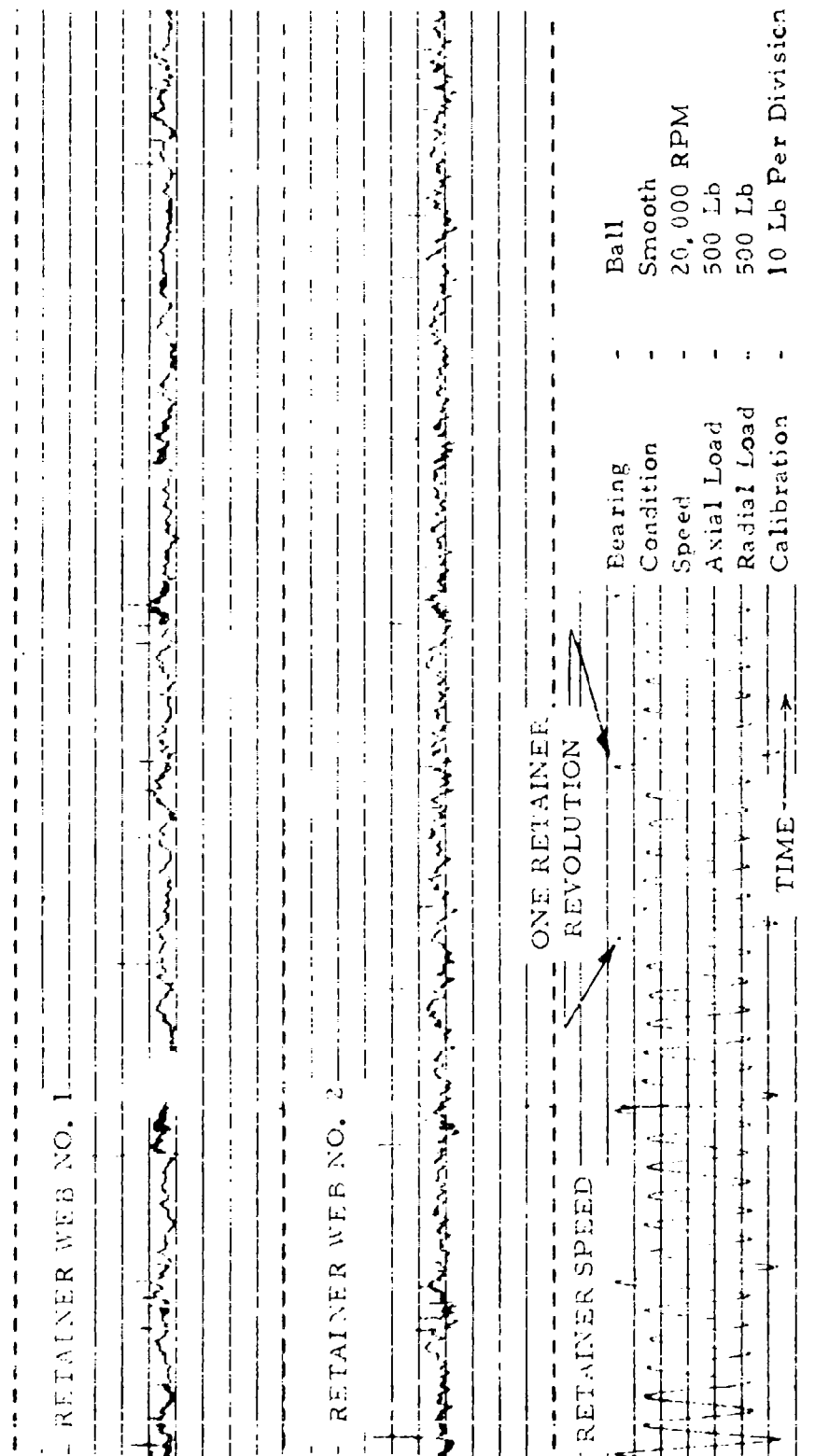


Figure 63. Retainer Web Force and Retainer Speed Versus Time, Showing Nature of Impact Loads.

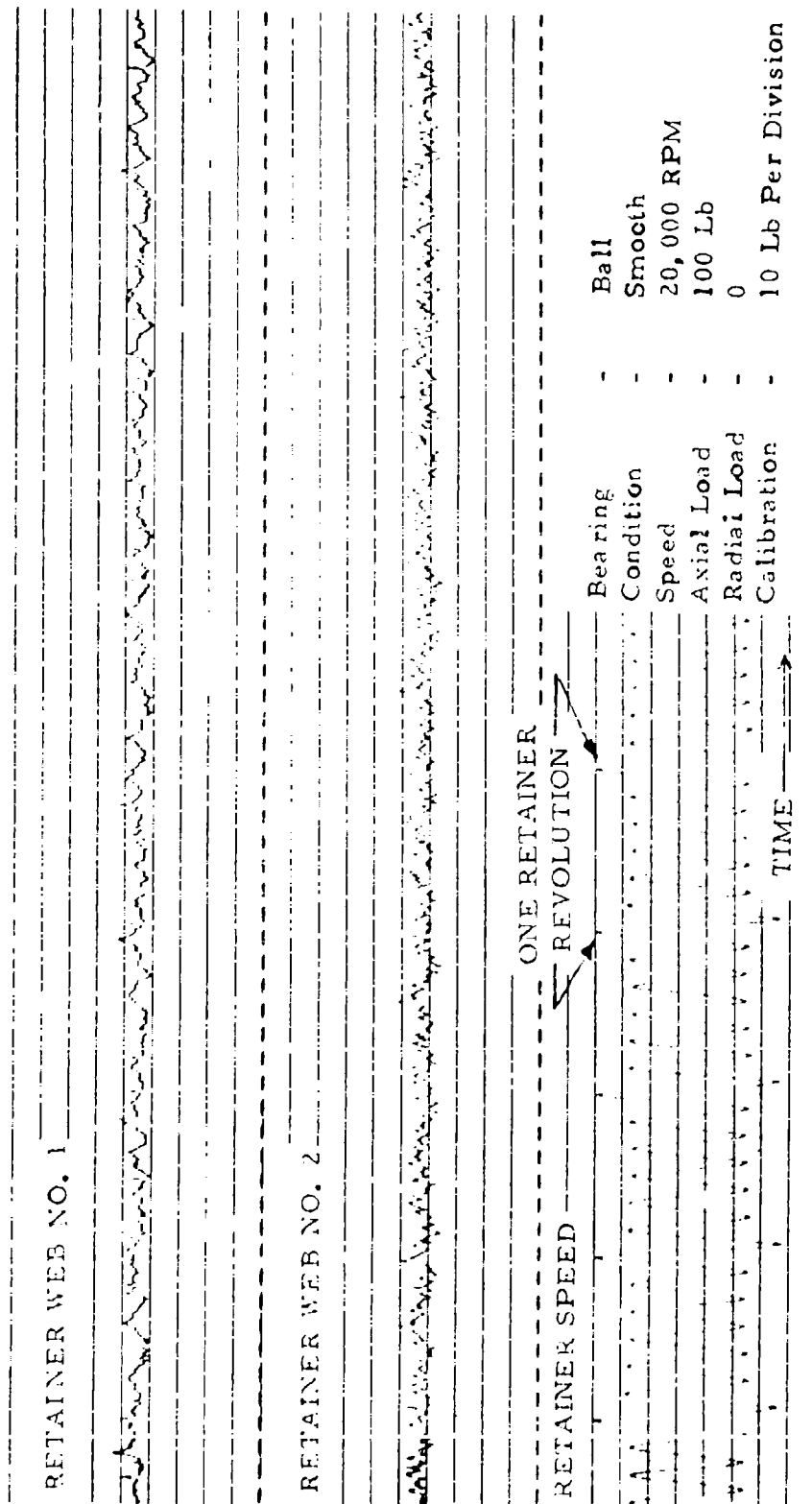


Figure 64. Retainer Web Force and Retainer Speed Versus Time, Showing Nature of Impact Loads.

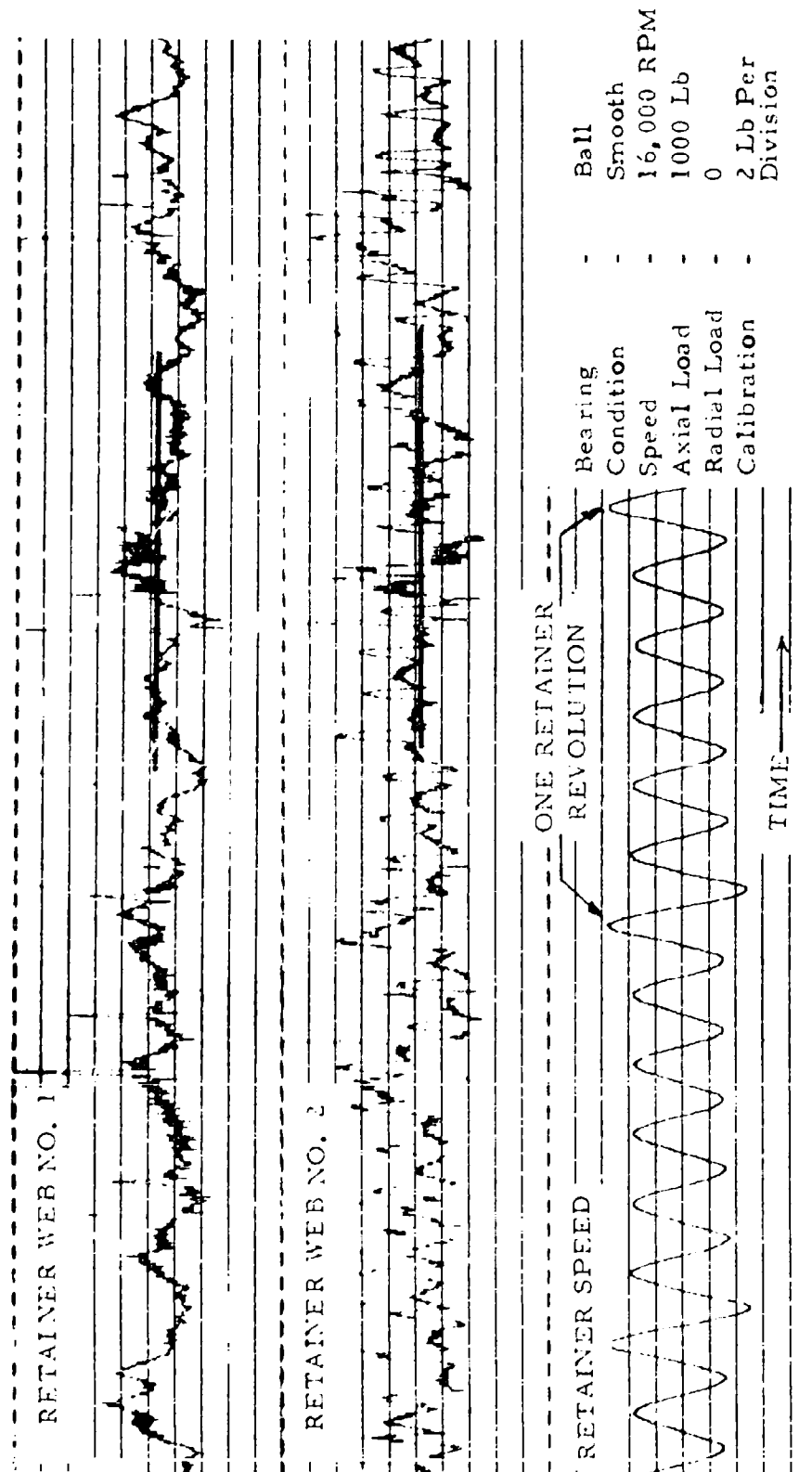


Figure 65. Retainer Web Force Expanded With Computed Web Force Superimposed.

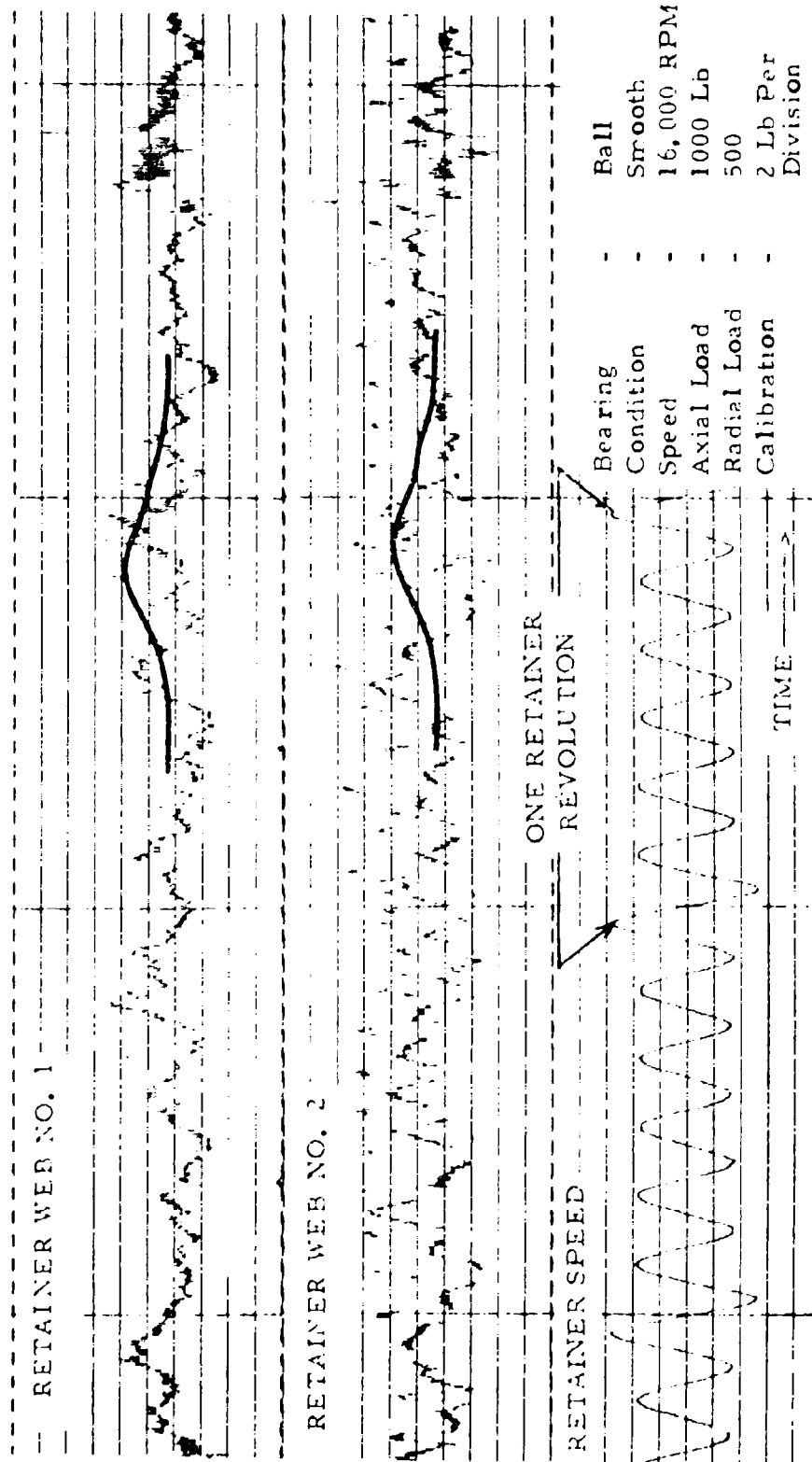
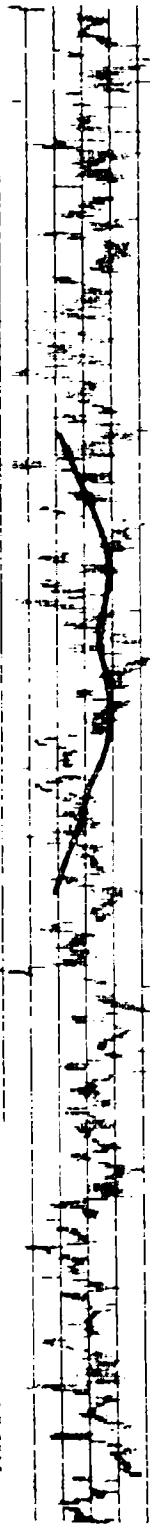


Figure 66. Retainer Web Force Expanded With Computed Web Force Superimposed.

RETAINER WEB NO. 1



RETAINER WEB NO. 2



ONE RETAINER

RETAINER SPEED

REVOLUTION

Bearing	-	Ball
Condition	-	Smooth
Speed	-	16,000 RPM
Axial Load	-	500 Lb
Radial Load	-	500 Lb
Calibration	-	2 Lb Per Division

TIME

Figure 67. Retainer Web Force Expanded With Computed Web Force Superimposed.

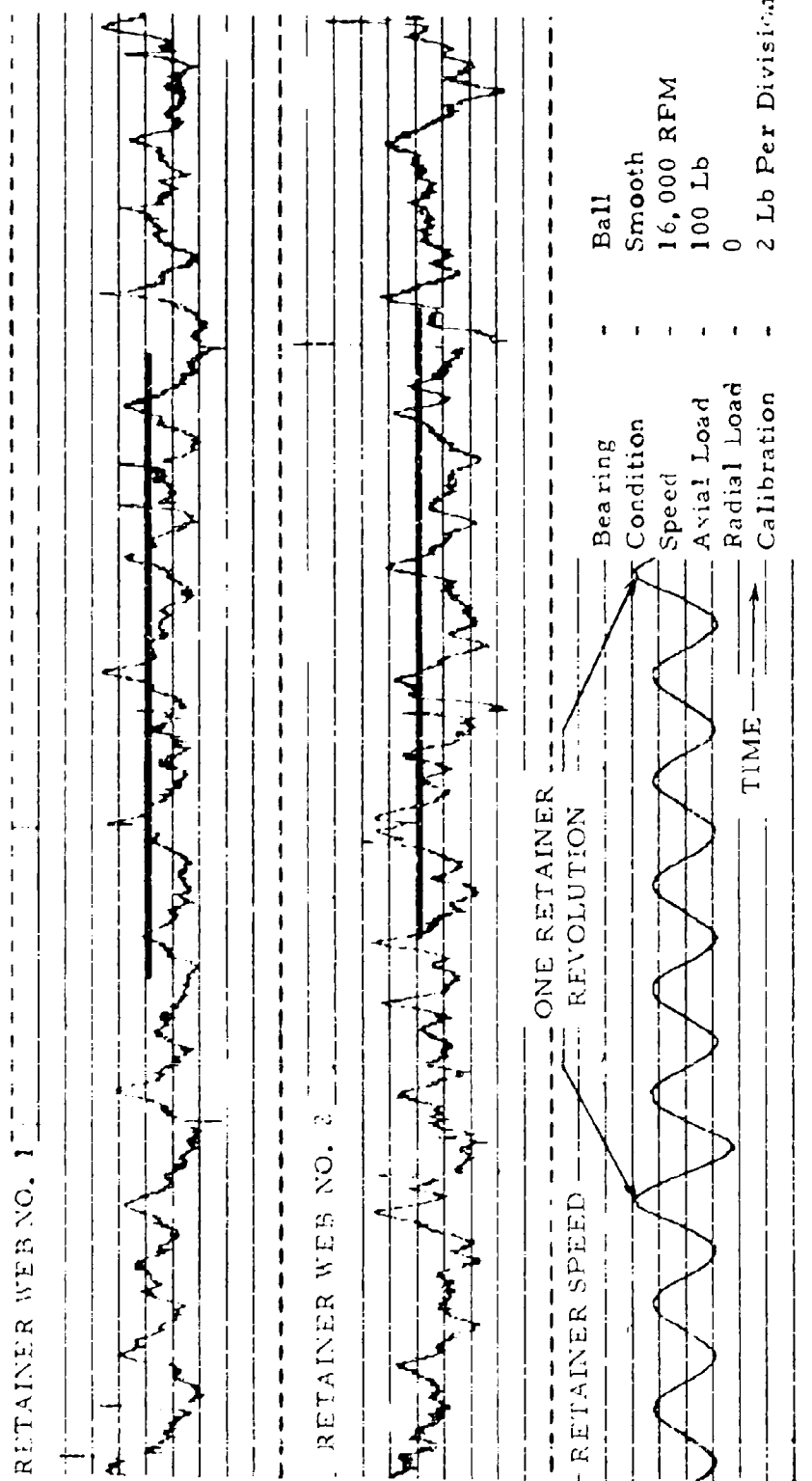


Figure 48. Retainer Web Force Expanded With Computed Web Force Superimposed.

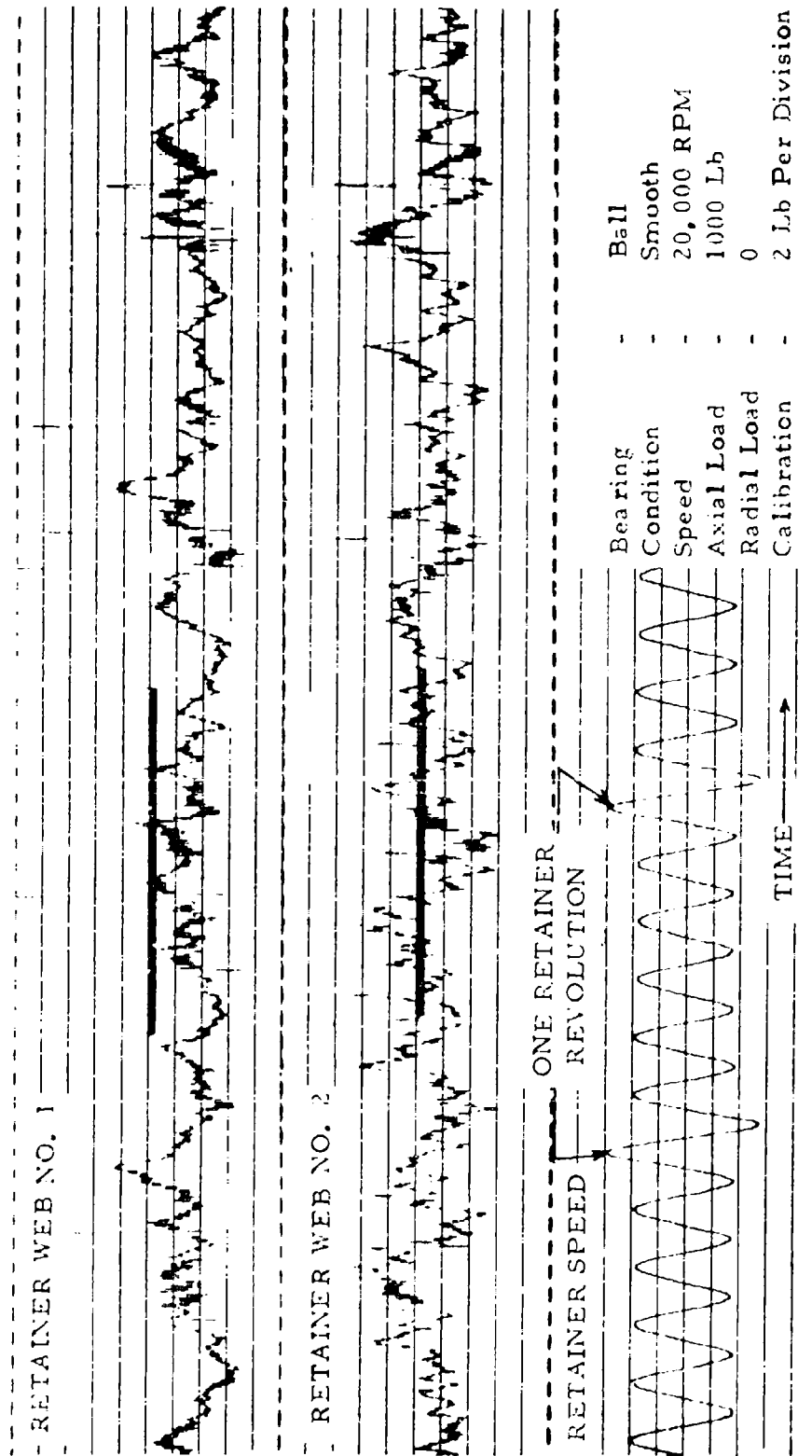


Figure 69. Retainer Web Force Expanded With Computed Web Force Superimposed.

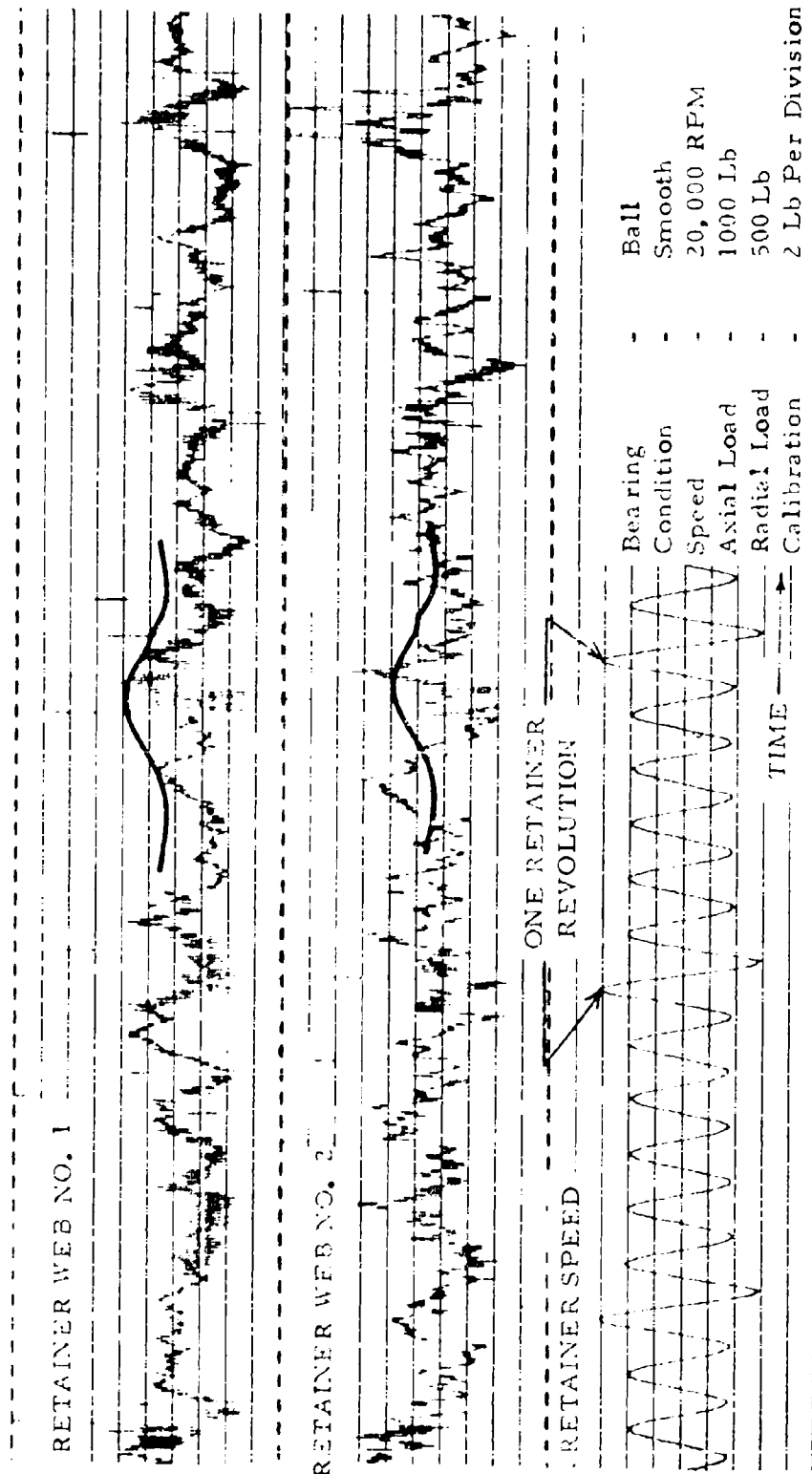


Figure 70. Retainer Web Force Expanded With Computed Web Force Superimposed.

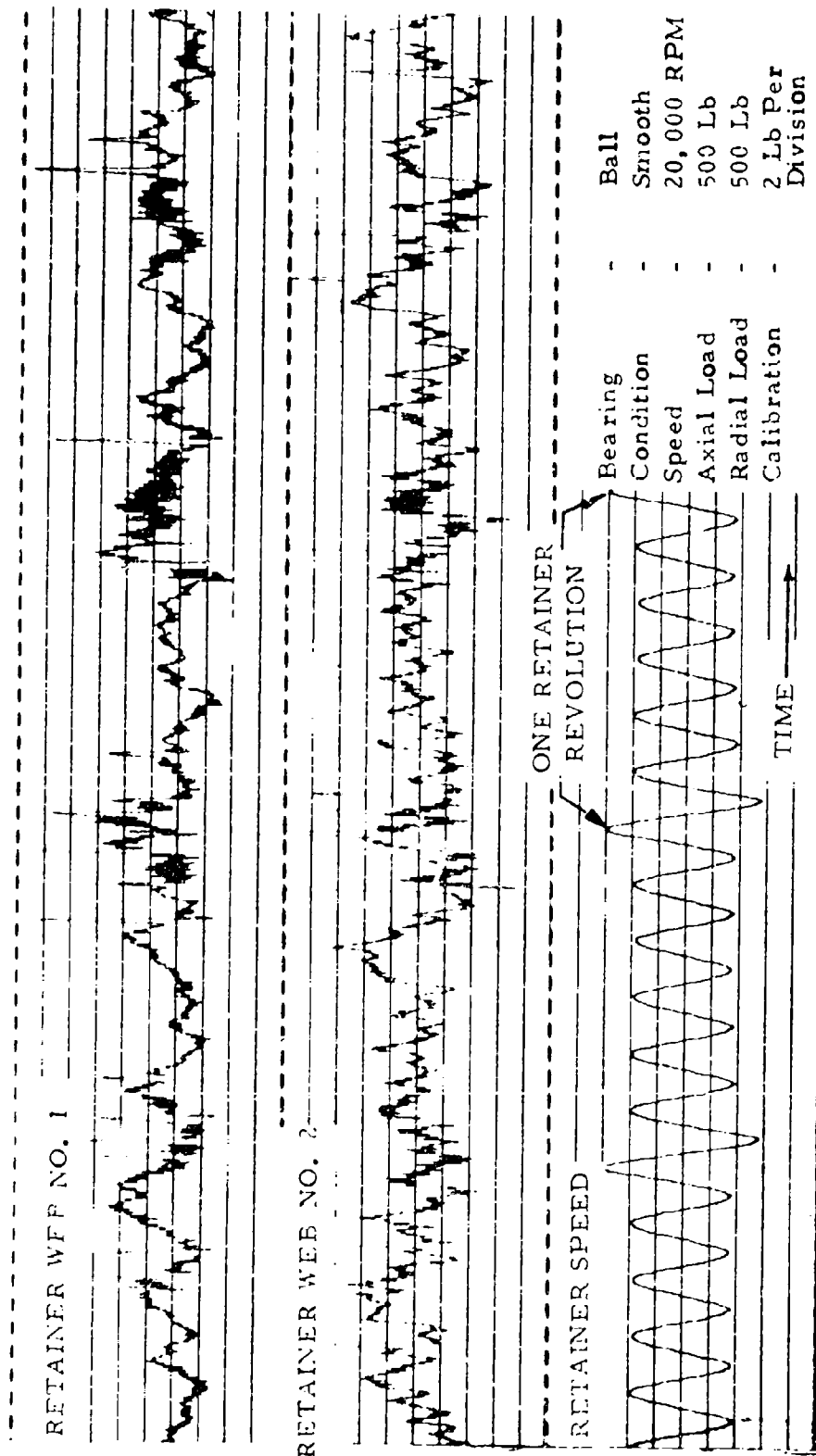


Figure 71. Retainer Web Force Expanded With Computed Web Force Superimposed.

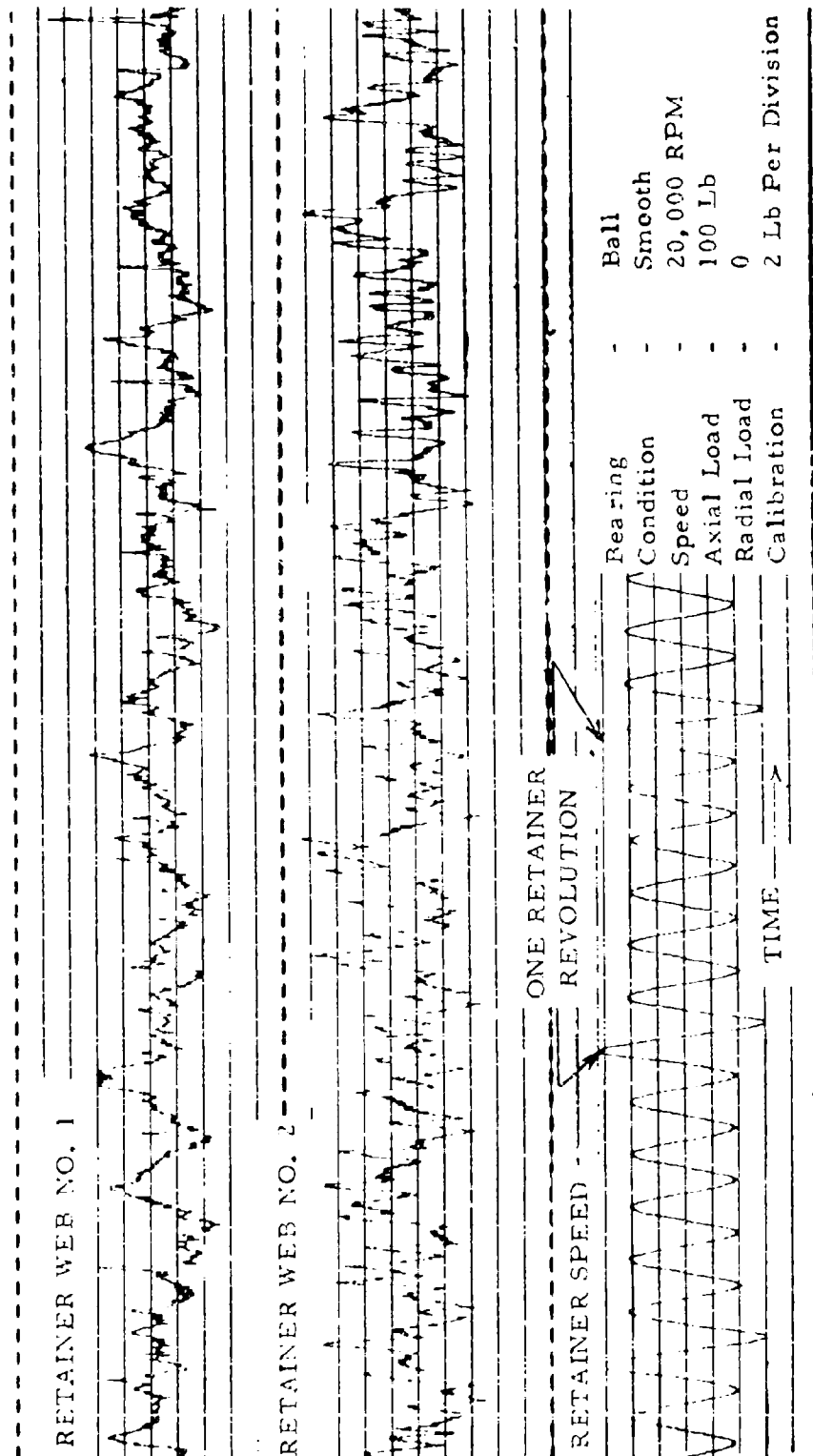


Figure 72. Retainer Web Force Expanded With Computer Web Force Superimposed.

The large, pulse-like force was later simulated in the laboratory by impact loading a ball against a retainer web. Results suggested the presence of dynamic ball/pocket forces resulting from accelerations of the ball within the pocket clearance or of the retainer itself. These dynamic effects were not predicted by the computer program.

With respect to the smaller vibratory signal, two approaches were taken in the analysis of the test data. First, ball azimuth versus retainer web force plots as determined by the computer program were superimposed on similar plots from the test program data (Figures 65 through 72). Second, a harmonic analysis of the computer-determined output was compared with similar analysis from the test data (Figures 73 through 75). Figure 75 shows the computer-determined harmonic analysis of the computed web force wave, and is normalized here to an arbitrary unit to compare ratios of harmonics rather than absolute values. Figures 73 and 74 show the average of 16 spectra obtained from experimental test tape recordings. Spectrum averaging was used to eliminate random signals that might be present in the experimental wave forces, since the harmonic analysis of any selected cycle could be distorted by random occurrences.

In the cases of pure thrust bearing loading (Figures 65, 68, and 69), where computed pocket force is a constant value of approximately 0.25 pound, the dynamic component determined experimentally (neglecting impact peaks) was between ± 3 and ± 4 pounds. It is suggested that the difference between the computed and measured force levels at these conditions, where the predicted force is nearly zero, is background or additional forces generated by conditions not considered in the computer analysis. Practically speaking, a 3- to 4-pound background force is of little consequence.

In the cases of combined thrust and radial loading (Figures 66, 67, and 70), the predicted and measured force levels are of the same magnitude, neglecting impact peaks. The computer program predicted approximately ± 1.5 to ± 2.0 pounds; the measured values were from ± 4 to ± 4.5 pounds. Note that the difference is not large in view of the background levels determined during pure thrust load tests.

Two of the test conditions, filtered and unfiltered, are shown in Figures 76 through 79. Frequencies higher than seven times retainer speed (seventh order) have been eliminated in the filtered wave.

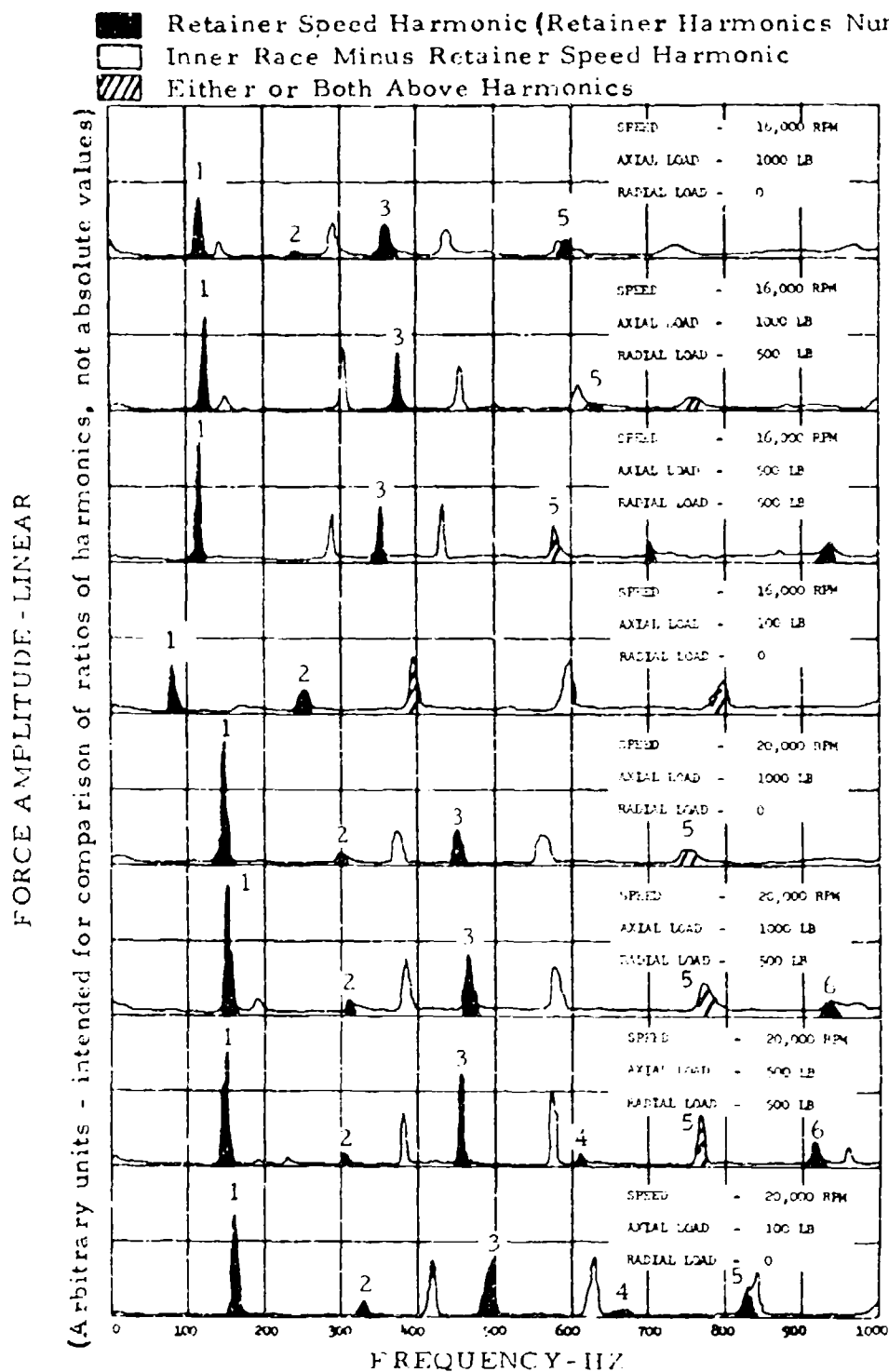


Figure 73. Harmonic Analysis of Experimentally Determined Retainer Web Force (Average of 16 Spectra) for Ball Bearing Smooth Race. Bearing Retainer Web No. 1.

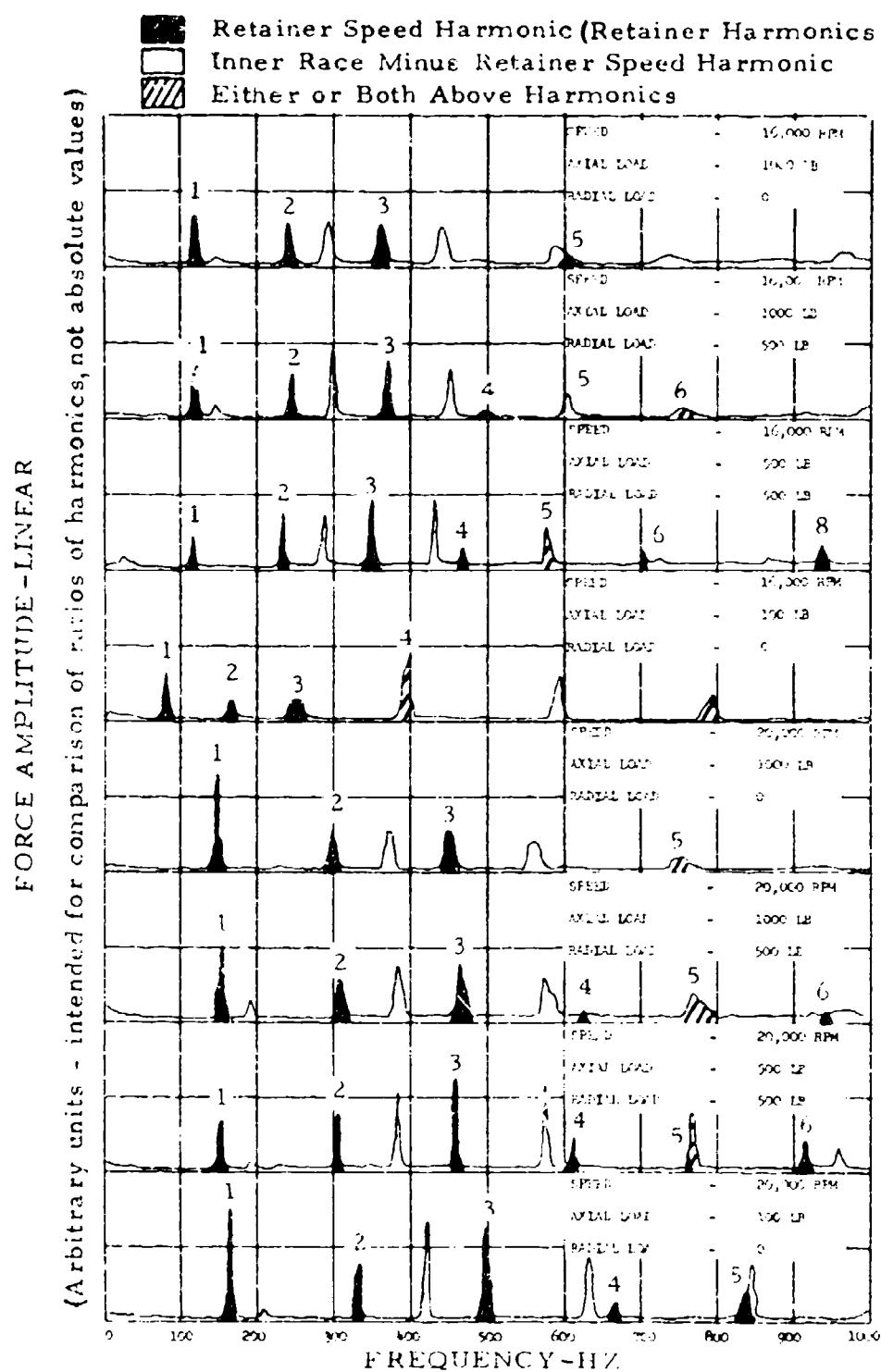


Figure 74. Harmonic Analysis of Experimentally Determined Retainer Web Force (Average of 16 Spectra) for Ball Bearing Smooth Race, Bearing Retainer Web No. 2.

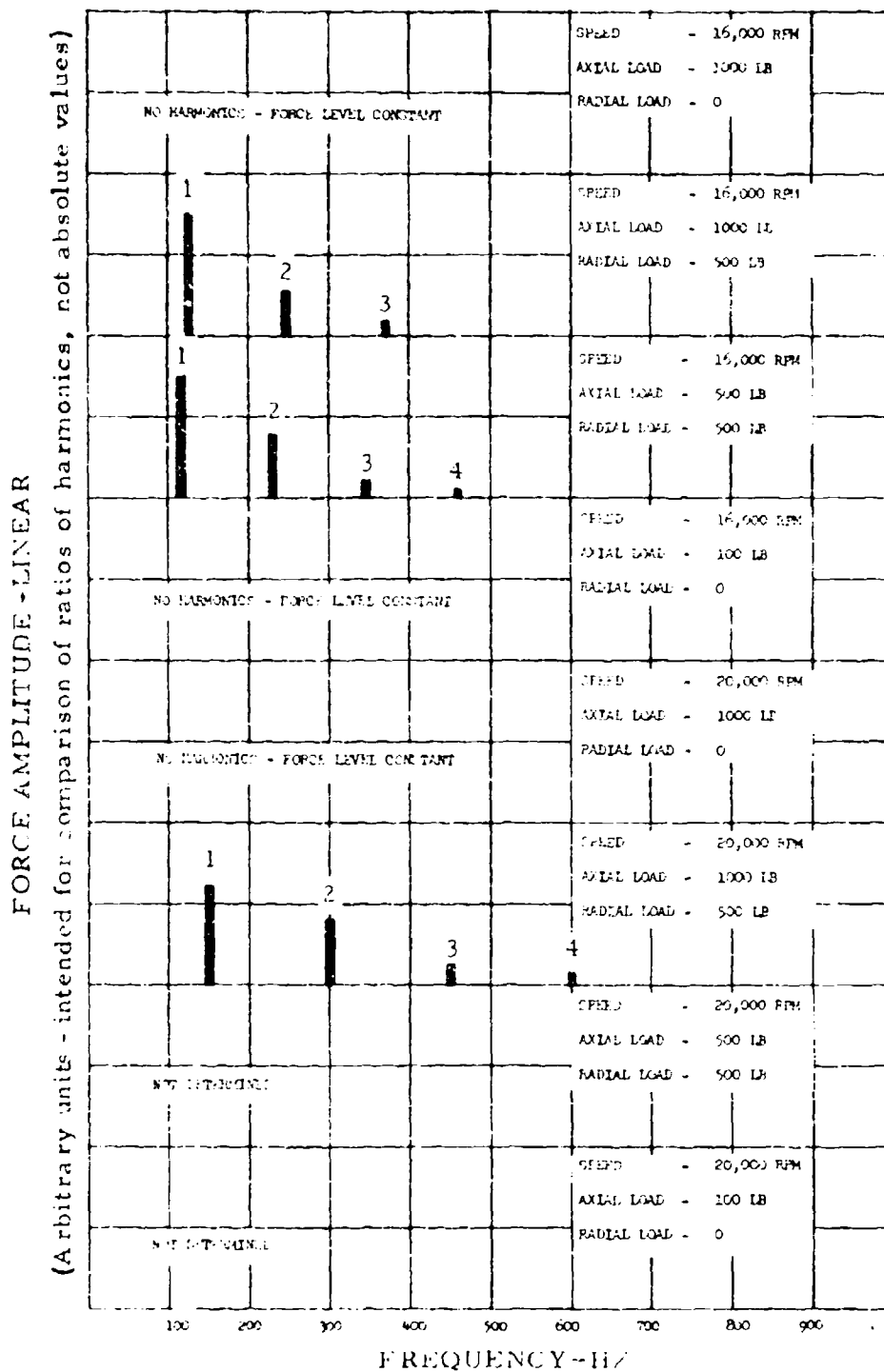


Figure 75. Harmonic Analysis of Computed Retainer Web Force for Ball Bearing Smooth Race.

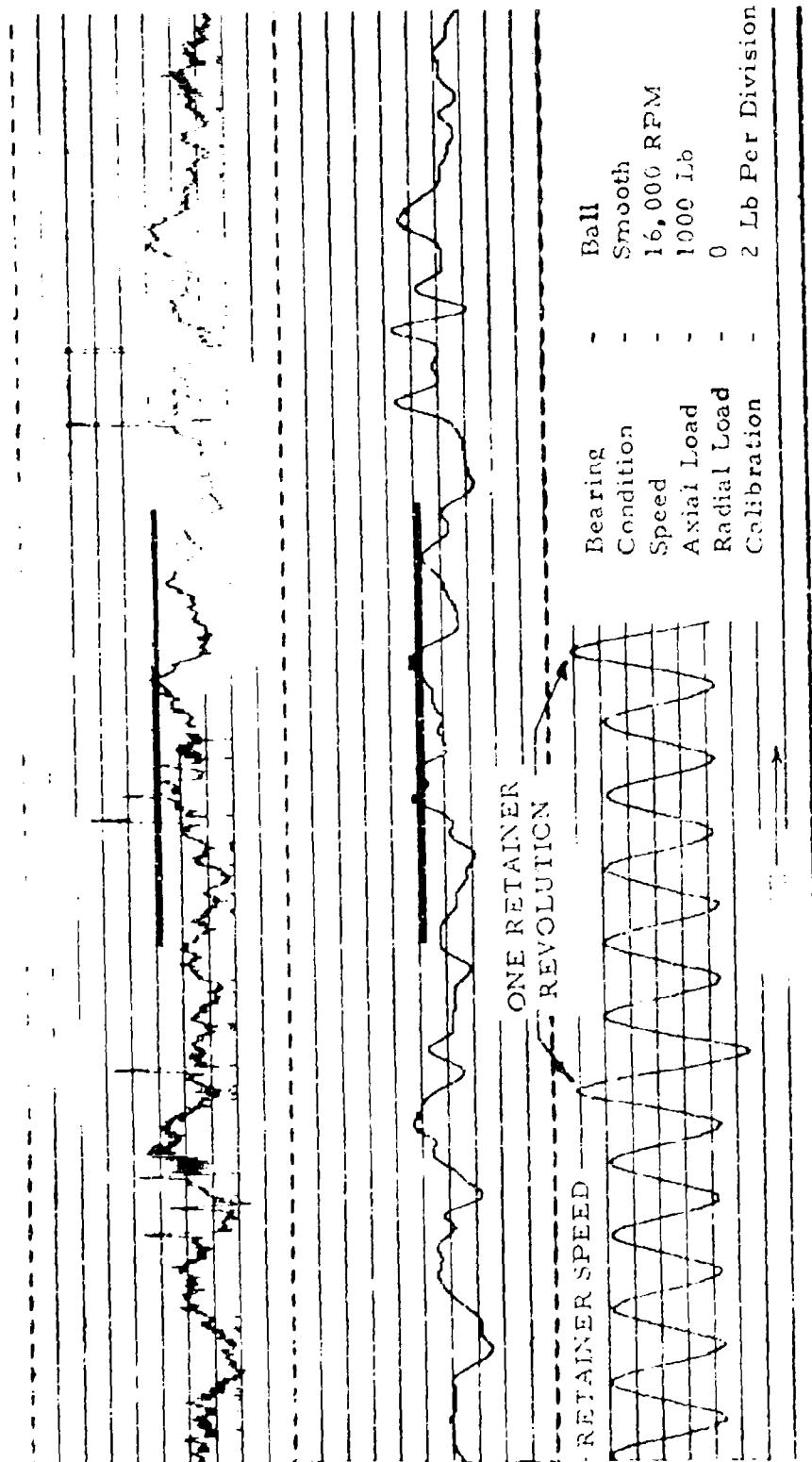


Figure 76. Retainer Web No. 1, Filtered and Unfiltered Retainer Force Wave Form With Computed Forces Superimposed. Frequencies Higher Than Seventh Order Retainer Speed Removed in Filtered Wave.

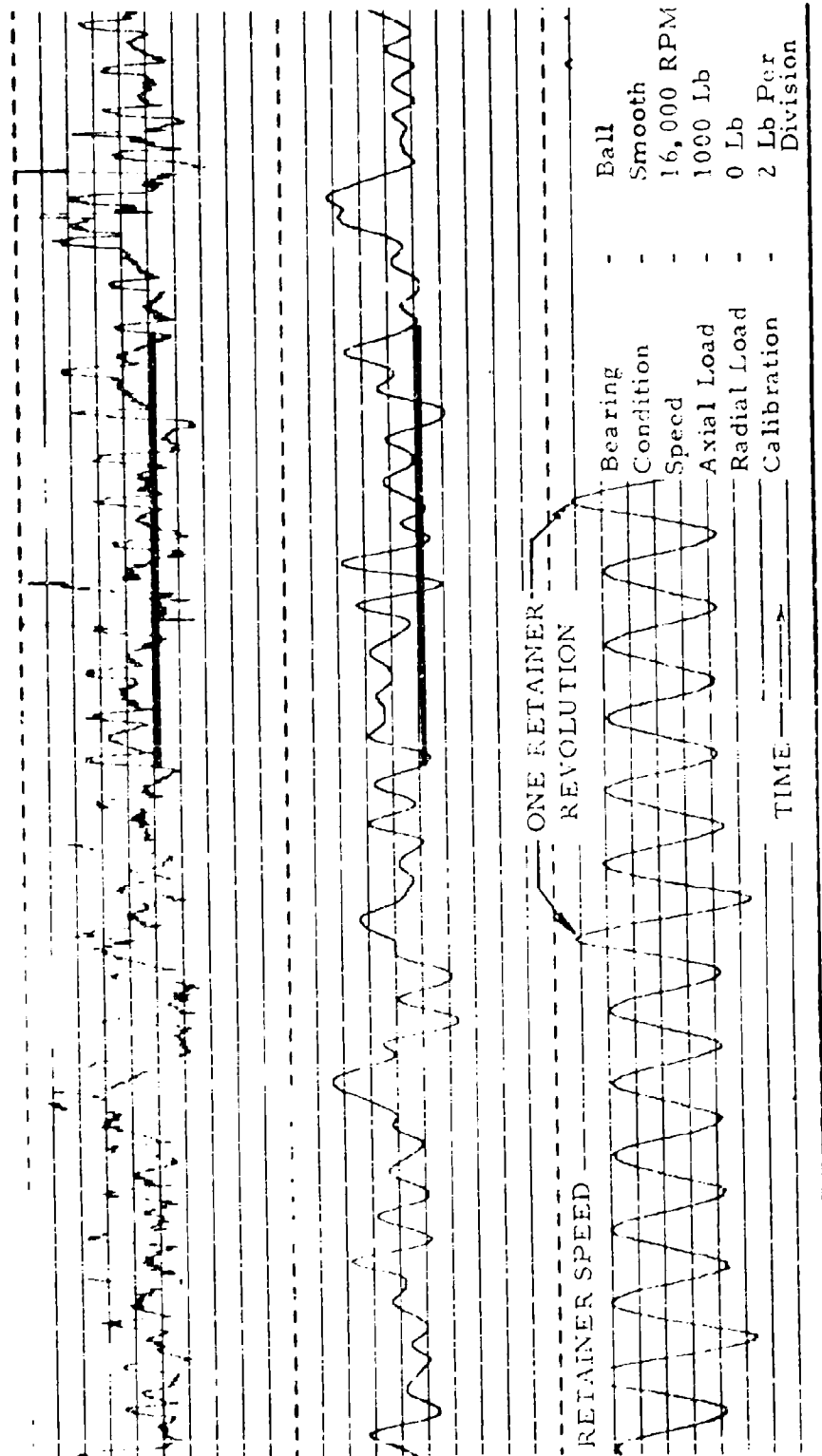


Figure 77. Retainer Web No. 2, Filtered and Unfiltered Retainer Force Wave Form With Computed Forces Superimposed. Frequencies Higher Than Seventh Order Retainer Speed Removed in Filtered Wave.

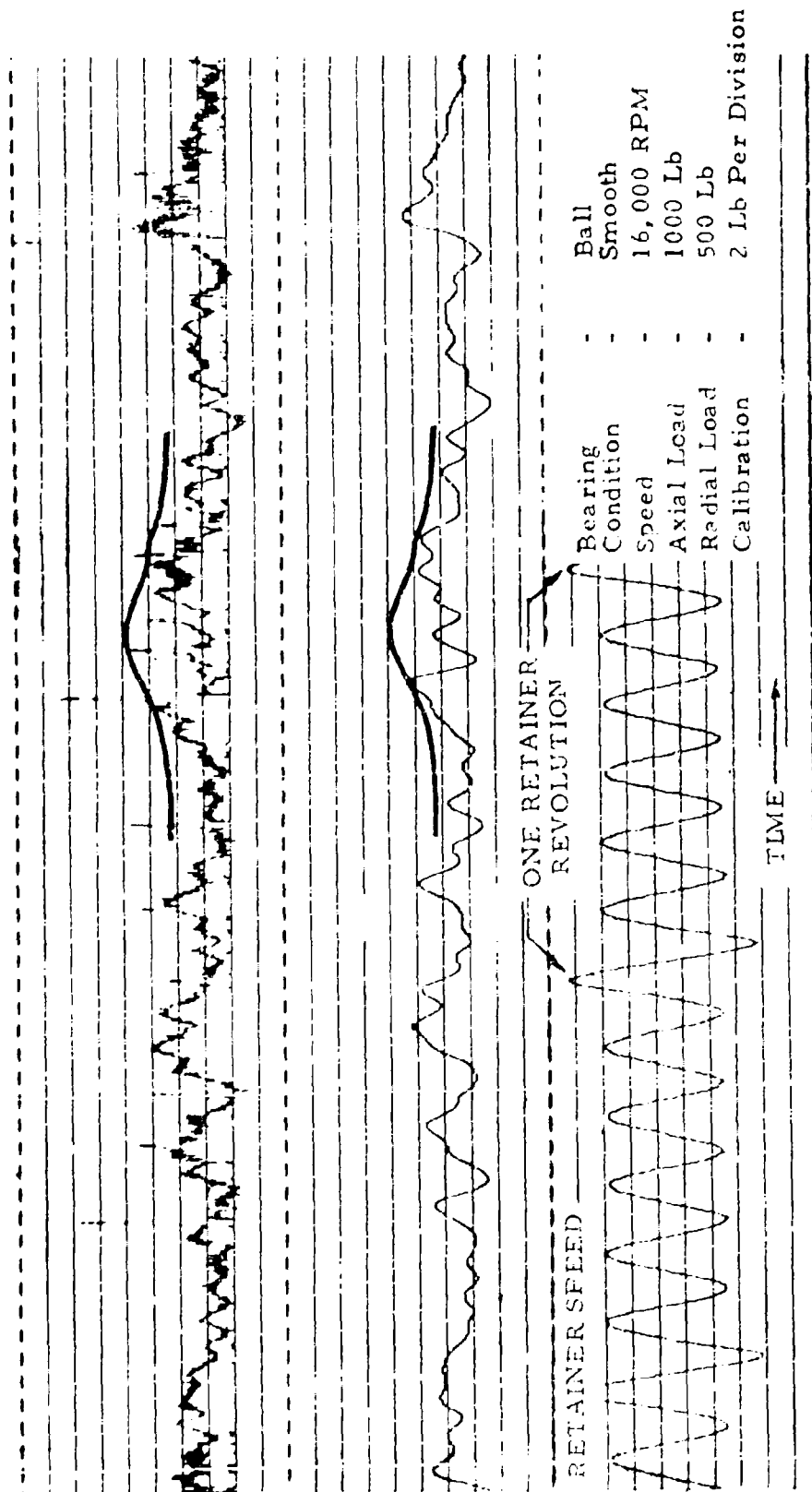


Figure 78. Retainer Web No. 1, Filtered and Unfiltered Retainer Force Wave Form
With Computed Forces Superimposed. Frequencies Higher Than Seventh
Order Retainer Speed Removed in Filtered Wave.

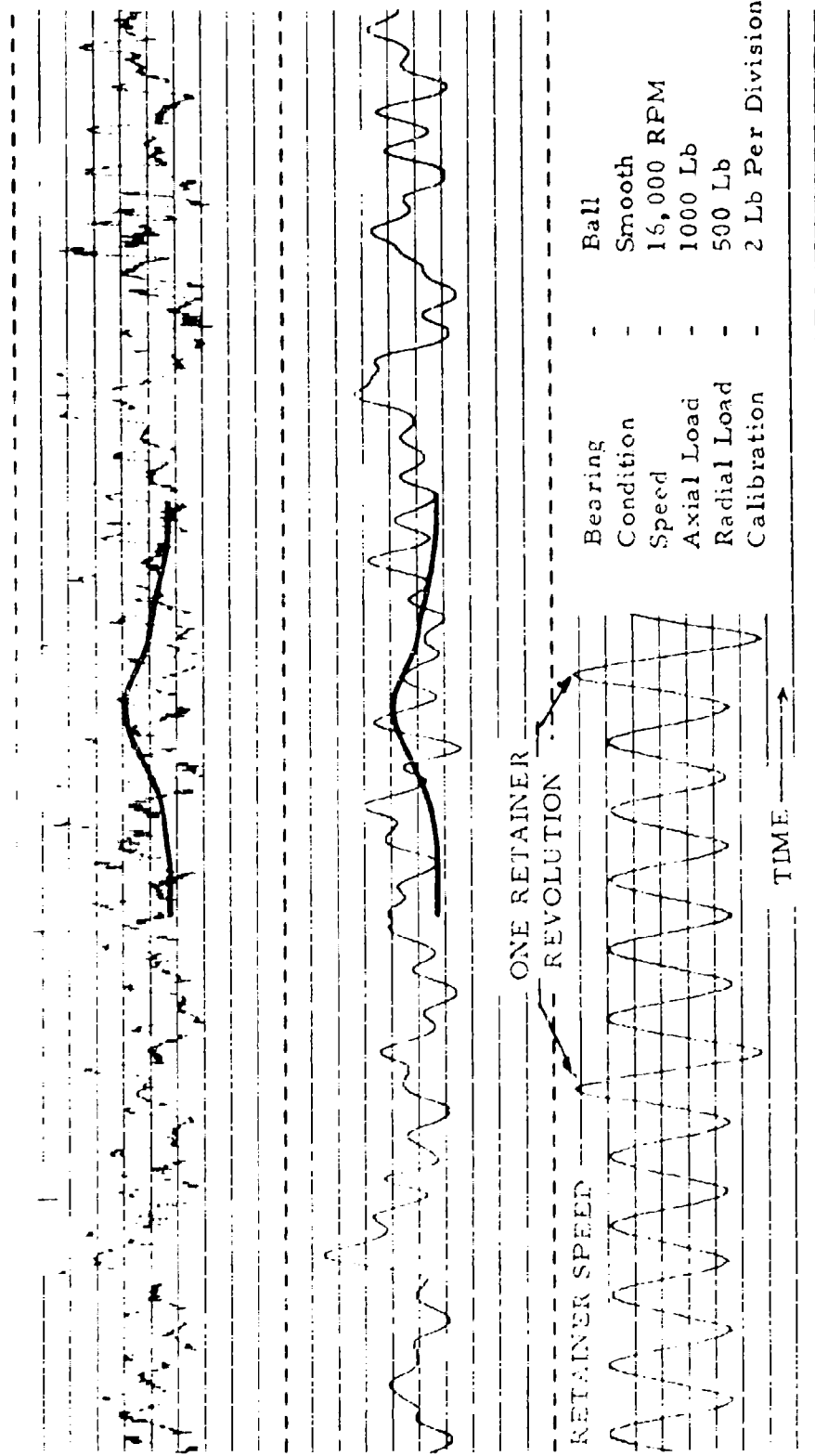


Figure 7a. Retainer Web No. 2, Filtered and Unfiltered Retainer Force Wave Form With Computed Forces Superimposed. Frequencies Higher Than Seventh Order Retainer Speed Removed in Filtered Wave.

Harmonic analysis (Figures 73 through 75) shows similar frequency components for computer and test results, but proportions of the harmonics are not comparable; in fact, two different retainer webs show different harmonic amplitudes. There are also more frequency components in the experimental data. Further experimentation and analysis are required to understand these differences between predicted and measured values and to explain the origin of the background force level described above.

A skid map is shown in Figure 80.

Build No. 3, Rough-Race Ball Bearing

Inner and outer race temperatures are summarized in Table XI. Ball force data from the rough bearing generally looked similar to that of the smooth bearing with pulse magnitudes reduced. Samples of data from the first two test points are shown in Figures 81 and 82. The distorted retainer speed signal is the result of magnetic tape saturation in one direction, but since the large peak is still discernible, the signal is still useful in establishing the time of a single ball cycle and the relationship between the location of the retainer and the leading zone. Figure 82 also shows the beginning of the deterioration of the No. 2 retainer-web strain-gage bridge.

Build No. 4, Smooth-Race Roller Bearing

Inner and outer race temperatures are summarized in Table XII.

Traces from the only functioning retainer-web strain-gage bridge for four test conditions are shown in Figures 83 through 86.

The roller force traces do not show the large pulse-like forces found in the ball force traces at the test conditions required for computer verification; however, these peaks were observed while sweeping to the test speed.

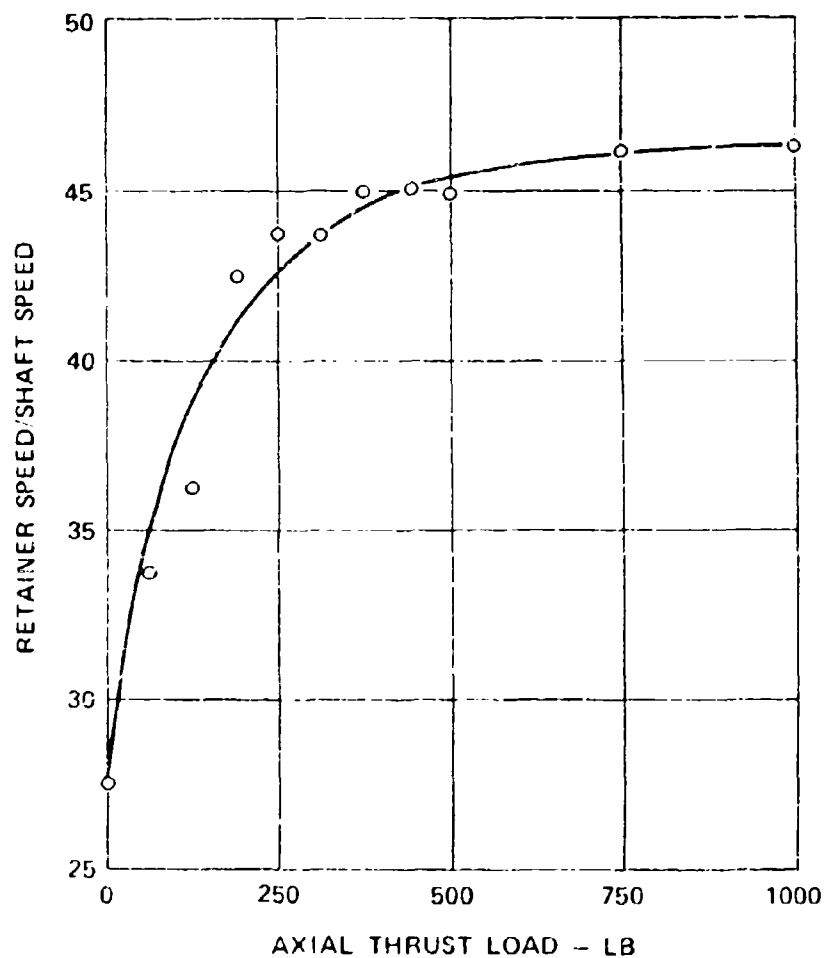


Figure 80. Retainer Speed Ratio Versus Axial Thrust Load.

TABLE XI. INNER AND OUTER RACE TEMPERATURES,
BUILD NO. 3

Data Point	Inner Race (° F)	Outer Race (° F)	ΔT (° F)
1	275	250	-25
2	340	265	-75
3	270	260	0
4	290	265	-25
5	265	275	10
6	320	285	-35
7	300	285	15
8	-	275	-

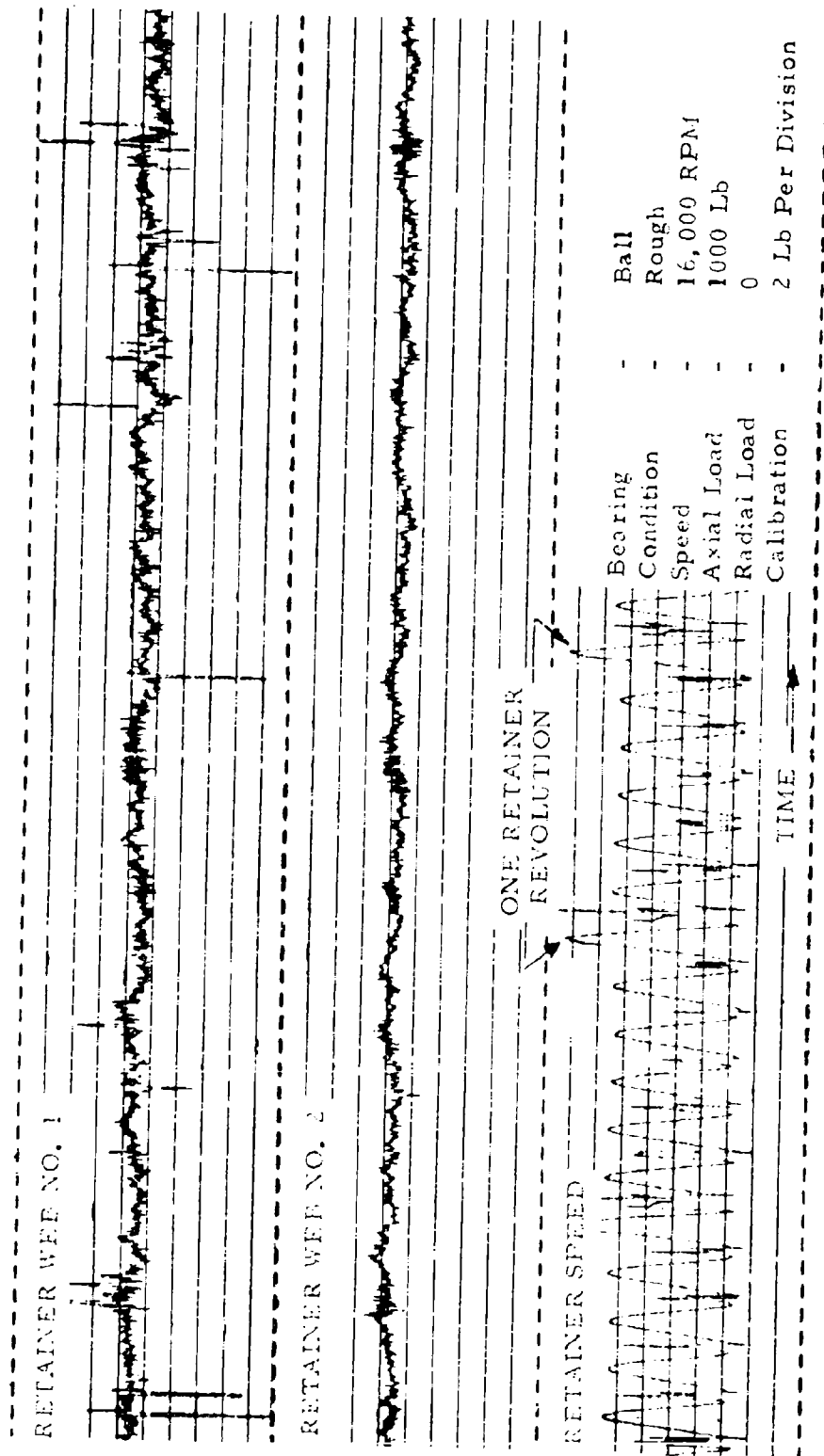


Figure 8i. Expanded Trace of Rough-Race Bearing Retainer Web Forces. Speed signal distortion is result of magnetic tape saturation.

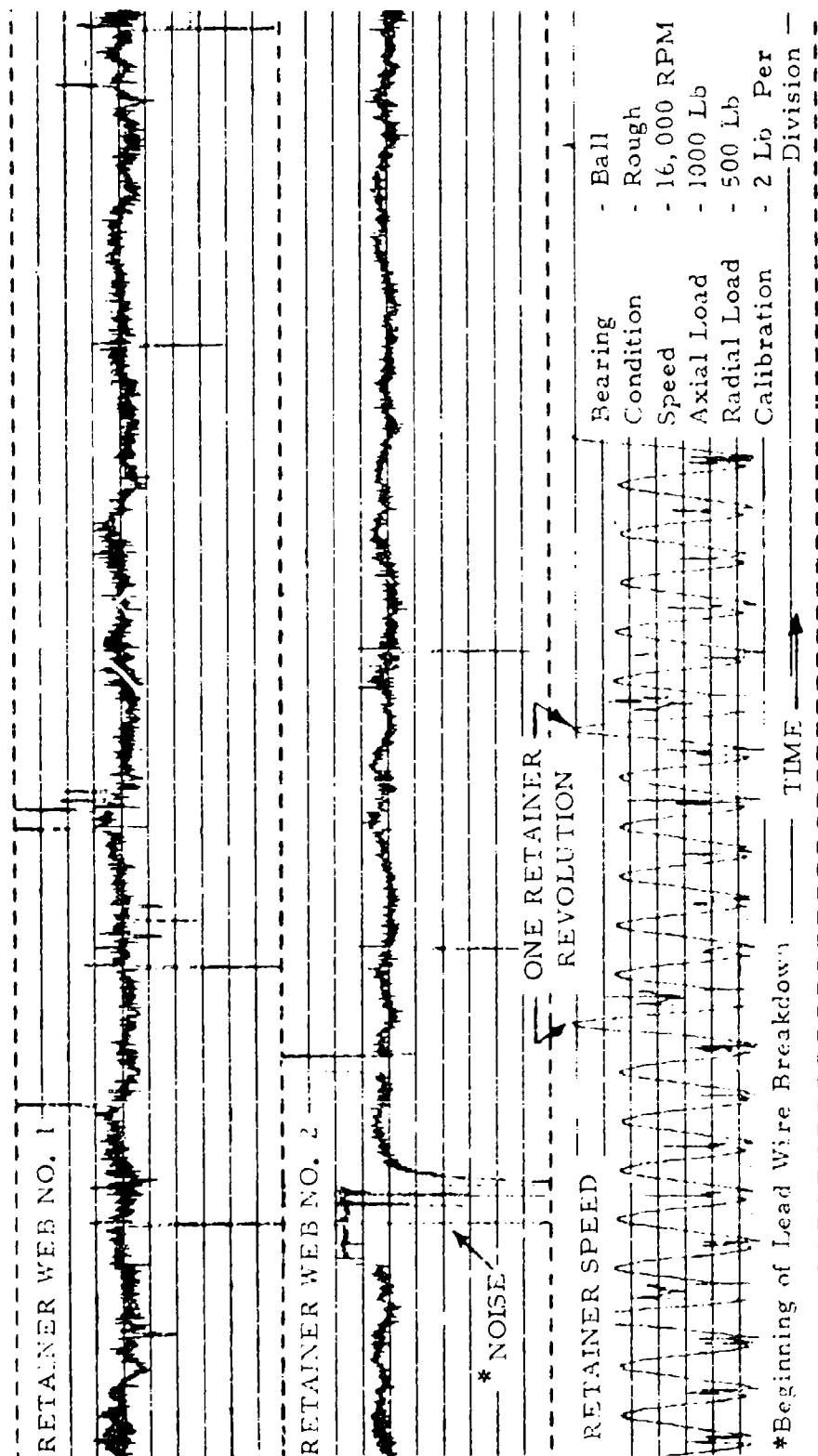


Figure 82. Expanded Trace of Rough-Race Bearing Retainer Web Forces. Speed signal distortion is result of magnetic tape saturation.

TABLE XII. INNER AND OUTER RACE TEMPERATURES, BUILD NO. 4			
Data Point	Inner Race (° F)	Outer Race (° F)	ΔT (° F)
1	200	225	25
2	180	215	25
3	168	195	27
4	130	165	35
5	230	225	-5
6	245	245	0
7	180	255	75
8	140	265	125

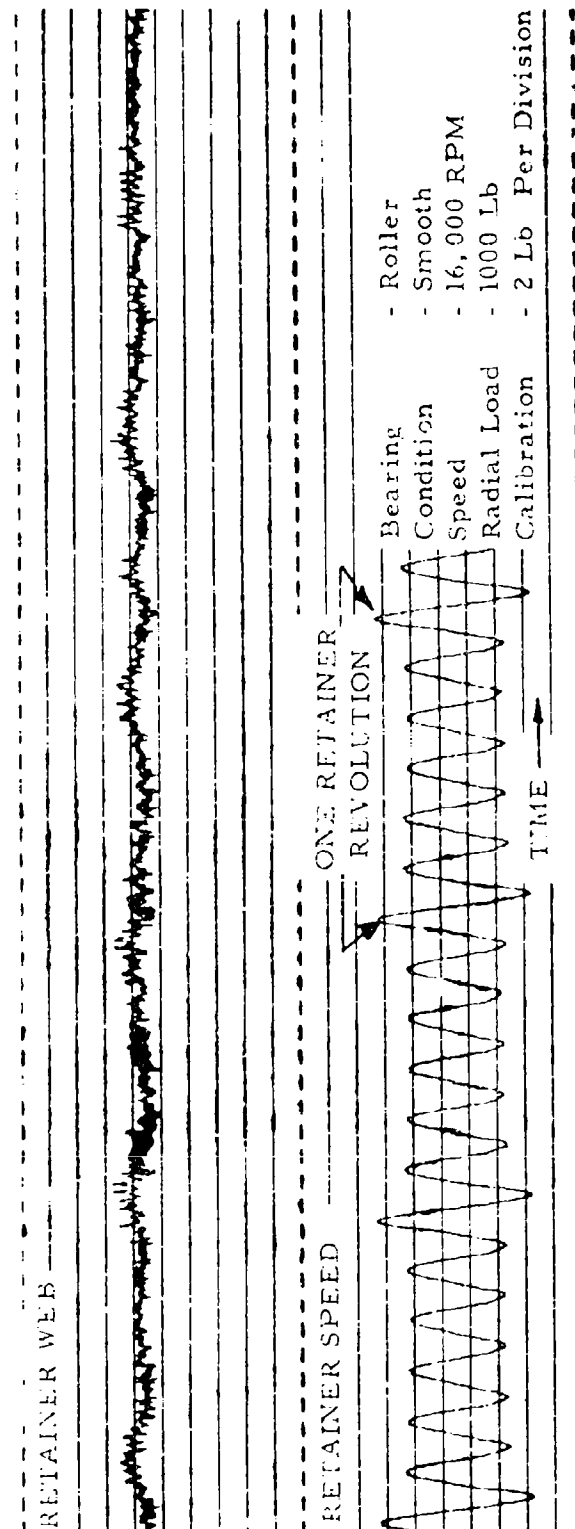


Figure 83. Bearing Retainer Web Force and Speed Versus Time.

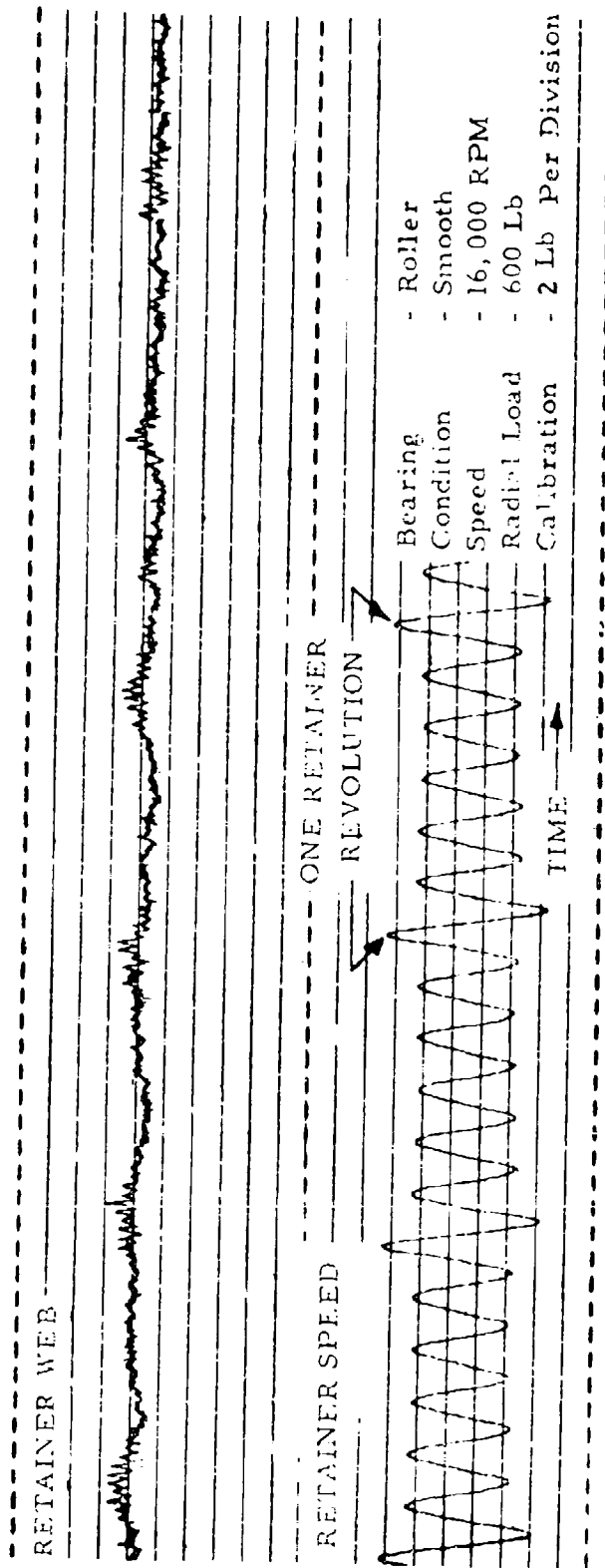


Figure 84. Bearing Retainer Web Force and Speed Versus Time.

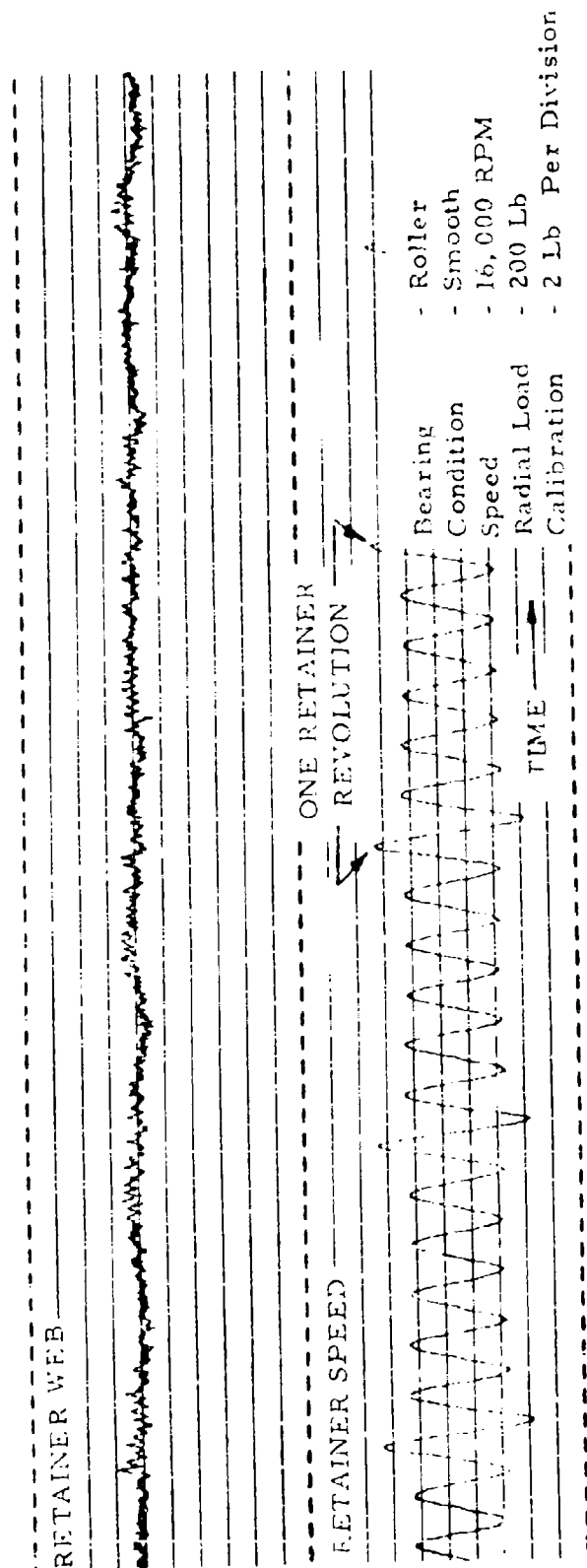


Figure 85. Bearing Retainer Web Force and Speed Versus Time.

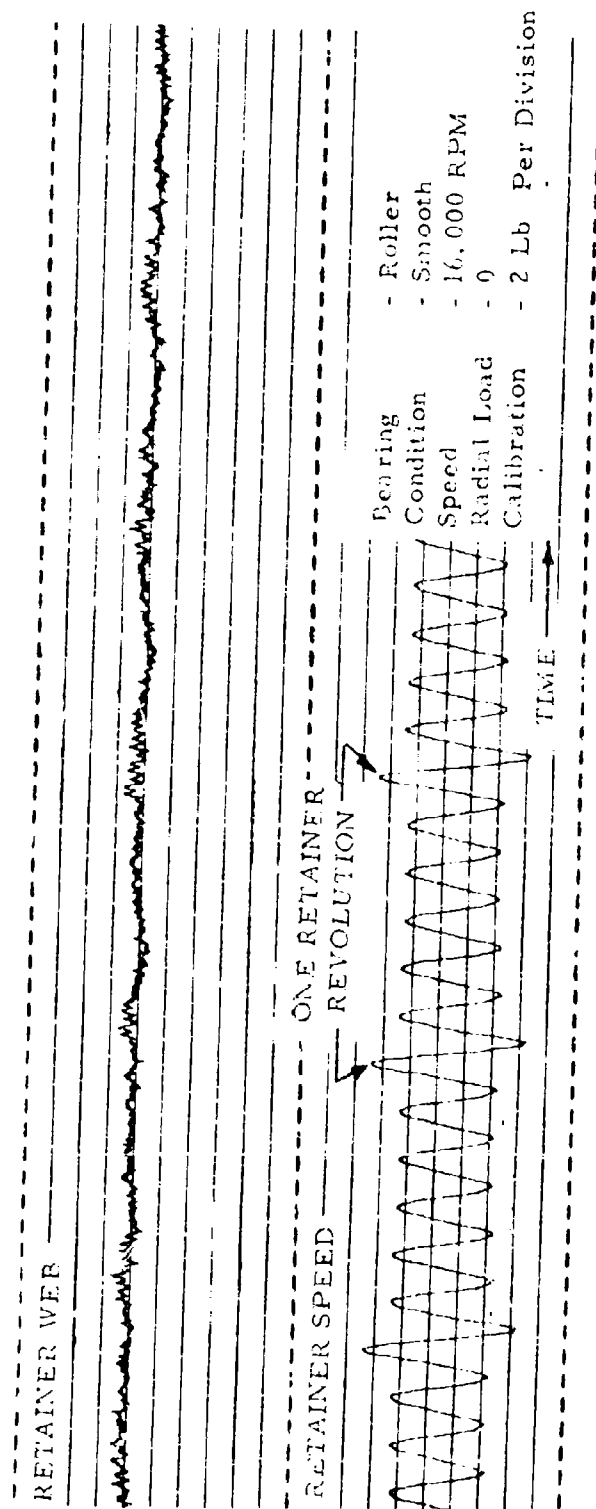


Figure 86. Bearing Retainer Web Force and Speed Versus Time.

COMPUTER PROGRAM RESULTS

BALL BEARING COMPUTER DECK

A listing of the ball bearing computer program FORTRAN source deck is presented in Appendix I. The program consists of a main section and eleven subroutines, each of which performs a specific function. This modular organization of the program facilitates the incorporation of alternate or improved mathematical models at a later date if revisions or modifications are indicated by future advances in the technology. For example, if it is desired to employ traction-slip data other than that reflected, only the subroutine FRCTN need be replaced.

The format for the input information required in the program is given in Appendix II. Cards signifying appropriate units for the input parameters and recommended values of convergence limits are included. Available options concerning the sequence of running numerous load cases with varying bearing definitions, lubricant descriptors, etc., are explained.

A typical problem with the input restated and the program output conveniently labeled for easy interpretation is presented in Appendix III.

BALL BEARING TYPICAL RESULTS

Retainer Pocket Loading and Lubrication

To illustrate the results desired of the computer program, the bearing problem shown in Table XIII, based on the test bearing in the experimental program, was adopted.

The bearing is analyzed at a constant inner ring speed of 20,000 rpm (2.0×10^6 DN) and an axial thrust load of 1,000 pounds. Externally applied radial loads were varied to determine their effect on pocket loading and lubrication. The effects of applied radial loads on the ball pocket load distribution are shown in Figure 87.

A positive pocket force indicates that the ball is driving the retainer assembly; conversely, a negative pocket force indicates that the ball is retarding the rotation of the retainer assembly. The results clearly indicate, as intuition dictates, that ball pocket loading is strongly dependent upon the relationship between the thrust and the radial load when operating under combined axial and radial externally applied loads. This dependency occurs because the unconstrained orbital velocity at each ball

TABLE XIII. BEARING PROBLEM PARAMETERS

Number of Balls	22
Ball Diameter	.531 in.
Pitch Diameter	4.724 in.
Nominal Contact Angle	30 deg
Outer Race Curvature	.515
Inner Race Curvature	.520
Clearance Change	-.0015 in.
Pilot Clearance (outer)	.029 in.
Pocket Clearance	.031 in.
Pressure Viscosity Coefficient	1.18×10^{-4} in. ² /lb
Temperature Viscosity Coefficient	1.53×10^{-2} °F ⁻¹
Viscosity at Inlet	3.86×10^{-6} lb-sec/in. ²
Thermal Conductivity	7.74×10^{-2} Btu/°F-hr/ft
Lubricant Density	8.97×10^{-5} lb-sec ² /in. ⁴

position would be different, owing to contact angle variations from position to position. Contact angle variations are strongly dependent on the magnitude of radial load relative to the axial load acting on the bearing. The calculated radial force acting between the pilot surface and the outer race land is shown as a parenthetic quantity in Figure 87. It is interesting to note the variation in this load component for the equal increments of externally applied radial loads. Note that for equal externally applied radial load increments from 500 to 750 pounds and from 750 to 1,000 pounds, the pilot surface contact force increase is 2.2 and 17.3 pounds, respectively. Additional cases were investigated with a thrust load of 500 pounds and a radial load of 1,000 pounds, and a pure radial load of 1,000 pounds with resulting pilot surface contact forces of 7.76 and 1.91 pounds, respectively. An axial-radial load ratio appears to exist (approximately 1:1) at which the pilot load is at a maximum value. This load component, in the case of an outer-piloted retainer, results in a retainer drag force; in the case of an inner-piloted retainer, it creates a retainer driving force. This effect might be theorized to be responsible for the skid recovery phenomenon often experienced on ball bearings at high speeds and extremely low thrust loads. Figure 88 illustrates the hydrodynamic ball-pocket film thickness as a function of azimuth angle for a thrust load of 1000 pounds and a radial load of 500 pounds. Also plotted on the same azimuth scale is the pocket loading to illustrate the strong dependence of film thickness upon load. For light loads, pocket film thicknesses are limited to pocket clearances in the analysis because often, with extremely light pocket loads, unrealistically large estimates will result.

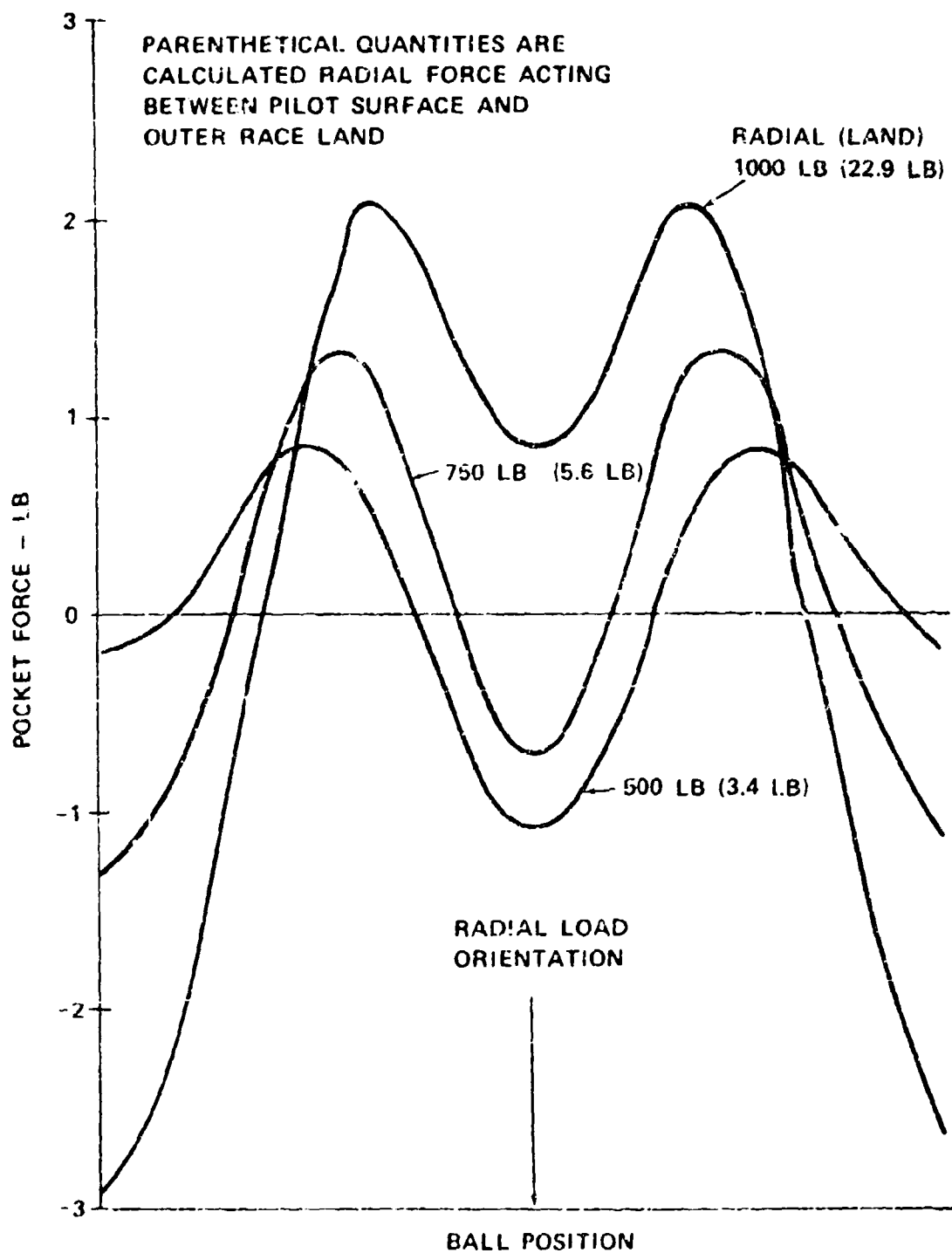


Figure 87. Pocket Loading Versus Radial Load (Axial Load = 1000 Pounds).

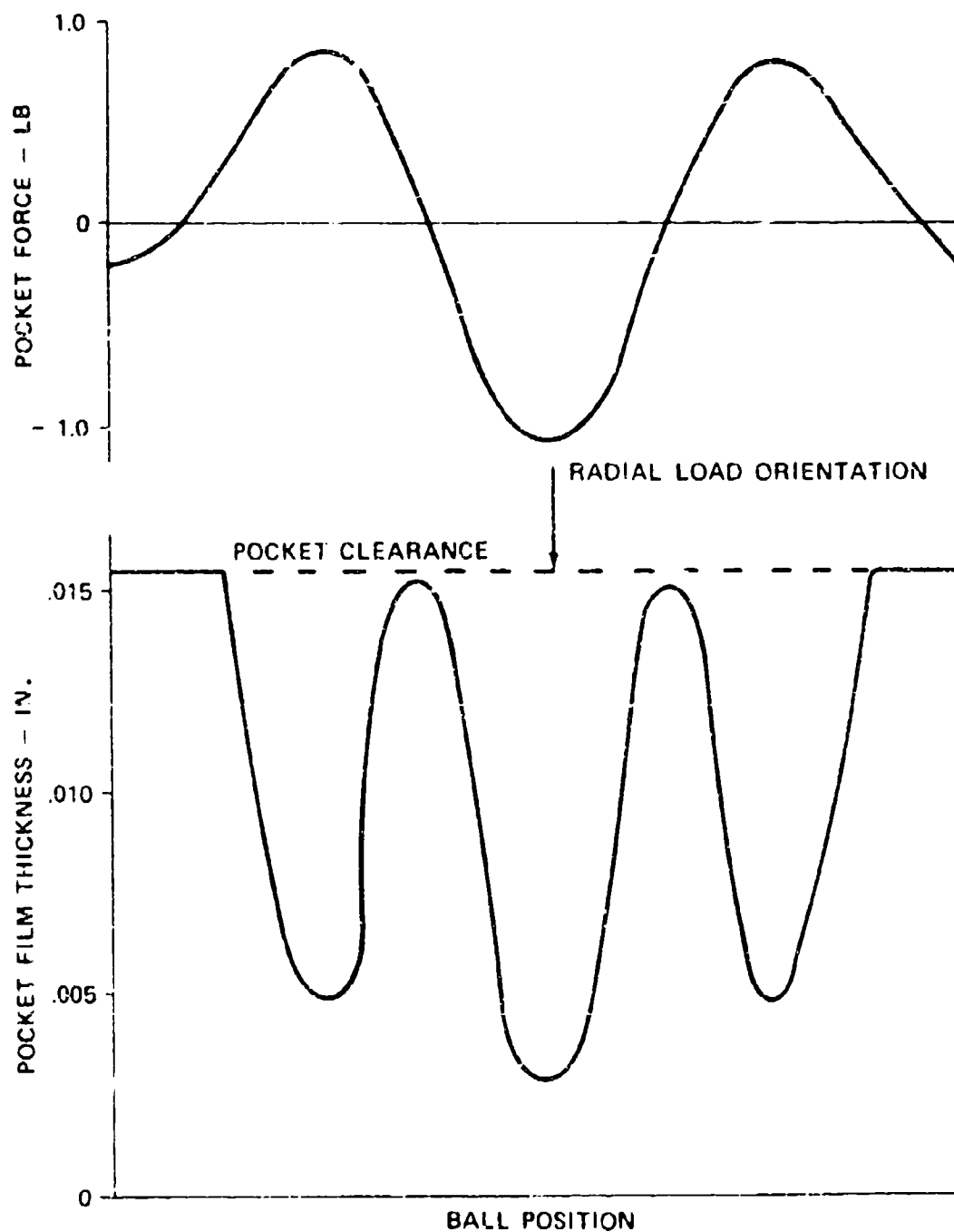


Figure 88. Pocket Film Thickness Versus Pocket Load
(Axial Load = 1000 Pounds, Radial Load = 500
Pounds).

Retainer Speed Variations (Skidding)

An important spinoff benefit derived from the retainer analysis reported herein is the ability to predict retainer skidding as a function of externally applied loads for high-speed angular-contact ball bearings. Figure 89 compares retainer speed results derived from the computer program with data obtained during the verification program. Also shown are the retainer speeds calculated using the elastic analysis (no slip), which is extensively used for bearing design today throughout industry. The zone depicted between the dashed lines in the gross skid regime is indicative of retainer speed variations encountered. Unlike previous results,⁹ retainer rotational velocities in this skid regime were not constant, and significant excursions were observed at constant thrust loads. This phenomenon is not considered to be of great importance from a design standpoint; what is significant is the break in the curve below which gross skidding occurs.

With respect to the difference between the elastic solution prediction and the EHD solution results, the difference in retainer speeds calculated at high thrust loads is predominantly the result of ball slip at the race contacts required to generate traction. Inner and outer race contact angles for this load case were essentially the same for the two different analytical solutions.

Ball Kinematics

The kinematics of a ball in a high-speed angular-contact bearing has provided bearing engineers and analysts with a wide area for disagreement over the last decade. The reason is that in an angular-contact ball bearing, pure rolling cannot occur simultaneously at both inner and outer race contacts.² Consequently, assumptions were required concerned with the spin velocities prevalent at the race contacts and the distribution of tractive force components required to offset ball gyroscopic moments. The major controversy centers about the race control concept previously discussed under "Introduction."

This concept is based upon the supposition that all the spin occurs at the contact where the resistance to spin (spin torque) is minimum, and that all traction in the gyroscopic plane occurs at the race contact which exhibits pure rolling (no slip). For example, a bearing with outer race control would have zero spin at the outer contact with the inner contact operating at the geometrically required spin level, while all the required traction force to resist gyroscopic precession would be developed at the outer contact.

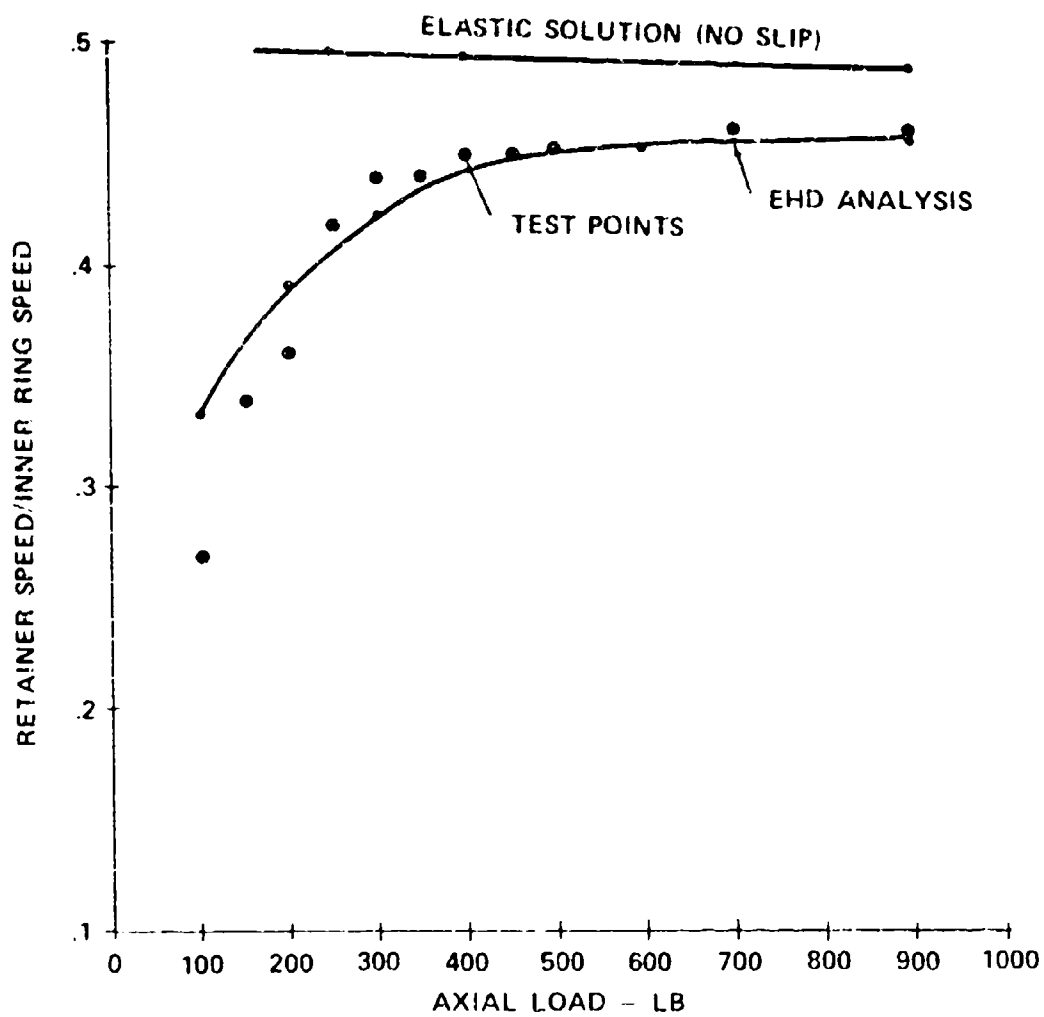


Figure 89. Retainer Speed Versus Axial Load.

The analysis developed herein is general and does not require these assumptions, and unbiased solutions can be obtained. Table XIV presents computer results pertaining to ball kinematics for varying thrust loads to explore this phenomenon in the skid regime and at high thrust loads. The cases studied are the same as those used for the skid curve, Figure 89. Also shown at the bottom of the table is the result of an elastic solution in which outer race control is assumed.

In Table XIV, $\dot{\alpha}_X$, $\dot{\alpha}_Y$, and $\dot{\alpha}_Z$ are the angular velocity components about the indicated axes. The angular velocity component $\dot{\alpha}_Y$ has a circumferential vectorial direction, i.e., gyroscopic precession. F_{X1} and F_{X2} are the tractive forces in the outer and inner contact areas, which are opposing the rotation $\dot{\alpha}_Y$. The ratio F_{X2} divided by F_{X1} compares these two force components. Outer race control would have $F_{X2} = F_{X2}/F_{X1} = 0$. The computer results do not rigorously substantiate this assumption, but F_{X2} is significantly less than F_{X1} , which indicates that the race control concept is, if not absolutely correct, practically useful from this standpoint. It is interesting to note that from a traction standpoint, bearings in the skid regime tend more toward race control than those that are operating at high thrust loads. Also, by comparing the 800-pound thrust load cases, it is seen that a greater value of $\dot{\alpha}_Z$ is predicted with the EHD analysis with a corresponding increase in gyroscopic moment and tractive force.

Another relationship that can be used to test the accuracy of the race control concept is the spin velocities at the race contact. Again, referring to Table XIV, it is evident that spin occurs predominantly at the inner contact as the control theory predicts. With regard to the behavior in the skid regime, values of $\dot{\alpha}_{S1}$ divided by $\dot{\alpha}_{S2}$ increase as gross skidding increases -- the opposite effect relative to race control behavior as observed with the tractive forces.

In general, kinematic behavior that is in relative agreement with the race control concept is not surprising, in that many successful bearings have been designed with the use of analytical techniques predicated upon its precepts.

TABLE XIV. BALL KINEMATICS; INNER RING SPEED = 20,000 RPM, RADIAL LOAD = 0									
Thrust (lb)	ω_X (rpm)	ω_Y (rpm)	ω_Z (rpm)	FX_1 (lb)	FX_2 (lb)	FX_2/FX_1	ω_{s1} (rpm)	ω_{s2} (rpm)	ω_{s1}/ω_{s2}
100	-67,640	1,696	8,470	-3.78	-0.05	.013	-7,854	-39,753	.198
200	-78,834	1,960	10,030	-5.30	-0.15	.028	-7,764	-44,826	.173
300	-84,104	2,052	11,641	-6.32	-0.27	.043	-7,210	-46,953	.154
500	-88,447	2,075	13,930	-7.75	-0.59	.076	-5,945	-47,820	.124
800	-89,566	1,990	17,210	-9.29	-1.25	.135	-4,540	-45,800	.099
800 (Elastic Solution)	-94,800	0	12,600	-8.2	0	0	0	-52,669	0

ROLLER BEARING COMPUTER DECK

A listing of the roller bearing computer program FORTIAN source deck is presented in Appendix IV. The program is structured in a manner similar to the ball bearing deck and consists of a main section and nine subroutines. Four subroutines are inactive in this listing as a result of the convergence problems encountered with the COEFCT routine. They are included in this listing since they were part of the initial effort.

The format for the program input is given in Appendix V. Directions for exercising various program input options are also given. A particular input requirement for the roller bearing program is found on card 9, columns 41 through 50. This input item causes the program to execute the specific case for the cage slip inputted. It is therefore required that the user input an appropriate series of cases to achieve a desired solution. The solution is obtained when the "Torque on Cage" output value approaches zero.

A typical problem and corresponding output is presented in Appendix VI.

ROLLER BEARING TYPICAL RESULTS

The bearing data shown in Table XV was used to illustrate the desired program output. This data represents the test roller bearing used during the experimental program.

The bearing was analyzed at an inner ring speed of 20,000 rpm, which results in a DN speed value of 2×10^6 . Radial loads were varied to determine slip speeds of the cage and other bearing outputs. To arrive at the desired solution, various cage slip speed assumptions were inputted. Each output case yielded residual cage torques which were plotted as shown in Figure 90. The final solutions for slip are obvious and can be inputted to obtain final results for each load case. Final results for cage slip speeds as a function of radial loading are shown in Figure 91. The iterative procedure was pursued for the 200-pound load case, the solution for which is shown in Appendix VIII.

TABLE XV. ROLLER BEARING PROBLEM PARAMETERS

Number of Rollers	28
Roller Diameter - in.	.4331
Roller Length - in.	.4331
Pitch Diameter - in.	4.7244
Diametral Clearance - in.	.0025
Retainer Pilot Clearance (Inner) - in.	.030
Pocket Clearance - in.	.0125
Pressure Viscosity Coefficient - in. ² /lb	9.6×10^{-5}
Temperature Viscosity Coefficient - $^{\circ}\text{F}^{-1}$	1.47×10^{-2}
Viscosity at Inlet - lb-sec/in. ²	7.35×10^{-7}
Thermal Conductivity - Btu/ $^{\circ}\text{F}$ -hr/ft	7.40×10^{-2}
Lubricant Density - lb-sec ² /in. ⁴	8.25×10^{-5}

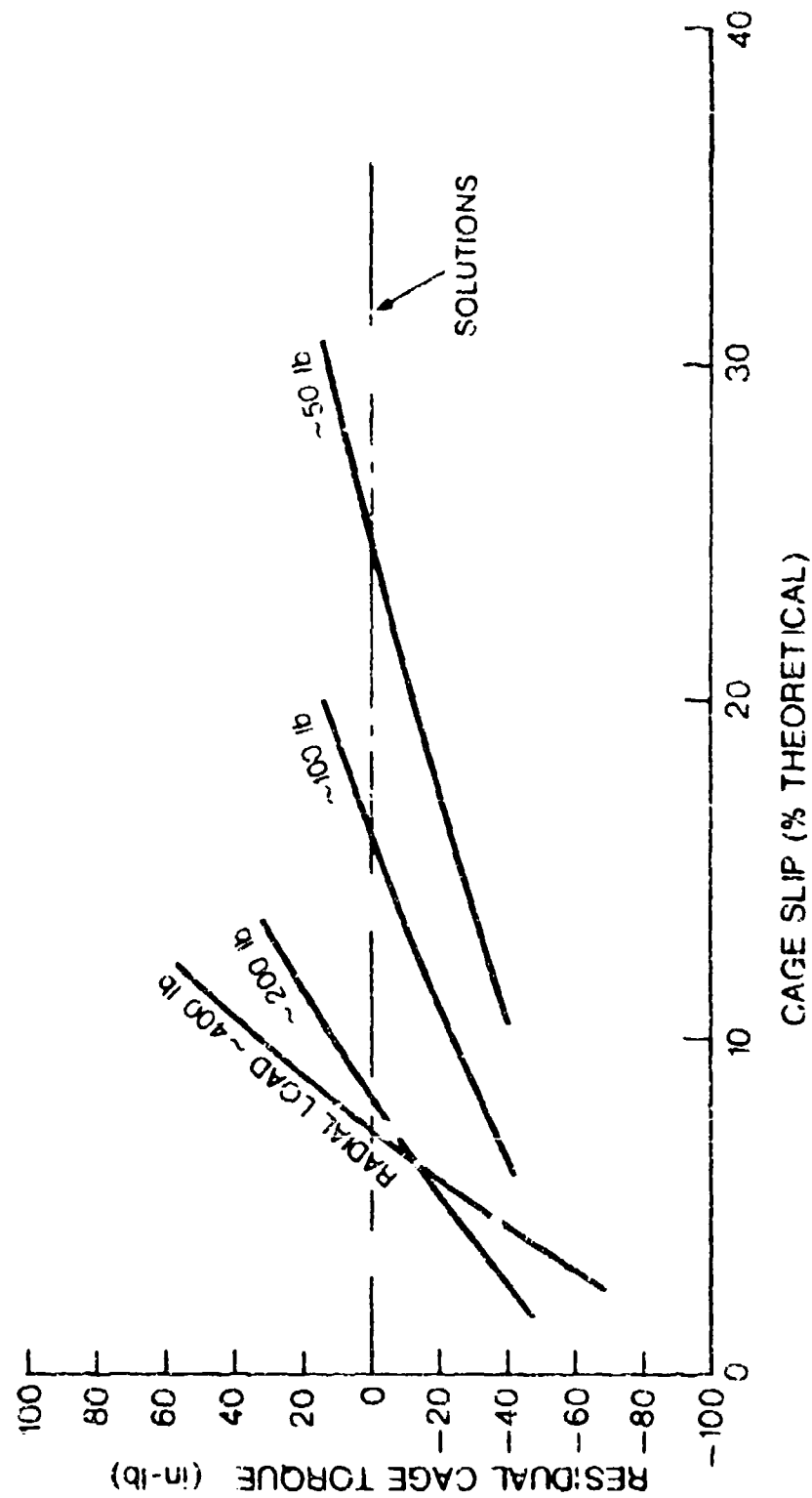


Figure 90. Roller Bearing Program: Data: Residual Cage Torque Versus Cage Slip
(Inner Race Speed = 20,000 RPM).

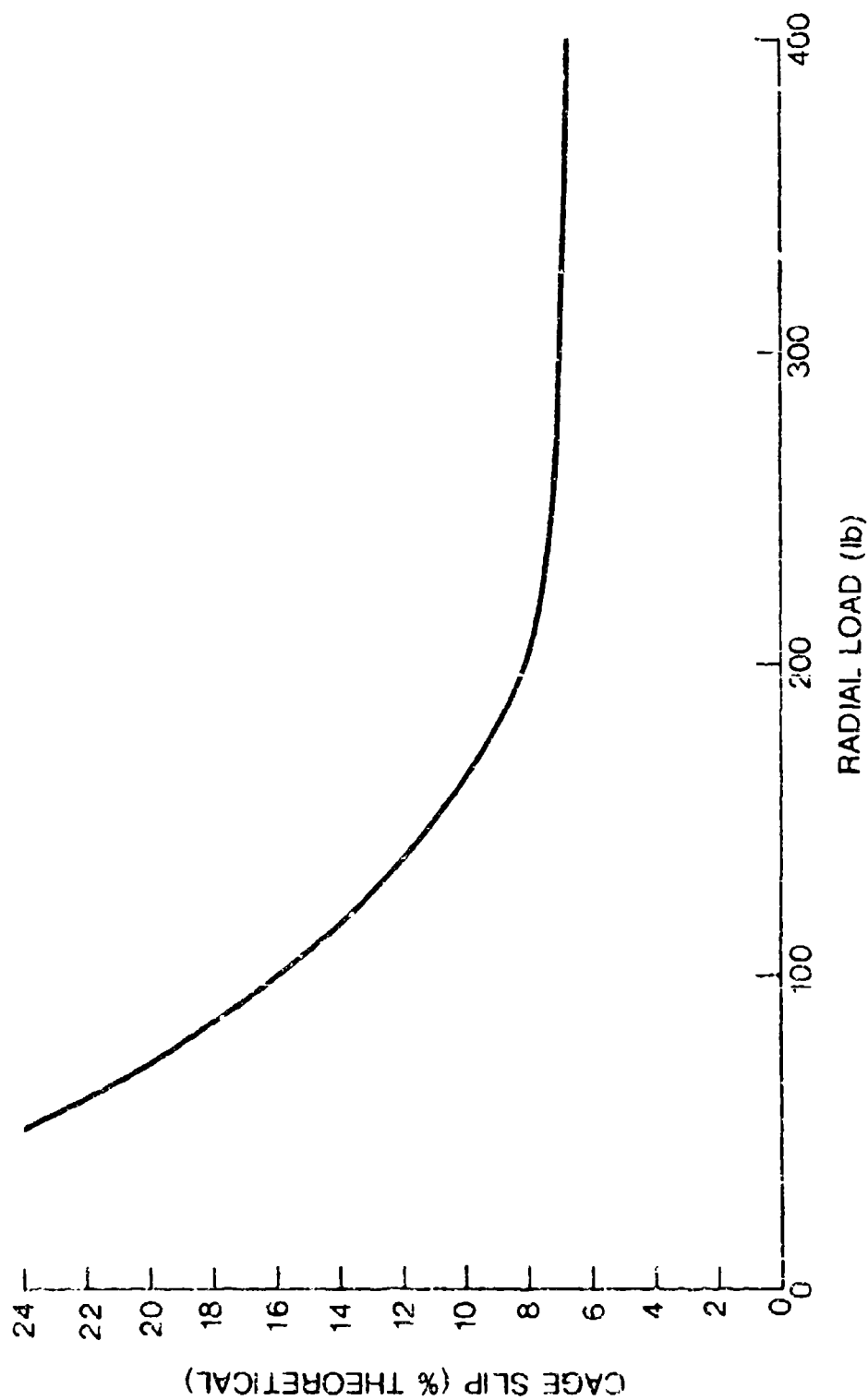


Figure 91. Roller Bearing Program Data; Cage Slip Versus Radial Load
(Inner Race Speed = 20,000 RPM).

CONCLUSIONS

1. Retainer pocket forces predicted by the computer analysis for the cases studied are small, approximately 5 pounds, and are in quantitative agreement with the basic pocket force cycles measured during the experimental test program. Existing differences between measured and predicted values can be attributed to dynamic shaft unbalance, imperfect bearing geometry, etc. However, superimposed upon these force levels are pulse-type forces that were measured at the retainer pockets. These forces were significantly larger than the former, on the order of 50 pounds, and are believed to be the result of impacts between the rolling elements and retainer pockets resulting from acceleration/deceleration of the rolling elements and/or retainer. Impact force levels dominate and constitute the major criteria in the establishment of the structural integrity of the high-speed retainer.
2. Lubricant film thicknesses developed at the rolling element-to-retainer pocket contacts are hydrodynamic in nature, and they are strongly dependent upon the contact force magnitudes.
3. Bearing kinematics resulting from the computer solutions that consider traction at the rolling element-to-race contacts are not widely different from analyses conducted hitherto that employ the race control assumptions. However, the new model does predict ball spin at both inner and outer contacts, gyroscopic precession, and resistance to gyroscopic precession at each of the inner and outer race contacts.
4. The computer analysis predicts regions of tractive ball instability at some load and speed conditions resulting from thermal effects in the EHD contact between balls and races.
5. Retainer slip at low-load conditions can be predicted by the computer program. Confirmation of the analysis for the test ball bearing employed during the program was obtained. Retainer pilot surface-to-race land contact force, which affects skidding characteristics, was found to be strongly dependent upon the ratio of the axial to radial loads applied to the bearing.

RECOMMENDATIONS

1. It is recommended that further work conducted to achieve a better understanding of overall bearing operation address the rheological behavior of EHD lubrication with particular emphasis on traction.

The effects of lubrication upon bearing operating characteristics are central to the analysis of rolling element bearings. The dynamics and kinematics of bearing operation are well understood in comparison with the equally important effects of the rheological behavior of the lubricant. Much of the lubricant information drawn upon in the analysis is an extrapolation of empirical data obtained in different operating regimes. The development of more extensive and sophisticated bearing analyses based upon the relatively underdeveloped technology of EHD lubrication will not substantially increase our overall understanding of high-speed bearing performance, especially in the light of the convergence problems encountered with available data as described in "Tractive Instability," page 53.

2. Attention should be directed toward further investigation of the cage pocket impact forces observed. Tests should be conducted on a greater variety of bearing configurations and operating conditions to achieve a more general verification of the observed results.

LITERATURE CITED

1. Dowson, D., and Higginson, G. R., ELASTOHYDRODYNAMIC LUBRICATION, Pergamon Press, Oxford, 1966.
2. Jones, A. B., THE MATHEMATICAL THEORY OF ROLLING-ELEMENT BEARINGS, Mechanical Design and Systems Handbook, Section 13, McGraw-Hill, New York, 1964.
3. Boness, R. J., THE EFFECT OF OIL SUPPLY ON CAGE AND ROLLER MOTION IN A LUBRICATED ROLLER BEARING, Journal of Lubrication Technology, Transactions of the ASME, Series F, Vol. 92, No. 1, 1970, pp. 39-53.
4. Crook, A. W., THE LUBRICATION OF ROLLERS. IV. MEASUREMENTS OF FRICTION AND EFFECTIVE VISCOSITY, Philosophical Transactions of Royal Society of London, Series A 255, 281.
5. Harris, T. A., AN ANALYTICAL METHOD TO PREDICT SKIDDING IN THRUST-LOADED ANGULAR-CONTACT BALL BEARINGS, Journal of Lubrication Technology, Vol. 93, No. 1, 1971, pp. 17-24.
6. Johnson, K. L., and Cameron, R., SHEAR BEHAVIOR OF ELASTO-HYDRODYNAMIC OIL FILM AT HIGH ROLLING CONTACT PRESSURES, Proceedings of the Institution of Mechanical Engineers, 1967-1968, Vol. 182, p 307.
7. Lundberg, G., ELASTISCHE BERÜHRUNG ZWEIER HALBRÄUME, VDI Forschung auf dem Gebiete des Ingenieurwesens, September-October 1939, Bd. 10, Nr. 5, pp. 201-252.
8. Plint, M. A., TRACTION IN ELASTOHYDRODYNAMIC CONTACTS, Proceedings of the Institution of Mechanical Engineers, 1967-1968, Vol. 182, p. 300.
9. Poplawski, J. V., and Mauriello, J. A., SKIDDING IN LIGHTLY LOADED HIGH-SPEED BALL THRUST BEARINGS, ASME Preprint 69-LUBS-20.
10. Walters, C. T., THE DYNAMICS OF BALL BEARINGS, Journal of Lubrication Technology, Vol. 93, No. 1, 1971, pp. 1-10.
11. McGrew, J. M., Gu, A., et al., ELASTOHYDRODYNAMIC LUBRICATION, Preliminary Design Manual, Technical Report AFAPL-TR-70-27, Mechanical Technology, Inc., November 1970.

APPENDIX I BALL BEARING COMPUTER PROGRAM FORTRAN SOURCE DECK

```

C      MAIN PROGRAM
REAL LURDEN
COMMON HSO(40),HSI(40)
COMMON ALPHA,AA(2),AMAJ(2,40),AMIN(2,40),APOCK(40),      RET,BETA
1,3(2),B3(2),BPCK(40),CAGEW,      CRV(2),      CRAD,COSR,CPH,CTHET,
200PR(5),CR(2),CF,C(2),CSP(2),COR(5),CLFA9S(2),CLFARP,DP(2,5),
30G(2,2),DCF(5),D9(2,5),DEX(2),DROP,D,DENS,DOL(4),DFL(4),DTV(5,5),
40ETER,DFL(2),DDELX(2,2),DXKOG(2),DFXVX(2),DFXVY(2),DFXWS(2),
50FXP(2),DFYVX(2),DFYVY(2),DFYWS(2),DFYP(2),DGSVX(2),DQSVY(2),DQSW
6(2),DQSP(2),DFX(2,5),DFY(2,5),DQS(2,5),DFPX(5),IFPZ(5),DQP(5),DMY(
75),DMZ(5),DPS(5,5),DPS1(5,5),DPA(2),DDELA(2),DPA(2),DFXA(2),DFYA
8(2),DOSA(2),DFXOME(2),DFYOME(2),DQSQME(2),DFPXA(2),DFPZA(2),DQPA(2
9),DVARA(5),DVARA2(5),DVOME(5),DGA(2),      E,EL
COMMON FRR(5),E2,FSAVE(2),      FLAT,F(2),FK,FRAD
1,ETAN,FFX(2,40),FFY(2,40),      GAGE,G2(2),GG(2),
2      HORIZ,HOR1,HOR2,HOR3,HOR4,      IQUIT,
3IPASS,      LPASS,LURDEN,      N,      IMFGAE,DMY,DMZ,
407,7MS(2),CMEX(40),CMFY(40),CMFZ(40),      PPOC(40),PL,
5PR,PC,PC,PO,PCCKET,PHI,PILOT,PX(2),PS1(5),P(2,40),      DMV,
6S(2),DQS(2,40),      R,RPM(2),      SINR,SPH,STHET,
7SR(2),SQ(2),      TOTL,T1,THET,TOL(11),TCRV,TSAVE(2),
8THICKR(2,40),THICKP(40),      VIS,VERT,VRT1,VRT2,VRT3,VRT4,VYR(2),
9VYR(2),VXR(2),VXP(40),VZP(40),VFC(5)
COMMON X(5),XN,XF(4),XF1(4),XK(2),XMZ,XMY,XPHI(40),XAFT(2,40),XOMS
1(2,40),XML,XMU1,      YE,YR,YC,YNUM
COMMON DZVYR,DZVX,DZWS,DZP2,XIN,XMASS
COMMON FX(2),FY(2)
COMMON IC,CTL(40),LCTL,ICNT,LQOP,1Q(2),Y1,Y2,Y3,Y4,Y5,Y6,Y7,Y8,Y9
1,Y10,GA(2,2),BA(2,2),DELA(2,2),H(2),HH(2),H1(2),H2(2),SRAL(2),
20RAL(2),CMEGA,CMF(40),DLX(2),DPSIX(2,2),DGYA(2),PA(2,2),DPSIA(2),
3XA(2),      KQNV,DAD(2,2),REYA,DGYRO(2),CAL,SAL,A1,A2,DN,T1,T2,T3,T4,
40ET,WIM,XA1(40),XA2(40),IPASS,REVX(40),REV7(40)
5,CAGED(2),RINGO(2),AREA(2),VFL(2),SORAG(2),RDRAG,DSORAG(2,4),
60ZDA1,FPZDA2,FPZOME,DRDRAG(4)
COMMON/TESTCOM/TEST1,TEST2
COMMON/RALTST/PLTST
COMMON/XTPA/VDRAG(2),CORAG(2),CFORCE
CALL ZFRO(ALPHA,DRDRAG(4))
GO TO 999
999  CONTINUE
DAD(1,1)=1.
DAD(2,1)=0.
DAD(1,2)=0.
DA(1,1)=0.
DA(1,2)=0.
DEX(1)=0.
DEX(2)=2.
DELA(1,1)=0.
DELA(1,2)=0.
H(2)=0.
H1(1)=0.
H1(1)=1.
H1(2)=0.
H2(1)=0.
H2(2)=1.
G4(1,1)=0.
G4(1,2)=0.
DCF(1)=0.
DCF(2)=0.

```

DOF(4)=0.	600
DOF(5)=0.	610
C(1)=1.	620
C(2)=-1.	630
2 READ(5,80)	640
WRITE(6,80)	650
CALL INPT	660
YMASS=1.3550693E-3*DENS*D**3	670
XIN=.1*YMASS*D**2	680
10 READ(5,1000)ALPHA,BETA,VIS,TI,FK,LUBDEN,D2VYR,D2VX	690
LCASF=0	700
IF(ALPHA)1,9,1	710
9 WRITE(6,81)	720
GO TO 2	730
1 WRITE(6,3)	740
1 FORMAT(1H /1H /1H /1H /1H /1H /23HO LUBRICANT PROPERTIES)	750
READ(5,1000)D2WS,D2P2,(TOL(K),K=1,9),CONST1,CONST2	760
WRITE(6,4)ALPHA	770
4 FORMAT(40H PRESSURE-VISCOSITY COEFFICIENT ,1P1E11.4)	780
WRITE(6,5)BETA	790
WRITE(6,6)VIS	800
5 FORMAT(40H TEMPERATURE-VISCOSITY COEFFICIENT ,1P1E11.4)	810
6 FORMAT(40H VISCOSITY AT INLET TEMPERATURE ,1P1E11.4)	820
WRITE(6,7)TI	830
7 FORMAT(40H INLET TEMPERATURE ,1P1E11.4)	840
WRITE(6,8)FK	850
8 FORMAT(40H THERMAL CONDUCTIVITY ,1P1E11.4)	860
WRITE(6,1001)LUBDEN	870
1001 FORMAT(40H LUBRICANT DENSITY ,1P1E11.4)	880
WRITE(6,5000)XMU	890
5000 FORMAT(40H BALL POCKET FRICTION COEFFICIENT ,1P1E11.4)	900
WRITE(6,5001)XMU1	910
5001 FORMAT(40H GAGE PILOT FRICTION COEFFICIENT ,1P1E11.4)	920
30 READ(5,1000)RPM(1),RPM(2),XF(1),XF(3),DOL(4),DOL(1),DOL(3),VLCTI	930
LCASF=LCASF+1	940
ICTL=VLCTI	950
IF(D2VYR.EQ.0.)D2VYR=.35	960
IF(D2VX.EQ.0.)D2VX=.05	970
IF(D2WS.EQ.0.)D2WS=.1	980
IF(D2P2.EQ.0.)D2P2=.05	990
1003 FORMAT(7F10.0,F9.0,11)	1000
IF(1CTL.LF.0)1CTL=1	1010
GGG=D*CONSR/E	1020
MEGAF=.5*(RPM(1)*(1.+GGG)+RPM(2)*(1.-GGG))	1030
4000 TAPS=CMEGAF	1040
1000 FORMAT(8F10.0)	1050
IF((RPM(1)-RPM(2)).EQ.0.) GO TO 10	1060
WRITE(6,81)	1070
WRITE(6,80)	1080
WRITE(6,71)LCASF	1090
WRITE(6,72)RPM(1)	1100
WRITE(6,73)RPM(2)	1110
WRITE(6,72)CMEGAF	1120
WRITE(6,74)XF(1)	1130
WRITE(6,75)XF(3)	1140
WRITE(6,76)DOL(4)	1150
WRITE(6,77)DOL(1)	1160
WRITE(6,78)DOL(3)	1170
WRITE(6,79)VLCTI	1180

71	FORMAT(40H)	OPERATION DATA FOR LOAD CASE NUMBER	,I2)	1190
72	FORMAT(40H)	OUTER RACE SPEED	,1P1E11.4)	1200
73	FORMAT(40H)	INNER RACE SPEED	,1P1F11.4)	1210
74	FORMAT(40H)	THRUST LOAD	,1P1F11.4)	1220
75	FORMAT(40H)	RADIAL LOAD	,1P1F11.4)	1230
76	FORMAT(40H)	MISALIGNMENT	,1P1F11.4)	1240
77	FORMAT(40H)	INITIAL AXIAL DEFLECTION	,1P1F11.4)	1250
78	FORMAT(40H)	INITIAL RADIAL DEFLECTION	,1P1E11.4)	1260
79	FORMAT(40H)	RACE CONTROL INDEX	,1P1E11.4)	1270
80	FORMAT(71H)			1280
1				1290
81	FORMAT(11H)			1300
82	FORMAT(40H)	THEORETICAL RACE SPEED	,1P1E11.4)	1310
83	FORMAT(1P3F11.4)			1320
	OMEGAE=.10471976*OMEGAE			1330
	IF (ABS(DDL(1))+ABS(DDL(3))+ABS(DDL(4)))13,13,14			1340
13	DDL(1)=DF(1)			1350
	DDL(3)=DFL(3)			1360
	DDL(4)=DFL(4)			1370
14	N=KN			1380
	IF (TOL(1).EQ.0.)TOL(1)=1.E-6			1390
	IF (TOL(2).EQ.0.)TOL(2)=1.E-6			1400
	IF (TOL(3).EQ.0.)TOL(3)=10.			1410
	TOL(3)=TOL(3)*.1047198			1420
	IF (TOL(4).EQ.0.)TOL(4)=1.			1430
	TOL(4)=TOL(4)*.1047198			1440
	IF (TOL(5).EQ.0.)TOL(5)=5.			1450
	TOL(5)=TOL(5)*.1047198			1460
	IF (TOL(6).EQ.0.)TOL(6)=1.E-6			1470
	IF (TOL(7).EQ.0.)TOL(7)=1.E-6			1480
	IF (TOL(8).EQ.0.)TOL(8)=1.E-6			1490
	IF (TOL(9).EQ.0.)TOL(9)=.5			1500
	TOL(9)=TOL(9)*.1047198			1510
	CONST1=.2			1520
	CONST2=1.			1530
	DO 34 K=1,4			1540
34	DFL(K)=DDL(K)			1550
	KINV=0			1560
	RPM(1)=RPM(1)*.10471976			1570
	RPM(2)=RPM(2)*.10471976			1580
	PL=4.*((1.-PE**2)/YE+(1.-PC**2)/YC)			1590
	DO 43 J=1,N			1600
43	CTL(J)=LCTL			1610
44	CONTINUE			1620
	DO 15 ITER=1,15			1630
	ATFST=0.0			1640
	DO 481 K=1,4			1650
481	SDRAG(K)=0.			1660
	ITPASS=ITER			1670
	TEMP1=.008*LUHPEA**25*SQRT(SQRT(VIS))			1680
	DO 400 K=1,2			1690
	VEL(K)=(RPM(K)-OMEGAE)*CAGFDI(K)*.5			1700
	SDRAG(K)=TEMP1*AREA(K)*ABS(VEL(K))*1.75/CLFARS(K)**25*.5*CAGFDI			1710
	1K)			1720
	SDRAG(K)=SIGN(SDRAG(K),VEL(K))			1730
400	VDRAG(K)=SDRAG(K)			1740
	BDRAG=LUBDEN*DO*(CLFARS(1)+CLFARS(2))*(E*OMEGAE)**2*.002			1750
	BDRAG=SIGN(BDRAG,OMEGAE)			1760
	DO 16 K=1,4			1770

16	XF1(K)=0.	1780
	DO 17 K=1,4	1790
	CFR(K)=0.	1800
	DO 17 L=1,4	1810
17	DIVIL(K)=0.	1820
	HOR17=0.	1830
	VERT=0.	1840
	HOR1=0.	1850
	HOR2=0.	1860
	HOR3=0.	1870
	HOR4=0.	1880
	VRT1=0.	1890
	VRT2=0.	1900
	VRT3=0.	1910
	VRT4=0.	1920
	DO 19 J=1,N	1930
	NUM=0	1940
	ICNT=0	1950
	LCJ=0	1960
	IPASS=J	1970
	DMF(J)=0.	1980
	XJ=J	1990
	IF(KCONV)52,52,53	2000
51	IF(ITER-1)52,55,52	2010
55	Y(3)=PPVX(J)	2020
	X(4)=0.	2030
	Y(5)=PPVZ(J)	2040
52	CALL A(2A3)A53*(X,1-1.1/XN	2050
	SPH=SIGN(PH)	2060
	CPH=COS(PH)	2070
	CALL(2,2)=CPH	2080
	CALL BALL(CONST1,CONST2,FPZ,QVX)	2090
	IF(ITER.EQ.0.0) GO TO 2054	2100
	WRITE(18,2052)ITER	2110
2052	FORMAT(1X,2H ITER=,F5.1)	2120
	GO TO 30	2130
2054	CONTINUE	2140
	IF(P(2,J))19,18,54	2150
54	ERR(4)=ERR(4)+PPDF(J)*.5*E2*FPZ*.5*0	2160
	IF(PLTEST.EQ.1.0)PLTEST=1.0	2170
19	CONTINUE	2180
	IF(KCONV)44,44,45	2190
44	DET=DTV(1,1)*DTV(2,2)-DTV(2,1)*DTV(1,2)	2200
	ERR(1)=XF1(1)*XF1(1)	2210
	ERR(3)=XF1(3)*XF1(3)	2220
	CORR(1)=(ERR(1)*DTV(2,2)-ERR(3)*DTV(1,2))/DET	2230
	CORR(3)=(DTV(1,1)*ERR(3)-DTV(2,1)*ERR(1))/DET	2240
	IF(ABS(CORR(1))-TOL(1))46,1515,1515	2250
46	IF(ABS(CORR(3))-TOL(3))47,1515,1515	2260
1515	CONTINUE	2270
	DEL(1)=DEL(1)-CORR(1)	2280
	DEL(3)=DEL(3)-CORR(3)	2290
	GO TO 15	2300
45	ERR(1)=XF1(1)*XF1(1)	2310
	ERR(2)=XF1(2)*XF1(2)	2320
	ERR(3)=XF1(3)*XF1(3)	2330
	IF(HOR17.EQ.0.0)HOR17=.01	2340
	IF(VERT.EQ.0.0)VERT=.01	2350
	TEMP2=SQRT(HOR17**2+VERT**2)	2360

	CFOPCE=TEMP2	2370
	KPLT=PILOT+.1	2380
	DO 402 K=1,2	2390
	DO 403 L=1,4	2400
403	DSORG(K,L)=G.	2410
	IF(K.NE.KPLT)GO TO 1402	2420
	TEMP=.5*XMU1*CAGEO1(K)*TEMP2	2430
	CDRAG(K)=SIGN(TEMP,VFL(K))	2440
	SDRAG(K)=CDRAG(K)+CDRAG(K)	2450
	TEMP=XMU1*CAGEO1(K)/TEMP2	2460
	TEMP=SIGN(TEMP,VFL(K))	2470
	DSORG(K,1)=(HOR1*HOR1+VERT*VRT1)/TEMP	2480
	DSORG(K,2)=(HOR1*HOR2+VERT*VRT2)/TEMP	2490
	DSORG(K,3)=(HOR1*HOR3+VERT*VRT3)/TEMP	2500
	DSORG(K,4)=(HOR1*HOR4+VERT*VRT4)/TEMP	2510
	TEMP=CAGEO1(K)**2*TEMP1*ARF1(K)*ARS(VFL(K))**.75*.4375/CLEAR5(K)**	2520
1.25	TEMP=SIGN(TEMP,VFL(K))	2530
	DSORG(K,4)=DSORG(K,4)+TEMP	2540
1402	CONTINUE	2550
	EP(4)=EP(4)+SDRAG(K)	2560
402	CONTINUE	2570
	TEMP=ATAN2(HOR1,VERT)	2580
	SNTI=SIN(TEMP)	2590
	CSTH=COS(TEMP)	2600
	TMP1=SNTI*XMU1*CSTH	2610
	TMP2=CSTH*XMU1*SNTI	2620
	TMP3=CSTH*XMU1*SNTI	2630
	TMP4=-SNTI*XMU1*CSTH	2640
	AY=-TEMP*TMP1	2650
	AZ=-TEMP*TMP3	2660
	OTMP21=(HOR1*HOR1+VERT*VRT1)/TEMP2	2670
	OTMP22=(HOR1*HOR2+VERT*VRT2)/TEMP2	2680
	OTMP23=(HOR1*HOR3+VERT*VRT3)/TEMP2	2690
	OTMP24=(HOR1*HOR4+VERT*VRT4)/TEMP2	2700
	DAY1=-TEMP2*TMP2*(VERT*HOR1-HOR1*VRT1)/(CSTH*VERT)**2-TMP1*OTMP21	2710
	DAY2=-TEMP2*TMP2*(VERT*HOR2-HOR1*VRT2)/(CSTH*VERT)**2-TMP1*OTMP22	2720
	DAY3=-TEMP2*TMP2*(VERT*HOR3-HOR1*VRT3)/(CSTH*VERT)**2-TMP1*OTMP23	2730
	DAY4=-TEMP2*TMP2*(VERT*HOR4-HOR1*VRT4)/(CSTH*VERT)**2-TMP1*OTMP24	2740
	DAZ1=-TEMP2*TMP4*(VERT*HOR1-HOR1*VRT1)/(CSTH*VERT)**2-TMP3*OTMP21	2750
	DAZ2=-TEMP2*TMP4*(VERT*HOR2-HOR1*VRT2)/(CSTH*VERT)**2-TMP3*OTMP22	2760
	DAZ3=-TEMP2*TMP4*(VERT*HOR3-HOR1*VRT3)/(CSTH*VERT)**2-TMP3*OTMP23	2770
	DAZ4=-TEMP2*TMP4*(VERT*HOR4-HOR1*VRT4)/(CSTH*VERT)**2-TMP3*OTMP24	2780
	DO 404 K=1,4	2790
404	OTV(4,K)=DIV(4,K)*DSORG(1,K)+DSORG(2,K)	2800
	IF(KPLT-2)33,42,33	2810
42	XF1(2)=XF1(2)+AY	2820
	XF1(3)=XF1(3)+AZ	2830
	OTV(2,1)=OTV(2,1)+DAY1	2840
	OTV(2,2)=OTV(2,2)+DAY2	2850
	OTV(2,3)=OTV(2,3)+DAY3	2860
	OTV(2,4)=OTV(2,4)+DAY4	2870
	OTV(3,1)=OTV(3,1)+DAZ1	2880
	OTV(3,2)=OTV(3,2)+DAZ2	2890
	OTV(3,3)=OTV(3,3)+DAZ3	2900
	OTV(3,4)=OTV(3,4)+DAZ4	2910
33	NN=4	2920
	CALL SIMULT(DTV,NN,ERR,COFR,IQUIT)	2930
	IF(IQUIT)24,24,25	2940
		2950

25	WRITE(6,26)	2960
26	FORMAT(14HSTAT 25, MAIN)	2970
	GO TO 30	2980
24	DO 27 K=1,3	2990
27	DFL(K)=DFL(K)-CORR(K)	3000
	OMEGA=OMEGA-CORR(4)	3010
	DO 28 K=1,4	3020
	IF (ABS(CORR(K))-TOL(K+5))28,15,15	3030
28	CONTINUE	3040
	GO TO 31	3050
15	CONTINUE	3060
	WRITE(6,29)	3070
29	FORMAT(1X,21HRETAINER LOOP FAILURE)	3080
C	STOP	3090
31	CALL OUTPT	3100
	IF (RTFST.EQ.1.0) WRITE(6,131)	3110
131	FORMAT(1X,17H B-L	3120
	GO TO 30	3130
47	KONV=1	3140
	IF (OMEGA)48,49,48	3150
49	VK=C.	3160
	XMEGA=0.	3170
	DO 50 J=1,N	3180
	IF (P(2,J))50,50,51	3190
51	VK=VK+1.	3200
	XMEGA=XMEGA+CMF(J)	3210
50	CONTINUE	3220
	OMEGA=XMEGA/VK	3230
	CMF(2)=XMASS*OMEGA**2	3240
	GO TO 48	3250
999	CALL ZERO(X,XMEGA)	3260
	GO TO 999	3270
2002	FORMAT(1P11E12,4)	3280
	END	3290

```

SUBROUTINE BALL(CONST1,CONST2,SPZ,VXX)
REAL LURDEN
COMMON HSC(40),HSI(40)
COMMON ALPHA,AA(2),AMAJ(2,40),AMIN(2,40),APACK(40),
1,B(2),BB(2),BFOCK(40),CAGEM,CRV(2),CRAD,CDSB,CPH,CTHET,BALL
200RR(5),CA(2),CF,C(2),CSP(2),COR(5),CLEAR(2),CLEARP,OP(2,5),BALL
32G(2,2),OCF(5),DB(2,5),DEX(2),DROP,D.DENS,DOL(4),DOL(4),DTV(5,5),BALL
40,TEP,DF(2),DDSLX(2,2),DXKDC(2),DFXVX(2),DFXVY(2),DFXWS(2),
50FXP(2),DFYVX(2),DFYVY(2),DFYWS(2),DFYP(2),DQSVX(2),DQSVY(2),DQSHSBALL
6(2),DQSP(2),CFX(2,5),DFY(2,5),DQS(2,5),DFPX(5),DFPZ(5),DQP(5),DMY(BALL
75),DMZ(5),DPSI(5,5),DPSI(5,5),DBA(2),DELA(2),DPA(2),DFXA(2),DFYABALL
8(2),DQSA(2),DFXOME(2),DFYOME(2),DQSOE(2),DFPXA(2),DFPZA(2),DQPA(2)BALL
9),DVARA(5),DVARA2(5),DVOME(5),DGAL(2),E,EL,BALL
COMMON ERR(5),F2,FSAVE(2),FLAT,F(2),FK,FRADBALL
1,FTAN,FFX(2,40),FFY(2,40),GAGE,G2(2),GG(2),BALL
2HORIZ,HOR1,HOR2,HOR3,HOR4,IQUIT,BALL
3JPASS,LPASS,LURDEN,N,OMEGAE,OMY,OMX,BALL
4M7,DMS(2),DMFX(40),DMFY(40),DMFZ(40),PP(40),PI,BALL
5PR,PE,PC,PD,POCKET,PHI,PILOT,PX(2),PSI(5),PI(2,40),QMV,BALL
6DS(2),QDS(2,40),P,RPM(2),SINP,SPH,STHET,BALL
7SB(2),SQ(2),TOTL,T1,THET,TOL(11),TCRV,TSAVE(2),BALL
8THICKR(2,40),THICKP(40),S,VERT,VRT1,VRT2,VRT3,VRT4,VYR(2),BALL
9VY9(2),VXB(2),VXP(40),VZP(40),VEC(5),BALL
COMMON X(5),XA,XF(4),XF(4),X(2),XMZ,XY,Y,XPHI(40),XHET(2,40),XOMSBALL
1(2,40),XPU,XMU1,YE,YR,YC,IUM,BALL
COMMON D2VVR,D2VX,D2WS,D2P2,XIN,XMASS,BALL
COMMON FX(2),FY(2),BALL
COMMON IC,CTL(40),LCTL,ICNT,LOCP,TQ(2),Y1,Y2,Y3,Y4,Y5,Y6,Y7,YR,Y9BALL
1,Y10,GA(2,2),BA(2,2),DELA(2,2),H(2),H1(2),H2(2),SBAL(2),BALL
2CBAL(2),OMEGA,OME(40),OCX(2),DPSIX(2,2),DGYA(2),PA(2,2),DPSIA(2),BALL
3KA(2),KUNV,DAG(2,2),REVR,DGYRO(2),CAL,SAL,A1,A2,DN,T1,T2,T3,T4,BALL
4TET,NUM,XA1(40),XA2(40),ITPASS,RFVX(40),RFVZ(40),BALL
5,CAGED(2),RINGDI(2),AREA(2),VEL(2),SDRAG(2),RDRAG,DSORG(2,4),BALL
6FZDA1,FZDA2,FZOME,DRDRAG(4),BALL
DIMENSION BQR(2)
COMMON/TESTCOM/TEST1,TEST2
COMMON/BALIST/BLTST
TEST1=0.0
I=JPASS
OPCK(J)=0.
APCK(J)=0.
APCK(J)=0.
VXX=0.
QYVY=0.
QVZW=0.
OPX=0.
EPZ=0.
QSP=0.
VXP(J)=0.
VZP(J)=0.
OPXWZ=0.
OPXWY=0.
OPZWX=0.
OPZWY=0.
QSP=0.
QSPWX=0.
QSPWZ=0.
QSPWY=0.
OX(J)=0.

```

52	DX(2)=0.	
	DY 52 K=3,5	RALL 600
	DZ 52 L=1,2	RALL 610
	DR(L,K)=0.	RALL 620
52	DR(L,K)=0.	RALL 630
	DEK(1)=0.	RALL 640
	DEK(2)=2.	RALL 650
610	A1=TCRV*SINR +DFL(1)+9* DFL(4)*CPH	RALL 660
	A2=TCRV*COSR+DFL(3)*CPH+DFL(2)*SPH-.5*PD	RALL 670
C	IF(X)NV<4C9,4C9,90	RALL 680
C80	X(1)<X(1)JK	RALL 690
C	X(2)<X(2)JK	RALL 700
C	GO TO 8	RALL 710
4C9	TEMP=A1	RALL 720
	A1A2=A1**2+A2**2	RALL 730
	ART=SQRT(A1A2)	RALL 740
	IF(ABS(A1)-1.E-6)1,1,2	RALL 750
2	IF(A1)3,3,4	RALL 760
3	TAG=-1.	RALL 770
	GO TO 5	RALL 780
1	IF(A2-TCRV-1.E-9)9,9,7	RALL 790
7	X(1)=0.	RALL 800
	X(2)=.55*(A2-TCRV)*CPV(1)	RALL 810
	GO TO 17	RALL 820
4	TAG=1.	RALL 830
5	IF((A2-CPV(1))**2<A1**2-CRV(2)**2,9,9,10	RALL 840
9	NLOAD=NLOAD+1	RALL 850
	IF(2,J)=0.	RALL 860
	RESTPN	RALL 870
10	A1=ABS(A1)	RALL 880
	TR=A1/A2	RALL 890
	IF(ART-TCRV)11,12,13	RALL 900
12	AX=A1*CPV(1)/ART	RALL 910
	AY=A2*CPV(1)/ART	RALL 920
16	XX=(AX*TR+AY-A2)/TR	RALL 930
	IF(XX)14,15,15	RALL 940
15	X(1)=1XX-.0*(AX-XX)*TAG	RALL 950
	Y(2)=AY-.6*(A2-AY)	RALL 960
17	A1=TEMP	RALL 970
	GO TO 9	RALL 980
11	CLAM=(CRV(1)**2+A1A2-CRV(2)**2)/(2.*CPV(1)*ART)	RALL 990
	ALAM=ATAN(SQRT(1.-CLAM**2)/CLAM)	RALL1000
	AL=ATAN(TR)-ALAM	RALL1010
	AX=CRV(1)*SIN(P1)	RALL1020
	AY=SQRT(CRV(1)**2-AX**2)	RALL1030
	GO TO 16	RALL1040
14	X(1)=.6*AX+TAG	RALL1050
	Y(2)=AY+.4*AX*TR	RALL1060
	GO TO 17	RALL1070
13	GO 18 L=1,2	RALL1080
	G=0*SQRT(1./(1.+TR**2))*C(L)/E	RALL1090
	T1=1./F(L)-2.*G/(1.+G)	RALL1100
	T2=4.-2./F(L)+T1	RALL1110
	CALL FLIPINT(T1,T2,FE,FK,CSE2,IOUIT)	RALL1120
	IF(10UIT)18,18,19	RALL1130
19	CONTINUE	RALL1140
	TEST=19.C	RALL1150
	OPTION	RALL1160
19	XX(1)=11.847711/CL*SQRT(FE*D/(EK**3*CSE2*Y211	RALL1170
		RALL1180

APIN=(ART-TCRV)/(1.+(XK(2)/XK(1))**.66666667)	RALL1190
APQ=ART-TCRV-APIN	RALL1200
AX=(CRV(1)+APC)*TR/SORT(1.4TR**2)	RALL1210
AY=SQRT((CRV(1)+APQ)**2-AX**2)	RALL1220
GJ TO 16	RALL1230
9 CVRG2=0.	RALL1240
2000 FORMAT(1X,1P10E12.4)	RALL1250
DO 21 IT=1,15	RALL1260
XY=XIN*(MFCDE*X(5)	RALL1270
Y47=-XIN*(MFCDF*X(4)	RALL1280
CVRG2=CVRG2+CONST1	RALL1290
IF(CVRG2-CONST2)22,22,23	RALL1300
23 CVRG2=CONST2	RALL1310
22 A(1)=ATAN(X(1)/X(2))	RALL1320
B(2)=ATAN((A1-X(1))/(A2-X(2)))	RALL1330
DO 24 K=1,2	RALL1340
SRIK1=SIN(B(K))	RALL1350
24 CR(K)=COS(B(K))	RALL1360
DB(1,1)=CB(1)**2/X(2)	RALL1370
DB(1,2)=-X(1)*DB(1,1)/X(2)	RALL1380
DB(2,1)=-CB(2)**2/(A2-X(2))	RALL1390
DB(2,2)=-DB(2,1)*(A1-X(1))/(A2-X(2))	RALL1400
E2=E+2.*(X(2)-CRV(1))*COS9	RALL1410
DEL(1)=SQRT(X(1)**2+X(2)**2)-CRV(1)	RALL1420
DEL(2)=SQRT((A1-X(1))**2+(A2-X(2))**2)-CRV(2)	RALL1430
DO 25 K=1,2	RALL1440
IF(DEL(K)-L.E-7)9.25,25	RALL1450
25 CONTINUE	RALL1460
DO 26 K=1,2	RALL1470
G2(K)=D*CR(K)/F2	RALL1480
GG(K)=1.+C(K)*G2(K)	RALL1490
T1=1./F(K)-2.*C(K)*G2(K)/GG(K)	RALL1500
T2=4.-2./F(K)+T1	RALL1510
CALL ELIPIN(T1,T2,FE,EK,CSE2,IQUIT)	RALL1520
IF(IQUIT)28,28,29	RALL1530
29 CONTINUE	RALL1540
TEST1=29.0	RALL1550
RETURN	RALL1560
28 CSEP=SQRT(CSE2)	RALL1570
CSP(K)=CSEP	RALL1580
ESAVE(K)=EE	RALL1590
SNP=SQRT(1.-CSE2)	RALL1600
TSAVE(K)=T2	RALL1610
YK(K)=11.847711/FL*SQRT(D*EE/(EX**2*CSE2*T2))	RALL1620
SJ(K)=XK(K)*SQRT(DEL(K))	RALL1630
DELX(K,1)=C(K)*SR(K)	RALL1640
DELX(K,2)=C(K)*CR(K)	RALL1650
CTAU=T1/T2	RALL1660
STAU=SQRT(1.-CTAU**2)	RALL1670
DTDG=2.*(T2-T1)*C(K)/(T2*GG(K))**2*STAU	RALL1680
DKDEP=(FE-EK*CSE2)/(SNP*CSEP)	RALL1690
DEDEP=(FE-EK)/SNP*CSEP	RALL1700
DEDTAU=(FE*SNP)**2*STAU*.5/(CSEP*(1.-2.*FF*(EX-FF)/SNP*(FE*DKDEP-	RALL1710
1FK*DEDEP)*CSEP))	RALL1720
DXKDEP=.5.9238555*SQRT(1./T2*EE*EK*.5)/EL*CSE2*(1FK*DEDEP-.3.*EE*	RALL1730
1XDEP)*CSEP+.2.*EK*FE*SNP)	RALL1740
DXKDT2=-XK(K)*.5/T2	RALL1750
26 DXKDG(K)=DXKDEP*DEDTAU*DTDG-DXKDT2*.2.*C(K)/GG(K)**2	RALL1760
DO 31 L=1,2	RALL1770

LPASS=!	BALL1780
DX(L)=DEL(L)*SC(L)	BALL1790
D(L,J)=DX(L)	BALL1800
RA(L)=1.23473241*ESAVE(L)*CSP(L)*EL*PX(L)*D/TSAVE(L)**2.33333333	BALL1810
AA(L)=RA(L)/CSP(L)	BALL1820
DO 32 K=1,2	BALL1830
CG(L,K)=-D/E2**2*(E2*SB(L)*DB(L,K)+CB(L)*DEX(K))	BALL1840
32 DP(L,K)=1.5*SC(L)*DDFLX(L,K)*DEL(L)*SQRT(CFL(L))*DXNG(L)*NG(L,K)	BALL1850
IF(KONV)31,2,403	BALL1860
403 VXR(L)=(IRPM(L)-CMFGAE)*.5*(F2+C(L)*D*CR(L))	BALL1870
VYB(L)=.5*C(L)*D*(X(3)*CB(L)-X(5)*SH(L))	BALL1880
VXA(L)=-.5*D*X(4)	BALL1890
QMS(L)=C(L)*(IRPM(L)-CMFGAE-X(3))*SB(L)-X(5)*C9(L)	BALL1900
QG=-F(L)*D	BALL1910
CF=XMASS*CMFGAE**2*.5*E2	BALL1920
CALL A2(FTJ(PG))	BALL1930
31 CONTINUE	BALL1940
IF(KONV)404,404,405	BALL1950
404 CALL BALL1	BALL1960
DO 406 K=1,2	BALL1970
IF(ABS(COR(K))-5.F-6)406,406,21	BALL1980
406 CONTINUE	BALL1990
X1(J)=X(1)	BALL2000
X2(J)=X(2)	BALL2010
407 CALL BALL2	BALL2020
IF(NHM)408,408,409	BALL2030
408 QME(J)=CMFGA	BALL2040
RETURN	BALL2050
405 PPOC(J)=FY(1)+FY(2)-QDRAG	BALL2060
QCH(1)=R(1)*57.235P	BALL2070
QCH(2)=R(2)*57.295H	BALL2080
IF(PPOC(J))36,38,36	BALL2090
36 T1=2.*D/POCKET	BALL2100
T2=4.-T1	BALL2110
CLFAPR=.5*(POCKET-D)	BALL2120
VZP(J)=X(3)*.5*D	BALL2130
VXP(J)=-X(5)*.5*D	BALL2140
CALL FLIP(X(1),T2,FF,EX,CSE2,LOUT)	BALL2150
IF(LOUT)33,33,34	BALL2160
34 CONTINUE	BALL2170
TEST1=35.0	BALL2180
RETURN	BALL2190
33 PPOCK(J)=1.23473241*EE*SQRT(CSE2)*PL*ABS(PPOC(J))*D/T2**2.33333333	BALL2200
APPOCK(J)=PPOCK(J)/SQRT(CSE2)	BALL2210
THICKP(J)=(V15*X(3)*.125*D**2*10.87/PPOC(J))*2/CLEARP	BALL2220
IF(THICKP(J)-10.F-6)401,402,402	BALL2230
402 FPX=V15*X(5)*(1.5*D)**2*.5*12.66/SQRT(CLEARP)	BALL2240
CPZ=V15*X(3)*(1.5*D)**2*.5*2.436/SQRT(CLEARP)	BALL2250
DFXP=0.	BALL2260
DFPZ=0.	BALL2270
DFPWX=0.	BALL2280
DFPWX=0.	BALL2290
DFPWX=FPZ/X(3)	BALL2300
DFPWX=FPZ/X(3)	BALL2310
GO TO 38	BALL2320
401 TEMP=XMI/SQRT(X(3)**2+X(5)**2)	BALL2330
FPX=TEMP*X(5)*PPOC(J)	BALL2340
CPZ=TEMP*X(3)*PPOC(J)	BALL2350
TEMP=TEMP*PPOC(J)/(X(3)**2+X(5)**2)	BALL2360

```

DEPX4X=-TEMP1*X(3)*X(5)
DEPXWZ=TEMP1*X(3)*X(5)
DEPXP=TEMP1*X(5)
DEPZWX=TEMP1*X(5)*X(5)
DEPZHZ=-TEMP1*X(3)*X(5)
DEPZP=TEMP1*X(3)
38 PS1(1)=-PX(1)*SB(1)+PX(2)*SB(2)+FX(1)*CB(1)-FX(2)*CB(2)-FPX
PS1(2)=-PX(1)*CB(1)+PX(2)*CB(2)-FX(1)*SB(1)+FX(2)*SB(2)+CF+FP7
PS1(3)=-FY(1)*CB(1)-FY(2)*CB(2)-FPZ)*D*.5+QS(1)*SD(1)-QS(2)*SB(2)
PS1(4)=-FX(1)+FX(2)*D*.5+XMY-JSP
PS1(5)=-FY(1)*SB(1)+FY(2)*SB(2)-FPX)*D*.5+2S(1)*CB(1)-QS(2)*CB(2)
1+XX4)
DO 42 K=1,2
DO 43 L=1,2
DEX(K,L)=DEXP(K)*DF(K,L)+.5*(RPM(K)-DMEGAF)*(DEX(L)-C(K)*D*SB(K)+DB(K,2510
13(K,L)=DEXVY(K)+.5*(C(K)*D*(X(3)*SB(K)+X(5)*CB(K))*DEXVY(K)+DB(K,2520
2)*C(K)+RPM(K)-DMEGAF-X(3))*CB(K)+X(5)*SB(K))*DEXWS(K)+DB(K,L)
DEY(K,L)=DEYP(K)+DP(K,L)+.5*(RPM(K)-DMEGAF)*(DEX(L)-C(K)*D*SB(K)+DB(K,2540
13(K,L)=DEYVY(K)+.5*(C(K)*D*(X(3)*SB(K)+X(5)*CB(K))*DEYVY(K)+DB(K,2550
2)*C(K)+RPM(K)-DMEGAF-X(3))*CB(K)+X(5)*SB(K))*DEYWS(K)+DB(K,L)
43 QS(K,L)=QDSP(K)+DP(K,L)+.5*(RPM(K)-DMEGAF)*(DEX(L)-C(K)*D*SB(K)+DB(K,2570
13(K,L)=QDSVY(K)+.5*(C(K)*D*(X(3)*SB(K)+X(5)*CB(K))*QDSVY(K)+DB(K,2580
2)*C(K)+RPM(K)-DMEGAF-X(3))*CB(K)+X(5)*SB(K))*QDSWS(K)+DB(K,L)
DEX(K,3)=-C(K)*(.5*D*CP(K)+DEXVY(K)+SB(K)+DEXWS(K))
DEY(K,3)=-C(K)*(.5*D*CP(K)+DEYVY(K)+SB(K)+DEYWS(K))
QDS(K,3)=-C(K)*(.5*D*CP(K)+QDSVY(K)+SB(K)+QDSWS(K))
DEY(K,4)=-.5*(DEXVX(K))
DEX(K,4)=-.5*(DEYVX(K))
QDS(K,4)=-.5*(QDSVX(K))
DEX(K,5)=-C(K)*(.5*D*SP(K)+DEXVY(K)-CB(K)+DEXWS(K))
DEY(K,5)=-C(K)*(.5*D*SP(K)+DEYVY(K)-CB(K)+DEYWS(K))
42 QS(K,5)=-C(K)*(.5*D*SP(K)+QDSVY(K)-CB(K)+QDSWS(K))
DEPX(1)=DEXP*(DEY(1,1)+DEY(2,1))
DEPX(2)=DEXP*(DEY(1,2)+DEY(2,2))
DEPX(3)=DEXP*(DEY(1,3)+DEY(2,3))+DEPXWX
DEPX(4)=DEXP*(DEY(1,4)+DEY(2,4))+DEPXWY
DEPX(5)=DEXP*(DEY(1,5)+DEY(2,5))+DEPXWZ
DEPZ(1)=DEPZP*(DEY(1,1)+DEY(2,1))
DEPZ(2)=DEPZP*(DEY(1,2)+DEY(2,2))
DEPZ(3)=DEPZP*(DEY(1,3)+DEY(2,3))+DEPZWX
DEPZ(4)=DEPZP*(DEY(1,4)+DEY(2,4))+DEPZWY
DEPZ(5)=DEPZP*(DEY(1,5)+DEY(2,5))+DEPZWZ
YSP(1)=QDSP*(DEY(1,1)+DEY(2,1))
YSP(2)=QDSP*(DEY(1,2)+DEY(2,2))
YSP(3)=QDSP*(DEY(1,3)+DEY(2,3))+YSPWX
YSP(4)=QDSP*(DEY(1,4)+DEY(2,4))+YSPWY
YSP(5)=QDSP*(DEY(1,5)+DEY(2,5))+YSPWZ
MY(1)=0.
MY(2)=0.
MY(3)=0.
MY(4)=0.
MY(5)=X(4)*DMEGAF
MY(1)=0.
MY(2)=0.
MY(3)=0.
MY(4)=-X(4)*DMEGAF
MY(5)=0.
DEP(1)=0.
DEP(2)=X(4)*DMEGAF*AF*2

```

```

BALL2370
BALL2380
BALL2390
BALL2400
BALL2410
BALL2420
BALL2430
BALL2440
BALL2450
BALL2460
BALL2470
BALL2480
BALL2490
BALL2500
BALL2510
BALL2520
BALL2530
BALL2540
BALL2550
BALL2560
BALL2570
BALL2580
BALL2590
BALL2600
BALL2610
BALL2620
BALL2630
BALL2640
BALL2650
BALL2660
BALL2670
BALL2680
BALL2690
BALL2700
BALL2710
BALL2720
BALL2730
BALL2740
BALL2750
BALL2760
BALL2770
BALL2780
BALL2790
BALL2800
BALL2810
BALL2820
BALL2830
BALL2840
BALL2850
BALL2860
BALL2870
BALL2880
BALL2890
BALL2900
BALL2910
BALL2920
BALL2930
BALL2940
BALL2950

```

```

      DCF(3)=0.                                BALL2960
      DCF(4)=0.                                BALL2970
      DCF(5)=0.                                BALL2980
      DO 40 K=1,5                              BALL2990
      DPG1(1,K)=-PX(1)*CB(1)*DB(1,K)-SB(1)*DP(1,K)+PX(2)*CB(2)*DB(2,K)+
1SB(2)*DP(2,K)-FX(1)*SC(1)*DB(1,K)+CB(1)*DFX(1,K)+FX(2)*SB(2)*DB(2,K)+
2CB(2)*DFX(2,K)-DFPX(K)                      BALL3020
      DPG1(2,K)=PX(1)*SB(1)*DB(1,K)-CB(1)*DP(1,K)-PX(2)*SB(2)*DB(2,K)+CB(2)*
1DP(2,K)-FX(1)*CB(1)*DB(1,K)-SB(2)*DFX(1,K)+FX(2)*CB(2)*DB(2,K)+
2SB(2)*DFX(2,K)+DFPZ(K)+DCF(K)              BALL3050
      DPG1(3,K)=-FY(1)*SB(1)*DB(1,K)+CB(1)*DFY(1,K)+FY(2)*SB(2)*DB(2,K)+
1CB(2)*DFY(2,K)-DFPZ(K))*5*DS(1)*CB(1)*DB(1,K)+SB(1)*DS(1,K)-
2DS(2)*CB(2)*DB(2,K)-SB(2)*DS(2,K)          BALL3080
      DPG1(4,K)=(FX(1,K)+DFX(2,K))*5*DS(1,K)+DP(K)    BALL3090
40   DPG1(5,K)=(FY(1,K)+CB(1,K)-SB(1,K)*DFY(1,K)+FY(2)*CB(2,K)+DB(2,K)+
1SB(2)*DFY(2,K)-DFPX(K))*5*DS(1,K)+SB(1,K)+CB(1,K)*DS(1,K)+
2DS(2)*SB(2)*DB(2,K)-CB(2,K)+DS(2,K)+DMZ(K)    BALL3120
C     DPG1(7,2)<DPG1(7,2)<XMAS5+DMFGAE+2      BALL3130
      NN=5                                      BALL3140
      DO 53 K=1,5                              BALL3150
      DO 53 L=1,5                              BALL3160
53   DPG1(L,K)=DPG1(L,K)                      BALL3170
      CALL SIMULT(DPG1,NN,PSI,COR,IQUIT)        BALL3180
      IF(IQUIT)44,44,45                       BALL3190
45   CONTINUE                                  BALL3200
      TEST1=45.0                               BALL3210
      RETURN                                    BALL3220
44   DO 47 K=1,5                              BALL3230
47   X(K)=X(K)-COR(K)*CVPG2                   BALL3240
      DO 48 K=1,5                              BALL3250
      IF(ABS(COR(K))-TOL(K))48,21,21          BALL3260
48   CONTINUE                                  BALL3270
      HCR12=HCR12-PPDC(J)*CPH-FPZ*SPH        BALL3280
      VERT=VERT+PDC(J)*SPH-FPX*CPH            BALL3290
      BLTEST=0.0                               BALL3300
      GO TO 54                                  BALL3310
21   CONTINUE                                  BALL3320
      BLTEST=1.0                               BALL3330
54   DBA(1)=CB(2)*2/(A2-X(2))                 BALL3340
      DBA(2)=-((A1-X(1))*(CB(2)/(A2-X(2))))*2  BALL3350
      DBA(1)=-D*DBA(1)*SR(2)/E2              BALL3360
      DBA(2)=-D*DBA(2)*SR(2)/E2              BALL3370
      DDELA(1)=SB(2)                          BALL3380
      DDELA(2)=C(2)                          BALL3390
      V1=-PX(2)*CB(2)-FX(2)*SB(2)            BALL3400
      V2=PX(2)*SB(2)-FX(2)*CB(2)            BALL3410
      V3=-.5*D*FY(2)*SB(2)+DS(2)*CB(2)      BALL3420
      V4=-.5*D*FY(2)+CB(2)-DS(2)*SB(2)      BALL3430
      KOUNT=0                                  BALL3440
      XPHI(J)=X(1)*57.295780                 BALL3450
      DMEX(J)=X(3)/.10471976                 BALL3460
      DMEY(J)=X(4)/.10471976                 BALL3470
      DMEZ(J)=X(5)/.10471976                 BALL3480
      DO 60 K=1,2                              BALL3490
      D(K,J)=PX(K)                            BALL3500
      XHET(K,J)=B(K)*57.295780               BALL3510
      AMAJ(K,J)=AA(K)*2.0                     BALL3520
      AMIN(K,J)=AB(K)*2.0                     BALL3530
      FFX(K,J)=FX(K)                          BALL3540

```

```

      FFY(K,J)=FY(K)                                BALL3550
      QDS(K,J)=QS(K)                                BALL3560
      XQMS(K,J)=QMS(K)/.10471276                  BALL3570
      QPA(K)=1.5*SQ(2)*QFLA(K)*PX(2)*DXKQ(2)*QGA(K)*XK(2)  BALL3590
      DFXA(K)=DFXP(2)*QPA(K)-(.5*Q*(-(RPM(2)-OMEGAE-X(3))*SR(2)+X(5)*CR(BALL3590
      12))*DFXVY(2)+(RPM(2)-OMEGAE-X(3))*CR(2)*X(5)*SR(2))*DFXWS(2))*QPA(BALL3600
      2(K)                                            BALL3610
      DFYA(K)=DFYP(2)*QPS(K)-(.5*Q*(-(RPM(2)-OMEGAE-X(3))*SR(2)+X(5)*CR(BALL3620
      12))*DFYVY(2)+(RPM(2)-OMEGAE-X(3))*CR(2)*X(5)*SR(2))*DFYWS(2))*QPA(BALL3630
      2(K)                                            BALL3640
      QDSA(K)=QDSP(2)*QPA(K)-(.5*Q*(-(RPM(2)-OMEGAE-X(3))*SR(2)+X(5)*CR(BALL3650
      12))*QDSVY(2)+(RPM(2)-OMEGAE-X(3))*CR(2)*X(5)*SR(2))*QDSWS(2))*QPA(BALL3660
      2(K)                                            BALL3670
      DFXOME(K)=-(E2+C(K)*Q*CR(K))*Q*DFXVY(K)-C(K)*SR(K)*DFXWS(K)  BALL3680
      DFYOME(K)=-(E2+C(K)*Q*CR(K))*Q*DFYVY(K)-C(K)*SB(K)*DFYWS(K)  BALL3690
      QDSOME(K)=-(E2+C(K)*Q*CR(K))*Q*QDSVY(K)-C(K)*SR(K)*QDSWS(K)  BALL3700
      DFPXA(K)=DFXP*DFYA(K)                        BAL 3710
      DFPZA(K)=DFPZ*DFYA(K)                        BALL3720
60  QDPA(K)=QDSP*DFYA(K)                            BALL3730
      DFXOME(1)=DFYOME(1)+DFYOME(2)                BALL3740
      XMYCME=XIN*X(5)                                BALL3750
      XMYCME=-XIN*X(4)                                BALL3760
      VEC(1)=V1*QPA(1)-SR(2)*QPA(1)+CB(2)*DFXA(1)+DFPXA(1)  BALL3770
      VEC(2)=V2*QPA(1)-CR(2)*QPA(1)-SR(2)*DFXA(1)-DFPZA(1)  BALL3780
      VEC(3)=V3*QPA(1)+.5*Q*CR(2)*DFYA(1)+SR(2)*QDSA(1)+.5*Q*DFPZA(1)  BALL3790
      VEC(4)=-.5*Q*DFXA(1)+QDPA(1)                  BALL3800
      VEC(5)=V4*QPA(1)-.5*Q*SR(2)*DFYA(1)+CB(2)*QDSA(1)+.5*Q*DFPXA(1)  BALL3810
      DO 66 K=1,5                                     BALL3820
      DVARA1(K)=0.                                     BALL3830
      DO 66 I=1,5                                     BALL3840
66  DPS1(L,K)=DPS1(L,K)                             BALL3850
      CALL SIMULT(DPS1,MN,VEC,DVARA1,IQUIT)          BALL3860
      KOUNT=KOUNT+1                                   BALL3870
      IF(IQUIT)61,61,62                             BALL3880
62  CONTINUE                                          BALL3890
      TEST1=62.0                                     BALL3900
      RETURN                                          BALL3910
61  VEC(1)=V1*QPA(2)-SR(2)*QPA(2)+CB(2)*DFXA(2)+DFPXA(2)  BALL3920
      VEC(2)=V2*QPA(2)-CR(2)*QPA(2)-SR(2)*DFXA(2)-DFPZA(2)  BALL3930
      VEC(3)=V3*QPA(2)+.5*Q*CR(2)*DFYA(2)+SR(2)*QDSA(2)+.5*Q*DFPZA(2)  BALL3940
      VEC(4)=-.5*Q*DFXA(2)+QDPA(2)                  BALL3950
      VEC(5)=V4*QPA(2)-.5*Q*SR(2)*DFYA(2)+CB(2)*QDSA(2)+.5*Q*DFPXA(2)  BALL3960
      DO 67 K=1,5                                     BALL3970
      DVARA2(K)=0.                                     BALL3980
      DO 67 I=1,5                                     BALL3990
67  DPS1(L,K)=DPS1(L,K)                             BALL4000
      CALL SIMULT(DPS1,MN,VEC,DVARA2,IQUIT)          BALL4010
      KOUNT=KOUNT+1                                   BALL4020
      IF(IQUIT)64,64,62                             BALL4030
64  VEC(1)=-CB(1)*DFXOME(1)+CB(2)*DFXOME(2)+DFXP*(DFYOME(1)+DFYOME(2))  BALL4040
      1)                                            BALL4050
      VEC(2)=SB(1)*DFXOME(1)-SB(2)*DFXOME(2)-XMASS*E2*OMEGAE-DFPZ*(DFYOME(1)+DFYOME(2))  BALL4060
      1ME(1)+DFYOME(2))                                BALL4070
      VEC(3)=-.5*Q*(CR(1)*DFYOME(1)-CR(2)*DFYOME(2))-SB(1)*QDSOME(1)+SB(BALL4080
      12)*QDSOME(2)+.5*Q*DFPZ*(DFYOME(1)+DFYOME(2))  BALL4090
      VEC(4)=-.5*Q*(DFXOME(1)+DFXOME(2))-XMYCME+QDSP*(DFYOME(1)+DFYOME(2))  BALL4100
      12))                                            BALL4110
      VEC(5)=-.5*Q*(DFYOME(1)+SB(1)-DFYOME(2)*SR(2))-CB(1)*QDSOME(1)+CB(BALL4120
      1)*QDSOME(2)-XMYCME+.5*Q*DFXP*(DFYOME(1)+DFYOME(2))  BALL4130

```


204

A3=-V1*DP2OME+SB(2)*DP2OME-CR(2)*DFXOME(2)	BALL4730
DTV(1,1)=DTV(1,1)+A1	BALL4740
DTV(1,2)=DTV(1,2)+A2*SPH	BALL4750
DTV(1,3)=DTV(1,3)+A2*CPH	BALL4760
DTV(1,4)=DTV(1,4)+A3	BALL4770
A1=-V2*DB2CA1+CR(2)*DP2DA1+SB(2)*DFXA(1)	BALL4780
A2=-V2*DB2CA2+CR(2)*DP2DA2+SB(2)*DFXA(2)	BALL4790
A3=-V2*DB2CMF+CR(2)*DP2OME+SB(2)*DFXOME(2)	BALL4800
DTV(2,1)=DTV(2,1)+A1*SPH-DFYA(1)*CPH	BALL4810
DTV(2,2)=DTV(2,2)+A2*SPH**2-DFYA(2)*SPH*CPH	BALL4820
DTV(2,3)=DTV(2,3)+A2*SPH*CPH-DFYA(2)*CPH**2	BALL4830
DTV(2,4)=DTV(2,4)+A3*SPH-DFYOME(2)*CPH	BALL4840
DTV(3,1)=DTV(3,1)+A1*CPH+DFYA(1)*SPH	BALL4850
DTV(3,2)=DTV(3,2)+A2*SPH*CPH+DFYA(2)*SPH**2	BALL4860
DTV(3,3)=DTV(3,3)+A2*CPH**2+DFYA(2)*SPH*CPH	BALL4870
DTV(3,4)=DTV(3,4)+A3*CPH+DFYOME(2)*SPH	BALL4880
DTV(4,1)=DTV(4,1)+.5*(DFPA1*E2+FP2DA1*D)+DDVXWX*DVARA1(3)	BALL4890
DTV(4,2)=DTV(4,2)+.5*(DFPA2*E2+FP2DA2*D)+DDVXWX*DVARA2(3)*SPH	BALL4900
DTV(4,3)=DTV(4,3)+.5*(DFPA2*E2+FP2DA2*D)+DDVXWX*DVARA2(3)*CPH	BALL4910
DTV(4,4)=DTV(4,4)+.5*(DFPOME*E2+FP2OME*D)+DDVXWX*DVOME(3)	BALL4920
RETURN	BALL4930
END	BALL4940

SUBROUTINE ELIPIN(TERM1,TERM2,FE,FK,CSE2,IER)	ELIP 10
CTAU=TERM1/TERM2	ELIP 20
SNF=.99999	ELIP 30
IER=0	ELIP 40
DO 1 I=1,30	ELIP 50
SNFS=SNF*SNF	ELIP 60
CSE2=1.-SNFS	ELIP 70
IF(CSE2)3,3,4	ELIP 80
3 WRITE(6,5)	ELIP 90
5 FORMAT(10HCELI PIN=)	ELIP 100
IER=1	ELIP 110
RETURN	ELIP 120
4 CTF2=CSE2/SNFS	ELIP 130
XLG=ALOG(1./CSE2)	ELIP 140
FE=1.+CSE2*(.444792040+CSE2*(.085099193+CSE2*(.040905094))+CSE2*(.2	ELIP 150
149697949+CSE2*(.091502240+CSE2*(.013929990)))*XLG	ELIP 160
FK=1.38629436+CSE2*(.097932891+CSE2*(.054544409+.032024666*CSE2))	ELIP 170
1+.5+CSE2*(.124750742+CSE2*(.060118519+.010944912*CSE2)))*XLG	ELIP 180
EUK=FK/FE	ELIP 190
CR=(1.-CTAU-2.*(EUK-1.)*CTF2)*SNFS*SNF/((1.-4.*SNFS)*EUK-2.*CSE2	ELIP 200
1EUK**2-6.)	ELIP 210
SNF=SNF-CR	ELIP 220
IF(ABS(CR)-5.E-7)2,1,1	ELIP 230
1 CONTINUE	ELIP 240
WRITE(6,6)	ELIP 250
6 FORMAT(10HCELI PIN=)	ELIP 260
IER=1	ELIP 270
2 RETURN	ELIP 280
END	ELIP 290

```

SUBROUTINE INPT                                INPT  10
REAL LURDEN                                    INPT  20
REAL*BW1,W2,WORD                               INPT  30
COMMON HSD(40),HSL(40)                        INPT  40
COMMON ALPHA,AA(2),AMAJ(2,40),AMIN(2,40),APOCK(40), BET,BETA INPT  50
1,B(2),BR(2),BPOCK(40), CAGEW, CRV(2), CRAD, COSB,CPH,CTHET, INPT  60
2CJRR(5),CB(2),CF,C(2),CSP(2),COR(5), CLEARS(2),CLEARP, DP(2,5), INPT  70
3DG(2,2),DCF(5),DD(2,5),DEX(2),DRDP,D,DEFS,DDL(4),DFL(4),DTV(5,5), INPT  80
4DFTF,DEL(2),DEFLX(2,2),DXKOG(2),DFXVX(2),DFXVY(2),DFXWS(2), INPT  90
5DFXP(2),DFYVX(2),DFYVY(2),DFYWS(2),DFYPI(2),DQSVX(2),DQSVY(2),DQSW INPT 100
6(2),DQSP(2),CFX(2,5),DFY(2,5),DQS(2,5),DFPX(5),DFPZ(5),DQP(5),DMY(INPT 110
75),DMZ(5),DPS(5,5),DPS1(5,5),DPS11(5,5),DPA(2),DDELA(2),DPA(2),DFXA(2),DFYA INPT 120
8(2),DQSA(2),DFXOMF(2),DFYOMF(2),DQSQME(2),DFPXA(2),DFPZA(2),DQPA(2 INPT 130
9),DVARA1(5),DVARA2(5),DVOMF(5), DGA(2), E,CI INPT 140
COMMON ERR(5),E2,FSAVE(2), FLAT,F(2),FK,FRAD INPT 150
1,FTAN,FFX(2,40),FFY(2,40), GAGE,G2(2),GG(2), INPT 160
2 HCRIZ,HOR1,HOR2,HOR3,HOR4, IQUIT, INPT 170
3JPASS, LPASS,LURDEN, N, OMEGAF,DMY,OMX, INPT 180
4MZ,OMS(2),OMEX(40),OMFY(40),OMEZ(40), PPOC(40),PL, INPT 190
5PZ,PF,PC,PD,POCKET,PHI,PILCT,PX(2),PSI(5),P(2,40), QMV, INPT 200
6DS(2),QDS(2,40), R,PPM(2), SINB,SPH,STHET, INPT 210
7SD(2),SQ(2), TOTI,TI,THET,TOL(11),TCRV,TSAVE(2), INPT 220
8THICKP(2,40),THICKP(40), VIS,VEP1,VRT1,VRT2,VRT3,VRT4,VYR(2), INPT 230
9VYR(2),VXR(2),VXP(40),VZP(40),VFC(5) INPT 240
COMMON X(5),XA,XF(4),XFI(4),XK(2),XMZ,XMY,XPHI(40),XRET(2,40),XOMS INPT 250
1(2,40),XMU,XMU1, YF,YR,YT,YNUM INPT 260
COMMON DZVVR,CZVX,DZWS,DZP2,XIN,XMASS INPT 270
COMMON FX(2),FY(2) INPT 280
COMMON IC,CTI(40),LCTL,ICNT,LDDP,TO(2),Y1,Y2,Y3,Y4,Y5,Y6,Y7,Y8,Y9 INPT 290
1,Y10,GA(2,2),RA(2,2),DFL3(2,2),H(2),HH(2),HI(2),H2(2),SBAI(2), INPT 300
2SFAI(2),OMEGA,OME(40),DCX(2),DPSIX(2,2),OGYA(2),PA(2,2),DPSIA(2), INPT 310
3YA(2), KQNV,DADI(2,2),REVR,DGYPO(2),CAL,SAL,A1,A2,ON,Y1,Y2,T3,T4, INPT 320
4DFT,KUN,XA(40),XA2(40),ITPASS,REVR(40),REV(40) INPT 330
5,CAGEFI(2),RINGOI(2),APFA(2), VFL(2),SURAG(2),BORAG,DORAG(2,4), INPT 340
6FPZ(2),FOPDA2,FOPOMF INPT 350
DATA W1,W2/5FCUTFR,5HIFNER/ INPT 360
1 FQWAT(RF10,C) INPT 370
2EADI(5,1)XN,F,E,BET,F(1),F(2),PD,POCKET INPT 380
3AT=RET INPT 390
4F(XV)2,2,5 INPT 400
5 STOP INPT 410
6EADI(5,1)YC,PC,YE,PF,YR,PD,DEFS,XMU,XMU1,CAGEW,CAGEFI(1),CAGEFI(2) INPT 420
1,RINGOI(1),RINGOI(2) INPT 430
HFT=RET/57.245780 INPT 440
SINB=SIN(RET) INPT 450
COSB=COS(RET) INPT 460
TCRV=(F(1)*F(2)-1.)*D INPT 470
4)PO+H? INPT 480
IF(YF)6,6,7 INPT 490
6 YE=29,F6 INPT 500
7 IF(YD)8,8,9 INPT 510
9 YR=29,F6 INPT 520
7 IF(PF)10,10,11 INPT 530
10 PF=.25 INPT 540
11 IF(PD)12,12,13 INPT 550
12 PD=.25 INPT 560
13 FL=4.4(1.-PD**2)/YR+(1.-PE**2)/YF INPT 570
2)40 K=1,2 INPT 580
40 CRV(K)=IF(K-.5)*D INPT 590

```

```

      Q=.5*F*CRV(2)*COSB
      41 K=1,2
      DIA=F+2.*C(K)*(F(K)*D-CRV(K)*COSB)
      DEPTH=APS(DIA-RINGDI(K))*0.5
      40TH=SQRT((F(K)*D)**2-(F(K)*D-DEPTH)**2)
      AREA(K)=3.14159*CAGEDI(K)*(CAGFW-WOTH)
41 CLEARSI(K)=ABS(RINGDI(K)-CAGEDI(K))*0.5
      PILOT=1.
      IF(CLEARSI(2).LT.CLEARSI(1))PILOT=2.
21 WRITE(6,19)
18 FORMAT(22H BEARING DESIGN DATA)
      WRITE(6,19)
19 FORMAT(129H0 NO. OF ELEMENT PITCH CONTACT RAINPT
1 OF CURVATURES CLEARANCE TYPE OF PILOT POCKET INPT
2 CAGE/129H ELEMENTS DIAMETER DIAMETER ANGLE CINPT
3 OUTER INNER INCREMENT PILOT CLEARANCE CLEARANCE INPT
6 WIDTH)
      WORD=W1
      IF(PILOT.EQ.2.)WORD=W2
      TEMP=2.*CLEARSI(1)
      IF(PILOT.EQ.2.)TEMP=CLEARSI(2)*2.0
      TEMP1=POCKET=0
      IF(DENS.EQ.0.)DENS=.283
      WRITE(6,50)XN,D,F,BAT,F(1),F(2),PD,WORD,TEMP,TEMP1,CAGFW
50 FORMAT(1P7E12.4,4X,4S,3X,1P3E12.4)
      WRITE(6,51)
51 FORMAT(130H0 1. D. OF 0. D. OF 1. D. OF 0. D. OF
1 MODULUS OF ELASTICITY POISSON'S RATIO INPT
2 ELEMENT/130H OUTER INNER CAGE CAGE INPT
3 RINGS CAGE ELEMENTS RINGS CAGE ELEMENT INPT
4S DENSITY)
      WRITE(6,52)RINGDI(1),RINGDI(2),CAGEDI(2),CAGEDI(1),YR,YC,YF,PR,PC,INPT
1PE,DENS
52 FORMAT(1P11E12.4)
      RETURN
      END
      SHORROUTINE OUTPT
      REAL LURDEN
      COMMON HSC(40),HSL(40)
      COMMON ALPHA,AA(2),AMAJ(2,40),AMIN(2,40),APOCK(40),
      1,B(2),BP(2),PPOCK(40), CAGFW, CRV(2), CRAD, COSB,CPH,CTHET, OUTP
200PR(5),CP(2),CF,C(2),OSP(2),COR(5), CLEARSI(2),CLEAPP, DP(2,5), OUTP
30G(2,2),ICF(5),DB(2,5),DEX(2),DRDP,D,DENS,DCL(4),DFL(4),OTV(5,5), OUTP
40ETFR,DFL(2),DDFLX(2,2),DXXDC(2),DFXVX(2),DFXVY(2),DFXWS(2), OUTP
50FXP(2),DFYVX(2),DFYVY(2),DFYWS(2),DFYP(2),DQSVX(2),DQSVY(2),DQSW,OUTP
60(2),DQSO(2),DFX(2,5),DFY(2,5),DQS(2,5),DFPX(5),DFP7(5),DQW(5),DMY(OUTP
75),DMZ(5),DPS(5,5),DPS1(5,5),DPS11(5,5),DBAT(2),DUELA(2),DPA(2),DEKAI(2),DFY4,OUTP
80(2),DQSA(2),DFXDM(2),DFYDM(2),DQSDME(2),DFPXA(2),DFP7A(2),DQPA(2)OUTP
90),DVARA1(5),DVARA2(5),DVOME(5), DGA(2), E,EL OUTP
COMMON ERR(5),F2,FSAVE(2), FLAT,F(2),FK,FRAD,OUTP
1,STAN,FFX(2,40),FFY(2,40), GAGE,G2(2),GC(2),OUTP
2 HOR17,HOR1,HOR2,HOR3,HOR4, IQUIT, OUTP
3DPASS, LPASS,LURDEN, N, OMEGAE,OMY,OMX, OUTP
4047,OMS(2),OMEX(40),OMEY(40),OMF(40), PPOC(40),PL,OUTP
50R,PE,PC,PD,POCKET,PHT,PILOT,PX(2),PSI(5),P(2,40), OMY,OUTP
60S(2),DQS(2,40), R,PPM(2), SINP,SPH,STHET, OUTP
7SH(2),SO(2), TOTL,T1,THET,TOI(11),YCRV,TSAVE(2), OUTP
8THICKP(2,40),THICKP(40), VIS,VFRT,VRT1,VRT2,VRT3,VRT4,VYR(2), OUTP
9VYR(2),VXR(2),VXP(40),VZP(40),VFC(5) OUTP
COMMON X(4),XN,XF(4),YF(4),YK(2),XMY,XMY,XPH(40),XRT(2,40),XDIS,OUTP
102,40),XMO,XMU1, YE,YR,YC,YNUM OUTP
COMMON D2VYR,D2VX,D2WS,D2P2,XIN,XMASS OUTP
COMMON FX(2),FY(2) OUTP
COMMON IC,TI(40),LOTL,ICNT,LDDP,TOI(2),Y1,Y2,Y3,Y4,Y5,Y6,Y7,Y8,Y9,OUTP

```

208

```

15  WRITE(6,6)J,XOMS(1,J),XOMS(2,J),THICKR(1,J),THICKR(2,J),HSD(J),HST(J)  OUTP 930
16  CONTINUE  OUTP 940
    WRITE(6,10)  OUTP 950
16  FORMAT(27H0  BALL/POCKET CONTACT DATA)  OUTP 960
    WRITE(6,17)  OUTP 980
17  FORMAT(83H0  ELEMENT  POCKET  PRESSURE ELLIPSE  SL  OUTP 990
    10ING VELOCITY  MIN. FILM)  OUTP1000
    WRITE(6,18)  OUTP1010
18  FORMAT(183H  NO.  FORCE  LENGTH  WIDTH  RAD)  OUTP1020
    1AL  AXIAL  THICKNESS)  OUTP1030
    GO 19 J=1,N  OUTP1040
    IF(19(J))19,19,20  OUTP1050
20  APOCK(J)=2,*APOCK(J)  OUTP1060
    BPOCK(J)=2,*BPOCK(J)  OUTP1070
    IF(THICKP(J).GT.CLEARP)THICKP(J)=CLEARP  OUTP1080
    WRITE(6,6)J,PPDC(J),APOCK(J),BPOCK(J),VZP(J),VXP(J),THICKP(J)  OUTP1090
19  CONTINUE  OUTP1100
    WRITE(6,70)  BORAG  OUTP1110
    WRITE(6,60)  OUTP1120
40  FORMAT(29H0  CAGE/PILOTING SURFACE DATA/34H0  VISCOS  COULOMB  OUTP1130
    :  NORMAL/33H  TORQUE  TORQUE  LOAD)  OUTP1140
70  FORMAT(25H0  VISCOS DRAG ON BALL #,1P1E11,4)  OUTP1150
    TEMP=VDRAG(1)+VDRAG(2)  OUTP1160
    KPLT=P(LCT)+1  OUTP1170
    YEMP=CORAG(KPLT)  OUTP1180
    WRITE(6,11)TEMP,TEMP1 ,CFORCE  OUTP1190
    RETURN  OUTP1200
    END  OUTP1210

```

```

SUBROUTINE SIMULT(A,N,D,X,KX)  SIMU 10
  DOUBLE PRECISION AMPY,EL,V,POW,AMPYI  SIMU 20
  1  FORMAT( 1  ELEMENTS ALL ZERO. POW NO.0 ,16 /)  SIMU 30
  IW=6  SIMU 40
  DIMENSION A(5,5),R(5),X(5),ROW(5),KOL(5)  SIMU 50
  GO 5050 J=1,N  SIMU 60
  TEMP=0.  SIMU 70
  GO 5051 K=1,N  SIMU 80
  IF(ABS(A(J,K))-TEMP)5051,5051,5052  SIMU 90
5052  TEMP=ABS(A(J,K))  SIMU 100
5051  CONTINUE  SIMU 110
  IF(TEMP.NE.0.) GO TO 15051  SIMU 120
  WRITE(IW,1) J  SIMU 130
  GO TO 5050  SIMU 140
C  GO 5053 K=1,N  SIMU 150
15051  GO 5053 K=1,N  SIMU 160
5053  A(J,K)=A(J,K)/TEMP  SIMU 170
  R(J)=P(J)/TEMP  SIMU 180
5050  CONTINUE  SIMU 190
  KOL(1)=1  SIMU 200
5001  GO 5002  IFOW=2,N  SIMU 210
5002  KOL(1POW)=KOL(1ROW-1)+1  SIMU 220
5004  GO 5025  KOUNT=1,N  SIMU 230
  LARGST=N-KOUNT+1  SIMU 240
  I  ASE=KOL(1)  SIMU 250
  J=JL=1  SIMU 260
5005  IF (N-KOUNT) 5035,5014,5006  SIMU 270
5006  AMPY = ABS ( A(1,1) )  SIMU 280
5007  GO 5010  IFOW=2,LARGST  SIMU 290
  AMPYI=ABS(A(1POW,1))  SIMU 300
5008  IF ( AMPY - AMPYI  1 5009, 5010, 5010  SIMU 310

```

5009 JCCL=IROW	SIMU 320
AMPY = A(3 (A(IROW,1))	SIMU 330
IFRASE=KCL(IROW)	SIMU 340
5010 CONTINUE	SIMU 350
5011 IF (KOL(1)-IFRASE) 5012,5014,5012	SIMU 360
5012 KCL(JCOL)=KCL(1)	SIMU 370
KOL(1)=IFRASE	SIMU 380
5014 IF (A(JCOL,1))5015,5035,5015	SIMU 390
5015 AMPY=A(JCOL,1)	SIMU 400
5017 DO 5019 IROW=2,N	SIMU 410
EL=A(JCOL,IROW)	SIMU 420
C IROW=IROW-1<#A2JCCL,IROW</AMPY	SIMU 430
ROW(IROW-1)=EL/AMPY	SIMU 440
5018 A(JCOL,IROW-1)=A(1,IROW-1)	SIMU 450
ROW(N)=1./AMPY	SIMU 460
A(JCOL,N)=A(1,N)	SIMU 470
5019 DO 5027 IROW=2,N	SIMU 480
AMPY=A(IROW,1)	SIMU 490
5020 DO 5021 JCOL=2,N	SIMU 500
EL=A(IROW,JCOL)	SIMU 510
C 5021 A(IROW-1,JCOL-1<#A(IROW,JCOL<-AMPY*ROW*JCOL-1<	SIMU 520
5021 A(IROW-1,JCOL-1)=EL-AMPY*ROW*JCOL-1	SIMU 530
5022 A(IROW-1,N)=AMPY*ROW(N)	SIMU 540
5023 DO 5024 JCOL=1,N	SIMU 550
KCL(JCOL)=KCL(JCOL+1)	SIMU 560
5024 A(N,JCOL)=KCL(JCOL)	SIMU 570
5025 KOL(N)=IFRASE	SIMU 580
5025 DO 5034 KCUNT=1,N	SIMU 590
5027 IF (KOL(KCUNT)-KCUNT) 5035,5034,5028	SIMU 600
5029 DO 5032 IROW=KCUNT,N	SIMU 610
5029 IF (KOL(IROW)-KCUNT) 5035,5030,5032	SIMU 620
5030 DO 5031 JCOL=1,N	SIMU 630
ROW(1)=A(JCOL,IROW)	SIMU 640
A(JCOL,IROW)=A(JCOL,KCUNT)	SIMU 650
5031 A(JCOL,KCUNT)=ROW(1)	SIMU 660
IFRASE=KCL(KCUNT)	SIMU 670
KOL(KCUNT)=KCL(IROW)	SIMU 680
KOL(IROW)=IFRASE	SIMU 690
GO TO 5034	SIMU 700
5032 CONTINUE	SIMU 710
GO TO 5035	SIMU 720
5034 CONTINUE	SIMU 730
997 IF (KX-31599.9000.798	SIMU 740
9000 KX=0	SIMU 750
RETURN	SIMU 760
999 DO 5042 IROW=1,N	SIMU 770
C 5042 X=IROW<#0.0	SIMU 780
5040 AMPY=0.	SIMU 790
C 5041 DO 5042 JCOL=1,N	SIMU 800
5041 DO 5042 JCOL=1,N	SIMU 810
EL=A(IROW,JCOL)	SIMU 820
V=B(JCOL)	SIMU 830
C 5042 X=IROW<# X=IROW<#A(IROW,JCOL<# B(JCOL<	SIMU 840
5042 AMPY=AMPY+EL*V	SIMU 850
5042 X(IROW)=AMPY	SIMU 860
KX=C	SIMU 870
RETURN	SIMU 880
5035 KX=1	SIMU 890
RETURN	SIMU 900
END	SIMU 910

__SUBROUTINE PALETTJ(RG)	HALF	10		
REAL LURDEN	HALF	20		
COMMON HSD(40),HSI(40)	HALF	30		
COMMON ALPHA,AA(2),AMAJ(2,40),AMIN(2,40),APOCK(40),	REF,RETABALF	40		
1,B(2),BR(2),BPCK(40),CAGEW,CRV(2),CHAD,CNSR,CPH,CTHF),	HALF	50		
2,CORR(5),CR(2),CF,C(2),CSP(2),COR(5),CLEARF(2),CLEARP,OP(2,5),	HALF	60		
3,DC(2,2),DCF(5),DR(2,5),DEX(2),DRPD,D,DEVS,DNL(4),DFL(4),DTV(5,5),	HALF	70		
4,DETFP,DFL(2),DDELX(2,2),DXXNG(2),DEXVX(2),DEXVY(2),DEXXS(2),	HALF	80		
5,DFXP(2),DFYVX(2),DFYVY(2),DFYWS(2),DFYP(2),DOSVX(2),DOSVY(2),DOSWSBALF	90			
6(2),DOSP(2),DFX(2,5),DFY(2,5),DOSI(2,5),DFPX(5),DFPZ(5),DOP(5),DMY(BALF	100			
75),DMZ(5),DPSI(5,5),DPSI1(5,5),DPA(2),DDELA(2),DPA(2),DFXA(2),DFYABALF	110			
8(2),DOSA(2),DFXOME(2),DFYOME(2),DOSOME(2),DFPXA(2),DFPZA(2),DOPA(2,BALF	120			
9),DVARA1(5),DVARA2(5),DVOME(5),DGA(2),	E,EL	130		
COMMON ERR(4),F2,FSAVE(2),	FLAT,F(2),FK,FRADRALF	140		
1,ETAN,FFX(2,40),FFY(2,40),	GAGE,G2(2),GG(2),BALF	150		
2	HCR12,HCR1,HCR2,HCR3,HCR4,	*QUIT, HALF	160	
3J ASS,	LPASS,LURDEN,	N,	OMEGAF,DMY,DMX, HALF	170
4,MS(2),MS(2),CFEX(40),DMEY(40),DMEZ(40),	PROG(40),PL	BALF	180	
5,SR,PE,PC,PD,POCKFT,PHI,PILOT,PX(2),PSI(5),P(2,40),	QMV,	BALF	190	
6,RS(2),DOS(2,40),	R,RPM(2),	SINR,SPH,STHET,	HALF	200
7,SB(2),SQ(2),	TOTL,TI,THET,TOL(1),TCRV,TSAVE(2),	BALF	210	
8,THICKR(2,40),THICKP(40),	VIS,VERT,VRT1,VRT2,VRT3,VRT4,VYR(2),	BALF	220	
9,VXB(2),VXB(2),VXP(40),VZP(40),VEC(5)		BALF	230	
COMMON X(5),XA,XF(4),XF1(4),XK(2),XNZ,XMY,XPHI(40),XBET(2,40),XOMS	BALF	240		
1(2,40),XMU,XMU1,	YE,YR,YC,YNUM	BALF	250	
COMMON D2VYR,D2VX,D2WS,D2PZ,XIN,XMASS		BALF	260	
COMMON FX(2),FY(2)		BALF	270	
COMMON IC,CIL(40),LCTL,TCNT,LODP,TO(2),Y1,Y2,Y3,Y4,Y5,Y6,Y7,Y8,Y9	BALF	280		
1,Y10,GA(2,2),PA(2,2),DELA(2,2),H(2),HH(2),H1(2),H2(2),SBAL(2),	BALF	290		
2,CBAL(2),OMEGA,DMF(40),DCX(2),DPSIX(2,2),DGYA(2),PA(2,2),DPSIA(2),	HALF	300		
3,XA(2),	KOMV,CAD(2,2),REVB,DGYRO(2),CAL,SAL,A1,A2,OM,I1,I2,I3,I4,	BALF	310	
4,DET,NUM,XA1(40),XA2(40),ITPASS,REVB(40),REVZ(40)		BALF	320	
5,CAGEFI(2),RINGDI(2),AREA(2),VEL(2),SDRAG(2),RDRAG,DSDRG(2,4),	BALF	330		
6,FPZDA1,FPZCA2,FPZOME		BALF	340	
DIMENSION U(3),V(3),WSS(3),WIT(3),SW(3),S1(3),S2(3),PHZ(3),Y(60),	BALF	350		
IRATIO(60),FFXX(3,3,6),FFYY(3,3,6),TMM(3,3,6)		BALF	360	
J=JPASS		BALF	370	
L=LPASS		BALF	380	
DVYR=D2VYR*ARS(VYR(L)-VYB(L))		BALF	390	
DVX=D2VX*ARS(VXR(L))		BALF	400	
DWS=D2WS*ARS(DMS(L)/.10472)		BALF	410	
O7=D2PZ*PX(L)		BALF	420	
IF(DVYR.LT.0.1)DVYR=0.1		BALF	430	
IF(DVX.LT.0.1)DVX=0.1		BALF	440	
IF(DWS.LT.0.1)DWS=0.1		BALF	450	
IF(O7.LT.0.1)O7=0.1		BALF	460	
IF(O7.GE.PX(L)) O7=0.9*PX(L)		BALF	470	
THICKR(L,J)=1.E6		BALF	480	
S1(1)=AA(1)		BALF	490	
S2(1)=BB(1)		BALF	500	
IDY=6		BALF	510	
IDY=20		BALF	520	
XIDY=IDY		BALF	530	
RJ=.5*D		BALF	540	
R3=-C(1)*.5*(E2/C8(L)+C(1)*D)		BALF	550	
WT=PX(L)		BALF	560	
WWS=-(DMS(L)/.10471976)		BALF	570	
WS=WWS		BALF	580	
U1=VYR(L)		BALF	590	

U2=VYP(1)	BALF 600
V1=-VXR(1)	BALF 610
OU=-OVYR	BALF 620
OW=-OVX	BALF 630
OWS=-OWS	BALF 640
OWS=OWS	BALF 650
OWT=OT	BALF 660
U(2)=U1+OU	BALF 670
U(3)=U1-OU	BALF 680
V(2)=V1+OV	BALF 690
V(3)=V1-OV	BALF 700
WSS(2)=WS+OWS	BALF 710
WSS(3)=WS-OWS	BALF 720
WTT(2)=WT+OWT	BALF 730
WTT(3)=WT-OWT	BALF 740
THETA=(T1-32.)/1.8	BALF 750
QXP=1./PJ+1./OP	BALF 760
QYP=1./PJ+1./OG	BALF 770
AAA=.5*QXP	BALF 780
OOO=.5*QYP	BALF 790
RXP=1./RXP	BALF 800
QYP=1./QYP	BALF 810
AMC=(AAA-OOO)/(AAA+OOO)	BALF 820
EP=3.14159265/(11.-PF**2)/VE+11.-PR**2)/VR)	BALF 830
U(1)=U1	BALF 840
V(1)=V1	BALF 850
WSS(1)=WS	BALF 860
WTT(1)=WT	BALF 870
QY=2./XIDY	BALF 880
DO 200 K=2,3	BALF 890
TEMP=(WTT(K)/WTT(1))*3333333	BALF 900
S1(K)=S1(1)*TEMP	BALF 910
200 S2(K)=S2(1)*TEMP	BALF 920
DO 45 I=1,3	BALF 930
OH7(I)=1.5*WTT(1)/(3.14159265 *S1(I)*S2(I))	BALF 940
SV(I)=.75*WTT(1)/S1(I)	BALF 950
45 CONTINUE	BALF 960
35 VIS3=VIS*EXP(PFTA*(T1-96.))	BALF 970
AL3=ALPHA+930.*ALPHA*(T1-86.)/(546.*(T1+460.))	BALF 980
IMH=.5*ALPHA**4*V(S**7*EP**3)*RXP**43	BALF 990
G1T=VIS3*(ALPHA/AL3)**6*(VIS/VIS3)**7	BALF1000
G2T=VIS3*PFTA/(K.*EK*.216)	BALF1010
II=1	BALF1020
IJ=1	BALF1030
KK=1	BALF1040
LL=1	BALF1050
MM=1	BALF1060
45 CF1Y=0.	BALF1070
CF1X=0.	BALF1080
TM2=C.	BALF1090
TM1=0.	BALF1100
CS=WSS(KK)*.10471076*(1/LL)	BALF1110
IF((KK.EQ.1).AND.(LL.EQ.1).AND.((11.NE.1).OR.(IJ.NE.1)))GO TO 49	BALF1120
IF((SS.EQ.0.)GO TO 45	BALF1130
YS=(U(1))-U2)/SS	BALF1140
IF((YS.GE.1.).OR.(YS.LE.(-1.)))GO TO 43	BALF1150
GO TO 44	BALF1160
43 Y(1)=1.+OY*.5	BALF1170
44 Z=1	BALF1180

44	Y(NN)=Y	BALF1190
	Y(1)=YS	BALF1200
41	Y(NN+1)=Y(NN)+DY	BALF1210
	RATIO(NN+1)=1.-Y(NN+1)*2	BALF1220
	NNN=NN+1	BALF1230
	IF(Y(NN).LT.(1.-5*DY))GO TO 41	BALF1240
	IF(Y(NN).CF.1.)NNN=NN-1	BALF1250
	NN=NN+1	BALF1260
	Y(MM)=YS-DY	BALF1270
	RATIO(MM)=1.-Y(MM)*2	BALF1280
	IF(Y(MM).LT.(1.-1))MM=MM-1	BALF1290
	IF(Y(MM+1).LE.(1.-1))GO TO 42	BALF1300
42	Y(MM+1)=Y(MM)-DY	BALF1310
	RATIO(MM+1)=1.-Y(MM+1)*2	BALF1320
	MM=MM+1	BALF1330
	IF(Y(MM).GT.(1.-5*DY))GO TO 42	BALF1340
	IF(Y(MM).LE.(1.-1))MM=MM-1	BALF1350
49	GO 50 M=2,MM	BALF1360
	UMAR=ARS((U(1)+U2-SS*Y(M))*5)	BALF1370
	Y=SWILL)*RATIO(M)	BALF1380
	HQ=HHH*UMAR*.77W*.13	BALF1390
	PPH2=PHZ(LL)*SQRT(RATIO(M))	BALF1400
	US=ARS(U2-U(1)+SS*Y(M))	BALF1410
	G11=G1Y*US*(HQ*PPH2)	BALF1420
	G22=G2Y*US**2	BALF1430
	G33=G3Y*PPH2	BALF1440
	CALL FRCIN *G11,G22,G33,FCOF,THETA<	BALF1450
	FCOF=7.5*SQRT(G11)	BALF1460
	FCOF=7.5*SQRT(G11)	BALF1470
	FIX=-FCOF*M*DY*S1(LL)	BALF1480
	IF((U(1)-SS*Y(M)).LT.U2)FIX=-FIX	BALF1490
	F1Y=-FCOF*M*V(JJ)/US*DY*S1(LL)	BALF1500
	FF1X=FF1X+F1X	BALF1510
	FF1Y=FF1Y+F1Y	BALF1520
	TFX=-F1X*Y(M)*S1(LL)	BALF1530
	TM1=TM1+TFX	BALF1540
	TFY=-FCOF*M*SS*S2(LL)**2*RATIO(M)*DY/(3.*US)	BALF1550
	TM2=TM2+TFY	BALF1560
	IF(HQ-THICKR(L,J))>01,201,50	BALF1570
201	THICKR(L,J)=HQ	BALF1580
50	CONTINUE	BALF1590
	TM=TM1+TM2	BALF1600
	FFXX(I,JJ,NN)=FF1X	BALF1610
	FFYY(I,JJ,NN)=FF1Y	BALF1620
	TMM(I,JJ,NN)=TM	BALF1630
	IF((I,GE.3).OR.(JJ,GT.1).OR.(KK,GT.1).OR.(LL,GT.1))GO TO 55	BALF1640
	II=II+1	BALF1650
	GO TO 48	BALF1660
55	II=1	BALF1670
	IF((JJ,GE.3).OR.(KK,GT.1).OR.(LL,GT.1))GO TO 56	BALF1680
	JJ=JJ+1	BALF1690
	GO TO 58	BALF1700
56	JJ=1	BALF1710
	IF((KK,GE.3).OR.(LL,GT.1))GO TO 57	BALF1720
	KK=KK+1	BALF1730
	NN=NN+1	BALF1740
	GO TO 48	BALF1750
57	KK=1	BALF1760
		BALF1770

```

IF (LL.GE.3) GO TO 58
LL=LL+1
VV=NN+1
G1 TO 49
58 CONTINUE
FXDU=(FFXX(2,1,1)-FFXX(3,1,1))/(2.*DU)
FXDV=(FFXX(1,2,1)-FFXX(1,3,1))/(2.*DV)
FXDWS=(FFXX(1,1,2)-FFXX(1,1,3))/(2.*DWS)
FXDW=(FFXX(1,1,4)-FFXX(1,1,5))/(2.*DWT)
FYDU=(FFYY(2,1,1)-FFYY(3,1,1))/(2.*DU)
FYDV=(FFYY(1,2,1)-FFYY(1,3,1))/(2.*DV)
FYDWS=(FFYY(1,1,2)-FFYY(1,1,3))/(2.*DWS)
FYDW=(FFYY(1,1,4)-FFYY(1,1,5))/(2.*DWT)
TMDU=(TMM(2,1,1)-TMM(3,1,1))/(2.*DU)
TMDV=(TMM(1,2,1)-TMM(1,3,1))/(2.*DV)
TMDWS=(TMM(1,1,2)-TMM(1,1,3))/(2.*DWS)
TMDW=(TMM(1,1,4)-TMM(1,1,5))/(2.*DWT)
FX(1)=FFXX(1,1,1)
FY(1)=FFXX(1,1,1)
TS(1)=TMM(1,1,1)
FXVX(1)=-FYDV
FYVY(1)=-FYDU
FXWS(1)=-FYDWS/.10471976
FXDP(1)=FYDW
FYVX(1)=-FXDV
FYVY(1)=-FXDU
FYWS(1)=-FXDWS/.10471976
FYDP(1)=FXDW
QDSVX(1)=-TMDV
QDSVY(1)=-TMDU
QDSWS(1)=-TMDWS/.10471976
QDSP(1)=TMDW
PSTURN
END

C) COMPUTE BALL
REAL LUBDEN
COMMON HSO(40),HSI(40)
COMMON AL2FA,FA(2),AMAJ(2,40),AMIN(2,40),APICK(40),
1,B(2),BP(2),BCECK(40),CAGEW,CRV(2),CRAO,CNSB,CPH,CTHET,
2CQRR(5),CP(2),CF,CI(2),CSP(2),CRR(5),CLEAR(2),CLEARP,DP(2,5),
3CG(2,2),CCF(5),DP(2,5),DEX(2),DRDP,D.DENS,DOL(4),DFL(4),DTV(5,5),
4CTEP,DFL(2),DDELX(2,2),DXKGG(2),DEXVX(2),DEXVY(2),DEXWS(2),
5DEXPI(2),DEXVX(2),DEXVY(2),DEXWS(2),DEXPI(2),DQSVX(2),DQSVY(2),DQSWSHALL
6(2),DQSP(2),DEX(2,5),DEY(2,5),DOS(2,5),DEPX(5),DEPZ(5),DOP(5),DMY(BALL
75),DMZ(5),DPSI(5,5),DPSII(5,5),DRA(2),DELA(2),DPA(2),DFXA(2),DFYABALL
8(2),DQSA(2),DEXOME(2),DEYOME(2),DOSOME(2),DEPXA(2),DEPZA(2),DQPA(2)BALL
9),DVAPA(5),DVARA(5),DVOME(5),DGA(2),
COMMON ERR(5),F2,FSAVE(2),
1,FTAN,FEF(2,40),FEY(2,40),
2HOR1,HOR2,HOR3,HOR4,
3JPASS,LPASS,LUBDEN,N,OMEGA,OMY,OMX,
4OM7,OMS(2),OMFY(40),OMFY(40),OMEZ(40),
5PR,PF,PC,PD,PUCKET,PHI,PILOT,PX(2),PSI(5),PI(2,40),
6OS(2),OS(2,40),R,RPM(2),SINH,SPH,SHFT,
7SP(2),SO(2),TOL,TI,THEI,TOL1(1),TCRV,TSAVE(2),
8THICKP(2,40),THICKP(40),VTS,VERT,VRT1,VRT2,VRT3,VRT4,VYR(2),
9VYR(2),VXV(2),VXP(40),VZP(40),VEC(5)
COMMON XI(5),XN,XF(4),XF(4),XK(2),XK2,XMY,XPHI(40),XBFT(2,40),XOMS(BALL
112,40),XMU,XMU1,YF,YR,YC,YNUM
COMMON DZVYR,DZVX,DZWS,DZP2,XIN,XMASS
COMMON FX(2),FY(2)
COMMON IC,CTI(40),LCTI,ICNT,LOOP,TQ(2),Y1,Y2,Y3,Y4,Y5,Y6,Y7,Y8,Y9(BALL
1,Y10,GA(2,2),BA(2,2),DELA(2,2),H1(2),HH(2),H1(2),H2(2),SHAL(2),
2PAL(2),OMEGA,OME(40),DCXI(2),DPSIX(2,2),DGYA(2),PA(2,2),DPSIA(2),
3XA(2),KONV,CAD(2,2),REFR,DQVRO(2),CAL,SAL,A1,A2,OM,TI,IZ,IS,IA,BALL

```

```

4001,NUM,XA1(40),XA2(40),IPASS,REVM(40),REV7(40)      BALL 320
5,CAC(501(2),PINGO1(2),AREA1(2),VEL(2),SDRAG(2),BDRAG,DSORG(2,4), BALL 330
6,PDZCA1,PDZCA2,PDZOME      BALL 340
J=IPASS      BALL 350
IC=CTL(J)      BALL 360
TAL=SF(1C)/(CF(1C)+C(1C)*D/E2)      BALL 370
ALX=ATAN(TAL)      BALL 380
SAL=SIN(ALX)      BALL 390
CAL=COS(ALX)      BALL 400
DO 1K=1,2      BALL 410
TEMP=R(K)-ALX      BALL 420
S1AL(K)=SIN(TEMP)      BALL 430
1 CHAL(K)=COS(TEMP)      BALL 440
T1=GG(1)*CBAL(2)      BALL 450
T2=GG(2)*CBAL(1)      BALL 460
OMX=T1+T2      BALL 470
Q=VR=E2*(RPM(1)-RPM(2))/GG(1)*GG(2)/(D*DN)      BALL 480
REVM(J)=REVB+CAL      BALL 490
REVZ(J)=-REVR*SAL      BALL 500
OMEGA=(T1+RPM(1)+T2+RPM(2))/DN      BALL 510
CC=XMASS*.5*E2*OMEGA**2      BALL 520
XMY=XIN*OMEGA*REVR*SAL      BALL 530
H(1)=7.*XMY/D      BALL 540
H(2)=H(1)      BALL 550
Y1=CB(1C)**2+C(1C)*G2(1C)      BALL 560
Y2=CB(1C)**2-SB(1C)**2      BALL 570
Y3=SB(1C)*CB(1C)      BALL 580
Y4=(CAL/Y1)**2      BALL 590

Y5=E2*(RPM(1)-RPM(2))/(D*DN**2)      BALL 600
Y6=OMEGA*DN      BALL 610
Y7=2./D*(H1(1C)*CB(1)-H2(1C)*CB(2))      BALL 620
Y8=2./D*(H1(1C)*SB(1)-H2(1C)*SB(2))      BALL 630
Y9=.5*D*Y7      BALL 640
Y10=.5*D*Y8      BALL 650
DO 2 K=1,2      BALL 660
Q4 X=(Y1+Y2*DB(1C,K)-Y3*(1-2.*Y3*DB(1C,K)+C(1C)*DG(1C,K)))*Y4      BALL 670
Z1=GG(1)*SPAL(2)*(DB(2,K)-DALX)      BALL 680
Z2=GG(2)*SEAL(1)*(DP(1,K)-DALX)      BALL 690
DOMBX=Y5*(DN*(1-GG(1)*DG(2,K)+GG(2)*DG(1,K))-GG(1)*GG(2)*(-Z1+CBAL(1)      BALL 700
1)*DG(1,K)-Z2-CBAL(1)*DG(2,K))+REVR*DEX(K)/E2      BALL 710
DOMEX=DN*(RPM(1)*(1-Z1+CBAL(2)*DG(1,K))-RPM(2)*(Z2+CBAL(1)*DG(2,K)+      BALL 720
1)*Y6*(1-Z1+CBAL(2)*DG(1,K)-Z2-CBAL(1)*DG(2,K))/DN**2      BALL 730
DCX(K)=XMASS*(E2*OMEGA*DOMEX+.5*OMEGA**2*DEX(K))      BALL 740
2 QGYRD(K)=XIN*(REVR*DOMEX+OMEGA*DOMBX)*SAL+REVB*OMEGA*CAL*DALX      BALL 750
T1=PX(1)*CB(1)+H(1C)*SB(1)      BALL 760
T2=PX(2)*CB(2)+H(1C)*SB(2)      BALL 770
T3=PX(1)*SB(1)-H(1C)*CB(1)      BALL 780
T4=PX(2)*SB(2)-H(1C)*CB(2)      BALL 790
DO 3 K=1,2      BALL 800
OPSIX(1,K)=T1*DB(1,K)-T2*DB(2,K)+DP(1,K)*SB(1)-DP(2,K)*SB(2)-Y7*      BALL 810
1 DGYPD(K)      BALL 820
3 OPSIX(2,K)=Y3*DP(1,K)+4*DB(2,K)+DP(1,K)*CB(1)-DP(2,K)*CB(2)+Y8      BALL 830
1 DGYPD(K)=DCX(K)      BALL 840
PSI(1)=PX(1)*SB(1)-PX(2)*SB(2)-H(1)*Y9      BALL 850
PSI(2)=PX(1)*CB(1)-PX(2)*CB(2)+H(1)*Y10-CF      BALL 860
QF1=OPSIX(1,1)*OPSIX(2,2)-OPSIX(2,1)*OPSIX(1,2)      BALL 870
COR(1)=(PSI(1)*OPSIX(2,2)-PSI(2)*OPSIX(1,2))/DET      BALL 880
COR(2)=(OPSIX(1,1)*PSI(2)-OPSIX(2,1)*PSI(1))/DET      BALL 890
DO 4 K=1,2      BALL 900
X(K)=X(K)-COR(K)      BALL 910
4 RETURN      BALL 920
END      BALL 930

```

SUBROUTINE BALL2	BALL	10
REAL LURDEN	BALL	20
COMMON HSO(40),HSI(40)	BALL	30
COMMON ALPHA,AA(2),AMAJ(2,40),AMIN(2,40),APOCK(40),	BET,RETBAIL	40
1,BL(2),BB(2),BPCK(40),CAGEM,CRV(2),CBAD,COSB,CPH,CTHET,	BALL	50
2,CORR(5),CP(2),CF,C(2),CSP(2),COR(5),CLEAR(2),CLFARP,	DP(2,5),	BALL
3,DG(2,2),DCF(5),DR(2,5),DEX(2),DROP,D,DENS,DDL(4),DFL(4),DTV(5,3),	BALL	80
4,DETER,DEL(2),DEFLX(2,2),DKNG(2),DFVX(2),DFVY(2),DFXWS(2),	BALL	90
5,DFXP(2),DFYVX(2),DFYVY(2),DFYWS(2),DFYP(2),DOSVX(2),DOSVY(2),DOSWSBALL		100
6(2),DOSP(2),DFX(2,5),DFY(2,5),DQS(2,5),DFPX(5),DFPZ(5),DQP(5),DMY(BALL		110
75),DMZ(5),OPSI(5,5),OPSI1(5,5),DBA(2),DELA(2),DPA(2),DFXA(2),DFYABALL		120
8(2),DQSA(2),DFXOME(2),DFYOME(2),DOSOME(2),DFPXA(2),DFPZA(2),DQPA(2)BALL		130
9),DVARA1(5),DVARA2(5),DVOHE(5),DGA1(2),	E,EL	BALL
COMMON FRR(5),F2,FSAVE(2),	FLAT,F(2),FK,FRAOBALL	150
1,FIAN,FFX(2,40),FFY(2,40),	GAGE,G2(2),GG(2),BALL	160
2	HOR(2),HOR1,HOR2,HOR3,HOR4,	IOU(2),
3JPASS,	IPASS,LURDEN,	N,
4OMZ,DMS(2),PMEX(40),OMEY(40),OMEZ(40),	OMEGAE,OMY,OMX,	BALL
5OR,PE,PC,PD,POCKET,PHI,PILQI,PI(2),PSI(5),PI2(40),	PROG(40),PL,BALL	190
6OS(2),QOS(2,40),	R,RPM(2),	SINH,SPH,STHET,
7SB(2),SO(2),	TOTL,TI,THET,TOL(11),TCPV,TSAYF(2),	BALL
8THICKR(2,40),THICKP(40),	VIS,VERT,VRT1,VRT2,VRT3,VRT4,VYR(2),	BALL
9VYU(2),VXB(2),VXP(40),VZP(40),VEC(5)		BALL
COMMON X(5),XA,XF(4),XF1(4),XK(2),XMZ,XMY,XPHI(40),XRFT(2,40),XOMSBALL		250
112,40),XMU,XMU1,	YE,YR,YC,YNUM	BALL
COMMON DZVYR,DZVX,DZWS,DZP2,XIN,XMASS		BALL
COMMON FX(2),FY(2)		BALL
COMMON IC,CTL(40),LCTL,ICNT,LOOP,TQ(2),Y1,Y2,Y3,Y4,Y5,Y6,Y7,Y8,Y9BALL		290
1,Y10,GA(2,2),BA(2,2),DELA(2,2),H(2),HH(2),H1(2),H2(2),SPAL(2),		BALL
2,CAL(2),CEGA,CM(40),DCX(2),OPSI(2),GGYA(2),PA(2,2),OPSI1(2),		BALL
3XA(2),	KENV,LA(2,2),REVB,DGYRO(2),CAL,SAL,A1,A2,DN,T1,T2,T3,T4,	BALL
4DET,NUM,XA1(40),XA2(40),ITPASS,REX(40),REVZ(40)		BALL
5,CAGFD(2),RNGDI(2),ARFA(2),VEL(2),SORAG(2),RDRAG,DSDAG(2,4),		BALL
6FPZA1,FPZA2,FPZME		BALL
J=JPASS		BALL
ICNT=ICNT+1		BALL
DO 1 K=1,		BALL
1 T(K)=AA(K)*PX(K)*FSAVE(K)/CSP(K)		BALL
2Q1=COS(R(2)-R(1))		BALL
IF(ICNT-3)2,3,3		BALL
3 IF(LOOP)4,4,5		BALL
4 LCP=1		BALL
IC=1		BALL
NUM=1		BALL
RETURN		BALL
2 IF(IC-1)6,6,7		BALL
6 IF(TQ(2)*B2R1-TQ(1))8,8,9		BALL
9 IC1=2		BALL
GO TO 10		BALL
9 IC1=1		BALL
GO TO 10		BALL
7 IF(TQ(1)*R2P1-TQ(2))11,11,12		BALL
12 IC1=1		BALL
GO TO 10		BALL
11 IC1=2		BALL
IF(IC1-IC)13,5,13		BALL
13 IC=IC1		BALL
NUM=1		BALL
RETURN		BALL

5	DTL(I)=IC	BALL 610
	NUM=C	BALL 620
	DLA(2,1)=SB(2)	BALL 630
	DLA(2,2)=CP(2)	BALL 640
	PA(2,1)=CR(2)*2/(A2-X(2))	BALL 650
	PA(2,2)=-(A1-X(1))*(CP(2)/(A2-X(2)))*2	BALL 660
	GA(2,1)=-D*PA(2,1)*SB(2)/E2	BALL 670
	GA(2,2)=-D*PA(2,2)*SB(2)/E2	BALL 680
	DO 14 K=1,2	BALL 690
	DALA=(Y1*Y2*PA(1C,K)-Y3*(-2.*Y3*PA(1C,K)+C(1C)*GA(1C,K)))*Y4	BALL 700
	DALA=(Y1*Y2*PA(1C,K)-Y3*(-2.*Y3*PA(1C,K)+C(1C)*GA(1C,K)))*Y4	BALL 710
	Z1=CG(1)*SBAL(2)*(PA(2,K)-DALA)	BALL 720
	Z2=CG(2)*SBAL(1)*(PA(1,K)-DALA)	BALL 730
	DDMPA=Y5*(DM*(-GG(1)*GA(2,K)+GG(2)*GA(1,K))-GG(1)*GG(2)*(-Z1+CRAL(1)*GA(1,K)-Z2-CRAL(1)*GA(2,K)))	BALL 740
	DDMPA=(DM*(RPM(1)*(-Z1+CRAL(2)*GA(1,K))-RPM(2)*(Z2+CRAL(1)*GA(2,K)+RPM(1)*(-Z1+CRAL(2)*GA(1,K)-Z2-CRAL(1)*GA(2,K)))/DM**2	BALL 750
	DDMPA=MASS*E2*DDMPA	BALL 760
	DDYA(K)=XIN*((PEVP*DDMPA+OMEGA*DDMPA)*SAL+REVB*DDMPA*CAL+DALA)	BALL 770
	DO 15 L=1,2	BALL 780
15	PA(L,K)=1.5*SG(L)*DLA(L,K)+DEL(1)*SORT(DLA(L))*DXXDG(L)*GA(L,K)	BALL 790
	DDSLA(1)=T1*DA(1,K)-T2*PA(2,K)+PA(1,K)*SB(1)-PA(2,K)*SB(2)-Y7*DDYA(L,K)	BALL 800
	DDSLA(2)=-T3*DA(1,K)+T4*PA(2,K)+PA(1,K)*CR(1)-PA(2,K)*CR(2)+Y8*DDYA(L,K)-DCA	BALL 810
	XA(1)=-DPSLA(1)*DDSLX(2,2)+DDSLA(2)*DDSLX(1,2))/DET	BALL 820
	XA(2)=(-DPSLA(2)*DDSLX(1,1)+DPSLA(1)*DDSLX(2,1))/DET	BALL 830
	PA(2,K)=PA(2,K)+DD(2,1)*XA(1)+DD(2,2)*XA(2)	BALL 840
	DLA(2,K)=DLA(2,K)+DDFLX(2,1)*XA(1)+DDFLX(2,2)*XA(2)	BALL 850
	PA(2,K)=1.5*SG(2)*DLA(2,K)+DEL(2)*SORT(DLA(2))*DXXDG(2)*GA(2,K)+DD(2,1)*XA(1)+DD(2,2)*XA(2)	BALL 860
14	DDYA(K)=DDYA(K)+DDY9(1)*XA(1)+DDY9(2)*XA(2)	BALL 870
	XF(1)=XF(1)+T4	BALL 880
	XF(2)=XF(2)+T2*CPH	BALL 890
	DO 16 K=1,2	BALL 900
	Y1=PA(2,1)*PA(1,K)+PA(2,2)*DA(2,K)	BALL 910
	Y2=PA(2,1)*PA(1,K)+PA(2,2)*DA(2,K)	BALL 920
	Y3=DDYA(1)*CAL(1,K)+DDYA(2)*DA(2,K)	BALL 930
	Y4=T2*Y1+Y2*SG(2)-H2(1C)*Y3*CB(2)/D22	BALL 940
	Y5=-T4*Y1+Y2*CP(2)+H2(1C)*Y3*SB(2)/D22	BALL 950
	DTV(1,K)=DTV(1,K)+Y4	BALL 960
	DTV(2,K)=DTV(2,K)+Y5*CPH	BALL 970
16	RTIMEH	BALL 980
	CND	BALL 990

```

SUBROUTINE FRCTN (G1,G2,G3,FCOE,THE1A)
DIMENSION AG1(13),AG2(13),AG3(13),FTN(13,7,7),U7(7,7),V7(7),VTN(637)
DIMENSION A1(13),A2(13),A3(13),A4(13),A5(13),A6(13),A7(13),A8(13),A9(13),
1A9(13),A10(13),A11(13),A12(13),A13(13),A14(13),A15(13),A16(13),
2A17(13),A18(13),A19(13),A20(13),A21(13),A22(13),A23(13),A24(13),
3A25(13),A26(13),A27(13),A28(13),A29(13),A30(13),A31(13),A32(13),
4A33(13),A34(13),A35(13),A36(13),A37(13),A38(13),A39(13),A40(13),
5A41(13),A42(13),A43(13),A44(13),A45(13),A46(13),A47(13),A48(13),
6A49(13)
EQUIVALENCE(VTN(1),FTN(1,1,1))
EQUIVALENCE(VTN(1),A1(1)),(VTN(14),A2(1)),(VTN(27),A3(1)),
1(VTN(40),A4(1)),(VTN(53),A5(1)),(VTN(66),A6(1)),(VTN(79),A7(1)),
2(VTN(92),A8(1)),(VTN(105),A9(1)),(VTN(118),A10(1)),(VTN(131),A11(1)),
3(VTN(144),A12(1)),(VTN(157),A13(1)),(VTN(170),A14(1)),(VTN(183),A15(1)),
4A16(1)),(VTN(196),A16(1)),(VTN(209),A17(1)),(VTN(222),A18(1)),
5(VTN(235),A19(1)),(VTN(248),A20(1)),(VTN(261),A21(1)),(VTN(274),A22(1)),
6A23(1)),(VTN(287),A23(1)),(VTN(300),A24(1)),(VTN(313),A25(1)),
7(VTN(326),A26(1)),(VTN(339),A27(1)),(VTN(352),A28(1)),(VTN(365),A29(1)),
8A30(1)),(VTN(378),A30(1)),(VTN(391),A31(1)),(VTN(404),A32(1)),
9(VTN(417),A33(1)),(VTN(430),A34(1)),(VTN(443),A35(1)),(VTN(456),A36(1)),
1A37(1)),(VTN(469),A37(1)),(VTN(482),A38(1)),(VTN(495),A39(1)),
2(VTN(508),A40(1)),(VTN(521),A41(1)),(VTN(534),A42(1)),(VTN(547),A43(1)),
3A44(1)),(VTN(560),A44(1)),(VTN(573),A45(1)),(VTN(586),A46(1)),(VTN(599),A47(1)),
4(VTN(612),A48(1)),(VTN(625),A49(1))
DATA A1 /0.0025,0.0007, 0.0014, 0.0023, 0.0067,
1 0.0135, 0.021, 0.037, 0.046, 0.052, 0.0615, 0.0695, 0.0775/
DATA A2 /0.0007, 0.002, 0.0039, 0.0065, 0.0150,
1 0.022, 0.027, 0.042, 0.0495, 0.054, 0.0625, 0.069, 0.0775/
DATA A3 / 0.0026, 0.0079, 0.014, 0.019, 0.029,
1 0.034, 0.038, 0.0485, 0.054, 0.059, 0.064, 0.0695, 0.0775/
DATA A4 / 0.0077, 0.017, 0.023, 0.027, 0.035,
1 0.04, 0.044, 0.051, 0.0555, 0.0605, 0.066, 0.071, 0.0775/
DATA A5 /0.019, 0.0285, 0.034, 0.037, 0.044, 0.048,
1 0.05, 0.056, 0.06, 0.0635, 0.067, 0.0725, 0.0775/
DATA A6 / 0.0215, 0.032, 0.037, 0.0415, 0.0475,
1 0.051, 0.054, 0.06, 0.0635, 0.066, 0.07, 0.073, 0.0775/
DATA A7 / 0.0245, 0.034, 0.04, 0.0435, 0.05,
1 0.054, 0.0565, 0.062, 0.0655, 0.0675, 0.071, 0.074, 0.0775/
DATA A8 /0.0002,0.0006, 0.0, 0.002, 0.004, 0.012,
1 0.019, 0.036, 0.047, 0.054, 0.0645, 0.0, 0.077/
DATA A9 /0.0006,0.002, 0.0, 0.0065, 0.015, 0.024,
1 0.028, 0.043, 0.052, 0.0575, 0.0645, 0.072, 0.077/
DATA A10 / 0.0027, 0.0081, 0.014, 0.019, 0.0285,
1 0.035, 0.0395, 0.051, 0.057, 0.061, 0.064, 0.0725, 0.077/
DATA A11 /0.0066, 0.015, 0.021, 0.025, 0.034, 0.04,
1 0.0445, 0.054, 0.06, 0.064, 0.069, 0.073, 0.077/
DATA A12 / 0.017, 0.0225, 0.029, 0.0345, 0.043,
1 0.049, 0.052, 0.059, 0.063, 0.066, 0.070, 0.073, 0.077/
DATA A13 / 0.019, 0.032, 0.039, 0.0415, 0.05, 0.054,
1 0.056, 0.061, 0.064, 0.067, 0.0715, 0.075, 0.077/
DATA A14 / 0.021, 0.0335, 0.041, 0.0455, 0.053,
1 0.056, 0.059, 0.064, 0.068, 0.07, 0.073, 0.076, 0.077/
DATA A15 / 0.0016, 0.0055, 0.0011, 0.0019, 0.0059, 0.011,
1 0.018, 0.033, 0.042, 0.048, 0.06, 0.068, 0.075/
DATA A16 / 0.007, 0.021, 0.0043, 0.007, 0.015, 0.023,
1 0.027, 0.039, 0.046, 0.052, 0.062, 0.07, 0.075/
DATA A17 / 0.0018, 0.0053, 0.01, 0.015, 0.0255,
1 0.034, 0.037, 0.049, 0.054, 0.058, 0.066, 0.073, 0.075/
DATA A18 / 0.0046, 0.011, 0.018, 0.024, 0.037,

```

U 0.039, 0.044, 0.0525, 0.057, 0.061, 0.068, 0.074, 0.075/	FRCT 600
DATA A19 / 0.0092, 0.017, 0.025, 0.03, 0.042,	FRCT 610
10.049, 0.052, 0.06, 0.064, 0.066, 0.073, 0.074, 0.075/	FRCT 620
DATA A20 / 0.015, 0.026, 0.034, 0.04, 0.049,	FRCT 630
1 0.054, 0.058, 0.063, 0.067, 0.069, 0.073, 0.075, 0.075/	FRCT 640
DATA A21 / 0.019, 0.029, 0.035, 0.043, 0.052,	FRCT 650
1 0.057, 0.06, 0.065, 0.069, 0.07, 0.074, 0.075, 0.075/	FRCT 660
DATA A22 / 0.0015, 0.0046, 0.01, 0.0017, 0.005, 0.01,	FRCT 670
1 0.016, 0.034, 0.04, 0.04, 0.059, 0.067, 0.073/	FRCT 680
DATA A23 / 0.00064, 0.002, 0.0039, 0.0004, 0.015,	FRCT 690
1 0.021, 0.026, 0.039, 0.046, 0.052, 0.062, 0.068, 0.073/	FRCT 700
DATA A24 / 0.0017, 0.0049, 0.009, 0.014, 0.025,	FRCT 710
1 0.031, 0.036, 0.047, 0.053, 0.057, 0.065, 0.0695, 0.073/	FRCT 720
DATA A25 / 0.043, 0.01, 0.017, 0.023, 0.033,	FRCT 730
1 0.047, 0.043, 0.052, 0.059, 0.061, 0.066, 0.07, 0.073/	FRCT 740
DATA A26 / 0.0079, 0.015, 0.024, 0.029, 0.04,	FRCT 750
1 0.046, 0.051, 0.057, 0.062, 0.064, 0.068, 0.071, 0.073/	FRCT 760
DATA A27 / 0.0145, 0.024, 0.033, 0.039, 0.049,	FRCT 770
1 0.053, 0.056, 0.062, 0.066, 0.067, 0.07, 0.072, 0.073/	FRCT 780
DATA A28 / 0.016, 0.027, 0.0355, 0.041, 0.052,	FRCT 790
1 0.056, 0.059, 0.064, 0.067, 0.069, 0.071, 0.073, 0.073/	FRCT 800
DATA A29 / 0.001, 0.0027, 0.0055, 0.0009, 0.0029,	FRCT 810
1 0.0067, 0.01, 0.025, 0.036, 0.043, 0.054, 0.062, 0.068/	FRCT 820
DATA A30 / 0.0044, 0.013, 0.0225, 0.0044, 0.012,	FRCT 830
1 0.013, 0.024, 0.034, 0.044, 0.048, 0.057, 0.063, 0.069/	FRCT 840
DATA A31 / 0.001, 0.0029, 0.0056, 0.0029, 0.0195,	FRCT 850
1 0.0255, 0.03, 0.042, 0.0485, 0.053, 0.06, 0.064, 0.068/	FRCT 860
DATA A32 / 0.0015, 0.0045, 0.0095, 0.013, 0.024,	FRCT 870
1 0.032, 0.036, 0.047, 0.053, 0.057, 0.063, 0.065, 0.069/	FRCT 880
DATA A33 / 0.0034, 0.0093, 0.0155, 0.021, 0.032,	FRCT 890
1 0.038, 0.042, 0.052, 0.056, 0.06, 0.064, 0.066, 0.068/	FRCT 900
DATA A34 / 0.0044, 0.017, 0.0245, 0.03, 0.04,	FRCT 910
1 0.0465, 0.051, 0.059, 0.061, 0.063, 0.066, 0.067, 0.068/	FRCT 920
DATA A35 / 0.012, 0.022, 0.0295, 0.035, 0.0455,	FRCT 930
1 0.051, 0.055, 0.061, 0.063, 0.065, 0.067, 0.068, 0.069/	FRCT 940
DATA A36 / 0.0005, 0.0014, 0.0027, 0.0045, 0.0014,	FRCT 950
1 0.0027, 0.0046, 0.013, 0.023, 0.029, 0.042, 0.052, 0.055/	FRCT 960
DATA A37 / 0.0012, 0.0042, 0.0095, 0.014, 0.024,	FRCT 970
1 0.0084, 0.013, 0.0245, 0.032, 0.037, 0.0455, 0.053, 0.055/	FRCT 980
DATA A38 / 0.004, 0.012, 0.024, 0.004, 0.011,	FRCT 990
1 0.017, 0.023, 0.0345, 0.039, 0.0425, 0.049, 0.0535, 0.055/	FRCT 1000
DATA A39 / 0.0015, 0.0042, 0.0084, 0.012, 0.023,	FRCT 1010
1 0.029, 0.033, 0.0395, 0.043, 0.045, 0.059, 0.0535, 0.055/	FRCT 1020
DATA A40 / 0.0034, 0.0094, 0.014, 0.0195, 0.03,	FRCT 1030
1 0.036, 0.04, 0.046, 0.049, 0.049, 0.051, 0.054, 0.055/	FRCT 1040
DATA A41 / 0.0054, 0.013, 0.02, 0.025, 0.0375,	FRCT 1050
1 0.042, 0.045, 0.049, 0.05, 0.052, 0.0525, 0.054, 0.055/	FRCT 1060
DATA A42 / 0.0071, 0.015, 0.023, 0.03, 0.04,	FRCT 1070
1 0.045, 0.049, 0.051, 0.052, 0.053, 0.054, 0.055, 0.055/	FRCT 1080
DATA A43 / 0.0003, 0.0009, 0.0019, 0.003, 0.0039,	FRCT 1090
1 0.0019, 0.003, 0.009, 0.016, 0.023, 0.037, 0.045, 0.051/	FRCT 1100
DATA A44 / 0.001, 0.0026, 0.0054, 0.009, 0.029,	FRCT 1110
1 0.0057, 0.0092, 0.021, 0.029, 0.034, 0.041, 0.047, 0.051/	FRCT 1120
DATA A45 / 0.0025, 0.0074, 0.015, 0.024, 0.032,	FRCT 1130
1 0.013, 0.019, 0.028, 0.035, 0.039, 0.045, 0.048, 0.051/	FRCT 1140
DATA A46 / 0.00054, 0.0016, 0.0033, 0.0052, 0.014,	FRCT 1150
1 0.022, 0.0265, 0.033, 0.04, 0.042, 0.0465, 0.047, 0.051/	FRCT 1160
DATA A47 / 0.013, 0.023, 0.0369, 0.041, 0.043,	FRCT 1170
1 0.029, 0.0325, 0.0395, 0.044, 0.046, 0.0485, 0.059, 0.051/	FRCT 1180


```

DATA A49          /0.0015, 0.041, 0.009, 0.012, 0.0235,      FRCT1190
1 0.0295, 0.033, 0.04, 0.044, 0.0465, 0.049, 0.0505, 0.051/   FRCT1200
DATA A49          /0.0018, 0.0052, 0.0094, 0.014, 0.0255,      FRCT1210
1 0.031, 0.035, 0.042, 0.045, 0.047, 0.05, 0.051, 0.051/   FRCT1220
DATA AG1          /1.E-8, 3.E-8, 5.E-8, 1.E-7, 3.E-7, 6.E-7,   FRCT1230
1 1.E-6, 3.E-6, 6.E-6, 1.E-5, 3.E-5, 1.E-4, 1.E-3/           FRCT1240
DATA AG2          /5.E-7, 1.E-6, 5.E-6, 1.E-5, 5.E-5, 5.E-4, 1.E-3 FRCT1250
1 /                                                         FRCT1260
DATA AG3          /13.32, 15.2, 17.9, 19., 21.19, 27.13, 100./   FRCT1270
IF(G1.EQ.0.) GO TO 240   FRCT1280
IF(G2.EQ.0.) GO TO 240   FRCT1290
DO 100 I=1,7            FRCT1300
DO 100 J=1,7            FRCT1310
IF(G1-AG1(I)) 40,60,80   FRCT1320
40 IF(G1.LT.AG1(I)) GO TO 70   FRCT1330
CALL TLUG(G1,UZ(I,J),AG1,FTN(1,I,J),13)   FRCT1340
GO TO 100              FRCT1350
60 UZ(I,J)=FTN(1,I,J)      FRCT1360
GO TO 100              FRCT1370
70 UZ(I,J)=EXP(ALOG(FTN(1,I,J))+(ALOG(FTN(2,I,J))-ALOG(FTN(1,I,J)))/   FRCT1380
1   (ALOG(AG1(2))-ALOG(AG1(1)))+(ALOG(G1)-ALOG(AG1(1))))   FRCT1390
100 CONTINUE            FRCT1400
DO 200 K=1,7            FRCT1410
IF(G3-AG3(K)) 140,160,160   FRCT1420
140 IF(G3.LT.AG3(K)) GO TO 170   FRCT1430
CALL TLUG(G3,VZ(K),AG3,UZ(1,K),7)   FRCT1440
GO TO 200              FRCT1450
160 VZ(K)=UZ(7,K)        FRCT1460
GO TO 200              FRCT1470
170 VZ(K)=UZ(1,K)-(UZ(2,K)-UZ(1,K))/(AG3(2)-AG3(1))*(AG3(1)-G3)   FRCT1480
IF (VZ(K).LE.0.0) VZ(K)=1.E-5   FRCT1490
200 CONTINUE            FRCT1500
IF(G2-AG2(7)) 204,206,206   FRCT1510
204 IF(G2.LT.AG2(7)) GO TO 207   FRCT1520
CALL TLUG(G2,F83,AG2,VZ,7)   FRCT1530
GO TO 210              FRCT1540
206 F83=EXP(ALOG(VZ(6))+(ALOG(VZ(7))-ALOG(VZ(6)))/(ALOG(AG2(7))-ALOG(   FRCT1550
1   AG2(6)))+(ALOG(G2)-ALOG(AG2(6))))   FRCT1560
GO TO 210              FRCT1570
207 F83=EXP(ALOG(VZ(2))+(ALOG(VZ(1))-ALOG(VZ(2)))/(ALOG(AG2(1))-ALOG(   FRCT1580
1   AG2(2)))+(ALOG(G2)-ALOG(AG2(2))))   FRCT1590
210 FCODE=ALOG(F83)-0.149*(ALOG(F83)-ALOG(130.))   FRCT1600
FCODE=EXP(FCODE)         FRCT1610
GO TO 250              FRCT1620
240 FCODE=0.            FRCT1630
250 CONTINUE            FRCT1640
RETURN                  FRCT1650
END                      FRCT1660

```

SUBROUTINE TLU(A,B,C,D,N)	TLUX 10
DIMENSION C(1),D(1)	TLUX 20
IF(N-1)1,2,3	TLUX 30
1 A=0.	TLUX 40
GO TO 100	TLUX 50
2 A=D(1)	TLUX 60
GO TO 100	TLUX 70
3 ML=1	TLUX 80
MJ=N	TLUX 90
4 IF(MJ-ML-1) 15,15,9	TLUX 100
5 M=(MJ+ML)/2	TLUX 110
IF(C(1)-C(2))11,2,10	TLUX 120
10 IF(C(M)-A)13,12,14	TLUX 130
11 IF(A-C(M))13,12,14	TLUX 140
12 A=D(M)	TLUX 150
GO TO 100	TLUX 160
13 MJ=M	TLUX 170
GO TO 8	TLUX 180
14 ML=M	TLUX 190
GO TO 8	TLUX 200
15 A=D(ML)+(D(MJ)-D(ML))*((A-C(ML))/(C(MJ)-C(ML)))	TLUX 210
100 RETURN	TLUX 220
END	TLUX 230

SUBROUTINE TLUG(A,B,C,D,N)	TLUG 10
DIMENSION C(1),D(1)	TLUG 20
IF(N-1)1,2,3	TLUG 30
1 A=0.	TLUG 40
GO TO 100	TLUG 50
2 A=D(1)	TLUG 60
GO TO 100	TLUG 70
3 ML=1	TLUG 80
MJ=N	TLUG 90
4 IF(MJ-ML-1) 15,15,9	TLUG 100
5 M=(MJ+ML)/2	TLUG 110
IF(C(1)-C(2))11,2,10	TLUG 120
10 IF(C(M)-A)13,12,14	TLUG 130
11 IF(A-C(M))13,12,14	TLUG 140
12 A=D(M)	TLUG 150
GO TO 100	TLUG 160
13 MJ=M	TLUG 170
GO TO 8	TLUG 180
14 ML=M	TLUG 190
GO TO 8	TLUG 200
15 A=EXP(ALOG(D(ML))+(ALOG(D(MJ))-ALOG(D(ML)))*((ALOG(A)-ALOG(C(ML)))/(ALOG(C(MJ))-ALOG(C(ML)))))	TLUG 210
1 / (ALOG(C(MJ))-ALOG(C(ML))))	TLUG 220
100 RETURN	TLUG 230
END	TLUG 240

APPENDIX II FORMAT FOR BALL BEARING COMPUTER INPUT INFORMATION

CARD NO.	COL. NO.	ITEM
1	1-10	NUMBER OF BALLS
	11-20	BALL DIAMETER - IN.
	21-30	PITCH DIAMETER - IN.
	31-40	CONTACT ANGLE - DEG.
	41-50	OUTER RACE CURVATURE FACTOR.
	51-60	INNER RACE CURVATURE FACTOR.
	61-70	CHANGE IN INTERNAL CLEARANCE (+ IF INCREASED)
2	71-80	DIAMETER OF CYLINDRICAL CAGE POCKET - IN.
	1-10	YOUNG'S MODULUS FOR CAGE - PSI.
	11-20	POISSON'S RATIO FOR CAGE.
	21-30	YOUNG'S MODULUS FOR BALLS - PSI. IF BLANK PROGRAM ASSUMES 29000000.
	31-40	POISSON'S RATIO FOR BALLS. IF BLANK PROGRAM ASSUMES .25.
	41-50	YOUNG'S MODULUS FOR RINGS. - PSI. IF BLANK PROGRAM ASSUMES 29000000.
	51-60	POISSON'S RATIO FOR RINGS. IF BLANK PROGRAM ASSUMES .25.
3	61-70	BALL MATERIAL DENSITY - LB/IN**2.
	71-80	COEFFICIENT OF SLIDING FRICTION OF BALL IN POCKET.
	1-10	COEFFICIENT OF SLIDING FRICTION OF CAGE ON PILOTING SURFACE.
	11-20	WIDTH OF CAGE - IN.
	21-30	O. D. OF CAGE - IN.
	31-40	I. D. OF CAGE - IN.
	41-50	I. D. OF OUTER RING - IN.
4	51-60	O. D. OF INNER RING - IN.
	61-80	LEAVE BLANK
	1-10	PRESSURE-VISCOSITY COEFFICIENT OF THE LUBRICANT - IN**2/LB.
	11-20	TEMPERATURE-VISCOSITY COEFFICIENT OF LUBRICANT - /F DEG.
	21-30	VISCOSITY OF LUBRICANT - LB-SEC/IN**2.
	31-40	INLET TEMPERATURE - F DEG.
	41-50	THERMAL CONDUCTIVITY OF LUBRICANT - BTU/F DEG - HR - FT.
5	51-60	DENSITY OF LUBRICANT - LB*SEC**2/IN**4
	61-70	PROPORTIONATE INCREMENT FOR THE VELOCITY OF THE RACE IN THE Y DIRECTION. SET TO .05 IF LEFT BLANK
	71-80	PROPORTIONATE INCREMENT FOR THE VELOCITY OF THE BALL IN THE X DIRECTION. SET TO .05 IF LEFT BLANK
	1-10	PROPORTIONATE INCREMENT FOR ANGULAR VELOCITY OF SPIN. SET TO .1 IF LEFT BLANK
	11-20	PROPORTIONATE INCREMENT FOR CONTACT LOAD. SET .05 IF BLANK
	21-30	TOLERANCE ON X(1) BALL CENTER COORDINATE. IF BLANK PROGRAM ASSUMES 1.E-6
	31-40	TOLERANCE ON X(2) BALL CENTER COORDINATE. IF BLANK PROGRAM ASSUMES 1.E-6
6	41-50	TOLERANCE ON BALL'S ANGULAR VELOCITY ABOUT X. IF BLANK PROGRAM ASSUMES 10 RPM.
	51-60	TOLERANCE ON BALL'S ANGULAR VELOCITY ABOUT Y. IF BLANK PROGRAM ASSUMES 1 RPM.
	61-70	TOLERANCE ON BALL'S ANGULAR VELOCITY ABOUT Z. IF BLANK

PROGRAM ASSUMES 5 RPM.

71-80	TOLERANCE ON DEFLECTION ALONG X - IN. IF BLANK PROGRAM ASSUMES 1.E-6
-------	--

6	1-10 TOLERANCE ON DEFLECTION ALONG Y - IN. IF BLANK PROGRAM ASSUMES 1.E-6
	11-20 TOLERANCE ON DEFLECTION ALONG Z - IN. IF BLANK PROGRAM ASSUMES 1.E-6
	21-30 TOLERANCE ON ANGULAR VELOCITY OF CAGE - RPM. IF BLANK PROGRAM ASSUMES .5 RPM
	31-80 LEAVE BLANK

7	1-10 RPM OF OUTER RING.
	11-20 RPM OF INNER RING.
	21-30 THRUST LOAD - LB.
	31-40 RADIAL LOAD - LB.
	41-50 MISALIGNMENT ABOUT Y - IN/IN.
	51-60 ESTIMATE OF DEFLECTION ALONG X - IN.
	61-70 ESTIMATE OF DEFLECTION ALONG Z - IN.
	71-80 PUNCH 2. IF BEARING WHEN RUNNING WITH BOUNDARY LUBRICATION COULD BE EXPECTED TO HAVE 'INNER-RACE CONTROL'. IF BLANK PROGRAM ASSUMES THAT 'OUTER-RACE CONTROL' WOULD EXIST.

NOTES TO RUN ADDITIONAL LOAD CASES WITH THE SAME SYSTEM REPEAT CARD NO. 7 FOR EACH NEW LOAD CASE

TO RUN NEW LUBRICANT PROPERTIES WITH SAME BEARING PLACE ONE BLANK AFTER LAST CARD NO. 7 AND READ IN NEW CARD NO. 4 ET SEQ.

TO READ NEW BEARING SYSTEM PLACE TWO BLANKS AFTER LAST CARD NO. 7 AND READ IN CARD NO. 1 ET SEQ.

APPENDIX III TYPICAL BALL BEARING PROBLEM FOR COMPUTER PROGRAM

BEARING DESIGN DATA

N2 OF ELEMENTS	ELEMENT NUMBER	PITCH DIAMETER	CONTACT ANGLE	RACE CURVATURES OUTER	INNER	CLEARANCE INCREMENT	TYPE OF PILOT	PILOT CLEARANCE	POCKET CLEARANCE	CAGE WIDTH
2422224	01	5.1132E-01	5.1740E-00	3.000E-01	5.1500E-01	5.2000E-01	OUTER	2.9000E-02	3.1000E-02	7.1600E-01
122424E	02	5.1132E-02	5.1740E-00	3.000E-01	5.1500E-01	5.2000E-01	OUTER	2.9000E-02	3.1000E-02	7.1600E-01
32042E	03	5.1132E-02	5.1740E-00	3.000E-01	5.1500E-01	5.2000E-01	OUTER	2.9000E-02	3.1000E-02	7.1600E-01

LUBRICANT PROPERTIES

PRESSURE-VISCOSITY COEFFICIENT = 1.1800E-04
 TEMPERATURE-VISCOSITY COEFFICIENT = 1.5400E-02
 VISCOSITY AT INLET TEMPERATURE = 3.8010E-04
 INLET TEMPERATURE = 1.0000E-02
 THERMAL CONDUCTIVITY = 7.7401E-02
 DENSITY = 3.9700E-05

BALL POCKET FRICTION COEFFICIENT = 1.0000E-02
 CASE PILOT SURFACE FRICTION COEFFICIENT = 1.1000E-02

ELEMENT NO.	SPINNING VELOCITY		MINIMUM FILM THICKNESS	
	OUTER	INNER	OUTER	INNER
1	-5.574E-03	-3.722E-04	8.941E-05	8.518E-05
2	-5.590E-03	-3.737E-04	8.934E-05	8.506E-05
3	-5.625E-03	-3.834E-04	8.915E-05	8.472E-05
4	-5.650E-03	-3.893E-04	8.883E-05	8.412E-05
5	-5.698E-03	-3.981E-04	8.833E-05	8.335E-05
6	-3.795E-03	-3.045E-04	8.762E-05	8.232E-05
7	-3.108E-03	-2.797E-04	8.685E-05	8.117E-05
8	-2.655E-03	-2.549E-04	8.601E-05	7.992E-05
9	-1.929E-03	-2.361E-04	8.513E-05	7.877E-05
10	-1.574E-03	-2.212E-04	8.440E-05	7.788E-05
11	-1.314E-03	-2.127E-04	8.393E-05	7.730E-05
12	-1.194E-03	-2.060E-04	8.375E-05	7.712E-05
13	-1.138E-03	-2.125E-04	8.397E-05	7.737E-05
14	-1.538E-03	-2.275E-04	8.467E-05	7.790E-05
15	-1.333E-03	-2.341E-04	8.521E-05	7.899E-05
16	-2.575E-03	-2.584E-04	8.610E-05	8.006E-05
17	-3.165E-03	-2.825E-04	8.695E-05	8.130E-05
18	-3.479E-03	-3.072E-04	8.777E-05	8.245E-05
19	-4.585E-03	-3.306E-04	8.850E-05	8.343E-05
20	-4.998E-03	-3.502E-04	8.867E-05	8.420E-05
21	-5.330E-03	-3.652E-04	8.918E-05	8.477E-05
22	-5.517E-03	-3.744E-04	8.935E-05	8.508E-05

BALL/POCKET CONTACT DATA

ELEMENT NO.	PRESSURE		SLIDING VELOCITY		MIN. FILM THICKNESS
	ORICE	LENGTH	RADIAL	AXIAL	
1	8.383E-01	1.492E-02	2.533E-03	-1.970E-03	3.116E-03
2	8.512E-01	1.464E-02	2.552E-03	-1.968E-03	2.972E-03
3	9.053E-01	1.495E-02	2.590E-03	-1.965E-03	2.860E-03
4	9.484E-01	1.721E-02	2.539E-03	-1.960E-03	2.613E-03
5	9.520E-01	1.695E-02	2.598E-03	-1.952E-03	2.619E-03
6	7.329E-01	1.579E-02	2.422E-03	-1.942E-03	3.965E-03
7	3.964E-01	1.285E-02	1.570E-03	-1.932E-03	1.354E-02
8	-9.473E-02	7.994E-03	1.224E-03	-1.927E-03	1.550E-02
9	-6.868E-01	1.575E-02	2.379E-03	-1.913E-03	4.352E-03
10	-1.211E-02	1.902E-02	2.917E-03	-1.907E-03	1.750E-03
11	-1.702E-00	2.092E-02	3.208E-03	-1.903E-03	7.052E-04
12	-1.940E-00	2.147E-02	3.292E-03	-1.903E-03	6.337E-04
13	-1.556E-00	2.077E-02	3.194E-03	-1.903E-03	7.260E-04
14	-1.227E-00	1.875E-02	2.876E-03	-1.907E-03	1.364E-03
15	-6.268E-01	1.499E-02	2.587E-03	-1.914E-03	5.270E-03
16	-3.850E-02	5.916E-03	9.071E-04	-1.923E-03	5.545E-02
17	4.384E-01	1.310E-02	2.040E-03	-1.933E-03	1.397E-02
18	7.590E-01	1.597E-02	2.650E-03	-1.943E-03	3.707E-03
19	9.119E-01	1.702E-02	2.610E-03	-1.953E-03	2.559E-03
20	9.473E-01	1.720E-02	2.686E-03	-1.960E-03	2.417E-03
21	9.079E-01	1.692E-02	2.594E-03	-1.961E-03	2.682E-03
22	8.555E-01	1.653E-02	2.550E-03	-1.969E-03	2.990E-03

WICUS DRAG IN BALL = 3.1950E 00

CASE/PILOTING 5/REACE DATA

WICUS	COULOMBS	NORMAL
TORQUE	TORQUE	LOAD
-2.449E-00	-3.915E-01	1.619E-01

14C9001 EXECUTION TERMINATING DUE TO ERROR COUNT FOR ERROR NUMBER 217

APPENDIX IV ROLLER BEARING COMPUTER PROGRAM FORTRAN SOURCE DECK

```

COMMON ALPHA,AL3, BETA, C(2),CAGED1(2),CAGEW,CAGET,CLCAGE(200009700
X1,CCRNFR,CP,CZ,CPI,CZ1, O,OROP,DENS,DENLUB,DEL1,DEL(2), 00008300
XDFDEL(2),DFYWX(2),DFPDH(2),DFZDH(2),DFPMX(2),DFZWX(2), 00008900
XF,FL,FO, FLAT,FLAT02,FK,FBARV,FD,FC,FY(2),FP(2),FZ(2),FY11, 00009000
XFY12,FP11,FP12,FZ11,FZ12,FILM,FFY(3), GAG,CAGE,G1T,G2T, 00009100
XHF,HMH,HP(2),HMN1,HMN2,HMN(2),HMRAC(2), 1SYS,ILOAD,ILUB,1SIGN, 00009200
XQUIT, JPASS, KPLT,KPASS, NUM,NUMY, OMEDCR, 00009300
XOMEGAE,CNF1,CMEGAX,CMX1,OMEX, PD,POCKET,PILOT,POCCLR, 00009400
XPX(2),PPI(9), RADIUS,PINGDI(2),RINGYM,ROLLYM, 00009500
XPRNGPR,ROLLPR,RMH,PPM(2),ROT,RFV,R(9), STR,STS(9) 00009600
COMMON TOTL,TOL(4),TOTL02,T1,THETA,TORQ,TORK, VHMN,VIS,VEINC,00009700
XVIS3,VY(2),VIC(3),VSS,V(2), XMU1,XMASS,XTM,XTREX,XN, 00009800
XYE,YNUM,YINC(2,50) 00009900
COMMON CPH,CAGECF, DXF7,DELTA,DRAG, FY1(2,50),FP1(2,50)00010000
X1,FZ1(2,50),FLIM(2,50), HOR,H1(2,50), ITER, NOLOAD, 00010100
XMEGX(50), P(2,50),PPP(9,2,50),PN,PXOUT, RR(9,2,50), 00010200
XSTS(9,2,50),SPH, VERT,VY1(2,50), XFZ,XTM(2,50) 00010300
COMMON /CHEC,IV 00010400
DIMENSION WORD(2) 00010500
DATA WORD(1),WORD(2)/4H OUT,4H IN / 00010600
1SYS=0 00010700
C(1)=1. 00010800
C(2)=-1. 00010900
GO TO 5
6 WRITE(6,650)
5 READ(5,10)XN,D,E,TOTL,FLAT,CORNER,RADIUS,DROP 00011000
IF(XN.EQ.0.)STOP 00011100
10 FORMAT(9E10.3) 00011200
NUM=XN 00011300
ILOAD=0 00011400
ILUB=0 00011500
1SYS=1SYS+1 00011600
GAG=D/E 00011700
READ(5,10)GAGE,PD,RINGDI(1),RINGDI(2),CAGED1(1),CAGED1(2),POCKET, 00011800
1CAGEW,RINGYM,ROLLYM,RINGPR,ROLLPR, XMU1,CAGEW,DENS,YNUM,(TOL( 00011900
2),K=1,4) 00012000
IF(DENS.EQ.0.)DENS=.283 00012100
IF(TOL(1).EQ.0.)TOL(1)=.000001 00012200
IF(TOL(2).EQ.0.)TOL(2)=.0000005 00012300
IF(TOL(3).EQ.0.)TOL(3)=1. 00012400
IF(TOL(4).EQ.0.)TOL(4)=.1 00012500
TOL(3)=TOL(3)*.1047198 00012600
TOL(4)=TOL(4)*.1047198 00012700
IF(XMU1.EQ.0.)XMU1=.1 00012800
IF(YNUM.EQ.0.)YNUM=5. 00012900
NUMY=YNUM 00013000
CALL RCALC(TOTL,FLAT,GAGE,RADIUS,DROP) 00013100
XN = NO. OF ROLLS 00013200
D = ROLL DIA. - IN 00013300
E = PITCH DIA. - IN 00013400
TOTL = TOTAL LENGTH OF ROLL - IN 00013500
FLAT = LENGTH OF FLAT PORTION OF ROLL - IN 00013600
CORNER = CORNER RADIUS OF ROLL - IN 00013700
RADIUS = CROWN RADIUS - IN 00013800
DROP = DROP OF ROLL CROWN - IN 00013900
GAGE = DISTANCE FROM END OF ROLL TO CROWN DROP REFERENCE POINT 00014000
- IN 00014100
PD = DIAMETRAL CLEARANCE - IN (+ IF BEARING IS LOOSE) 00014200
RINGDI(1) = I.D. OF OUTER RING - IN 00014300
RINGDI(2) = O.D. OF INNER RING - IN 00014400
CAGED1(1) = O.D. OF CAGE - IN 00014500
CAGED1(2) = I.D. OF CAGE - IN 00014600
POCKET = POCKET LENGTH IN ROLLING DIRECTION - IN 00014700

```



```

C CAGEW = WIDTH OF CAGE - IN 00014800
C RINGYM = YOUNG'S MODULUS FOR RINGS - PSI 00014900
C ROLLYM = YOUNG'S MODULUS FOR ROLLS - PSI 00015000
C RINGPR = POISSON'S RATIO FOR RINGS 00015100
C ROLLPR = POISSON'S RATIO FOR ROLLS 00015200
C CAGEWT = WEIGHT OF CAGE - LB 00015300
C YMU1 = COEFFICIENT OF COULOMB FRICTION FOR PILOT SURFACES 00015400
FLAT2=.5*FLAT 00015500
TOTL2=.5*TOTL-CORNER 00015600
RHH=SQRT(RADIUS**2-FLAT2**2) 00015700
READ(5,20) 00015800
FORMAT(1H1,79H 00015900
20 1 /IX,79H 00016000
2 00016100
WRITE(6,20) 00016200
WRITE(6,30)1SYS 00016300
37 FORMAT(30H0 DESIGN DATA FOR BEARING NO.,13) 00016400
WRITE(6,40) 00016500
40 FORMAT(130H0 NO. OF ROLL PITCH TOTAL FL00016600
1AT CROWN CROWN GAGE DIAMETRAL I.D. OF 00016700
2 I.D. OF/129H ROLLERS DIAMETER DIAMETER LENGTH 00016800
3 LENGTH DROP RADIUS POINT CLEARANCE OUTER R00016900
4NG INNER RING) 00017000
WRITE(6,50)XN,D,F,TOTL,FLAT,DROP,RADIUS,GAGE,PD,RINGDI(1),RINGDI(200017100
11 00017200

50 FORMAT(1P1E12,4) 00017300
WRITE(6,50) 00017400
62 FORMAT(128H0 O.D. OF I.D. OF TYPE OF CAGE/RING CLEARA00017500
INCE POCKET CAGE YOUNG'S MODULUS POISSON00017600
25 RAT:0/129H CAGE CAGE PILOT OUTER IN00017700
3MER CLEARANCE WIDTH PINGS ROLLS RINGS 00017800
4 ROLL S 00017900
PILOT=1. 00018000
IF(ABS(RINGDI(2)-CAGEDI(2)).LT. ABS(RINGDI(1)-CAGEVI(1)))PILOT=2. 00018100
KPLT=PILOT 00018200
CLCAGE(1)=ABS(RINGDI(1)-CAGEDI(1)) 00018300
CLCAGE(2)=ABS(RINGDI(2)-CAGEDI(2)) 00018400
WRD=WORD(KPLT) 00018500
POCCLP=POCKET-D 00018600
IF(RINGYM.EQ.O.)PINGYM=29.E6 00018700
IF(ROLLYM.EQ.O.)ROLLYM=29.E6 00018800
IF(RINGPR.EQ.O.)RINGPR=.25 00018900
IF(ROLLPR.EQ.O.)ROLLPR=.25 00019000
FI=.6366198*(1.-RINGPR**2)/RINGYM*(1.-ROLLPR**2)/ROLLYM 00019100
WRITE(6,70)CAGEDI(1),CAGEDI(2),WRD,CLCAGE(1),CLCAGE(2),POCCLP,CAGE00019200
70 1W,RINGYM,ROLLYM,RINGPR,ROLLPR 00019300
FORMAT(1P2E12,4,3X,46,3X,1P8F12,4) 00019400
WRITE(6,75) 00019500
75 FORMAT(45H0 FRICTION MATERIAL CORNER CAGE/46H COF00019600
1E DENSITY RADIUS HEIGHT) 00019700
WRITE(6,30) XMU1,DENS,CORNER,CAGEWT 00019800
XMASS=D**2*TOTL*DENS/491.9797 00019900
80 READ(5,10)ALPHA,BETA,VIS,TI,EK,DEMLUB 00020000
IF(1ALPHA,LE,Q,J)GO TO 6 00020100
ILUB=ILUB+1 00020200
C ALPHA = PRESSURE-VISCOSITY COEFFICIENT - IN**2/LB 00020300
C BETA = TEMPERATURE-VISCOSITY COEFFICIENT - 1/(DEG F) 00020400
C VIS = VISCOSITY AT INLET TEMPERATURE - LB*SEC/IN**2 00020500
C TI = INLET TEMPERATURE - DEG F 00020600
C EK = THERMAL CONDUCTIVITY - BTU/(DEG F)/HR/FT 00020700
C DEMLUB = LUBRICANT DENSITY - LB SEC**2/IN**4 00020800
READ(5,30) 00020900
90 FORMAT(1H0,79H 00021000
1 00021100

```

WRITE(6,81)	00021200
81 FORMAT(1H /1H /1H /1H /1H /23HQ LUBRICANT PROPERTIES)	00021300
WRITE(6,90)	00021400
WRITE(6,82)ALPHA	00021500
82 FORMAT(40H PRESSURE-VISCOSITY COEFFICIENT ,1P1E11.4)	00021600
WRITE(6,83)BETA	00021700
83 FORMAT(40H TEMPERATURE-VISCOSITY COEFFICIENT ,1P1E11.4)	00021800
WRITE(6,84)VIS	00021900
84 FORMAT(40H VISCOSITY AT INLET TEMPERATURE ,1P1E11.4)	00022000
WRITE(6,85)TI	00022100
85 FORMAT(40H INLET TEMPERATURE ,1P1E11.4)	00022200
WRITE(6,86)FK	00022300
86 FORMAT(40H THERMAL CONDUCTIVITY ,1P1E11.4)	00022400
WRITE(6,87)DENLUB	00022500
87 FORMAT(40H LUBRICANT DENSITY ,1P1E11.4)	00022600
115 READ(5,10)RPM(1),RPM(2),FBARV,ROT,OMEDCR,VEINC,MF	00022700
IF(RPM(1).EQ.0.)AND.(RPM(2).EQ.0.))GO TO 80	00022800
ILOAD=ILOAD+1	00022900
WRITE(6,120)ILOAD,ISYS	00023000
120 FORMAT(26H1 INPUT DATA FOR LOAD NO.,13,13H, BEARING NO.,13/34H0	00023100
1RPM, OF RPM, OF RADIAL/33H OUTER INNER L00023200	
2401	00023300
IF(VEINC.EQ.0.)VEINC=.0025	00023400
C IF(MF.EQ.0.)MF=.00001	00023500
C	00023600
WRITE(6,90)RPM(1),RPM(2),FBARV	00023700
WRITE(6,7551)	00023800
7551 FORMAT(1X)	00023900
WRITE(6,7550)OMEDCR	00024000
7550 FORMAT(1X,17HPERCENT CAGE SLIP,1P1E15.4)	00024100
RPM(1)=RPM(1)*.1047198	00024200
RPM(2)=RPM(2)*.1047198	00024300
OMEGAE=.5*(RPM(1)*(1.+GAM)+RPM(2)*(1.-GAM))*1.-OMEDCR	00024400
IF(OMEDCR.EQ.0.)OMEDCR=.1+OMEGAE	00024500
OMEGE=OMEGAE	00024600
OMEGAE=OMEGAE-OMEDCR	
ISIGN=1	00024700
REV=0.	00024800
IF(ROT)121,123,121	00024900
121 REV=ROT*.1047198	00025000
WRITE(6,122)PCT	00025100
122 FORMAT(16H0 LOAD ROTATES AT,1P1E11.4,4H RPM)	00025200
GO TO 125	00025300
123 WRITE(6,124)	00025400
124 FORMAT(21H0 LOAD IS STATIONARY)	00025500
125 EP=2.7/((1.-RINGPR**2)/RINGYM+(1.-ROLLPR**2)/ROLLYM)	00025600
THETA=(TI-32.)/1.8	00025700
VIS3=VIS*EXP(BETA*(TI-86.))	00025800
AL3=ALPHA+930.*ALPHA*(TI-86.)/(156.*(TI+460.))	00025900
G1T=VIS3*ALPHA/AL3+.6*VIS/VIS3**.7	00026000
G2T=VIS3*BETA/(1.728*FK)	00026100
RMN=.58*ALPHA**+.6*VIS**+.7*EP**+.03	00026200
IF(VD.GT.0.)DELZ=DELZ+.5*PD	00026300
TI=0	00026400
TORQ=0.	00026500
TORK=-9.0	
CME1=OMEGAE	00026600
126 FN=0.	00026700
IQUIT=0	00026800
TORQ-TORK	00026900
TORK=0.	00027000
DO 130 K=1,2	00027100
VY(K)=.5*(E+C(K)*D)*(RPM(K)-OMEGAE)	00027200

130	FD=FD+.25*CLCAGE(K)*TOTL*DENLUB*(.25*(RINGDI(K)+CAGEDI(K))*OMEGAE	00027300
	1**2*OMEGAE/ABS(OMEGAE)	00027400
	FC=XHASS+.5*F*OMEGAE**2	00027500
	IV=0	00027600
	CALL NOCON	00027700
	IF(IV:132,132,131	00027800
131	WR:YF(6,8601)	00027900
8001	FORMAT(IX,10H**HP EXCEEDED 1.0E2 IN NOCON**)	00028000
	GO TO 115	00028100
132	DEL2=.005*0	00028200
	IF(TOUT)140,140,115	00028300
140	DO 240 ITER=1-15	00028400
	XF2=0.	00028500
	XF2=0.	00028600
	NOLoad=0	00028700
	DO 230 J=1,NJM	00028800
	JPASS=J	00028900
	XJ=J	00029000
	PHI=6.283185*(XJ-1.)/XM	00029100
	CPH=COS(PHI)	00029200
	DELTA=DEL2*CPH+.5*PD	00029300
	DEL(1)=.55*DELTA	00029400
	DEL(2)=DELYA-DEL(1)	00029500
	DO 200 IT=1,15	00029600
	IF(DEL(2)-1.E-8)141,141,142	00029700
141	NOLoad=NOLoad+1	00029800
	P(2,J)=0.	00029900
	GO TO 230	00030000
142	DO 190 K=1,2	00030100
	KPASS=K	00030200
145	CALL RCLL	00030300
	IF(IQU)1170,170,150	00030400
150	WRITE(6,160)J,IT,ITER,K	00030500
160	FORMAT(9HMAIN 145,414)	00030600
	GO TO 115	00030700
170	IF(PX(K))171,171,172	00030800
171	P(2,J)=0.	00030900
	NOLoad=NOLoad+1	00031000
	GO TO 230	00031100
172	DO 180 I=1,NJMY	00031200
	PR(L,K,J)=R(L)	00031300
	PPP(L,K,J)=PPJ(L)	00031400
180	STYS(L,K,J)=STS(L)	00031500
	XTRM(K,J)=XTRFM	00031600
	P(K,J)=PX(K)	00031700
190	CONTINUE	00031800
	PS11=-P(1,J)+P(2,J)+FC	00031900
	X1=-DFDEL(1)-DFDEL(2)	00032000
	X1=PS11/X1	00032100
	DEL(1)=DEL(1)-X1	00032200
	DEL(2)=DELTA-DEL(1)	00032300
	IF(ABS(X1)-TOL(1))220,200,200	00032400
200	CONTINUE	00032500
	WRITE(6,210)J	00032600
210	FORMAT(9HMAIN 200,14)	00032700
	GO TO 115	00032800
220	DET=-DFDEL(1)-DFDEL(2)	00032900
	DP2DEL=-DFDEL(1)/DET	00033000
	XF2=XF2+P(2,J)*CPH	00033100
	DXF2=DXF2+CP2DEL*DFDEL(2)*CPH**2	00033200
230	CONTINUE	00033300
	X1=DXF2-FEARY1/DXF2	00033400
	DEL2=DEL2-X1	00033500
	IF(ABS(X1)-5.*TOL(1))255,240,240	00033600

240	CONTINUE	00033700
	WRITE(6,250)X1	00033800
250	FORMAT(9HOMAIN 240,1P1E12.4)	00033900
C	GO TO 115	00034000
C	255 OMEGA=OMEGAF	
	TORR=0.	
	TORR=0.	00034200
	MOR=0.	00034300
	VERT=0.	00034400
	DO 310 J=1,NUM	00034500
	IF(P(2,J))1310,310,2551	00034600
2551	XJ=J	00034700
	PHI=6.283185*(XJ-1.)/XM	00034800
	SPH=SIN(PHI)	00034900
	CPH=COS(PHI)	00035000
	OMEGAX=(RPM(1)-OMEGAF)*(F+0)/D	00035100
	JPASS=J	00035200
	DO 265 I=1,30	00035300
	CP1=CP*ABS(OMEGAX)	00035400
	CZ1=CZ*OMEGAX	00035500
	DO 261 K=1,2	00035600
	WMRAC(K)=0.0	00035700
	KPASS=K	00035800
	DO 260 L=1,NUMY	00035900
	RL(L)=RR(L,K,J)	00036000
	RPI(L)=RPP(L,K,J)	00036100
260	STS(L)=SSTS(L,K,J)	00036200
	CALL TPAC	00036300
261	CONTINUE	00036400
	TEMP=FY(1)+FY(2)-FD	00036500
	TH=1	00036600
	IF(TEMP.(1.0.0))TH=2	
	HP(1)=HF	00036700
	HP(2)=HF	
	DO 262 ITH=1,30	00036800
	CALL POCFLM(ITH)	00036900
	PS11=FP(11)-APS(TEMP)	
	OPS11H=DFPDH(11)	00037100
	TEMP1=PS11/OPS11H	00037200
	HP(11)=HP(11)-TEMP1	00037300
	IF(HP(1).GT.1.0E2)GO TO 9000	00037400
	IF(HP(2).GT.1.0E2)GO TO 4000	00037500
	GO TO 2650	00037600
9000	WRITE(6,7500)	00037700
7500	FORMAT(1X,21H**HP EXCEEDED 1.0E2**)	00037800
	GO TO 115	00037900
2650	ABS(T.3P1).LE.TOL(2)GO TO 264	00038000
262	CONTINUE	00038100
	WRITE(6,263)J	00038200
263	FORMAT(1X,9HOMAIN 262,13)	00038300
C	GO TO 115	00038400
264	PS12=(FY(1)-FY(2)-FZ(11))*5*D	00038500
	DH0WX=-DFPWX(11)/DFPDH(11)	00038600
	OPS12W=(DFYWX(1)-DFYWX(2)-DFZWX(11)-DFZOH(11)*DH0WX)*5*D	00038700
	TEMP=PS12/OPS12W	00038800
	OMEGAX=OMEGAX-TEMP	00038900
	IF(ABS(TEMP).LE.TOL(3))GO TO 300	00039000
265	CONTINUE	00039100
	WRITE(6,266)J	00039200
266	FORMAT(1X,9HOMAIN 265,13)	00039300
C	GO TO 115	00039400
300	IF(1H.EQ.1)HP(2)=POCCLR-HP(1)	00039500
	IF(1H.EQ.2)HP(1)=POCCLR-HP(2)	00039600
	DO 305 K=1,2	00039700
	FY1(K,J)=FY(K)	00039800

```

      FP1(K,J)=FP(K)
      FZ1(K,J)=FZ(K)
      VY1(K,J)=V(K)
      FL1(K,J)=HMRAC(K)
      H1(K,J)=H1(K)
305  CONTINUE
      OMEGX1(J)=OMEGAX
      X1=-C(IH)*(FP(IH)*CPH+FZ(IH)*SPH)
      X2=C(IH)*(FP(IH)*SPH-FZ(IH)*CPH)
      HMR=HMR+X1
      VERT=VERT+X2
      TORK=TORK+C(IH)*(FP(IH)*E+FZ(IH)*POCKET)*.5
310  CONTINUE
      VEL=(RPM(KPLT)-OMEGAE)*RINGDI(KPLT)*.5
      XMUP=XMUP+VEL/ABS(VEL)
      Y1=-XMUP*VERT+HMR
      X2=XMUP*HMR+VERT
      ANG=ATAN2(X1,X2)
      CAGECF=CAGEW+BEV**2*CLCAGE(KPLT)/772.8
      PN=HMR/(XMUP*COS(ANG)+SIN(ANG))-CAGECF
      DRAG=D.
      DO 320 K=1,2
      AREA=3.141593*RINGDI(K)*(CAGEW-TOTL)
      VEL=(RPM(K)-OMEGAE)*CAGED1(K)*.5
320  DRAG=DRAG+.008*SQR(SQR(VIS+ABS(VEL)**7*DENLUB**3/1.5*CLCAGE(K)))
      TORK=TORK+(XMUP*(PN+CAGECF)+DRAG)*CAGED1(KPLT)*.5
7900  FORMAT(1X,9HMAIN BODY,14,1P5E10.5)
      TOL(5)=.001
      IF(ABS(TORK)-TOL(5))390,390,330
C 330  IF(TORK)331,331,333
C 331  OMEGAE=OMEGAE-OMEDCR
      GO TO 126
C 335  OMEDCR=OMEDCR/5.0
      TORK=TORK
      OMEGAE=OMEGAE-OMEDCR
C  WRITE(6,7500)111,OMEGAE,OMEL,OMEDCR,TORK,TORD
C  GO TO 126
390  WRITE(6,2000)
2000  FORMAT(1H1)
      WRITE(6,400)11,OAD,1SYS
400  FORMAT(27H OUTPUT DATA FOR LOAD NO.,13,12H BEARING NO.,13)
      WRITE(6,410)
410  FORMAT(60H BEARING RPM OF PERCENT TORQUE CAGE
      11LOT)
      WRITE(6,420)
420  FORMAT(60H REACTION CAGE CAGE SLIP ON CAGE
      11OAD)
      OMEGAE=OMEGAE/.1047198
      TEMP=(RPM(1)*(1.+GAM)+RPM(2)*(1.-GAM))/2094396
      TEMP=(TEMP-OMEGAE)/TEMP*100.
      WRITE(6,430)XFZ,OMEGAE,TEMP,TORK,PN
430  FORMAT(1P2E12.4,OP1F9.2,3X,1P2E12.4)
      WRITE(6,440)
440  FORMAT(32H OUTPUT DATA FOR RACE CONTACTS)
      WRITE(6,450)
450  FORMAT(115H ELEMENT ELEMENT CONTACT LOAD MEAN
      1COMPRESSIVE STRESS PATTERN EXTREMITY SLIP VELOCITY)

```

```

WRITE(6,460)
460 FORMAT(117H  NUMBER  AZIMUTH  OUTER  INNER  OUT00045900
1ER  INNER  OUTER  INNER  OUTER  INNER) 00046000
DO 490 J=1,NUM
IF(P(2,J))490,490,470
470 XJ=J
PHI=360.*(XJ-1.)/XN
SSTS(9,2,J)=.7853982*SSTS(NUMY,2,J)
SSTS(9,1,J)=.7853982*SSTS(NUMY,1,J)
WRITE(6,480)J,PHI,P(1,J),P(2,J),SSTS(9,1,J),SSTS(9,2,J),XTRM(1,J),
XTRM(2,J),VVI(1,J),VVI(2,J)
480 FORMAT(17,5X,1P9F12.4) 00046500
490 CONTINUE 00046600
IF(NLOAD)515,515,500
SSTS(9,2,J)=.7853982*SSTS(NUMY,2,J)
WRITE(6,510)PXMIT,STR,XTRM,VSC
510 FORMAT(12H  THE REST ,12X,1P1F12.4,12X,1P1F12.4,12X,1P1F12.4,12X, 00046700
1P1F12.4) 00046800
515 WRITE(6,520) 00046900
520 FORMAT(56H0  ELEMENT  MIN. FILM THICKNESS  TRACTIVE FORCE00047000
1) 00047100
WRITE(6,530) 00047200
530 FORMAT(57H  NUMBER  OUTER  INNER  OUTER  INNE00047300
1P) 00047400
DO 550 J=1,NUM
IF(P(2,J))550,550,540
540 WRITE(6,480)J,FLIM(1,J),FLIM(2,J),FYI(1,J),FYI(2,J) 00047500
550 CONTINUE 00047600
IF(NLOAD)565,565,550
565 WRITE(6,640)FILM,YF 00047700
565 WRITE(6,570) 00047800
570 FORMAT(34H0  OUTPUT DATA FOR POCKET CONTACTS) 00047900
WRITE(6,580) 00048000
580 FORMAT(94H0  ELEMENT  RPM OF  NORMAL POCKET LOAD  TANGEN00048100
1TAL POCKET LOAD  MIN. FILM THICKNESS) 00048200
WRITE(6,590) 00048300
590 FORMAT(92H  NUMBER  ROLLER  FORE  AFT  FOR00048400
1F  AFT  FORE  AFT) 00048500
DO 610 J=1,NUM
IF(P(2,J))610,610,600
600 CMGX(J)=CMGX(J)/.2047198
WRITE(6,480)J,CMGX(J),FPI(1,J),FPI(2,J),FZ1(1,J),FZ1(2,J),H1(1,J),H1(2,J)
1,H1(2,J)
610 CONTINUE 00048600
IF(NLOAD)115,115,620
CMX)=CMX)/.1047198
WRITE(6,630)CMX1,FP11,FP12,FZ11,FZ12,HMN1,HMN2
630 FORMAT(12H  THE REST ,1P8F12.4) 00048700
DO TO 115 00048800
640 FORMAT(12H  THE REST ,1P1F12.4,12X,1P1F12.4) 00048900
650 FORMAT(1H) 00050000
END 00050800

```

SUBROUTINE RCALC(TOYL, FLAT, GAGE, RADIUS, DROP)	00056300
DOUBLE PRECISION DRP, RDIUS, FLT, TTL, GAG, A1, A2, NSORT	00056400
RDIUS=RADIUS	00056500
DRP=DROP	
FLT=FLAT	00056800
TTL=TCTL	00056900
GAG=GAGE	00057000
IF(RADIUS) 10, 10, 20	00056600
10 A1=(1.500*TTL-GAG)**2	
A2=(1.500*FLT)**2	00057200
RDIUS=NSORT(((A1-A2-DRP**2)/(2.00*DRP))**2+A1)	00057300
RDIUS=RDIUS	00057400
RETURN	00057300
20 A1=NSORT(RDIUS**2-(1.500*FLT)**2)	00057600
A2=NSORT(RDIUS**2-(1.500*TTL-GAG)**2)	00057700
DRP=A1-A2	00057800
DRP=DRP	00057900
RETURN	00058000
END	00058100

	SUBROUTINE PCL1	00058200
	COMMON ALPHA, A1, 2, BETA, C(2), CAGEF(2), CAGEW, CAGEWT, CLCAGE(2)	00058300
	X), CRRNEP, C0, C7, C01, C71, 0, 0000, DENS, DENLUR, DEL7, DEL(2),	00058400
	XDEF(2), DEFVWX(2), DEFQW(2), DEFZWH(2), DEFVWX(2), DEFZWH(2),	00058500
	YC, EL, C0, F1, AT, FLAT02, FK, FBABV, FO, FC, FY(2), FP(2), FZ(2), FY1,	00058600
	XY12, F011, F012, F211, F212, FILM, FFY(3), GAM, GAGE, G1T, G2T,	00058700
	YHE, HWH, HD(2), HMN1, HMN2, HMN(2), HMRAC(2), [SYS, ILQAD, ILUR, ISGN,	00058800
	Y1OUT, IPASS, KPLT, KPASS, NIM, NUMY, QMEDCR,	00058900
	YMEGAC, CMF1, CMGAX, CMX1, CMEX, PD, POCKET, PILOT, POCLR,	00059000
	YRX(2), OPT(9), RADIUS, PINGDI(2), RINGYM, ROLLYM,	00059100
	X0, XGPD, PCLLP0, PMH, PEM(2), RNT, REV, R(9), STR, STS(9)	00059200
	COMMON T0TL, T0L(4), T0TL02, T1, THETA, T0RC, T0RK, V4MIN, VIS, VEINC,	00059300
	XVTS3, VY(2), VINC(2), VSS, V(2), XMU1, XMASS, XTM, XTREM, XN,	00059400
	YVF, YNIJM, YINC(2, 50)	00059500
	COMMON CPH, CAGECF, DXFZ, DELTA, DRAG, FY(2, 50), F01(2, 50)	00059600
	X), F71(2, 50), FLIM(2, 50), HQR, H1(2, 50), ITER, N0LOAD,	00059700
	XMEGAX(50), P(2, 50), PPD(9, 2, 50), PN, PXMIT, RR(9, 2, 50),	00059800
	XSSTS(9, 2, 50), SPH, VERT, VV1(2, 50), XF7, XTREM(2, 50)	00059900
	J=JPASS	00060000
	K=KPASS	00060100
	DX(K)=0,	00060200
	DEFEL(K)=0,	00060300
	XTREM=SQRT(2.*RADIUS*DEFEL(K)+FLAT02**2)	00060400
	IF(XTREM-T0TL02)15,15,10	00060500
11	XTREM=T0TL02	00060600
15	EFL= XTREM-FLAT02	00060700
	YINC=EFL/(YNIJM-1.)	00060800
	CF=XTREM	
	YINC(K, J)=YINC	00060900
	YH=XTREM+YINC	00061000
	SMINC=1,	00061100
	DO 30 I=1, NIJM	00061200
	OPT(I)=0,	00061300
	STS(I)=0,	00061400
	XH=XH-YINC	00061500
	SM=0.-SMINC	00061600
	SMINC=-SMINC	00061700
	IF(I-1)30,20,20	00061800
20	SM=1,	00061900
	GO TO 40	00062000
30	IF(I-NIJM)40,20,40	00062100
40	DELX=DEFEL(K)+.5*(FLAT02**2-XH**2)/RADIUS	00062200
	IF((DELX-1, F-0), (F, C.0) GO TO 30	
43	D(L)=.5*0-DEL(K)+DEFX	00062300
	GMA=2.*D(L)/E	00062400
	TEMP=C.F7*DELX**1.111111/EFL**1.111111	00062500
	DO 50 IIT=1,15	00062600
	IF(TEMP)30,30,45	00062700
45	A1=SQRT(EFL*TEMP*D*(1.+C(K)*GMA))	00062800
	A2=1, 8944+ALOG(EFL/(2.*A1))	00062900
	A3=A2*E1*TEMP	00063000
	A4=(A2-DEFX)/(EL*(A2-.5))	00063100
	TEMP=TEMP-A4	00063200
	IF(ABS(A2-DEFX)-T0L(1))70,70,50	00063300
50	CONTINUE	00063400
	DO 10 I=1, NIJM	00063500
40	FORMAT(9HCPCL 50)	00063600
	STOP	00063700
	END	00063800


```

TEMP=EV(1)-CF
T4=7
UP(2)=HC
DO 40 I=1,40
CALL DDFLH(TH)
DS(1)=F2(TH)-APS(TEMP)
DDSTH=DDFCH(TH)
TF(1)=DS(1)/DDSTH
UP(TH)=F2(TH)-TEMP
IF(ABS(TEMP),LE,C(12))GO TO 45
40 CONTINUE
45 DS(2)=(FV(1)-F2(TH))*500
DMQX=-DDMX(TH)/DDDH(TH)
DDSTW=(DFYWX(1)-DF2WX(TH)-DF2DH(TH)*DMQX)*500
TEMP=DS(2)/DDSTW
TEMP=.5*DS(2)/DDSTW
DMEGAX=DMEGAX-TEMP
IF(ABS(TEMP),LE,TOL(3))GO TO 55
50 CONTINUE
55 HP(1)=DDCLR-HP(2)
CY12=0
CO11=CO(1)
CO12=CO(2)
F711=F7(1)
F712=F7(2)
XTM=XTDFM
STG=STG(NUMY)
VSS=V(1)
FILM=VHMIN
VF=FY(1)
HMN1=HMN(1)
HMN2=HMN(2)
HMN1=DDCLR-FMA2
DMX1=DMEGAX
GETURN
END
SUBROUTINE DDFLH(TH)
COMMON ALPHA,AL3, RFTA, C(2),CAGEF(12),CAGEW,CAGEWT,CLCAGE(200)74700
Y1,COEF,CO,CO2,CO3,CO4, D,DF2D,DFNS,DFNLUB,DEL2,DEL(2), 00074800
XDFEL(2),DFYWX(2),DDFCH(2),DF2DH(2),DDMX(2),DF2WX(2), 00074900
VF,FI,FO, FLAT,FLAT2,FK,FRARV,FO,FC,FY(2),FO(2),FZ(2),FY(1), 00075000
XFV(2),CO11,CO12,F711,F712,FILM,VF(1), GAM,GAGE,GIT,G2T, 00075100
VFE,HFH,HP(2),HMN1,HMN2,HMN(2),HMPAC(2), ISYS,ILRAD,ILUB,ISIGN, 00075200
XTOUT, IPASS, KPLT,KPASS, NUM,NUMY, DMOCR, 00075300
YMEGAX,CVE1,DMEGAX,CVY,DMEX, D,POCKET,PILOT,DDCLR, 00075400
XV(2),DDT(2), RADUIS,PINGO(2),RINGYM,ROLLYM, 00075500
V2INC2,DEL(2),PMH,PPM(2),POT,REV,P(2), STG,STS(2), 00075600
COMMON TOL,TOL(4),TOLF2,T1,THET4,TORG,TORX, VHMIN,VIS,VINC,00075700
XV(2),VY(2),VINC(2),VSS,V(2), XMM1,XMASS,XTM,XTDFM,XV, 00075800
XVC,VMUM,VINC(2,50) 00075900
COMMON COH,CAGECE, DMEX,DELTA,DRAG, FY(2,50),FO(2,50)00076000
X1,F71(2,50),FILM(2,50), HCR,H(2,50), ITCR, NOLRAD, 00076100
XMEGAX(50), F(2,50),FPH(5,2,50),PH,OXO(1), PP(9,2,50), 00076200
XSTS(9,2,50),SPH, VERT,VY(2,50), VF7,XTFM(2,50) 00076300
FFI=TCT(2)-FLAT2

```

2) INC=FFI/(YNUM-1.)	00076500
TEM0)=2*INC/3.	00076600
DO 5 K=1,3	00076700
CO(K)=0.	00076800
CF(K)=0.	00076900
DEODH(K)=0.	00077000
DEODH(K)=0.0	
DE2WX(K)=0.0	
5) DE2DH(K)=0.	00077100
K=14	00077200
CONT=1.	00077300
YH=Y(71.72)*INC	00077400
DO 40 I=1,NUMV	00077500
SM=2.-SM*INC	00077600
IC(1-1)20,10,2)	00077700
10) SM=1.	00077800
DO 10 3)	00077900
20) IC(1-1)20,10,2)	00078000
30) SM*INC=SM*INC	00078100
YH=YH-2*INC	00078200
A)=DMH-SCRT(0.80)115**2-YH**2)	00078300
A)=.5*(XH**2-FLAT(2**2)/RADIUS	
HDX=H(K)+A)	00078400
IC(HDX = 1,0-4140,40,3)	
31) A2=,C(1-A)	00078500
C(1-A2)*A2**2	00078600
C(1-A2)*A2*SCRT(A2)	00078700
C(1-A2)*C(K)+SM*CC(1)/HDX	00078800
TEM0)=C(1)/HDX	00078900
F2(K)=F2(K)+SM*CC(1)/TEM0	00079000
DEODH(K)=DEODH(K)-SM*CC(1)/HDX**2	00079100
DE2DH(K)=DE2DH(K)-.5*SM*CC(1)/(HDX*TEM0)	00079200
40) CONT=1	
HDX(K)=HDX	00079300
CF(K)=2.*CF(K)+TEM0)+CC(1)*FLAT/HDX	00079400
C(K)=2.*CF(K)+TEM0)+CC(1)*FLAT/TEM0	00079500
DEODH(K)=2.*DEODH(K)+TEM0)-CC(1)*FLAT/HDX**2	00079600
DE2DH(K)=2.*DE2DH(K)+TEM0)-CC(1)*FLAT/(HDX*TEM0)*.5	00079700
DE2WX(K)=CF(K)/AP5(CMCH,K)	00079800
50) DE2WX(K)=CF(K)/CMGAX	00079900
RETURN	00080000
END	00080100
SUBROUTINE TRACE	00080200
COMMON ALPHA,FL2, RFTA, (2),CAGE0(2),CAGEW,CAGEWT,CLCAGE1	00080300
X1,COPNEP,CP,CZ,CPI,CZ1, D,200,DENS,DENLUP,DEL2,DEL12,	00080400
XDEP(2),DEYLY(2),DEODH(2),DE2DH(2),DE2WX(2),DE2WX(2),	00080500
YE,FL,CP, FLAT,FLAT02,EK,PHARV,ED,EC,FY(2),EP(2),EZ(2),EY11,	00080600
XEV12,EP11,EP22,F711,F712,F11H,FEY(3), GAM,GAGE,GIT,G2T,	00080700
XHG,HKG,HO(2),HMK,HMN2,HMN(2),HMPAC(2), ISYS,ILDAD,ILJAB,ISIGN,	00080800
V10HIT, JPASS, KBIT,KPASS, NUM,NUMV, GMFDR,	00080900
YOMEGAE,OMF1,CASEGAX,CMY1,OMEX, PD,POCKET,PILOT,POCCLR,	00081000
XDV(2),CPI(2), RADIUS,RING0(2),RINGYM,RLIYM,	00081100
X2INCPE,OC(1),DD,DMH,DEM(2),OCT,DEV,OC(9), STR,STS(9)	00081200
COMMON TOT1,TOT1(4),TOTLO2,T1,THEFA,TOR0,TORK, VMIN,VIS,VFINC,	00081300
XVTS3,VY(2),VINC(2),VCS,V12), XH01,XMASS,XTH,XTRM,XN,	00081400
XVE,VNIM,VINC(2,50)	00081500
COMMON CPH,CAGECF, XVE2,DELTA,ORAG, FY112,501,EP112,500001,600	
X1,FY112,501,FL1M12,501, FOR,HL12,501, IFR, NOLGAS,	00081700
YMERGX(5,1), P12,501,PPP(9,2,50),PN,PKOUT, PR(9,2,50),	00081800
XSTS10,7,501,COH, VERV,VV1(2,50), XE2,XTRM(2,50)	00081900
1-JPASS	00082000
K=KPASS	00082100
22=-1(K)0,5*(C+C(K)*D)	00082200

DEK=2.*VFINC*APS(CMEGAX)	00082300
DO 20 I=1,3	00082400
CMEY=CMEGAX*VINC(I)*APS(CMEGAX)	00082500
CMINC=1.	00082600
CEV(I)=0.	00082700
DO 70 L=1,NI*NY	00082800
CM=2.-SMINC	00082900
XP=1./I./P2+1./P(1,1)	00083000
IF(L-1)20,10,20	00083100
CM=1.	00083200
DO 70 30	00083300
IF(L-NI*NY)30,10,30	00083400
CMINC=-SMINC	00083500
IF(PPT(I)-L)370,70,40	
40 VPD1=CMEY*P(I)*C(K)	00083600
VS=VY(K)-VPD1	00083700
IF(VS)51,50,51	
50 IF(6,53)VY(K),VPC1,VS,CMEY,2(I),C(K)	
53 FORMAT(1X,4HTPAC,1PAF15.4)	
51 VPAR=(VY(K)+VPC1)*.5	00083800
VAP=ABS(VPAR)	00083900
VS=ABS(VS)	00084000
VHMIN=HHH*(VAP**7/PPT(I)**.13*XP**4.3	00084100
C1=G1*US/(VHMIN*STS(L))	00084200
G2=G2*VSC**2	00084300
C2=A1*STS(L)	00084400
CALL COEFCT(G1,G2,G3,CDE,THETA)	00084500
CALL COEFCT(G1,G2,G3,CDE,THETA)	00084600
CDE=5.*SCOT(C1)	
CDE=7.5*SCOT(C2)	00084600
FFY(I)=FFY(I)+SM*PPT(I)*CDE	00084700
CONTINUE	00084800
CEV(I)=2.*(FFY(I)+YINC(K,1)/3.+PPT(NI*NY)*FLAT02-CDE)*US/VS	00084900
CONTINUE	00085000
RY(K)=FFY(I)	00085100
DEYX(K)=(FFY(2)-FFY(3))/DEN	00085200
H2RAC(K)=VHMIN	00085300
V(K)=VS	00085400
RETURN	00085500
END	00085600

SUBROUTINE T11(A,B,C,D,N)	
DIMENSION C(1,2,1)	
IF(N-1)1,2,3	
1 0=0.	
DO 10 100	
2 0=C(1)	
DO 10 100	
3 M=1	
WHILE	
4 IF(M-M-1)15,15,0	
5 M=(M+M)/2	
IF(C(1)-C(2))1,2,10	
10 IF(C(M)-0)12,12,14	
11 IF(4-C(M))3,12,14	
12 0=C(M)	
DO 10 100	
13 0=0	
DO 10 100	
14 M=0	
DO 10 100	
15 0=C(M)+C(M)-C(M)*((A-C(M))/(C(M)-C(M)))	
DO 10 100	
END	

SUBROUTINE COEFFICIENTS, G2, G3, ECODE, TIME, A1									
DIMENSION AG1(13), AG2(7), AG3(7), FTN(13, 7, 7), U7(7, 7), VZ(7), VTN(637) FRCT									2
DIMENSION A1(13), A2(13), A3(13), A4(13), A5(13), A6(13), A7(13), A8(13), FRCT									3
A9(13), A10(13), A11(13), A12(13), A13(13), A14(13), A15(13), A16(13), FRCT									4
A17(13), A18(13), A19(13), A20(13), A21(13), A22(13), A23(13), A24(13), FRCT									5
A25(13), A26(13), A27(13), A28(13), A29(13), A30(13), A31(13), A32(13), FRCT									6
A33(13), A34(13), A35(13), A36(13), A37(13), A38(13), A39(13), A40(13), FRCT									7
A41(13), A42(13), A43(13), A44(13), A45(13), A46(13), A47(13), A48(13), FRCT									8
A49(13), FRCT									9
EQUIVALENCE(VTN(1), FTN(1, 1, 1))									
EQUIVALENCE(VTN(1), A1(1)), (VTN(14), A2(1)), (VTN(27), A3(1)),									
1(VTN(40), A4(1)), (VTN(53), A5(1)), (VTN(66), A6(1)), (VTN(79), A7(1)), FRCT									11
2(VTN(92), A8(1)), (VTN(105), A9(1)), (VTN(118), A10(1)), (VTN(131), A11(1) FRCT									
3), (VTN(144), A12(1)), (VTN(157), A13(1)), (VTN(170), A14(1)), (VTN(183) FRCT									
4, A15(1)), (VTN(196), A16(1)), (VTN(209), A17(1)), (VTN(222), A18(1)), FRCT									
5(VTN(235), A19(1)), (VTN(248), A20(1)), (VTN(261), A21(1)), (VTN(274), FRCT									
A22(1)), (VTN(287), A23(1)), (VTN(300), A24(1)), (VTN(313), A25(1)), FRCT									
7(VTN(326), A26(1)), (VTN(339), A27(1)), (VTN(352), A28(1)), (VTN(365), FRCT									
A29(1)), (VTN(378), A30(1)), (VTN(391), A31(1)), (VTN(404), A32(1)), FRCT									
9(VTN(417), A33(1)), (VTN(430), A34(1)), (VTN(443), A35(1)), (VTN(456), FRCT									
A36(1)), (VTN(469), A37(1)), (VTN(482), A38(1)), (VTN(495), A39(1)), FRCT									
2(VTN(508), A40(1)), (VTN(521), A41(1)), (VTN(534), A42(1)), (VTN(547), FRCT									
A43(1)), (VTN(560), A44(1)), (VTN(573), A45(1)), (VTN(586), A46(1)), (VTN(600) FRCT									
4(529), A47(1)), (VTN(612), A48(1)), (VTN(625), A49(1)) FRCT									
DATA A1 / 2.0025, 0.0207, 0.0014, 0.0023, 0.0067, FRCT									25
1 0.0135, 0.021, 0.027, 0.046, 0.057, 0.0615, 0.0685, 0.0775, FRCT									26
DATA A2 / 2.0207, 0.002, 0.0039, 0.0065, 0.0150, FRCT									27
1 0.022, 0.027, 0.042, 0.0495, 0.054, 0.0625, 0.069, 0.0775, FRCT									28
DATA A3 / 0.0226, 0.0079, 0.014, 0.018, 0.028, FRCT									29
1 0.034, 0.0395, 0.0485, 0.054, 0.058, 0.064, 0.0695, 0.0775, FRCT									30
DATA A4 / 2.0277, 0.017, 0.023, 0.027, 0.035, FRCT									31
1 0.04, 0.044, 0.051, 0.0565, 0.0605, 0.066, 0.071, 0.0775, FRCT									32
DATA A5 / 0.019, 0.0285, 0.034, 0.037, 0.044, 0.048, FRCT									33
1 0.05, 0.056, 0.06, 0.0635, 0.069, 0.0725, 0.0775, FRCT									34
DATA A6 / 0.0215, 0.032, 0.037, 0.0415, 0.0475, FRCT									35
1 0.051, 0.054, 0.06, 0.0635, 0.066, 0.07, 0.073, 0.0775, FRCT									36
DATA A7 / 0.0245, 0.034, 0.04, 0.0425, 0.05, FRCT									37
1 0.054, 0.0565, 0.062, 0.0655, 0.0675, 0.071, 0.074, 0.0775, FRCT									38
DATA A8 / 0.0002, 0.0035, 0.012, 0.032, 0.006, 0.012, FRCT									39
1 0.015, 0.016, 0.017, 0.054, 0.0645, 0.072, 0.077, FRCT									40
DATA A9 / 0.0006, 0.0022, 0.004, 0.0065, 0.015, 0.024, FRCT									41
1 0.028, 0.043, 0.052, 0.0575, 0.0665, 0.072, 0.077, FRCT									42
DATA A10 / 0.0027, 0.0081, 0.014, 0.019, 0.0295, FRCT									43
1 0.035, 0.0395, 0.051, 0.057, 0.061, 0.069, 0.0725, 0.077, FRCT									44
DATA A11 / 0.0064, 0.015, 0.021, 0.025, 0.034, 0.04, FRCT									45
1 0.0445, 0.054, 0.06, 0.064, 0.069, 0.073, 0.077, FRCT									46
DATA A12 / 0.012, 0.0225, 0.029, 0.0345, 0.043, FRCT									47
1 0.049, 0.052, 0.059, 0.063, 0.065, 0.07, 0.073, 0.077, FRCT									48
DATA A13 / 0.010, 0.032, 0.039, 0.0415, 0.05, 0.054, FRCT									49
1 0.056, 0.061, 0.064, 0.067, 0.0715, 0.075, 0.077, FRCT									50
DATA A14 / 0.021, 0.0335, 0.041, 0.0455, 0.053, FRCT									51
1 0.056, 0.059, 0.064, 0.068, 0.07, 0.073, 0.076, 0.077, FRCT									52
DATA A15 / 0.0016, 0.0055, 0.011, 0.0019, 0.0059, 0.011, FRCT									53
1 0.018, 0.023, 0.042, 0.048, 0.06, 0.068, 0.075, FRCT									54
DATA A16 / 0.007, 0.021, 0.0043, 0.007, 0.015, 0.023, FRCT									55
1 0.027, 0.039, 0.046, 0.052, 0.062, 0.07, 0.075, FRCT									56
DATA A17 / 0.0018, 0.0053, 0.01, 0.015, 0.0255, FRCT									57
1 0.034, 0.037, 0.048, 0.054, 0.059, 0.064, 0.073, 0.075, FRCT									58
DATA A18 / 0.0044, 0.011, 0.018, 0.024, 0.037, FRCT									59

U 0.030, 0.044, 0.0525, 0.057, 0.061, 0.068, 0.074, 0.075/	FRCT	60
DATA A19 / 0.0782, 0.017, 0.025, 0.03, 0.042,	FRCT	61
1 0.048, 0.052, 0.06, 0.064, 0.066, 0.071, 0.074, 0.075/	FRCT	62
DATA A20 / 0.015, 0.024, 0.034, 0.04, 0.049,	FRCT	63
1 0.054, 0.058, 0.063, 0.067, 0.069, 0.073, 0.075, 0.075/	FRCT	64
DATA A21 / 0.016, 0.028, 0.036, 0.043, 0.052,	FRCT	65
1 0.057, 0.06, 0.065, 0.068, 0.07, 0.074, 0.075, 0.075/	FRCT	66
DATA A22 / 0.0015, 0.0016, 0.01, 0.0017, 0.005, 0.01,	FRCT	67
1 0.016, 0.014, 0.014, 0.046, 0.059, 0.067, 0.073/	FRCT	68
DATA A23 / 0.0064, 0.002, 0.0019, 0.0064, 0.015,	FRCT	69
1 0.071, 0.026, 0.039, 0.046, 0.052, 0.062, 0.068, 0.073/	FRCT	70
DATA A24 / 0.0017, 0.0048, 0.009, 0.014, 0.025,	FRCT	71
1 0.071, 0.076, 0.047, 0.053, 0.057, 0.065, 0.0685, 0.071/	FRCT	72
DATA A25 / 0.043, 0.01, 0.017, 0.023, 0.033,	FRCT	73
1 0.09, 0.042, 0.052, 0.058, 0.061, 0.066, 0.07, 0.073/	FRCT	74
DATA A26 / 0.0078, 0.016, 0.024, 0.029, 0.04,	FRCT	75
1 0.044, 0.051, 0.057, 0.062, 0.064, 0.068, 0.071, 0.073/	FRCT	76
DATA A27 / 0.0145, 0.024, 0.033, 0.039, 0.049,	FRCT	77
1 0.057, 0.058, 0.062, 0.066, 0.067, 0.07, 0.072, 0.073/	FRCT	78
DATA A28 / 0.016, 0.027, 0.0355, 0.041, 0.052,	FRCT	79
1 0.056, 0.059, 0.064, 0.067, 0.068, 0.071, 0.073, 0.073/	FRCT	80
DATA A29 / 0.0011, 0.0027, 0.0055, 0.0009, 0.0029,	FRCT	81
1 0.0059, 0.01, 0.025, 0.034, 0.042, 0.054, 0.062, 0.068/	FRCT	82
DATA A30 / 0.0044, 0.012, 0.0026, 0.0044, 0.012,	FRCT	83
1 0.019, 0.024, 0.036, 0.044, 0.049, 0.057, 0.063, 0.068/	FRCT	84
DATA A31 / 0.001, 0.0029, 0.0056, 0.019, 0.0185,	FRCT	85
1 0.0255, 0.02, 0.042, 0.0495, 0.053, 0.06, 0.064, 0.068/	FRCT	86
DATA A32 / 0.0015, 0.0045, 0.0045, 0.013, 0.024,	FRCT	87
1 0.032, 0.034, 0.047, 0.052, 0.057, 0.063, 0.065, 0.068/	FRCT	88
DATA A33 / 0.0038, 0.0093, 0.0155, 0.021, 0.032,	FRCT	89
1 0.038, 0.042, 0.052, 0.056, 0.06, 0.064, 0.066, 0.068/	FRCT	90
DATA A34 / 0.0098, 0.017, 0.0245, 0.03, 0.04,	FRCT	91
1 0.0445, 0.051, 0.058, 0.061, 0.067, 0.066, 0.067, 0.068/	FRCT	92
DATA A35 / 0.012, 0.022, 0.0295, 0.035, 0.0455,	FRCT	93
1 0.051, 0.055, 0.061, 0.063, 0.065, 0.067, 0.068, 0.069/	FRCT	94
DATA A36 / 0.0005, 0.0014, 0.0027, 0.0045, 0.0014,	FRCT	95
1 0.0027, 0.0046, 0.013, 0.022, 0.029, 0.042, 0.052, 0.055/	FRCT	96
DATA A37 / 0.0012, 0.0042, 0.0085, 0.014, 0.044,	FRCT	97
1 0.0044, 0.013, 0.0245, 0.032, 0.037, 0.0445, 0.053, 0.055/	FRCT	98
DATA A38 / 0.0014, 0.012, 0.0274, 0.004, 0.011,	FRCT	99
1 0.017, 0.022, 0.0245, 0.039, 0.0425, 0.049, 0.0535, 0.055/	FRCT	100
DATA A39 / 0.0015, 0.0042, 0.008, 0.012, 0.022,	FRCT	101
1 0.025, 0.032, 0.0395, 0.045, 0.059, 0.0535, 0.055/	FRCT	102
DATA A40 / 0.0034, 0.0084, 0.014, 0.0195, 0.03,	FRCT	103
1 0.024, 0.04, 0.044, 0.048, 0.049, 0.051, 0.054, 0.055/	FRCT	104
DATA A41 / 0.0056, 0.013, 0.02, 0.024, 0.0375,	FRCT	105
1 0.042, 0.045, 0.049, 0.05, 0.052, 0.0525, 0.054, 0.055/	FRCT	106
DATA A42 / 0.0071, 0.015, 0.023, 0.03, 0.04,	FRCT	107
1 0.045, 0.048, 0.051, 0.052, 0.053, 0.054, 0.055, 0.055/	FRCT	108
DATA A43 / 0.0003, 0.0009, 0.0011, 0.003, 0.009,	FRCT	109
1 0.0019, 0.002, 0.009, 0.016, 0.023, 0.037, 0.045, 0.051/	FRCT	110
DATA A44 / 0.0001, 0.0026, 0.0058, 0.0009, 0.029,	FRCT	111
1 0.0057, 0.0002, 0.021, 0.029, 0.034, 0.041, 0.047, 0.051/	FRCT	112
DATA A45 / 0.0025, 0.0074, 0.0015, 0.0024, 0.0072,	FRCT	113
1 0.012, 0.018, 0.028, 0.035, 0.039, 0.045, 0.048, 0.051/	FRCT	114
DATA A46 / 0.0054, 0.0016, 0.0033, 0.0052, 0.014,	FRCT	115
1 0.022, 0.0265, 0.035, 0.04, 0.042, 0.0465, 0.049, 0.051/	FRCT	116
DATA A47 / 0.0013, 0.0036, 0.0069, 0.011, 0.023,	FRCT	117
1 0.029, 0.025, 0.0335, 0.044, 0.046, 0.0495, 0.059, 0.051/	FRCT	118

DATA AG8	/0.0015, 0.041, 0.003, 0.012, 0.0235,	FRCT 119
1 0.0295, 0.033, 0.04, 0.044, 0.0475, 0.049, 0.0505, 0.051/		FRCT 120
DATA AG9	/0.0018, 0.0012, 0.0004, 0.014, 0.0255,	FRCT 121
1 0.031, 0.035, 0.042, 0.045, 0.047, 0.05, 0.051, 0.051/		FRCT 122
DATA AG1	/1.E-8, 3.E-8, 6.E-8, 1.E-7, 3.E-7, 6.E-7,	FRCT 123
1 1.E-6, 3.E-6, 6.E-6, 1.E-5, 3.E-5, 1.E-4, 1.E-3/		FRCT 124
DATA AG2	/5.E-7, 1.E-6, 5.E-6, 1.E-5, 5.E-5, 5.E-4, 1.E-3	FRCT 125
1 /		FRCT 126
DATA AG3	/13.32, 15.2, 17.8, 19., 21.19, 27.13, 100./	FRCT 127
IF (G1.EQ.0.) GO TO 240		
IF (G2.EQ.0.) GO TO 240		
DO 100 I=1,7		
DO 100 J=1,7		
IF (G1-AG1(I)) 40,60,60		
4) IF (G1.LT. AG1(I)) GO TO 70		
CALL TLUC(G1,U7(I,J),AG1,FTN(1,I,1),13)		
GO TO 100		
60 U7(I,J)=FTN(12,I,J)		
GO TO 100		
70 U7(I,J)=EXP(ALCG(FTN(1,I,J))+[ALOG(FTN(2,I,J))-ALOG(FTN(1,I,J))]/		
13LOG(AG1(2))-ALOG(AG1(1))]*[ALOG(G1)-ALOG(AG1(1))])		
130 CONTINUE		
DO 200 K=1,7		
IF (G3-AG3(7)) 140,160,160		
14) IF (G3.LT. AG3(7)) GO TO 170		
CALL TLUC(G3,VZ(K),AG3,U7(1,K),7)		
GO TO 200		
140 VZ(K)=U7(7,K)		
GO TO 200		
170 VZ(K)=U7(1,K)-(U7(2,K)-U7(1,K))/(AG3(2)-AG3(1))*(AG3(1)-G3)		
IF (VZ(K).LE.0.0) VZ(K)=1.E-5		
200 CONTINUE		
IF (G2-AG2(7)) 204,206,206		
204 IF (G2.LT. AG2(7)) GO TO 207		
CALL TLUC(G2,FR3,AG2,VZ,7)		
GO TO 210		
206 FR3=EXP(ALOG(VZ(6))*[ALOG(VZ(7))-ALOG(VZ(6))]/[ALOG(AG2(7))-ALOG(A		
1G2(6))]*[ALOG(G2)-ALOG(AG2(6))])		
GO TO 210		
207 FR3=EXP(ALOG(VZ(2))*[ALOG(VZ(7))-ALOG(VZ(2))]/[ALOG(AG2(7))-ALOG(A		
1G2(2))]*[ALOG(G2)-ALOG(AG2(2))])		
210 FCOE=ALOG(FR3)-0.149*[ALOG(THETA)-ALOG(30.)]		
FCOE=EXP(FCOE)		
GO TO 250		
240 FCOE=0.		
250 CONTINUE		
RETURN		
END		

SUBROUTINE TLUC(A,B,C,D,N)	TLU00010
DIMENSION C(1),D(1)	TLU00020
IF (N-1) 1,2,2	TLU00030
1 B=0.	TLU00040
GO TO 100	TLU00050
2 B=D(1)	TLU00060
GO TO 100	TLU00070
3 M=1	TLU00080
M=N	TLU00090
4 IF (M)-M-1) 14,15,9	TLU00100
5 M=(M+M)/2	TLU00110
IF (C(1)-C(2)) 1,2,10	TLU00120
11 IF (C(M)-A) 12,12,14	TLU00130

11 IF(A-C(M))17,12,14	TLU00140
12 B=D(M)	TLU00150
GO TO 100	TLU00160
13 M1=M	TLU00170
GO TO A	TLU00180
14 M1=M	TLU00190
GO TO B	TLU00200
15 A=C(M1)+(C(M1)-D(M1))*(A-C(M1))/(C(M1)-C(M1))	TLU00210
177 RETURN	TLU00220
END	TLU00230
SUBROUTINE TLUG(A,P,C,D,N)	TLUG0010
DIMENSION C(1),D(1)	TLUG0020
IF(N-1)1,2,3	TLUG0030
1 B=0.	TLUG0040
GO TO 100	TLUG0050
2 B=D(1)	TLUG0060
GO TO 100	TLUG0070
3 M1=1	TLUG0080
M11=N	TLUG0090
4 IC(M11-M1-1) 15,16,9	TLUG0100
5 M=(M11+M1)/2	TLUG0110
IF(C(1)-C(2))11,2,10	TLUG0120
11 IF(C(M)-A)12,12,14	TLUG0130
11 IF(A-C(M))17,12,14	TLUG0140
12 B=D(M)	TLUG0150
GO TO 100	TLUG0160
13 M1=M	TLUG0170
GO TO A	TLUG0180
14 M1=M	TLUG0190
GO TO B	TLUG0200
15 B=EXP(ALOG(D(M1))*(ALOG(D(M11))-ALOG(D(M1)))+(ALOG(A)-ALOG(C(M1))))	TLUG0210
1 / (ALOG(C(M11))-ALOG(C(M1))))	TLUG0220
177 RETURN	TLUG0230
END	TLUG0240

Reproduced from
best available copy.



APPENDIX V
FORMAT FOR ROLLER BEARING
COMPUTER PROGRAM INPUT INFORMATION

MAIN PROGRAM			00000100
CARD	COL.	ITEM	00000200
1	1-10	NO. OF ROLLS (50 MAXIMUM)	00000300
	11-20	ROLL DIA. - IN.	00000400
	21-30	PITCH DIA. - IN.	00000500
	31-40	TOTAL LENGTH OF ROLL - IN.	00000600
	41-50	LENGTH OF FLAT PORTION OF ROLL - IN.	00000700
	51-60	ROLL CORNER RADIUS - IN.	00000800
	61-70	ROLL CROWN RADIUS - IN. DO NOT READ IF CROWN DROP IS GIVEN	00000900
	71-80	ROLL CROWN DROP - IN. DO NOT READ IF CROWN RADIUS IS GIVEN	00001000
			00001100
2	1-10	DISTANCE FROM ROLL END TO POINT WHERE CROWN DROP IS MEASURED - IN.	00001200
	11-20	DIAMETRAL CLEARANCE - IN. + IF LOOSE.	00001300
	21-30	I.D. OF OUTER RING - IN.	00001400
	31-40	O.D. OF INNER RING - IN.	00001500
	41-50	O.D. OF CAGE - IN.	00001600
	51-60	I.D. OF CAGE - IN.	00001700
	61-70	LENGTH OF CAGE POCKET IN THE ROLLING DIRECTION - IN.	00001800
	71-80	WIDTH OF CAGE - IN.	00001900
3	1-10	MODULUS OF ELASTICITY FOR RINGS - PSI. IF BLANK PROGRAM ASSUMES 29,000,000.	00002000
	11-20	SAME FOR ROLLS.	00002100
	21-30	POISSON'S RATIO FOR RINGS. IF BLANK PROGRAM ASSUMES .25	00002200
	31-40	SAME FOR ROLLS.	00002300
	41-50	COEFFICIENT OF SLIDING FRICTION FOR CAGE/PILOT CONTACT.	00002400
	51-60	WEIGHT OF CAGE - LB.	00002500
	61-70	ROLL DENSITY - LB/IN**3. IF BLANK PROGRAM ASSUMES .283	00002600
	71-80	TOLERANCE ON ELASTIC APPROACH OF ROLL TO RACE - IN. IF BLANK PROGRAM ASSUMES .000,000,1	00002700
4	1-10	TOLERANCE ON FILM THICKNESS AT ROLL/POCKET CONTACT - IN. IF BLANK PROGRAM ASSUMES .000,000,5 IN.	00002800
	11-20	TOLERANCE ON ANGULAR VELOCITY OF ROLL ABOUT OWN CENTER - RPM. IF BLANK PROGRAM ASSUMES 1.	00002900
	21-30	TOLERANCE ON ANGULAR VELOCITY OF CAGE - RPM. IF BLANK PROGRAM ASSUMES .1	00003000
	31-40	LEAVE BLANK.	00003100
	1	PUNCH 1 (NO DECIMAL POINT)	00003200
	2-80	TITLE CARD. WRITE ANYTHING.	00003300
6	1	LEAVE BLANK.	00003400
	2-80	WRITE ANYTHING.	00003500
7	1-10	PRESSURE-VISCOSITY COEFFICIENT OF LUBRICANT. IN**2/LB.	00003600
	11-20	TEMPERATURE-VISCOSITY COEFFICIENT OF LUBRICANT - 1/(DEG F)	00003700
	21-30	VISCOSITY OF LUBRICANT AT INLET TEMPERATURE - LB*SEC/IN**2.	00003800
	31-40	INLET TEMPERATURE OF LUBRICANT - DEG F.	00003900
	41-50	THERMAL CONDUCTIVITY OF LUBRICANT - BTU/(DEG F)/HR/FT.	00004000
	51-60	LUBRICANT DENSITY - LB*SEC**2/IN**4.	00004100
	61-80	LEAVE BLANK.	00004200
8	1	PUNCH ZERO	00004300
	2-80	IDENTIFICATION DATA FOR LUBRICANT. PUNCH ANYTHING.	00004400

9	1-10	RPM OF OUTER RING.	00005900
	11-20	RPM OF INNER RING.	00006000
	21-30	RADIAL LOAD - LR. (POSITIVE SIGN)	00006100
	31-40	RPM OF ROTATING LOAD. IF LOAD IS STATIONARY LEAVE	00006200
		BLANK.	00006300
	41-50	FACTOR WHICH MULTIPLIES CAGE SPEED TO GET CAGE SPEED	00006400
		DECREMENT. IF BLANK PROGRAM ASSUMES .1	00006500
	51-60	PROPORTIONALITY FACTOR FOR FINITE DIFFERENCE IN THE	00006600
		ANGULAR VELOCITY OF A ROLL ABOUT ITS OWN CENTER.	00006700
		IF BLANK PROGRAM ASSUMES .05	00006800
	61-70	STARTING VALUE FOR MINIMUM FILM THICKNESS AT	00006900
		ROLL/POCKET CONTACT - IN. IF BLANK PROGRAM ASSUMES	00007000
		.0005 IN.	00007100
	71-90	LEAVE BLANK.	00007200
			00007300
		TO RUN ADDITIONAL LOAD CASES WITH SAME LUBRICANT	00007400
		REPEAT CARD 9 AS REQUIRED	
			00007600
		TO RUN ADDITIONAL LUBRICANTS PLACE ONE BLANK AFTER	00007700
		LAST CARD 7 AND READ CARD 5 ET. SEQ.	00007800
			00007900
		TO RUN NEW BEARING CONFIGURATION PLACE TWO BLANKS	00008000
		AFTER LAST CARD 7 AND READ CARD 1 ET. SEQ.	00008100
			00008200
		TO STOP PLACE THREE BLANK CARDS AFTER LAST CARD 7.	00008300
			00008400
			00008500

$$u = 1, \dots, m, \quad v = 1, \dots, n, \quad w = 1, \dots, m, \quad t = 1, \dots, n$$

1. The first step is to identify the problem or question that needs to be answered.

$$\frac{\partial^2 \phi}{\partial x^2} = -\frac{q}{\epsilon_0}$$

OUTPUT DATA FOR LOAD NO. 1 BEARING NO. 2

BEARING REACTION	ROW OF CAGE	PERCENT CAGE SLIP	TORQUE ON CAGE	CAGE PILOT NORMAL LOAD
7.001E 02	4.0943E 03	10.02	6.6891E 01	1.9838E 01

OUTPUT DATA FOR RACE CONTACTS

ELEMENT NUMBER	ELEMENT AZIMUTH	CONTACT LOAD		MEAN COMPRESSIVE STRESS		PATTERN EXTREMITY		SLIP VELOCITY	
		OUTER	INNER	OUTER	INNER	OUTER	INNER	OUTER	INNER
1	7.0	1.6263E 02	1.4205E 02	8.5242E 04	8.7831E 04	1.6415E-01	1.6092E-01	9.7878E 01	1.2718E 02
2	6.0007E 01	7.8287E 01	5.8128E 01	6.0951E 04	5.8051E 04	1.4723E-01	1.4271E-01	8.3379E 01	1.4168E 02
4	3.0007E 02	7.8286E 01	5.8128E 01	6.0950E 04	5.8051E 04	1.4723E-01	1.4271E-01	8.3380E 01	1.4168E 02
THE REST	7.8286E 01			1.1867E 04		1.3213E-01		2.7620E 00	

ELEMENT NUMBER	MIN. FILM THICKNESS		TRACTION FORCE	
	OUTER	INNER	OUTER	INNER
1	6.2125E-05	6.2268E-05	9.2945E 00	9.3499E 00
2	6.7479E-05	6.9053E-05	4.6405E 00	4.6826E 00
6	6.7479E-05	6.9053E-05	4.6495E 00	4.6826E 00
THE REST	7.7876E-05		1.1860E-02	

OUTPUT DATA FOR POCKET CONTACTS

ELEMENT NUMBER	ROW OF ROLLER	NORMAL POCKET LOAD		TANGENTIAL POCKET LOAD		MIN. FILM THICKNESS	
		FORE	AFT	FORE	AFT	FORE	AFT
1	-7.7022E 04	1.4628E 01	0.0	-5.4609E-02	0.0	5.0747E-05	9.8492E-03
2	-2.6696E 04	5.5084E 00	0.0	-3.3110E-02	0.0	1.5073E-04	9.7492E-03
6	-2.6696E 04	5.5084E 00	0.0	-3.3110E-02	0.0	1.5074E-04	9.7492E-03
THE REST	-5.8634E 04	0.0	4.0136E 00	0.0	-2.7844E-02	9.7111E-03	1.9804E-04

APPENDIX VII
MIL-L-23699-TYPE OIL PROPERTIES
AVAILABLE FOR USE IN PROGRAM INPUTS

The following pressure-viscosity data* for Aeroshell Turbine Oil 555 is typical of the Mil-L-23699 class of lubricants. Pertinent properties for the formulated fluid are as follows:

Thermal Conductivity (Btu/ft ² -hr-°F-ft)	Kinematic Viscosity (cs)	Density (g/ml)	Reciprocal Asymptotic Isoviscous Pressure, (psi) ⁻¹
100°F .098	28.2	.980	.942
210°F -	5.3	.935	.691
300°F .078	2.4	.897	.602
500°F .075	-	-	-

*Data provided by William R. Jones, Jr., Research Engineer, NASA
Lewis Research Center, Cleveland, Ohio.

Reproduced from
best available copy.

1	2	3	4	5	6	7	8	9	10	11	12	13	14	15	16	17	18	19	20	21	22	23	24	25	26	27	28	29	30	31	32	33	34	35	36	37	38	39	40	41	42	43	44	45	46	47	48	49	50	51	52	53	54	55	56	57	58	59	60	61	62	63	64	65	66	67	68	69	70	71	72	73	74	75	76	77	78	79	80	81	82	83	84	85	86	87	88	89	90	91	92	93	94	95	96	97	98	99	100
1	2	3	4	5	6	7	8	9	10	11	12	13	14	15	16	17	18	19	20	21	22	23	24	25	26	27	28	29	30	31	32	33	34	35	36	37	38	39	40	41	42	43	44	45	46	47	48	49	50	51	52	53	54	55	56	57	58	59	60	61	62	63	64	65	66	67	68	69	70	71	72	73	74	75	76	77	78	79	80	81	82	83	84	85	86	87	88	89	90	91	92	93	94	95	96	97	98	99	100

Year	Number of cases	Number of deaths
1970	100	10
1971	120	12
1972	150	15
1973	180	18
1974	200	20
1975	220	22
1976	250	25
1977	280	28
1978	300	30
1979	320	32
1980	350	35
1981	380	38
1982	400	40
1983	420	42
1984	450	45
1985	480	48
1986	500	50
1987	520	52
1988	550	55
1989	580	58
1990	600	60
1991	620	62
1992	650	65
1993	680	68
1994	700	70
1995	720	72
1996	750	75
1997	780	78
1998	800	80
1999	820	82
2000	850	85
2001	880	88
2002	900	90
2003	920	92
2004	950	95
2005	980	98
2006	1000	100
2007	1020	102
2008	1050	105
2009	1080	108
2010	1100	110
2011	1120	112
2012	1150	115
2013	1180	118
2014	1200	120
2015	1220	122
2016	1250	125
2017	1280	128
2018	1300	130
2019	1320	132
2020	1350	135
2021	1380	138
2022	1400	140
2023	1420	142
2024	1450	145
2025	1480	148
2026	1500	150
2027	1520	152
2028	1550	155
2029	1580	158
2030	1600	160
2031	1620	162
2032	1650	165
2033	1680	168
2034	1700	170
2035	1720	172
2036	1750	175
2037	1780	178
2038	1800	180
2039	1820	182
2040	1850	185
2041	1880	188
2042	1900	190
2043	1920	192
2044	1950	195
2045	1980	198
2046	2000	200
2047	2020	202
2048	2050	205
2049	2080	208
2050	2100	210

INPUT DATA FOR BEARING NO. 9, BEARING NO. 3			
REACTION	REACTION	REACTION	REACTION
1	2.000E-04	2.000E-04	2.000E-04
PERCENT CAGE SLIP	9.500E-02		
LOAD IS STATIONARY			

INPUT DATA FOR BEARING NO. 9, BEARING NO. 3			
REACTION	REACTION	REACTION	REACTION
1	2.000E-04	2.000E-04	2.000E-04
PERCENT CAGE SLIP	9.500E-02		
LOAD IS STATIONARY			

INPUT DATA FOR BEARING NO. 9, BEARING NO. 3			
REACTION	REACTION	REACTION	REACTION
1	2.000E-04	2.000E-04	2.000E-04
PERCENT CAGE SLIP	9.500E-02		
LOAD IS STATIONARY			

INPUT DATA FOR BEARING NO. 9, BEARING NO. 3			
REACTION	REACTION	REACTION	REACTION
1	2.000E-04	2.000E-04	2.000E-04
PERCENT CAGE SLIP	9.500E-02		
LOAD IS STATIONARY			

INPUT DATA FOR BEARING NO. 9, BEARING NO. 3			
REACTION	REACTION	REACTION	REACTION
1	2.000E-04	2.000E-04	2.000E-04
PERCENT CAGE SLIP	9.500E-02		
LOAD IS STATIONARY			